Volcanogenic copper-zinc sulphide deposits and their geological setting, in the central portion of the murchison greenstone belt, North eastern Transvaal, South Africa

Robert Spencer Taylor

Frontispiece. View from the L locality, along the southern slopes of the Carrolls Peak - Tshutshu Range towards the J locality. Hole ML2 is in progress.

VOLCANOGENIC COPPER-ZINC SULPHIDE DEPOSITS AND THEIR GEOLOGICAL SETTING, IN THE CENTRAL PORTION OF THE MURCHISON GREENSTONE BELT, NORTHEASTERN TRANSVAAL, SOUTH AFRICA.

ROBERT SPENCER TAYLOR

B.Sc., A.R.S.M., M.I.M.M.

A thesis submitted for the degree of Doctor of Philosophy at the University of Durham.

July 1981

ABSTRACT

The Murchison greenstone belt is of Archaean age, and occurs within the Kaapvaal Craton of South Africa. The greenstone sequence consists of high-magnesia basalts, overlain by tholeiitic basalts, and, on the northern flank of the Belt, rhyolitic tuffs and lavas form the top of the volcanic pile. All units are overlain by clastic sediments. The entire sequence is intruded by numerous, large, sills of tholeiitic composition; and a large gabbroic complex occupies the base of the rhyolite pile.

Collapse and deformation of the sequence produced a tight syncline with a subhorizontal fold axis and vertical axial plane. Low Grade metamorphism accompanied the folding, with temperatures in the range 450-480^{o} and a pressure of about 5.6kbar. Plutons of tonalitic magma were emplaced along the margins of the Belt. Subsequent cooling of these superimposed a thermal metamorphism onto the existing fabric.

Massive copper-zinc sulphide deposits were formed immediately following the rhyolitic volcanism. Two main, and three minor, deposits were studied in the central part of the Murchison Belt. At the larger deposit, the massive sulphide body is underlain by altered tuff. This alteration comprises an inner core of chlorite with pyrrhotite and chalcopyrite, and an outer, ill-defined sericitic zone containing pyrite and sphalerite. Bulk chemical analyses show an increase in total iron, and decrease in Al_2O_3 and K_2O towards the core of the alteration zone. The massive

sulphides form a stratiform lens of sphalerite, pyrite, pyrrhotite, and chalcopyrite. Relict, original textures suggest formation as unconsolidated sulphidic sediments on the sea-floor. The lower sulphide horizons were originally rich in chalcopyrite and silica, with only minor sphalerite. As the sulphides accumulated, sphalerite replaced the silica. The upper sulphide horizons show no such replacement, and are generally rich in sphalerite. The other main deposit is similar, but has no underlying alteration zone.

A model is presented to account for these, and other, copper-zinc deposits in the Murchison Belt. Following rhyolitic volcanism, sea-water percolated through the underlying rocks, became heated, and set up a system of circulating, hot brines, capable of leaching metals from the rocks. Discharge along pre-existing fractures, precipitated sulphides at the rock/sea-water interface. Initial solutions were hot, with a high Cu/Zn ratio, whilst later, cooler solutions were zinc rich, and deficient in copper.

LIST OF CONTENTS

	Page
Abstract	i
List of Contents	iii
List of Figures	viii
List of Plates	xi
List of Tables	xvi
List of Maps	xvii
Acknowledgements	xviii
CHAPTER I: INTRODUCTION	
1.1 Location	1
1.2 General Geology	2
1.3 History of Mining Activity	3
1.3.1 Ancient Mineworkers	3
1.3.2 European Mining Activity	3
1.4 Previous Geological Investigations	4
CHAPTER II: PRESENT INVESTIGATION - A BRIEF REVIEW	
2.1 Aims	10
2.2 Methods of Exploration	11
2.2.1 Ground Holding Position	11
2.2.2 Field Techniques	11
2.2.3 Geological Interpretation	13
CHAPTER III: VOLCANIC MASSIVE SULPHIDE DEPOSITS - A REVIEW	
3.1 Introduction	16
3.2 Classification	16
3.2.1 Type I - "Archaean"	17
3.2.2 Type II - "Besshi"	20
3.2.3 Type III - "Kuroko"	21
3.2.4 Type IV - "Cyprus"	22
3.2.5 Type V - "Proterozoic"	23
3.3 Ore Genesis	24
3.4 Stratigraphic Controls	28
3.5 Massive Sulphide Deposits and Crustal Evolution	29
3.6 Applications in Mineral Exploration	31
3.7 The Murchison Range	31
CHAPTER IV: REGIONAL GEOLOGY OF THE MURCHISON RANGE	
4.1 Regional Setting	36
4.1.1 Introduction	36
4.1.2 Nature of the Greenstone Belts of the Kaapvaal Craton	36

		Page
	4.1.3 The Granite - Greenstone Model	38
	4.1.4 Nature of the Early Crust	39
4.2	General Geology	41
	4.2.1 Introduction	41
	4.2.2 Malati Subgroup	41
	4.2.3 Leydsdorp Subgroup	41
	4.2.4 Rubbervale Subgroup	42
	4.2.5 Gravelotte Subgroup	43
	4.2.6 Rooiwater Igneous Complex	44
	4.2.7 Basic Sills	45
	4.2.8 Later Intrusives	45
	4.2.8a Serpentinites	46
	4.2.8b Dykes	46
	4.2.8c Younger Granites	46
4.3	Structural History	46
4.4	Metamorphism	48
4.5	Mineralization	49
	4.5.1 General	49
	4.5.2 Fe-Zn-Cu Sulphide Deposits	51
4.6	Interpretation of Stratigraphy	53
	4.6.1 Special Note	57
CHAPTER V: DETAILED GEOLOGY OF STUDY AREA		
5.1	Location	64
5.2	Geology	64
	5.2.1 Introduction	64
	5.2.2 Rubbervale Subgroup	65
	5.2.3 Rubbervale Subgroup - Transition Zone	68
	5.2.4 Gravelotte Subgroup	70
	5.2.5 Basic Sills	75
	5.2.6 Rooiwater Igneous Complex	76
	5.2.6a Introduction	76
	5.2.6b Gabbro Phase	77
	5.2.6c Hornblende Granite Phase	78
	5.2.6d Summary	80
	5.2.7 Post-Greenstone Intrusives	81
	5.2.7a Younger Granites	81
	5.2.7b Later Dolerites	81
5.3	Structure	81
	5.3.1 Structures	81
	5.3.2 Distribution of Schistosity	84
	5.3.3 Fracturing	85
	5.3.4 Dykes	86
	5.3.5 Discussion	86
5.4	Metamorphic Petrology	87
	5.4.1 Introduction	87
	5.4.2 Pre-Metamorphic Minerals	88
	5.4.3 Metamorphic Petrology	89
	5.4.3a Regional Dynamothermal Metamorphism	89
	5.4.3b Thermal Metamorphism	106
	5.4.3c Rooiwater Igneous Complex	112
	5.4.3d Summary	115

		Page
CHAPTER VI: GEOCHEMISTRY		
6.1	Introduction	131
6.2	Results	131
	6.2.1 Rubbervale Subgroup	132
	6.2.1a Flows	132
	6.2.1b Tuffs	133
	6.2.1c Transition Zone	134
6.3	Summary and Discussion	134
6.4	Conclusions	136
CHAPTER VII: MINERALIZATION IN THE RUBBERVALE SUBGROUP		
7.1	General	145
	7.1.1 Introduction	145
	7.1.2 Previous Investigations	145
	7.1.3 Present Investigation	146
7.2	J Locality	148
	7.2.1 Introduction	148
	7.2.2 Geology	149
	7.2.2a Footwall Flows	149
	7.2.2b Footwall Tuffs	149
	7.2.2c Footwall Alteration Zone	150
	7.2.2d Massive Sulphides	153
	7.2.2e Hangingwall Aluminous Cherts	156
	7.2.2f Acid Porphyries	156
	7.2.2g Sediments	157
	7.2.2h Intrusives	157
	7.2.3 Summary and Discussion	158
7.3	Main Gossan Zone	159
	7.3.1 Introduction	159
	7.3.2 Geology	170
	7.3.2a Footwall Sequence	171
	7.3.2b Mineralized Zone	172
	7.3.2c Hangingwall Sequence	175
	7.3.2d Intrusives	176
	7.3.2e Metamorphism and Deformation	177
	7.3.3 Summary	178
7.4	D Locality	179
	7.4.1 Introduction	179
	7.4.2 Geology	179
7.5	The L and W Localities	188
	7.5.1 Introduction	188
	7.5.2 Geology	189
	7.5.2a Footwall Sequence	190
	7.5.2b Mineralized Zone	191
	7.5.2c The Hangingwall Acid Porphyries	196
	7.5.3 Summary	197
CHAPTER VIII: ORE MINERALOGY		
8.1	Introduction	204
8.2	J Locality	204
	8.2.1 Pyrite in Footwall Tuffs	204
	8.2.1a Fine Granular Pyrite	205

		Page
	8.2.1b Zoned Euhedra	205
	8.2.1c Fragmented, Banded Masses	205
	8.2.1d Interpretation	206
	8.2.2 Footwall Stringer Sulphide Zone	207
	8.2.2a Introduction	207
	8.2.2b Pyrite	208
	8.2.2c Other Sulphides	208
	8.2.3 Massive Sulphides	209
	8.2.3a Introduction	209
	8.2.3b Pyrite	210
	8.2.3c Sphalerite	217
	8.2.3d Chalcopyrite	219
	8.2.3e Pyrrhotite	220
	8.2.3f Magnetite	221
	8.2.3g Miscellaneous Sulphides	221
	8.2.3h Silicates	222
	8.2.4 Summary and Discussion	223
	8.2.5 Paragenetic Sequence	226
8.3	Main Gossan Zone	226
	8.3.1 Introduction	226
	8.3.2 Pyrite	245
	8.3.3 Pyrrhotite	246
	8.3.4 Chalcopyrite	247
	8.3.5 Sphalerite	247
	8.3.6 Silicates	247
	8.3.7 Summary and Discussion	248
8.4	L-W Locality	249
	8.4.1 Introduction	249
	8.4.2 Pyrite	257
	8.4.3 Sphalerite	258
	8.4.4 Chalcopyrite	259
	8.4.5 Pyrrhotite	259
	8.4.6 Miscellaneous	259
	8.4.7 Summary	260
8.5	Sphalerite Geobarometer	264
	8.5.1 Introduction	264
	8.5.2 Methods	265
	8.5.3 Results	265

CHAPTER IX: FOOTWALL ALTERATION

9.1	Introduction	267
9.2	Alteration Zone - Geochemistry	267
9.3	Solutions	270
9.4	Murchison Greenstone Belt	271
	9.4.1 J Locality	271
	9.4.2 MGZ Locality	272
9.5	Summary and Discussion	273

	Page
CHAPTER X: DISCUSSION	
10.1 Geology	279
10.2 Copper-Zinc Sulphide Deposits	280
10.3 Model for Sulphide Formation	281
10.4 Implications for Exploration in the Murchison Greenstone Belt	282
10.4.1 Copper-Zinc Deposits	282
10.4.2 Antimony Deposits	283
LIST OF REFERENCES	287
APPENDIX A: SAMPLE COLLECTION	301
APPENDIX B: ELECTRON MICROPROBE ANALYSES	306
APPENDIX C: WHOLE ROCK ANALYSES	345
APPENDIX D: ETCH TECHNIQUES FOR SULPHIDES	360

LIST OF FIGURES

		Page
1.	Locality Map of the Murchison Range.	7
2.	Generalized Geology of the Eastern Half of the Murchison Greenstone Belt.	8,9
3.	Stratigraphy of the Murchison Range According to Van Eeden et al. (1939).	59
4.	Stratigraphy of the Eastern Portion of the Murchison Range Compared to the Barberton Mountain Land.	60
5.	Various Stratigraphic Proposals for the Murchison Range.	61
6.	North-South Section, and Development of the Murchison Greenstone Belt.	62,63
7.	Generalized Stratigraphic Section Through the Transition Zone.	90
8.	Stratigraphic Section Through the Gravelotte Subgroup on the Farm Solomons Mine.	91
9.	Stratigraphic Sequence Through the Chloritoid and Antimony Bars.	92
10.	S_1 Pole Plots.	93
11.	Schematic Interpretation of the Structure of the Murchison Range.	94
12.	Fracture Trends.	95
13.	Dyke Trends.	96
14.	Pressure-Temperature Diagram, After Winkler (1974)	117
15.	Chlorite Compositions.	118
16.	Epidote Compositions.	118
17.	Feldspar Composition: Regional Metamorphism.	119
18.	Feldspar Composition: Thermal Metamorphism.	119
19.	Feldspar Composition: Rooiwater Igneous Complex.	119
20.	Mica Compositions.	120
21.	Garnet Compositions: Thermal Metamorphism.	120
22.	Amphibole Compositions: Thermal Metamorphism.	121

Page

23. Amphibole Compositions: Basic Sills & Gabbro. 121

24. Plot of Alumina versus Alkalies for Rubbervale Subgroup. 138

25. Alkali Plot of Rubbervale Subgroup. 139

26. Plots of K_2O vs. Ba, and Rb; and Na_2O vs. Sr, and Y, for Rubbervale Subgroup. 140

27. Plot of Zr/TiO_2 vs. Nb/Y for Rubbervale Subgroup. 141

28. Triangular Plot of TiO_2, Y+Zr, and Cr for Basic Sills. 142

29. Generalized Stratigraphic Sequence at the J Locality. 160

30. Diamond Drill Section 300E, Holes MM1 and MM3, J Locality. 161

31. Fragment Size in Footwall Tuffs at the J Locality. 162

32. Alteration in Footwall Tuffs at the J Locality. 163

33. Sulphide Distribution in Footwall Alteration Zone at the J Locality. 164

34. True Thickness of Massive Sulphide Lens at the J Locality. 165

35. Geological Map of the MGZ Locality. 180

36. Stratigraphic Sequence at the MGZ Locality. 181

37. Diamond Drill Section 4345E, Holes MS3 and MS1, MGZ Locality. 182

38. Longitudinal Section in the Plane of Mineralization, MGZ Locality. 183

39. Geological Map of the D Locality. 184

40. Stratigraphic Logs of Selected Boreholes at the L and W Localities. 200

41. Geological Map of the L Locality. 201

42. T-X Projection Onto the FeS-ZnS Join of Sphalerite+Pyrite+Hexagonal Pyrrhotite (in Kbar), from Scott (1976). 266

43. Diagramatic Section Through a Hypothetical Alteration Zone. 275

Page

44. J Locality: Footwall Alteration Zone. 276

45. Chlorite Composition: Footwall Alteration Zone at the J Locality. 277

46. MGZ Locality: Footwall Tuffs. 278

47. Diagramatic Section of a Convection Cell. 285

48. Copper-Zinc and Antimony Deposits of the Murchison Range. 286

Figure to Accompany Special Note: Litho-stratigraphy of the Gravelotte Group According to SACS (1980). 58

LIST OF PLATES

		Page
Frontispiece:	View from the L Locality, along the southern slopes of the Carrolls Peak - Tshutshu range towards the J Locality.	
1.	View from Carrolls Peak looking east along the Murchison Range.	14
2.	View from Carrolls Peak looking west along the Murchison Range.	15
3.	Hexagonal cooling joints in felsic intrusive on Rooiwater.	97
4.	Flow banding and flow-breccia in rhyolites, Maranda.	97
5.	Coarse felsic pyroclastic rocks, Maranda.	98
6.	Graded bedding; greywackes from Gravelotte Subgroup, Solomons Mine.	98
7.	Graded bedding; greywackes from the Antimony Bar.	99
8.	Original bedding, S_0, folded and cut by an axial plane cleavage, S_1.	99
9.	Blocks of coarse tuff from the Rubbervale Subgroup.	100
10.	S_1 and S_2 in tuffs from the Rubbervale Subgroup, Solomons Mine.	101
11.	S_1 and S_2 in thin section.	101
12.	F_2 fold in greywackes of the Antimony Bar.	102
13.	Flow banded rhyolite from Rubbervale Subgroup, Solomons Mine.	102
14.	Stages in recrystallization of quartz phenocrysts.	123
15.	Original, twinned, feldspar phenocryst; now almost pure albite. Sample SM204.	125
16.	Devitrification spherulites of quartz and alkali feldspar in acid porphyry, W locality. Sample MA18W2.	125
17.	Quartz grain with inclusions; representing an original, devitrification spherulite. Sheared tuff, sample SM11S1.	125
18.	Typical basic sill. Sample MA4K1.	125

		Page
19.	Typical braided, metamorphic texture in quartz+ chlorite+sericite schist. Sample MA28W2.	127
20.	Coarse biotite and quartz in pressure shadow to quartz phenocryst. Sample MS7/4.	127
21.	Homotropic biotite with relict S_1. Sample MA28W2.	127
22.	Poikiloblastic garnets, W locality. Sample MA9W2.	127
23.	Coarse amphibole with relict S_1. Sample MA4J4.	129
24.	Zoned amphibole from basic sill. Sample SM401.	129
25.	Porphyroblastic albite with S_1 relicts. Sample MA16W2.	129
26.	Crush texture in quartz diorite phase of the Rooiwater Igneous Complex. Sample SM12.	129
27.	Granophyric texture in quartz diorite phase of the Rooiwater Igneous Complex. Sample CD21.	130
28.	Typical alteration in footwall to the J massive sulphide deposit.	166
29.	Chert horizon in the footwall of the J massive sulphide deposit.	167
30.	Massive sulphide intersection from hole MM5A, J Locality.	167
31.	Banded pyrite+sphalerite ore, J massive sulphide deposit.	168
32.	Slump structures in banded silicate-sulphide horizon, J massive sulphide deposit.	168
33.	Banded massive sulphides, J massive sulphide deposit.	169
34.	Pillar of gossan in the Ancient Working at the MGZ deposit, Solomons Mine.	185
35.	Sulphide intersection from hole MS1, MGZ locality.	186
36.	Vertical L_1 lineations on gossan pillar in the Ancient Working at the MGZ locality, Solomons.	187
37.	Massive sulphide intersection from hole MMD2, D Locality.	187
38.	Brecciation and flow-banding in rhyolites from the W Locality.	202

Page

39. Slump structures in tuff horizon from the footwall volcanic rocks at the W Locality. 203

40. F_1 fold in quartz+sphalerite layer from the W Locality. 203

41. Successive stages in the growth, aggregation and metamorphic recrystallization of pyrite in a chlorite schist horizon in the footwall in the J massive sulphide deposit. Sample MA14J11. 229

42. Zoned pyrite euhedron from a chlorite schist horizon in the footwall to the J massive sulphide deposit. Sample MA9J11b. 230

43. Fragment of zoned pyrite. Chlorite schist horizon, footwall to the J massive sulphide deposit. Sample MA9J11b. 230

44. Fragment of zoned pyrite, with overgrowth of pyrite, sphalerite, and chalcopyrite. Sample MA9J11b. 230

45. Rare, fractured, amphibole crystal healed with pyrrhotite. Sulphide mineralization in the footwall alteration zone to the J massive sulphide deposit. Sample MA4J4. 230

46. Chlorite schist horizon from footwall tuffs, J deposit. 231

47. Banded pyrite+sphalerite ore. Possible slump structures, pyrite balls and concretions. 231

48. Layered sulphides. Basal horizon of pyrite+ sphalerite+chalcopyrite with fragments of chlorite schist. 231

49. Unstructured, sieve-textured pyrite. Massive sulphides, J locality. Sample MA17J11. 233

50. Radial, sieve-textured pyrite. Massive sulphides, J locality. Sample MA17J11. 233

51. Fragmented, sieve-textured pyrite. Massive sulphides, J locality. Sample MA18J11b. 233

52. Fragment of sieve-textured pyrite with concentric zonation. Massive sulphides, J locality. Sample MA18J11b. 233

53. Banded sphalerite+pyrite ore. Massive sulphides, J locality. Sample MA6J15a. 235

54. Banded sphalerite+pyrite ore. Euhedral and sieve-textured pyrite. Massive sulphides, J locality. Sample MA6J15a. 235

		Page
55.	Banded sphalerite+pyrite ore. Massive sulphides, J locality. Sample MA6J15a.	235
56.	Massive pyrite. Typical aggregate. Massive sulphides, J locality. Sample MA1J15.	236
57.	Massive pyrite. Grain with silica inclusions in core. Massive sulphides, J locality. Sample MA2J15.	236
58.	Massive pyrite. Zoned pyrite with irregular grain boundary. Massive sulphides, J locality. Sample MA1J15.	236
59.	Coarse, subhedral pyrite, with embayments. Massive sulphides, J locality. Sample MA15J11a.	238
60.	Coarse, subhedral pyrite, with embayments, and silica inclusions in centre of grain. Massive sulphides, J locality. Sample MA15J11a.	238
61.	Chalcopyrite blebs outlining sphalerite grains. Massive sulphides, J locality. Sample MA2J18.	238
62.	Etched sphalerite grains, with bent twin lamellae. Massive sulphides, J locality. Sample MA2OJ11.	238
63.	Mutual boundary textures in sphalerite - pyrrhotite - chalcopyrite horizon. Massive sulphides, J locality. Sample MA15J11c.	239
64.	Oval "domains" of sphalerite in mutual boundary textured massive sulphides, J locality. Sample MA16J11c.	239
65.	Etched chalcopyrite showing granular texture and twin lamellae. Massive sulphides, J locality. Sample MA15J11c.	241
66.	Hexagonal pyrrhotite replaced by magnetic, monoclinic pyrrhotite. Footwall stringer sulphides, J locality. Sample MA4J4.	241
67.	Pyrite, probably replacing pyrrhotite. Massive sulphides, J locality. Sample MA9J15.	241
68.	Poikiloblastic (?), magnetite with chalcopyrite inclusions. Massive sulphides, J locality. Sample MA15J11d.	241
69.	Large, porphyroblastic, pyrites with feathery chalcopyrite in pressure shadows. Chlorite schist unit, MGZ locality.	251
70.	Large, fractured, pyrite with infilling pyrrhotite. Mineralized chert unit, MGZ locality. Sample SM3S2.	251

Page

71. Large, fractured, pyrite, partially replaced by pyrrhotite. Mineralized chert unit, MGZ locality. Sample SM5S3. 251

72. Large, fractured, pyrite, set in silicate, with a thin pyrrhotite and chalcopyrite rim. Chlorite schist unit, MGZ locality. Sample SM1S2a. 251

73. Stages in the growth, aggregation, and metamorphic recrystallization of pyrite, with entrapment of silica. Mineralized chert unit, MGZ locality. Sample SM3S2. 253

74. Pyrrhotite radially overgrowing pyrite. Mineralized chert unit, MGZ locality. Sample SM5S3. 255

75. Hexagonal pyrrhotite partially replaced by magnetic, monoclinic pyrrhotite. Mineralized chert unit, MGZ locality. Sample SM4S2b. 255

76. Intergrown pyrrhotite and Mg-chlorite. Chlorite schist unit, MGZ locality. Sample SM4AS3. 255

77. Fractured amphibole crystal, healed with pyrrhotite. Chlorite schist unit, MGZ locality. Sample SM4AS3. 255

78. Coarse, quartz and sphalerite band in micaceous schist, L locality. Sample MA2L1. 262

79. Corroded pyrite in sphalerite and quartz, L locality. Sample MA3L1. 262

80. Angular sphalerite, interstitial to sericite, and parallel to schistosity, W locality, Sample MA16W2. 262

81. Garnet enclosing sphalerite, W locality. Sample MA23W2. 262

Page

LIST OF TABLES

1. Classification of Massive Sulphide Deposits. 33,34

2. Comparison of Metal Content with Underlying Rock Sequence, Massive Sulphide Deposits. 35

3. Gravelotte Subgroup: Sediments, Compared with Similar Rocks from the Barberton Mountain Land. 103

4. Mean and Range of Chemical Analyses of the Various Rock Types. 143,144

5. J Locality. Pyrite Analyses from the Massive Sulphides. 242

6. J Locality. Massive Sulphides. 243

7. Unknown Phases in Sample MA9J15 from Massive Sulphides, J Locality. 244

8. MGZ Locality. Massive Sulphide Unit. 256

9. Sphalerite Analyses from the W Locality. 263

LIST OF MAPS

(inside pocket on back cover)

1. 1:20,000 scale Detailed Geology, Central Part of the Murchison Greenstone Belt.

2. 1:2,000 scale Geology of the J Locality.

3. 1:1,000 scale Geology of the W Locality.

4. 1:20,000 scale Simplified Geology showing sample localities.

ACKNOWLEDGEMENTS

The field work and sample collection, which forms the basis of this thesis was conducted whilst the author was employed by African Selection Trust Exploration (Pty.) Ltd., and I would like to thank Dr. J. Kenyon for permission to use this data.

Messrs. J.B. Rogers and P.E. Winter, formerly of A.S.T.E., and Mr. W.G. Garlick, consultant, receive my thanks for their help and encouragement whilst in the field. I also extend my gratitude to Don Maximo Casañ-Daries who, as Senior Field Assistant, was responsible for the non-geological aspects of the Murchison Project.

The past two years at Durham University were spent under the tenure of a N.E.R.C. Special Competition Studentship award, and this is gratefully acknowledged.

I thank Professor G.M. Brown, former Head of Department of Geological Sciences, and Professor M.H.P. Bott, present Head, for making available the research facilities of the Department.

Mr. R. Phillips, my supervisor, and Dr. D.M. Hirst are to be thanked for their help and time given during this project.

Dr. J.G. Holland and Mr. R. Hardy gave instruction and advice on X-ray fluorescence analysis, Dr. A. Peckett on electron microprobe analysis, Messrs. G. Randall and L. MacGregor prepared thin sections and polished mounts,

and Mr. G. Dresser has aided in photographic work.

I would also like to take this opportunity to thank all past and present members of the academic and technical staff who have, during the past two years, given me generous help and advice, particularly: Dr. C.H. Emeleus, Messrs. D. Asbery, A. Carr, and R. Lambert. Also thanks to my associates for their help and hindrance: R.M. Foster, R.H. Hunter, A.P. Jones and M. Ozcelik.

Mrs. C.L. Mines kindly, and efficiently, typed this thesis, and I extend my thanks to her.

Finally, none of this would have been accomplished without the support and understanding of my wife, Myra, and our two sons, Tristen and Oliver-Denzil.

CHAPTER I

INTRODUCTION

1.1 Location

The Murchison Range is one of several Archaean greenstone belts lying within the Kaapvaal Craton of South Africa in a region known as the northeastern Transvaal Lowveld. Other greenstone belts in the region are the Pietersberg, the Sutherland, and the Barberton Mountain Land, the latter being approximately 190 km south of the Murchison Range, fig. 1.

The Murchison greenstone belt consists of a pile of metamorphosed volcanic and sedimentary rocks trending east-northeast for a total distance of 140 km. The belt extends from beneath the Proterozoic Escarpment in the west to the Kruger National Park in the east, immediately north of Palabora, where it disappears beneath a cover of the Karroo rock sequence. From a width of 14 km in the west, the belt gradually tapers to 5 km in the east where it bifurcates near the Park boundary.

The linear nature of the Range is emphasized by the near vertical dipping strata, of which the more resistant form prominent parallel ridges extending from the Escarpment to the township of Gravelotte. From here the ridges diminish in height and eventually merge into the relatively flat surrounding plains.

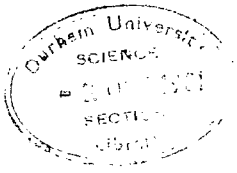

1.2 General Geology

The volcanic and sedimentary rocks comprising the Murchison greenstone belt can be divided into four major lithological units. The lowermost unit forms the southern flank of the Belt and is represented by a series of ultramafic metalavas which have been equated with the Lower Ultramafic Unit of the Barberton greenstone model (Viljoen and Viljoen, 1969a; Viljoen et al., 1979). Overlying these are tholeiitic and magnesian metalavas and chlorite schists, equated to the Mafic to Felsic Unit of the Barberton model. In the northern part of the Belt a thick sequence of felsic tuffs and flows, representing an ancient stratavolcano, is probably stratigraphically above the tholeiitic metalavas. Conformably overlying the volcanic sequences are clastic sediments, arenaceous in the centre and east, but argillaceous in the west. Intrusive along the northern flank of the belt is a gabbroic complex termed the Rooiwater Igneous Complex, fig.2.

Following intrusion of the Rooiwater Igneous Complex, the pile of volcanic and sedimentary rocks was folded into a tight isoclinal syncline, giving the belt its characteristic east-northeast linear trend. Plutons of tonalitic composition were intruded into the northern edge of the Rooiwater Igneous Complex, and to the south a zone of potash-rich pegmatites and early granites fragmented the ultramafic metalavas.

In spite of the intense deformation and the granitic intrusions the grade of metamorphism within the volcanic and sedimentary rocks remains low. Amphibolite facies is

found adjacent to the granites, but most of the rocks have only been subjected to upper greenschist facies metamorphism.

1.3 History of Mining Activity

1.3.1 Ancient Mineworkers

Traces of the earliest attempts to exploit the mineral wealth of the area can be seen as deep excavations and pits parallel to the strike of various gold, copper and copper-zinc "reefs". Schwellnus (1937) and Trevor (1912) ascribe a pre-European, possibly pre-Bantu origin to these "ancient workings", and Van Eeden et al. (1939) describe several of these workings as being "...distinct from the prospecting trenches, shafts, etc. made by Europeans...and were not made during living memory."

1.3.2 European Mining Activity

In 1870 Button and Sutherland found auriferous quartz near the present town of Gravelotte, but this attracted little attention until 1886 when prospectors from the Woodbush and Haernertsburg goldfields arrived. By 1888 the gold rush was in full swing, and the town of Leydsdorp was founded in 1890. However, by 1892, the heavy toll taken by malarial fever, high transport costs and only traces of gold forced many prospectors to abandon the area. Mining operations were carried out spasmodically until 1928 when a renewed "boom" began.

Gold mining was concentrated in the vicinity of prominent quartzite horizons within the sedimentary assemblage. North and east of the present town of Gravelotte, gold was extracted from carbonate and quartz "reefs" and banded ironstone horizons forming the so-called "Antimony Line",

(Van Eeden et al., 1939). In the south of the Murchison Belt, mineralization is confined to prominent quartzites between Leydsdorp and Gravelotte townships, continuing eastwards to the La France trigonometrical beacon.

Numerous other small mines and prospects occur elsewhere in the greenstone belt.

In 1928 the exploitation of antimony as a byproduct of gold mining commenced and in 1934 the Consolidated Murchison (Transvaal) Goldfields and Development Company was registered to produce antimony with gold as a byproduct from reefs along the "Antimony Line". Today, production continues from four mines, which together constitute the largest antimony producer in the western world.

South of the Murchison greenstone belt, reaction between beryllium-bearing pegmatites and ultramafic greenstone xenoliths led to the formation of beryl and emerald deposits. One large mine is in operation at present.

Despite spasmodic prospecting no other minerals are presently being mined in the Murchison Range, although sub-economic deposits of copper-nickel and copper-zinc are known to exist.

1.4 Previous Geological Investigations

Early publications by Sawyer (1892), Wilson-Moor (1896) and Merensky (1905) dwelt on the known gold deposits of the area. Mellor (1906) gave an account of a traverse through the Murchison Range describing the area as "...a basement of extremely ancient rocks with numerous later acid and basic intrusions." A more complete account of the geology of the Murchison Range was given in a Geological Survey

Memoir by Hall (1912) who subdivided the Lowveld into greenstone schists and basic schists overlain by phyllites, quartzites etc., and intruded by Older Granite, gneiss and sheared basic rocks. These were all assigned to the Swaziland System. Hall was the first to equate the quartzites to the Moodies Group sediments of the Barberton Mountain Land.

In 1939, Van Eeden et al. in a detailed investigation described the geology, structure and mineralization of the Murchison Range east of Leydsdorp. Rocks assigned to the Swaziland System were subdivided into three divisions depending on their relationship to the prominent quartzite horizons. Intrusive into these was the Rooiwater Igneous Complex, and everything was intruded by Old Granites.

This work was the first to describe the structure and stratigraphy of the volcanic and sedimentary assemblage, and provided a basis for later investigators.

In 1975 Minnitt produced an M.Sc. thesis covering the extreme east of the Murchison Range where he recognized a basal sequence of altered ultramafic metalavas, overlain by massive and pillowed mafic basalts. His interpretation of these was closely based on that proposed for the Barberton Mountain Land by Viljoen and Viljoen (1969a) and Anhaeusser (1972); see figure 4.

Recent reports by Jantski (1978) and Viljoen et al. (1979) have put forward proposed stratigraphic subdivisions for the Murchison greenstone belt. These are discussed fully under "Stratigraphy", chapter 4, section 4.2.

Early publications concerning mineralization within the Murchison greenstone belt concentrated on gold,

Merensky (1905), Mendelsohn (1938), and later on antimony, Cilliers (1975), Pearton (1975), Van Vuuren (1975), Muff (1978) and Viljoen et al. (1978). Van Eeden et al. (1939) and Viljoen et al. (1978) also discuss other mineral occurrences. The mineralogy of the Letaba copper-zinc deposit and the Monarch cinnabar deposit were described by Hausman in 1959.

Although the Murchison greenstone belt has been the subject of numerous geological investigations, these are mainly concerned with gold and antimony mineralization, with only a passing reference to copper and zinc. Similarly the geology of the northern flank of the belt has been neglected, especially the pile of felsic tuffs and flows which contain the copper-zinc deposits, and provide important clues as to the structure of the greenstone belt.

FIG 1 LOCALITY MAP OF THE MURCHISON RANGE

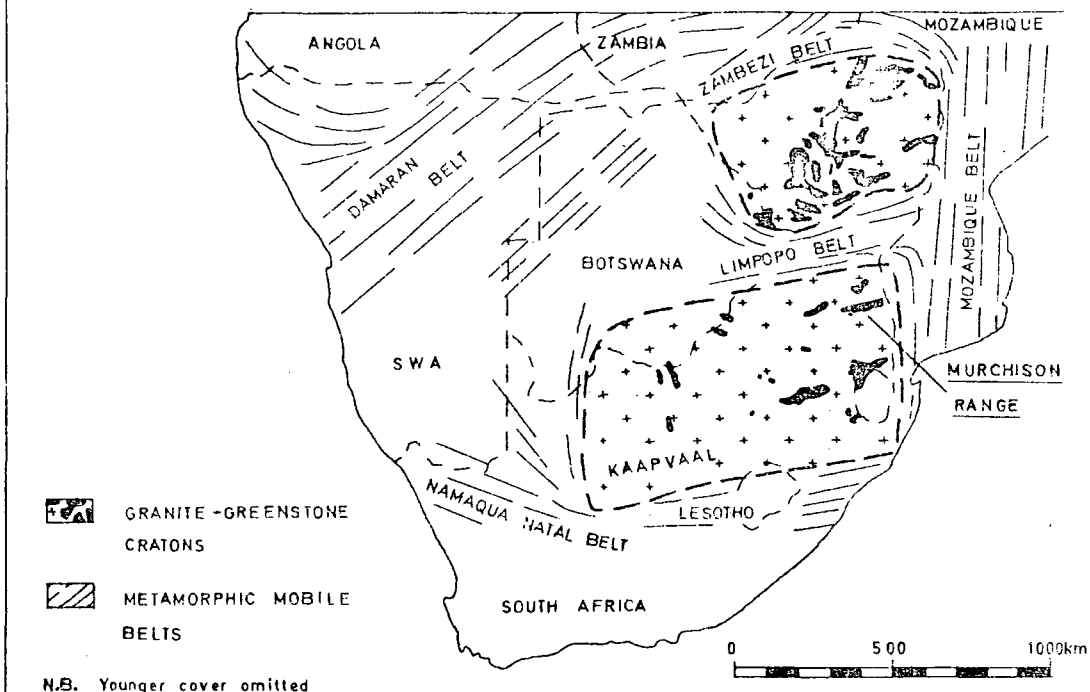

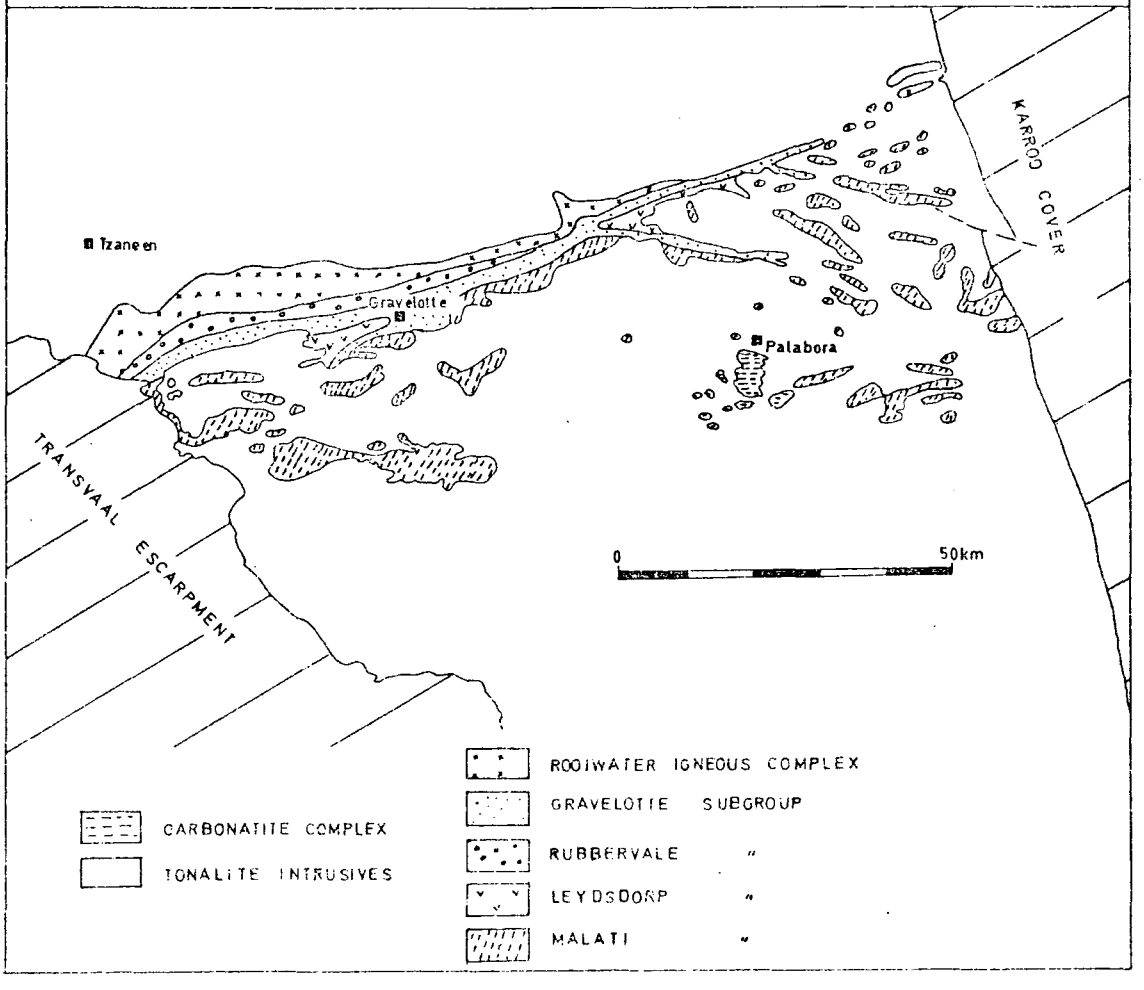

Figure 2: Generalized Geology of the Eastern Half of the Murchison Greenstone Belt.

Intrusive Younger Granites

Quartz-Diorite
Gabbro
} Rooiwater Igneous Complex

Sediments — Gravelotte Subgroup
Felsic tuffs and lavas — Rubbervale Subgroup
Tholeiite basalts — Leydsdorp Subgroup
High-magnesia basalts — Malati Subgroup
} Swaziland System

Quartzite bars; cb - chloritoid, ab - antimony, sb - spitzkop, lb - louskop

Working Mines

Abandoned mines or prospects.

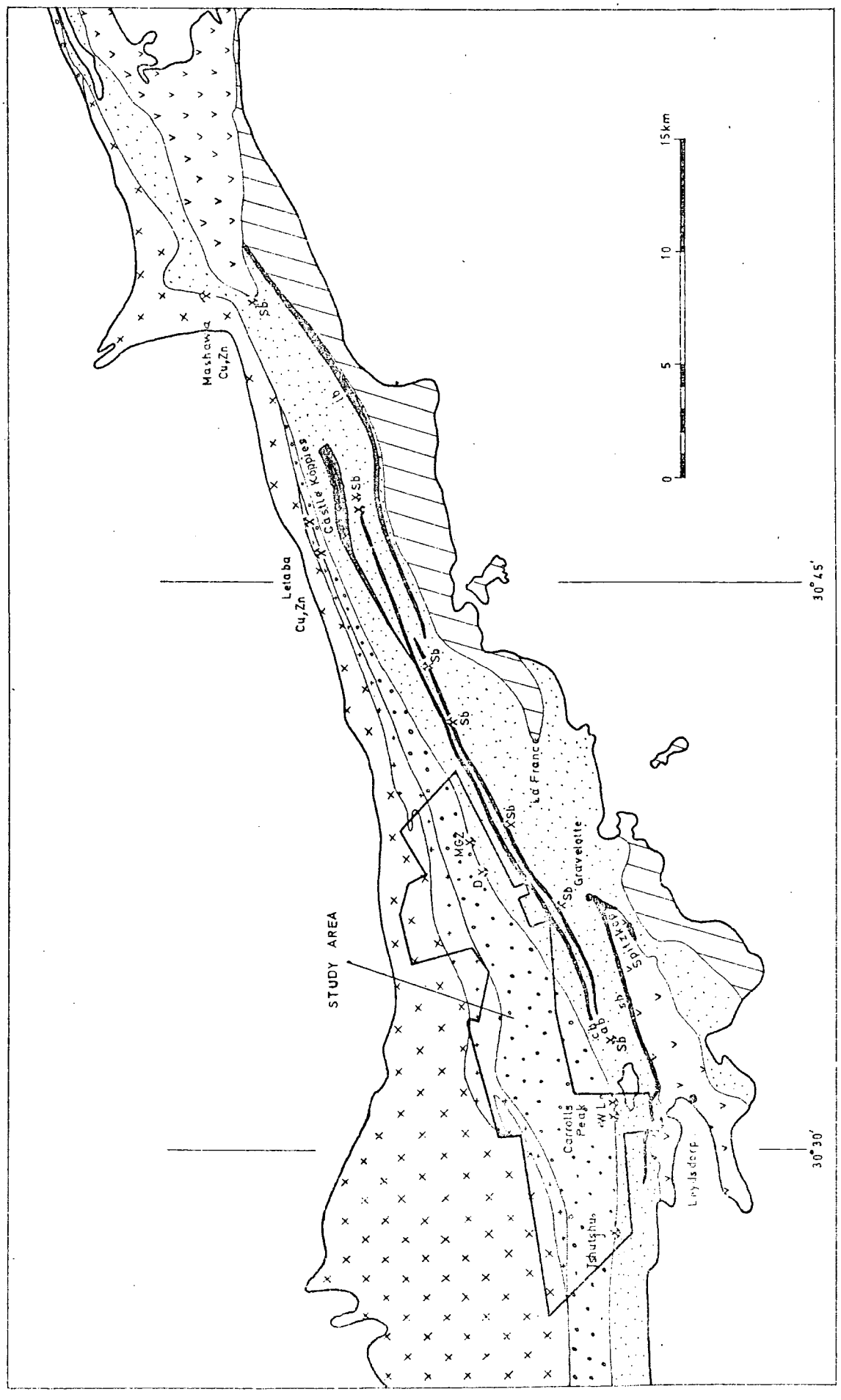
Mashawja
Cu,Zn
Letaba
Cu,Zn
Castle Kopjes
Sb
La France
Gravelotte
Spitzkop
STUDY AREA
Carrolls
Peak
Leydsdorp
30°45'
30°30'
0
5
10
15km

CHAPTER II

PRESENT INVESTIGATION: A BRIEF REVIEW

2.1 Aims

The Geological Survey Memoir of 1939 mentions the presence of Ancient Workings within the Murchison Range (Van Eeden et al., 1939, p.29), three of which were reported to contain malachite and azurite. These three are located within, or at, the southern contact of the "Quartz Porphyry Group", which consists of felsic volcanic rocks and has now been designated the Rubbervale Sub Group (Viljoen et al., 1979); also fig. 5. These ancient workings are on the farms Solomons Mine, Plaatveld and Vlaklaagte (the old Letaba Coppers Mine), and Mashawa (the old Mashawa Coppers Mine).

From a reconnaissance of these workings and from old company reports, it was concluded that they represent the surface expressions of massive pyritic copper-zinc sulphide lenses. The largest is the Letaba Coppers Mine, which is reported to contain 560,000 tonnes of 1.6% Cu and 5.7% Zn (for a summary see Hammerbeck, 1976). It was thus felt that the area held potential for the discovery of further massive sulphide deposits. Similarities between these deposits, their host rocks, and the massive Cu-Zn sulphide deposits in the Canadian Shield were noted.

In May 1975 the present writer, when employed by African Selection Trust Exploration, was given the task of prospecting for, exploring and evaluating any such deposits. As of February 1979 three massive Cu-Zn sulphide deposits and one area of disseminated zinc sulphide mineral-

ization had been discovered. One of these massive deposits, on the farm Solomons Mine, was the sub-surface continuation of an Ancient Working.

2.2 Methods of Exploration

2.2.1 Ground Holding Position

Another company owns the mineral rights to a number of farms and holds mineral claims over a large portion of the Murchison greenstone belt. These holdings are concentrated on the two old copper-zinc workings, the Letaba Coppers Mine and the Mashawa Coppers Mine, and on the antimony-gold mineralization along the "Antimony Line". Elsewhere mineral rights belong to the individual farm owners, or to the South African Government.

In 1975 African Selection Trust Exploration acquired prospecting options covering portions of eight adjacent farms in the central section of the Murchison Range, near the town of Gravelotte. These farms are Solomons Mine 762LT, Mon Desir 782LT, Gravelotte 783LT, Rubbervale 784LT, Beesplaas 676LT, Cottondale 674LT, Rooiwater 673LT, and Maranda 675LT. The area covers 25 km of strike along the pile of felsic volcanic rocks, or the "Quartz Porphyry Group", where these have their thickest development. See map 1 and fig.2. General views of this study area can be seen in plates 1 and 2, taken from Carrolls Peak trigonometrical beacon.

2.2.2 Field Techniques

Initially geological interpretations were based on the map accompanying the 1939 Geological Survey Memoir (Van Eeden et al., 1939). This was later revised, and the structure and stratigraphy extensively altered.

From pre-existing maps, aerial photographs and an initial geological reconnaissance the following field work was done:

a) the strike of the formations was determined accurately to allow location of a suitable base line on each farm

b) pegged lines at 200 m spacing were laid out perpendicular to this base line, with coloured stakes at 50 m intervals along the lines

c) soil samples were taken every 25 m along the lines, at a depth of 25 cm. These were analysed for total hot extractable Cu, Ni, Zn and Pb by atomic absorption at the company's Johannesburg laboratory

d) a ground, proton precession magnetometer survey was carried out in conjunction with the above soil survey

e) a base map was constructed, to 1:10,000 scale, incorporating the above data, and the same base map was used for detailed geological mapping

f) a further geophysical survey, using the Pulse Electromagnetic (PEM) technique (Crone, 1975) was conducted over the zone of greatest mineral potential as indicated by e) above, with stations at 25 m intervals along the pegged lines. Later the line spacing was reduced to 100 m.

g) Anomalies encountered from soil geochemistry, the PEM survey, prospecting, and geological mapping, were further investigated and the more promising were tested by air-flush and diamond-drilling.

2.2.3 Geological Interpretation

Rock exposure is limited to small scattered outcrops and occasional hills east of Rubbervale farm, and to the hills of the Carrolls Peak-Tshutshu range west of this. The sedimentary rocks, in the south of the study area have virtually no surface exposure until the more resistant quartzites and cherts of the Antimony Line are reached, representing a vertical thickness of approximately 1500 m. Similarly, to the north, the Rooiwater Igneous Complex is very poorly exposed within the study area. See plates 1 and 2.

Areas of very little or no exposure are generally flat lying and covered with up to 10 m of uniform brown loamy soil overlying a 20 cm quartz "pebble" layer. Scree and talus slopes have formed along the base and flanks of the larger hills.

However, geological continuity and interpretation along strike was aided by soil geochemistry, the geophysical surveys and a photogeological interpretation of the area. Extensive air-flush drilling along lines of inclined, overlapping holes across the geological strike, combined with limited diamond-drilling was used in areas of no exposure to trace and extend zones of mineralization.

From a compilation of this data, an accurate geological map was constructed.

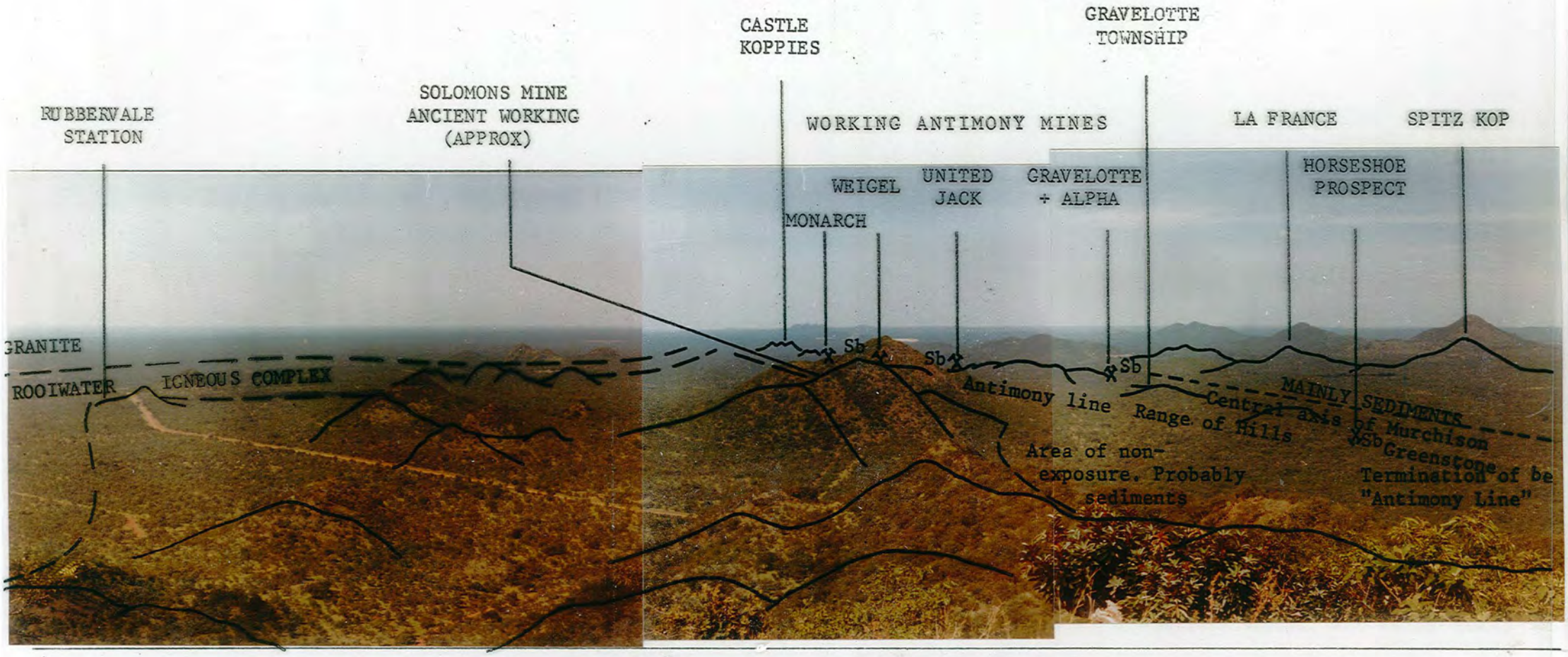

RUBBERVALE SUB-GROUP: TUFFS AND FLOWS

Plate 1. View from Carrolls Peak looking East along the Murchison Range.

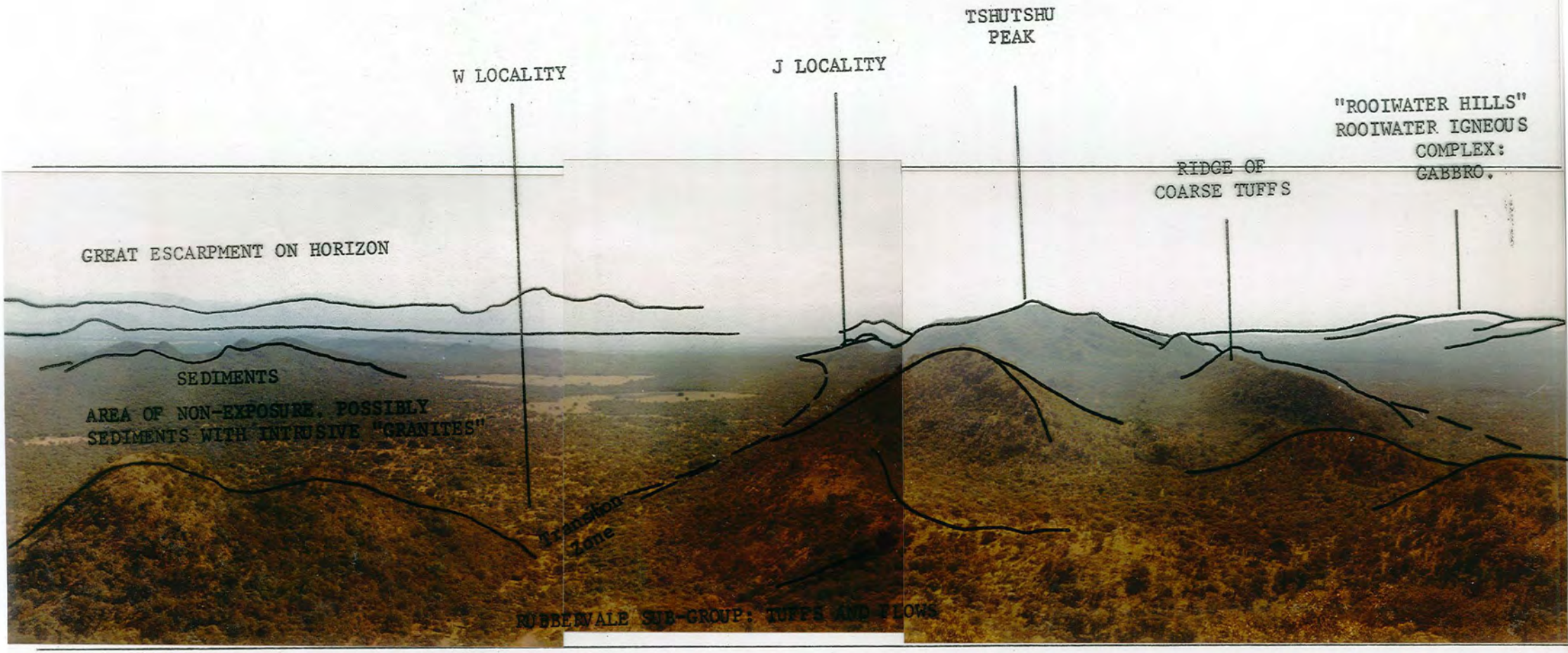

Plate 2. View from Carrolls Peak looking West along the Murchison Range.

CHAPTER III

VOLCANOGENIC MASSIVE SULPHIDE DEPOSITS - A REVIEW

3.1 Introduction

Over the past decade, numerous papers and articles have appeared, related to volcanogenic massive sulphide deposits. The more general papers include those by Sangster (1972), Hutchinson (1973), Constantinou and Govett (1973), Sillitoe (1973), Lambert and Sato (1974), Spence and de Rosen Spence (1975), and Solomon (1976). These deal with all aspects of ore formation and geological setting and attempt to classify the deposits.

Briefly, massive sulphide deposits within volcanic rock sequences occur as lenses and blanket-like bodies conformable with, and apparently formed at the same time as the enclosing rocks. Laterally and vertically the massive sulphide bodies grade into sulphide, oxide or manganese-bearing cherts. Commonly underlying the deposits is a pipe-shaped zone of altered rock locally carrying significant amounts of disseminated and stringer-type sulphides.

Textures within the sulphide lens, such as fine mineral banding, brecciation, slumping and graded bedding indicate a sedimentary-style of deposition.

3.2 Classification

Differences in tectonic and stratigraphic setting, host rock lithologies, and mineralogy can, and have been used to set up broad classification categories for these volcanogenic massive sulphide deposits (Hutchinson, 1973; Large, 1977).

The following five categories have been modified after Hutchison (1973), and are summarized in table 1.

3.2.1 Type I - "Archaean"

These deposits are almost exclusively confined to the Archaean era, and occur within greenstone belts of cratonic nucleii. Massive sulphide deposits are especially well developed in the Canadian Shield (Sangster, 1972; Spence and de Rosen Spence, 1975; Sangster and Scott, 1976), but lesser known examples occur in other Shield areas, e.g. Australia (Reynolds et al., 1975), South Africa (this thesis), India (Deb, 1979), and Saudi Arabia (Moore, 1975).

The greenstone belts comprise thick piles of deformed volcanic rocks and sediments, surrounded by granitic plutons. Within the volcanic pile, mafic and high-magnesia basalts and ultramafic lavas are overlain by a differentiated sequence of tholeiitic basalts and rhyolites, and a final capping of sediments (Viljoen and Viljoen, 1969a; Annhaeusser et al., 1969; Annhaeusser, 1972). Stratiform massive sulphide deposits are found within or at the top of the tholeiitic basalt-rhyolite sequence, commonly overlying felsic, often pyroclastic, volcanic rocks (Sangster, 1972; Spence and de Rosen Spence, 1975; Sangster and Scott, 1976).

The regional tectonic environment appears to be unique to the Archaean, dominated by vertical, gravity tectonics, with the volcanic piles accumulating in rift-like valleys or troughs of crustal downwarping (Annhaeusser, 1972, 1973; Baer et al., 1978). The high-magnesia basalts and ultramafic lavas are considered to represent primitive ocean crust (Viljoen and Viljoen, 1969b, Annhaeusser, 1972) and

similarities to modern-day island-arc complexes have been noted (Annhaeusser, 1972, 1973).

The most common, local host rocks to the sulphide deposits are rhyolites, often pyroclastic, which may be associated with, or intruded by "quartz porphyry" bodies (Evans, 1944; Pollock et al., 1972; Sangster, 1972; Hopwood, 1976). In any one mining district, deposits tend to occur along a particular horizon, often marked by a thin, base-metal bearing chert or tuff (Sangster, 1972; Roberts, 1975). The deposits are conformably overlain by further volcanic rocks or sediments.

The massive sulphide body takes the form of a lens or pod, stratiform and stratabound, commonly overlying a stockwork of anastomosing sulphide veinlets in a pipe of generally altered, commonly pyroclastic, footwall rock (Reynolds et al., 1975; Spence and de Rosen Spence, 1975; Sangster and Scott, 1976; Large, 1977).

Mineralogy is fairly simple; various proportions of pyrite, pyrrhotite, sphalerite, chalcopyrite and magnetite being present. Galena and sulphosalts are notably absent or present only in minor quantities. Zonation occurs within the massive lens, with chalcopyrite concentrated with pyrrhotite and magnetite at the base, grading upwards into a pyrite + sphalerite-rich assemblage. Mineral banding is common (Hutchinson, 1973; Large, 1977; Jambor, 1979). Overall, the deposits are zinc rich with respect to copper, and contain appreciable recoverable silver. Sulphates, especially bedded sulphates, are absent.

Alteration tends to be confined to the stratigraphic footwall, although a certain amount of bleaching can occur in the hangingwall sequence (H. Squair - personal communication, 1978). The zone of visible alteration tends to be pipe shaped and to occupy a larger area than the overlying massive sulphide lens. Chlorite, and locally sericite, are present within the zone which is enriched in MgO and FeO and depleted in Na_2O and K_2O with respect to the surrounding unaltered rocks (Spitz and Darling, 1978; Riverin and Hodgson, 1980). Sulphides are dominantly pyrrhotite-chalcopyrite with lesser pyrite and sphalerite (Large, 1977; Jambor, 1979).

In Fiji, several small Fe-Zn-Cu sulphide deposits are associated with acid pyroclastic rocks of Oligocene-Miocene age (Lawrence and Savage, 1976; Colley and Greenbaum, 1980). These occur towards the top of a tholeiitic sequence of basalts with minor rhyolites, which forms the base of the Fijian island-arc complex, i.e. the immature island-arc stage of Mitchell and Bell (1973). These deposits are in all respects similar to the Archaean, type I deposits but do not contain appreciable pyrrhotite. The tholeiitic volcanic sequence is covered by a calc-alkaline sequence containing "Kuroko" or type III massive sulphide deposits (Colley and Greenbaum, 1980).

3.2.2 Type II - "Besshi"

According to Mitchell and Bell (1973) Besshi-type massive sulphide deposits occur in thick sedimentary and volcanic accumulations in the arc-trench gap of island-arc complexes. A varied assemblage of thick marine, generally deep water sediments with volcanic and volcaniclastic rocks host the deposits; tholeiitic basalts are common. These assemblages develop during the growth of subaerial and submarine volcanic complexes of immature arc development, where topographic troughs occur around the volcanoes and in the arc-trench area. The result is deep burial and regional high temperature metamorphism (Mitchell and Bell, 1973), although high pressure "blueschist facies" metamorphic rocks develop in the arc-trench area (Myashiro, 1973). Sulphide deposits tend to occur at specific horizons within this pile, which often comprise volcaniclastic or pyroclastic rocks.

The massive sulphides form bedded pyritic deposits containing variable amounts of chalcopyrite and lesser sphalerite. Pyrrhotite is abundant towards the base of the deposits (Kanehira and Tatsumi, 1970; Mitchell and Bell, 1973). Galena and barite are also present in minor amounts. Stockwork mineralization is common beneath the massive ore, and comprises veinlets of pyrite and chalcopyrite (Strauss and Model, 1974). Deposits of the "Besshi" type are intimately associated with the processes of plate tectonics (Mitchell and Bell, 1973) and are confined to the Phanerozoic era (350 MY to Present). Due to the variable host-rock lithology and mineralogy, the deposits themselves show affinities to other "types" such as

"Archaean" and "Kuroko" (see for example Hutchinson, 1973).

3.2.3 Type III - "Kuroko"

This type is named after the polymetallic, massive sulphide ores of Japan (Lambert and Sato, 1974) where they are associated with a calc-alkaline volcanic sequence of basalt-andesite-rhyolite, and clastic sediments. These volcanic rocks formed during the late or mature stage of island-arc development (Mitchell and Bell, 1973; Lambert and Sato, 1974; Colley and Greenbaum, 1980).

The majority of deposits classified as "Kuroko" occur at or near the top of calc-alkaline derived dacitic sequences, although other host rocks may include tholeiitic volcanic rocks (Egin, 1978), and clastic sediments at the edges of the volcanic pile (Lambert and Sato, 1974). In the Japanese kuroko deposits, domes of "white rhyolite" commonly contain the stockwork part of the sulphide deposit (Tatsumi and Clark, 1971; Tatsumi and Wanatabe, 1971; Lambert and Sato, 1974).

The massive sulphide deposits characteristically show well developed mineral zoning from a pyrite + chalcopyrite + quartz stockwork to massive stratiform pyrite + chalcopyrite and an upper sequence of massive stratiform sphalerite + galena + barite. Sulphosalts and tellurides are concentrated in this upper portion. The sulphides are frequently capped by ferruginous cherts (Hutchinson, 1973; Lambert and Sato, 1974; Large, 1977). The relative abundance of these zones differs considerably between orebodies, and in many cases one or more are lacking(Lambert and Sato, 1974; Egin, 1978).

Associated with Kuroko deposits are lenses and beds of massive gypsum-anhydrite, and barite. Sulphates also form in the gangue to the massive ore.

Surrounding the Kuroko-type deposits are well developed zones of clay-rich alteration. Associated with the footwall stockwork ore, this alteration comprises quartz with a little sericite and Mg chlorite. Surrounding this and the stratiform ore is a zone of sericite, sericite-montmorillonite, Mg-chlorite and minor kaolinite. Enclosing these zones, and extending into the hangingwall sequence is an alteration characterised by Fe-chlorite and the development of albite, K-feldspar and quartz. In general, silica is enriched in the footwall stockwork zone, Na is leached, and Fe and Mg enriched in all alteration zones.

3.2.4 Type IV - "Cyprus"

This type of deposit is associated with basic volcanism, and is found within or at the top of pillow lava sequences of the upper part of ophiolite complexes (Hutchinson, 1973; Constantinou and Govett, 1973). These are now interpreted as slices of oceanic crust and the tectonic environment of formation was one of crustal rifting, either at mid-ocean ridge spreading systems or in back-arc basins (Hutchinson, 1973; Mitchell and Bell, 1973; Hollister, 1981).

The host rocks are pillowed, oceanic, tholeiitic lavas; felsic volcanic rocks are absent or rare, and sediments are insignificant but may include chemical cherts, banded iron-stones and manganstones. The deposits may be overlain by thin pelagic sediments, or further oceanic tholeiite or island-arc tholeiitic lavas (Hutchinson, 1973; Pearce, 1981; Alabaster and Pearce, 1981).

The sulphides form pods and lenses of massive, poorly-banded pyrite, with lesser chalcopyrite and minor, though variable, amounts of sphalerite, gypsum and barite. The galena, magnetite and pyrrhotite content is negligible. The massive ores are commonly capped by pyritic or ochrous mudstones (Constantinou and Govett, 1973). Underlying the massive ore is a zone of altered lava containing a core of stockwork pyrite + chalcopyrite + quartz veinlets. This footwall alteration zone is characterized by disseminated pyrite or chlorite, with silicification increasing in intensity upwards into the stockwork vein system.

3.2.5 Type V - "Proterozoic"

Although not often hosted by volcanic rocks, deposits of this type are included here because of their essentially similar mode of formation and mineralogy to the above mentioned deposits. The regional and tectonic setting is continental margin, with development of fault bounded marginal basins, intercratonic troughs, continental downwarps, and failed triple junctions (Lambert, 1976; Hodgson and Lydon, 1977; Raybould, 1978; Russell et al., 1981). These troughs develop over subsiding areas of basement consisting of earlier sediments, volcanic rocks or continental crust, and are generally continental on one side, open marine on the other (Lambert, 1976). Sulphide deposits in the basins tend to be best developed in areas where the underlying basement is thickest, and form at certain stratigraphic horizons near the base of the trough-filled sediment-volcanic rock pile, soon after a major period of subsidence (Hodgson and Lydon, 1977; Russell, 1981).

Host rocks to the massive sulphide deposits are varied, dominantly fine-grained, clastic, shallow to deep water sediments with occasional carbonates and thin, volcanic rock horizons. The enclosing trough is generally comprised of a thick sequence of varied, usually clastic, sedimentary and minor volcanic rocks (Walker et al., 1977; Lambert, 1976).

The deposits themselves are characteristically large, >100mt ore, isolated bodies spaced at roughly 18 km intervals along particular stratigraphic horizons (Russell et al., 1981). They are stratiform, well layered, with a blanket-like shape, grading laterally into pyritic, zinc-rich sediments. Sulphide banding is common, consisting of fine, <1 mm, monominerallic laminations. Mineralogy is dominantly pyrite, sphalerite and galena with lesser chalcopyrite which tends to be concentrated near, or at, the entry point of the mineralizing solutions (Lambert, 1976; Walker et al., 1977).

Alteration within the footwall sequence is generally restricted and weak. Associated faults may contain replacement copper deposits, and probably acted as feeder channels to the stratiform ore bodies (Lambert, 1976; Walker et al., 1977; Rye and Williams, 1981).

3.3 Ore Genesis

From present evidence, it appears that the solutions responsible for the formation of the various types of massive sulphide deposit originated as ocean water, percolating along fissures and micro-fractures in the pile of volcanic or sedimentary rocks, or oceanic crust (Kajiwara, 1973; Andrews and Fyfe, 1976; Solomon, 1976; Large, 1977;

Ohmoto and Rye, 1979; Taylor, 1979; Edmond, 1981). This water became heated, either by the local geothermal gradient (Russell et al., 1981), cooling of oceanic crust (Andrews and Fyfe, 1976), or by magmatic heat sources (Hodgson and Lydon, 1977; Alabaster and Pearce, 1981). The water circulated within the permeable rocks as geothermal convection cells of 10 km radius by 4-5 km depth (Solomon, 1976).

Re-equilibration between the heated ocean waters and the surrounding rocks leached elements such as Ca, Si, K, Ba from the rocks and added Mg and SO_4 (Bischoff and Dickson, 1975; Humphris and Thompson, 1978a,b; Mottl and Holland, 1978; Seyfried and Bischoff, 1981). The resulting acidic, chloride-rich brines are capable of leaching Fe, Mn, Cu, Pb, Zn, Ni, Au, and Ag from the rocks. Discharge from the system occurs along relatively small channels, usually fractures or fault zones, onto the sea-floor or land surface (Solomon, 1976; Hodgson and Lydon, 1977). At the discharge point, mixing with cold sea water precipitates the dissolved ions as stratiform sulphide deposits, or as subsurface replacement deposits if the hydrostatic pressure is insufficient to prevent boiling (Finlow-Bates and Large, 1978).

On entering the sea floor, the mineralizing solutions, if not boiling, were buoyant and hot, with densities in the order of 0.75 (Solomon and Walshe, 1979). They would rise as plumes, mixing almost instantaneously with the surrounding seawater and precipitating fine grained sulphides (Turner and Gustafson, 1978; Solomon and Walshe, 1979; RISE Project Group, 1980). From fluid inclusion data

and theoretical calculations the temperature of formation of the various types of massive sulphide deposit range from $< 150^{o}C$ for McArthur River, type V, (Solomon, 1976); 200-250^{o}C up to 320^{o}C for the Japanese kuroko deposits (Lambert and Sato, 1974; Large, 1977); 310^{o}C for the Cyprus deposits (Spooner and Bray, 1977); and $380 \pm 30^{o}C$ from direct observation of presently active discharge systems on the East Pacific Rise, type IV (RISE Project Group, 1980).

Quenching of the ascending solutions would precipitate first pyrite, chalcopyrite, and pyrrhotite at low sulphur fugacities, followed by sphalerite, pyrite and galena (Large, 1977). According to Solomon and Walshe (1979) pyrite and chalcopyrite are precipitated and fall out of the plume at or adjacent to the discharge point, whilst sphalerite, pyrite and galena precipitate within the plume and are carried up into the surrounding sea to fall out above, and laterally beyond, the chalcopyrite-rich precipitate. This could account for the metal zonation found in this type of deposit, and the lateral metal-rich cherts. Manganese tends to be carried further afield, leading to the extensive Mn-rich haloes around some massive sulphide bodies, e.g. Meggen (Gwosdz and Krebs, 1977), and Tynagh (Russell, 1975). Repeated zoning and repetitive mineral banding can be readily explained by variations in size and duration of the plume, repeated collapse, and "double-diffusion" effects; see Turner and Gustafson (1978).

Within the footwall sequence, the host rocks undergo progressive alteration from reactions between the ascending, hot, mineral-bearing fluids and the cold, water-saturated,

often porous or fractured rock. This is most notable in the immediate area of the discharge where the mineralizing fluids dominate the system. Alteration appears to occur as two co-existing phases, crosscutting veins filled with alteration minerals and sulphides representing former fluid channelways, and a more diffuse alteration between these (Riverin and Hodgson, 1980).

The different metal abundances in each of the five types of massive sulphide deposit outlined above, may be explained by the nature of the underlying prism of rock within which the geothermal convection cells are established, and from which they extract the various metals.

From table 2 it can be seen that copper is a common constituent where the rocks are dominated by basalts, with zinc becoming a major constituent in the differentiated basalt-rhyolite piles associated with Archaean type deposits. Experimental work by Bischoff and Dickson (1975) and Humphris and Thompson (1978b) shows that zinc should occur with copper in Cyprus-type deposits. The general paucity of zinc in these deposits (Constantinou and Govett, 1973) was suggested by Solomon and Walshe (1979) to be due to lateral dispersion of sphalerite from the plume of ascending mineralized fluids. However, such lateral zinc-rich sediments have not been recorded.

Lead is concentrated by reworking of volcanic and sedimentary material, being a fairly abundant element in continental crust (Laznicka, 1976). Lead thus becomes a major component only in those deposits underlain by such

rock sequences. Lead is virtually absent from Cyprus-type deposits, rare in the Archaean-type, and of minor importance in Besshi-type deposits. Only in Kuroko and Proterozoic-type massive sulphide deposits does lead occur in substantial quantities.

Thus there is an increase in variety, thickness and differentiation of the associated volcanic and sedimentary sequences from Cyprus to Archaean to Besshi to Kuroko to Proterozoic types of sulphide deposit, with a parallel sequence from simple to more complex metal associations.

3.4 Stratigraphic Controls

Massive sulphide deposits, of all five types, in any one mining district tend to occur along one particular stratigraphic horizon (Sangster, 1972; Constantinou and Govett, 1973; Lambert and Sato, 1974; Roberts, 1975; Spence and de Rosen Spence, 1975; Russell et al., 1981). Along these horizons, deposits, or clusters of deposits, tend to concentrate at specific intervals, e.g. Cyprus-type deposits at 9 km intervals in Oman (Pearce, 1981) and Proterozoic-type deposits at 18 km intervals (Russell et al., 1981). Major faults or fault zones may occur in proximity to these deposits and appear to have acted as ore-fluid conduits or discharge channels (Lambert, 1976; Walker et al., 1977).

With the exception of the Proterozoic-type, the particular "mineralized" stratigraphic horizon often marks the end of a volcanic cycle. This is commonly felsic and pyroclastic (Lambert and Sato, 1974; Spence and de Rosen Spence, 1975). For Cyprus-type deposits, the horizon

separates sequences of basaltic lavas (Constinantou and Govett, 1973; Alabaster and Pearce, 1981).

It has also been noted that many deposits form immediately following periods of subsidence in the volcanic or sedimentary basin (Hodgson and Lydon, 1977; Russell et al., 1981). Ohmoto (1978) proposed a mechanism of caldera collapse following effusive volcanism and growth of the volcanic-sedimentary pile, resulting in cracking and fracturing of the pile and allowing percolation of sea-water. The subsequent establishment of geothermal convection cells leads to the eventual formation of massive sulphide deposits.

In the case of Proterozoic-type deposits, where volcanism is absent or rare, subsidence occurs early in the history of basin sedimentation, with the result that sulphide deposits form near the base of the accumulating pile (Solomon, 1976; Hodgson and Lydon, 1977; Russell et al., 1981).

To account for Cyprus-type massive sulphide deposits in the Oman ophiolite sequence, Pearce (1981) and Alabaster and Pearce (1981) suggest that intrusion of magma set up geothermal convection cells producing the sulphide deposits. These were later covered by effusive, island-arc volcanics from this magma chamber.

Spacing of sulphide deposits along a particular horizon can be linked to the diameter of the underlying convection cell which fed the deposit (Solomon, 1976).

3.5. Massive Sulphide Deposits and Crustal Evolution

The Earth's crust has evolved in three stages, each characterized by its own, rather unique tectonic regime

(Sutton, 1967; Annhaeusser, 1973).

The Archaean Era, ending circa 2600MYBP, was dominated by vertical, gravity-induced tectonics (Eriksson, 1980), producing linear troughs or graben on a thin, unstable crust of oceanic (Viljoen and Viljoen, 1969b; Annhaeusser, 1972) or granitic composition (Sutton, 1967; Hunter, 1974a). These troughs formed locii for volcanic chains of basalt- to rhyolite volcanism and the widespread development of type I, Archaean, massive sulphide deposits. Subsequent deformation of these troughs and emplacement of tonalitic plutons gave rise to typical granite-greenstone terrain (Annhaeusser et al., 1969) and the stabilization of these cratonic nucleii.

In the following Proterozoic Era consolidation of these cratonic nucleii formed large stable areas containing intracratonic oceans and enabling extensive platform sedimentation to develop (Annhaeusser, 1973; Hunter, 1974b). Thick crustal sequences enabled lead to be concentrated and type V, Proterozoic, massive sulphide deposits in intercratonic troughs and basins began to form from about 1800MYBP onwards.

These large landmasses became progressively unstable and fragmented, marking the end of the Proterozoic Era at circa 250-350MYBP (Annhaeusser, 1973). This fragmentation was accompanied by processes of modern sea-floor spreading and "plate tectonics" (Vine and Matthews, 1963; Sawkins et al., 1974).

One consequence of continental fragmentation and development of crustal plates is the formation of arcuate

or linear, narrow, tectonically unstable zones associated with constructive and destructive plate boundaries, the so-called island-arcs and mid-ocean ridges. These provide ideal sites for volcanic activity and subsequent establishment of geothermal convection cells to produce massive sulphide deposits of types II, III and IV (Mitchell and Bell, 1973), and possibly type I (Colley and Greenbaum, 1980).

3.6 Applications In Mineral Exploration

In prospecting for massive sulphide deposits of the types outlined above, the regional tectonic setting and nature of the volcanic and/or sedimentary pile, and possibly its relationship to island-arc development, should determine the type of deposit most likely to be encountered.

In general massive sulphide deposits associated with vulcanism tend to be formed during the waning stages of volcanic activity, and where this is cyclic, occur towards the end of one particular cycle. In any one mining district there is one particular stratigraphic horizon along which most of the deposits are regularly spaced either as clusters of small deposits, or as isolated, larger deposits. Regional fault patterns may also influence the loci of sulphide deposits. Each type of deposit has a characteristic footwall alteration zone which usually covers a larger area than the massive sulphide body.

3.7 The Murchison Range

Within the volcanic and sedimentary rocks of the Murchison Range, volcanogenic, massive, sulphide deposits

are located along the southern contact between felsic flows and tuffs, and clastic sediments. The four known deposits occur at between 14 and 19 km intervals along this horizon in two cases more than one sulphide lens is present. The lateral equivalent to the massive deposits is a pyritic, zinc-rich chert.

The sulphide deposits comprise varying amounts of pyrite, pyrrhotite, sphalerite and chalcopyrite and contain recoverable silver but no gold. Galena is virtually absent, and bedded sulphates have not been observed. The mode of occurrence is a bedded, syn-volcanic, conformable lens of massive sulphide, underlain by a zone of stockwork pyrite + pyrrhotite + chalcopyrite within highly altered volcanic rocks.

From the classification scheme outlined above, these massive sulphide deposits are characteristic of the type I, or Archaean group.

TABLE 1. CLASSIFICATION OF MASSIVE SULPHIDE DEPOSITS

TYPE	METALS	TECTONIC SETTING	HOST ROCK
I ARCHAEAN	Fe,Zn,Cu, minor Ag, Sn.	Archaean greenstone belts. Crustal downwarping, development of linear troughs filled with extensive volcanics.	Tholeiitic basalt-rhyolite or andesite. Minor chemical and volcanic sediments. Deposits commonly hosted by felsic pyroclastics, rarely flows. Local cherts. Sequence overlain by clastic sediments or further volcanic rocks.
II BESSHI	Fe,Cu, Lesser Zn, Pb, Ba.	Crustal downwarping, accumulation of thick volcanic-sedimentary sequences in inter-island arc gaps, arc-trench gap, back-arc areas. Immature to mature stage of island arc development.	Varied sedimentary-volcanic pile. Deep water sediments. Tholeiitic basalts common. Sequence often highly deformed and metamorphosed.
III KUROKO	Fe,Pb,Zn, Cu,Ag,Ba, minor Au, Te.	Crustal downwarping, subduction zone. "Second differentiation" of oceanic and continental crust. Calc-alkaline volcanic suite. Mature stage of island arc development. Deposits occur in waning stages.	Calc-alkaline basalt-andesite-dacite. May be tholeiitic. Basement of older rocks, island arc tholeiites, continental crust. Extensive pyroclastics often host to deposits. May be covered by or grade laterally into thick clastic sediments.
IV CYPRUS	Fe,Cu, minor Zn.	Crustal accretion. Tensional regime at sites of oceanic ridge centres. Back-arc basin or oceanic crust prior to arc development.	Ophiolite sequences. Oceanic basalts and pillow lavas.
V PROTER-OZOIC	Fe,Pb,Zn, Cu,Ag.	Continental margin basins, intercratonic troughs, continental downwarps, fault-bounded troughs. Deposits formed soon after basin subsidence. Basement of varied, older, rocks.	Dominantly fine, clastic, shallow to deep water sediments. Minor volcanic rocks. Overlain by thick sedimentary and/or volcanic succession. Deposits commonly in lower part of basinal accumulation.

FORM OF DEPOSIT	FOOTWALL ALTERATION	EXAMPLES	REFERENCE
Stratiform and stratabound pods and lenses of massive sulphide generally overlying pipe-shaped stockwork of sulphide veins within a larger zone of altered rock. Massive sulphides are commonly banded and layered. Zoned from Cu-rich base to Zn-rich top. Absence of sulphates. Pb absent or very minor.	Sericite with chlorite core. Fe and Mg enrichment. Pyrite, pyrrhotite and chalcopyrite.	Noranda district. Murchison Range. Fiji (Miocene age).	Sangster (1972).
Conformable, fairly extensive Cu-rich deposits. Stratiform. Pyrite dominant. May have stockwork sulphides.	Stockwork of quartz + pyrite + chalcopyrite veins.	Japan, Besshi. Iberian pyrite belt.	Kanehira and Tatsumi (1970).
As type I. Pb major component. Zoned from Cu-rich base to Pb+Zn-rich top. Stratiform and cross-cutting gypsum-anhydrite. Bedded barite. Sulphosalts common towards top of deposit. Overlain by Fe-Mn bearing cherts.	Clay alteration zone with silicified core. Stockwork of pyrite + chalcopyrite + quartz veins.	Japan, Kuroko; Fiji; Roseberry; Woodlawn; Pontid Belt, Turkey.	Lambert and Sato (1974).
Stratiform and stratabound pods and lenses of massive cupreous pyrite. Minor sphalerite, usually towards top of deposit. Bedded sulphates absent. Covered by ochrous sediments.	Chloritization of lavas. Pyrite development. Stockwork of pyrite + chalcopyrite + quartz veins.	Cyprus, Oman, Nova Scotia.	Constantinou and Govett (1973).
Stratiform, well layered, blanket-like form. Commonly found in topographical lows, bounded by prominent faults. Normally large, isolated deposits.	Weak to absent. Replacement Cu deposits in nearby fault zones.	Mt. Isa, McArthur River, Sullivan, Tynagh, Navan, Rammelsberg, Meggen.	Lambert (1976).

Table 2. Comparison of Metal Content with Underlying Rock Sequence, Massive Sulphide Deposits

TYPE	UNDERLYING ROCK SEQUENCE	(1)	METAL CONTENT	(1)
IV CYPRUS	Oceanic basalts, pillowed tholeiites ophiolite sequences.	↓ Increasing variation/differentiation of volcanic rocks. Thicker crust.	Fe, Cu, (Zn, Ba)	Increase in number of major metal components. Pb content increases. ↓
I ARCHAEAN	Tholeiitic basalt-rhyolite sequences. High-magnesia basalts.		Fe, Cu, Zn, (Ag)	
II BESSHI	Clastic and volcanic sediments, tholeiitic basalts, minor felsic volcanic rocks		Fe, Cu, (Zn, Pb, Ba)	
III KUROKO	Calc-alkaline volcanic rocks, island-arc tholeiites, older rocks, continental crust, varied sediments.		Fe, Zn, Pb, Cu, Ag, Au, Ba	
V PROTER-OZOIC	Varied volcano-sedimentary sequence. Older basement, continental crust.		Fe, Pb, Zn, Cu, Ag, Au	

(1) NOT time dependent trends.

CHAPTER IV

REGIONAL GEOLOGY OF THE MURCHISON RANGE

4.1 Regional Setting

4.1.1 Introduction

The Murchison Range of northeastern Transvaal is one of several greenstone belts surrounded by intrusive "granites." This granite-greenstone terrain, of Archaean age, is known as the Kaapvaal Craton, and is surrounded by linear belts of highly deformed volcanic and sedimentary rocks, the so-called "mobile belts", fig.1. Proterozoic and younger, sedimentary basins overlie parts of the Craton, which today is exposed over a width of circa 150 km, as a strip of low-lying, rather monotonous land known as the Transvaal Lowveld. This tract extends southwards from the Soutpansberg Mountains into Natal, where it is terminated by the Namaqua-Natal Mobile Belt. It is covered in the East by the Karroo cover sequence and in the west by the Transvaal sedimentary basin.

The greenstone belts form linear, e.g. Murchison Range, or cuspate, e.g. Barberton Mountain Land, tracts of meta-volcanic and metasedimentary rocks, distinctly different from the more complex suite of intrusive granitic, gneissic and migmatitic rocks forming the bulk of the Craton.

4.1.2 Nature of the Greenstone Belts of the Kaapvaal Craton.

Over the past decade, numerous investigations have been conducted into the nature of the granite-greenstone terrain. Much of this was done on the Barberton Mountain

Land and surrounding area, which thus serves as a model for greenstone belt development. See for example Annhaeusser et al. (1969), Viljoen and Viljoen (1969a,b,c), Annhaeusser (1972), Hunter (1974a), Robb (1978) and Erikisson (1980). From these studies, the greenstone belts are seen to comprise a wide variety of igneous, volcanic and sedimentary rocks, collectively grouped into the Swaziland Supergroup (Annhaeusser et al., 1969). This Supergroup can be divided into a predominantly volcanic group, the Onverwacht Group, overlain by argillaceous and arenaceous sedimentary assemblages, the Fig Tree and Moodies Groups respectively (Viljoen and Viljoen, 1969a; Annhausser, 1972).

The Onverwacht Group is subdivided into a lower assemblage, the Lower Ultramafic Unit, and an overlying Mafic to Felsic Unit. The two are separated by a persistent and distinctive chert and carbonate sediment, the Middle Marker.

The Lower Ultramafic Unit is largely composed of mafic and ultramafic extrusive volcanic rocks characterized by a high magnesia content, a high Ca/Al ratio, and low alkali content. These distinctive ultramafic metalavas have been assigned to a new class of igneous rock, the "komatiites" (Viljoen and Viljoen, 1969b). Other rocks present include felsic tuffs, intrusive bodies of feldspar and quartz porphyry, and layered, differentiated ultramafic bodies.

The Mafic to Felsic Unit consists of cyclic alternations of tholeiitic basalts, "andesites", dacites and rhyodacites, with tholeiitic basalts dominating. The amount of felsic material increases towards the top of the Unit becoming

increasingly tuffaceous, with intercalated cherts and volcanic sediments (Viljoen and Viljoen, 1969a,c). Layers of carbonate, volcanoclastic debris, chert, local turbidites and, possibly, evaporitic sequences occur at the top of the Unit (Lowe and Knauth, 1977).

Conformably overlying the Onverwacht Group is an assemblage of largely deep water pelitic sediments, the Fig Tree Group, overlain in turn by cyclic successions of conglomerate, quartzite and shales, collectively termed the Moodies Group (Viljoen and Viljoen, 1969a; Condie et al., 1970; Annhaeusser, 1972; Eriksson, 1980).

4.1.3 The Granite-Greenstone Model

Some early models of Archaean crustal development in Southern Africa compare the greenstone belts to modern-day island-arc complexes, invoking processes of subduction or "crustal downwarping" (Annhaeusser, 1972). Later models emphasize the important role of gravity, with the volcanic greenstone pile being deposited in rift-bounded basins or troughs (Hunter, 1974a; Eriksson, 1980). Sediments were derived from the shoulders of the rift, concomitant with rift spreading. Emplacement of granitic plutons was controlled by vertical tectonics, with localized lateral compression.

The granitic terrain surrounding these greenstone belts appears to have formed in three distinct episodes (Hunter, 1974a; Robb, 1978). Early tonalitic gneisses and migmatites were derived from partial melting of basaltic rocks at mantle depths, a possible source being basal greenstone volcanic rocks depressed into the regime of anatexis (Annhaeusser, 1973).

These plutons were generally emplaced as diapirs around, and along, the margins of the greenstone belts. The formation of tonalitic plutons and their emplacement coincided with, and was probably a result of, the sagging and first deformation of the volcanic pile. Sedimentation of the Fig Tree Group was initiated, followed by sediments of Moodies type as the basin became shallower with the upwelling and subsequent erosion of the plutons. In the Kaapvaal Craton, north of the Barberton Mountain Land, this event took place between 3400 MYBP, or earlier, and 3200 MYBP (Robb, 1978). The next stage, at circa 3200 MYBP in the Barberton area, involved the widespread introduction of potassic magma. This appears to have followed the main period of downwarping and sagging of the volcano-sedimentary pile, with cessation of sedimentation, and may have given rise to the low-grade greenschist-amphibolite facies metamorphism characteristic of the greenstone belts (Annhaeusser et al., 1969).

A final event concerned the intrusion of discrete granitic bodies whose Sr-isotope values suggest a crustal pre-history. This took place between 3200 MYBP and 2600 MYBP (Robb, 1978).

4.1.4 Nature of the Early Crust

The nature of the early Archaean crust, especially that on which the greenstone belts were deposited, has been the subject of much controversy.

Hunter (1974a), working on the Barberton Mountain Land and surrounding granitic terrain, proposed an early crust comprising a bimodal dacite-tholeiitic association developed from melts formed by a sinking hydrous lithosphere.

Deformation of this resulted in the formation of banding. Localized sedimentation and volcanism were followed by metamorphism producing the Ancient Gneiss Complex. This formed the early crust in which graben-like rifts were produced and infilled by the volcanic and sedimentary sequences of the greenstone belts.

On the other hand, Annhaeusser (1972) and Viljoen and Viljoen (1969b,c) considered the early crust in Southern Africa to be relatively thin, 5 to 7 km, and of oceanic-type. This primeval crust was predominantly ultramafic in composition and portions of it are considered to be represented by the Lower Ultramafic Unit. Similar rocks are preserved at the base of many greenstone belts. The abrupt change in chemistry to the overlying Mafic to Felsic Unit, and the separation of the two units by the chemical and volcanic sediments of the Middle Marker, would suggest that greenstone belts represent chains of differentiated, tholeiite-dominated, volcanic rocks erupted onto pre-existing oceanic crust.

Viljoen and Viljoen (1969b) point to the abundant rafts and xenoliths of the Lower Ultramafic Unit within the granitic terrain of the Kaapvaal Craton, in areas between discrete greenstone depositories. They suggest that, prior to invasion by early tonalitic magma, the Lower Ultramafic Unit covered much of the Kaapvaal Craton, probably as a succession of reduced thickness in areas between the large accumulations in the greenstone troughs.

A granitic component to the crust was certainly present by the end of the Middle Felsic Unit, and supplied detritus to the overlying Fig. Tree and Moodies Groups

(Condie et al., 1970; Lowe and Knauth, 1977; Eriksson, 1980).

4.2 General Geology

4.2.1 Introduction

In the present study,the volcanic and sedimentary rocks comprising the Murchison greenstone belt have been divided into four Subgroups, and were intruded by the Rooiwater Igneous Complex prior to collapse of the pile and emplacement of granitic plutons. At the base of the sequence is the Malati Subgroup, overlain by the Leydsdorp and Rubbervale Subgroups, and finally the Gravelotte Subgroup, fig.5.

4.2.2 Malati Subgroup

Rocks belonging to this subgroup occupy most of the southern flank of the Murchison greenstone belt, and constitute the xenoliths of greenstone material within the granitic terrain to the south. The main rock types are actinolite+tremolite+chlorite schists, considered to represent original basaltic komatiites similar to the Geluk-type of the Barberton Mountain Land (Viljoen and Viljoen, 1969b; Minnitt, 1975; Viljoen et al., 1979). Other rocks include talcose schists, felsic tuffs and tholeiitic metalavas. These rocks are equated to the Lower Ultramafic Unit of the Barberton greenstone model (Minnitt, 1975), fig.4.

4.2.3 Leydsdorp Subgroup

In the east of the Murchison Belt, on the farm Wildebees, Minnitt (1975), described a sequence of carbonated tholeiitic lavas, magnesium-rich tholeiitic lavas and minor komatiites, stratigraphically overlying the Malati subgroup.

Towards the top of the sequence, chlorite schists, banded ironstones and porphyry bodies are present. Similar rock types crop out near the town of Leydsorp where they are conformably overlain by quartzitic sediments. In both areas, these rock sequences form wedge shaped outcrops occupying the cores of anticlinal structures (Viljoen et al., 1979). This subgroup is equated to part of the Mafic to Felsic Unit of the Barberton greenstone model (Minnitt, 1975; Viljoen et al., 1979).

4.2.4 Rubbervale Subgroup

Representatives of this Subgroup occur as elongate, wedge-shaped outcrops of felsic tuff and lava lying south of, and intruded by, the Rooiwater Igneous Complex, and conformably overlain to the south by clastic sediments of the Gravelotte Subgroup. The maximum thickness of the subgroup, 3700 m, is on the farm Rubbervale, and thins eastwards to disappear on the farm Hartebees. Minnitt (1975) described a thin sequence of quartz porphyries and cherts in the far north-east of the Belt as being the lateral equivalents to these tuffs and lavas. Rocks of the Rubbervale Subgroup only occur along the northern flank of the Murchison greenstone belt.

Quartz+sericite+chlorite schists, after felsic tuffs, are the dominant rock type, with lesser, massive and schistose quartz+sericite+albite rocks representing altered lava flows and high-level intrusives. The felsic tuffs are characterized by the presence of numerous blue quartz phenocrysts, giving rise to the term "Quartz Porphyry Group" by Van Eeden et al. (1939).

The present writer considers the volcanic rocks to have originally formed a thick pile of tuffs and lavas, whose centre now lies immediately to the west of the farm Maranda, thinning laterally east and west.

Minnitt (1975) describes an extensively developed zone of chloritic schists stratigraphically overlying and grading upwards from basalts of the Leydsdorp Subgroup, on the farm Wildebees. Jantski (1978) suggests that these are volcaniclastic sediments, laterally equivalent to the volcanic pile of the Rubbervale Subgroup. Unfortunately contacts between type members of each group have not been located.

It is suggested that this Subgroup, together with the Leydsdorp Subgroup, be equated to the Mafic to Felsic Unit of the Barberton greenstone model (Viljoen and Viljoen, 1969a).

4.2.5 Gravelotte Subgroup

Conformably overlying volcanic rocks of the Rubbervale and Leydsdorp Subgroups is a thick sequence of dominantly clastic sediments. These sediments have been termed the Gravelotte Subgroup (Viljoen et al., 1979) and essentially comprise the No.2 Division of Van Eeden et al. (1939).

These sediments occupy the core of the greenstone belt throughout its entire length where they form a low valley, due to their comparative ease of weathering. Within the sequence several resistant horizons of quartzite, grit and chert give rise to prominent topographical ridges or "bars". The more important of these are the parallel Chloritoid and Antimony "Bars" which are traceable from Crown Land south of the Rubbervale-Gravelotte farm boundary, eastwards to

Castle Koppies (Van Eeden et al., 1939). Several quartzite horizons also extend through the south of the Belt between Leydsdorp and Gravelotte townships, forming part of the Spitz Kop - La France range of hills. A further quartzite horizon, the Louws Kop Bar, occurs in the east of the area (Viljoen et al., 1979).

Rock types comprise quartz+chlorite schists representing original greywacke-turbidite sediments, quartz+muscovite schists, quartzite, grit and chert horizons, a variety of carbonate-rich rocks, talc and talc+carbonate rocks, minor lavas and banded iron formations. Although the sequence is dominantly arenaceous in the central and eastern sectors of the Murchison greenstone belt, argillaceous sediments are prominent in the west.

Apart from the quartzite horizons exposure is virtually nil and obscures the relationship between the Antimony and Chloritoid Bars, in the north, and those of the Spitz Kop - La France range in the south of the Belt. Both sets of "Bars" overlie volcanic sequences, and both young towards the central valley of the Murchison greenstone belt. It is concluded that they are probably lateral equivalents and help to define a synclinal structure along the central valley of the belt (see section 4.3).

4.2.6 Rooiwater Igneous Complex

This term was proposed by Van Eeden et al. (1939) for the largely gabbroic sequence of rocks forming the rugged, rather irregularly rounded, and fairly continuous ENE trending range on the extreme northern edge of the Murchison greenstone belt. This range becomes less pronounced east of

the farm Gravelotte. A quartz-diorite phase forms a narrow, featureless, easterly-tapering belt south of the gabbros.

Between the gabbro hills and the felsic volcanic ridge to the south is a long, low-lying valley, where exposure is scanty, being obscured by a mantle of deep red soil (Van Eeden et al., 1939). Sufficient exposure is available, however, on the farm Solomons Mine, to show the Rooiwater Igneous Complex to be intrusive into the Rubbervale Subgroup.

East of the farm Mashawa, the Complex continues as a thin strip of gabbro sills or sill-like intrusives.

4.2.7 Basic Sills

Volcanic and sedimentary rocks belonging to the Rubbervale and Gravelotte Subgroups have been intruded by numerous, large sills of tholeiitic composition. Thicknesses of up to 200 m, and strikes of 7 km, have been recorded. Many are multiphase or polyphase intrusives, and nearly all run parallel to the local bedding. In the study area they comprise up to 20% of the total stratigraphic thickness. The sills weather easily and are rarely exposed at the surface. However, due to their water retaining properties they support a denser-than-normal tree and vegetation growth and show up well as lineaments on aerial photographs.

These basic sills are considered by the writer to be associated with the Rooiwater Igneous Complex, as a precursor to the main intrusive phase. Previous writers however have variously described them as interbedded lava flows (Viljoen et al., 1979), mafic tholeiitic lavas (Viljoen et al., 1978), and hornfelsic tuffs (Minnitt, 1975).

4.2.8 Later Intrusives

Van Eeden et al. (1939) recognized three varieties of

post-greenstone intrusive.

4.2.8a Serpentinites

Serpentine bodies occur at various localities along the Murchison Range, commonly within the sedimentary assemblage. According to Van Eeden et al. (1939) they appear to be younger than the lavas and sediments and probably belong to the Rooiwater Igneous Complex.

4.2.8b Dykes

a) Dykes of syenite lamprophyre occur in the south of the Range and are related to the intrusion of the Palabora Carbonatite complex, dated at 2060MYBP (Palabora Mining Company Geological Staff, 1976).

b) Karroo dolerites which follow the regional fracture pattern along 040° and 140° trends.

4.2.8c Younger Granites

A series of acid plutons surround and intrude the Murchison greenstone belt. A suite of trondjhemitic gneisses has been mapped by Minnitt (1975) in the east of the Belt. Their diapiric mode of intrusion has caused the bifurcation and arcuate nature of the schist belt there. South of the Murchison belt, an early granite, the Willi granite, was intruded along the 125° magnetic trend (Jantski - personal communication, 1978). Much of the southern contact of the Murchison greenstone belt is intruded by a belt of leucocratic, potash-rich pegmatites, seldom exceeding 1 km in width (Viljoen et al., 1979).

4.3 Structural History

During the final stages of, or following sedimentation of, the Gravelotte subgroup, the Rooiwater Igneous Complex was

emplaced as an essentially horizontal body, into the base of the pile of felsic volcanic rocks which constitute the Rubbervale Subgroup (see chapter 5).

Following this, the trough of volcanic and sedimentary rocks collapsed under the action of gravity on an unstable crust (Annhaeusser, 1973). This developed a tight, steep syncline, with F_1 along a subhorizontal fold axis, and gave the Belt its characteristic linear ENE trend. Due to the initial asymmetric distribution of the various lithologies, only the sedimentary unit is repeated either side of the major fold structure.

Axial plane cleavage to the F_1 fold produced a penetrative schistosity S_1, trending 080-100° magnetic, along which the metamorphic mineral fabric developed. Continued vertical stretching rotated the original bedding parallel to S_1 and produced mineral lineations, L_1, along the axis of maximum strain, i.e. vertical (Hopwood, 1978), fig. 11. Further flattening of the strain ellipsoid along the S_1 plane produced localized buckle or intrafolial folds about vertical fold axes parallel to L_1 lineations (Hopwood, 1978). The axial plane surface of these F_2 folds is not parallel to S_1, but varies from 125-135° magnetic and is parallel to a non-penetrative axial plane cleavage S_2, along which micro-slip and shear relieve the extension in the S_1 plane (Hopwood, 1978; Ramsay, 1967).

This S_2 direction was important in influencing the emplacement of early granite plutons, e.g. the Willi granite in the south of the Belt (Jantski - personal communication) 1978, 1979), the alignment of greenstone xenoliths and

wedges, and the direction of protruberances between adjacent plutons (Viljoen et al., 1978).

Depression of the root zones of the greenstone sequence into the zone of anatexis led to the production of ton alitic melts which were emplaced along or into the margins of the greenstone belt (Annhaeusser, 1973). Plutons intruding the core of the syncline produced local antiform structures or doming effects, for example the area between the towns of Leydsdorp and Gravelotte where the Spitz Kop "Bar" defines a north east plunging anticlinal structure (Viljoen et al., 1979; J. de Waal - personal communication, 1979).

Minor vertical adjustments created localized, small-scale kink bands and chevron folds.

Cooling of the granite-greenstone "block",and possibly even later unroofing, caused brittle fracture along 040°, 140° and 000° magnetic trends. These directions were utilized by later Karroo dolerites (Van Eeden et al., 1939; see also chapter 5).

4.4 Metamorphism

The Murchison greenstone sequence has been subjected to metamorphism of the greenschist facies grade with narrow zones of amphibolite facies along the margins of the belt (Minnitt, 1975). This style of metamorphism is characteristic of greenstone belt development (Annhaeusser, 1972).

Collapse of the volcano-sedimentary assemblage, isoclinal folding and early intrusion of granitic plutons produced the planar and linear metamorphic fabric of the greenschist facies assemblage. Subsequent pluton emplacement and cooling superimposed a thermal, low pressure metamorphism of upper

greenschist to amphibolite facies grade.

In the south of the Murchison greenstone belt, potash rich pegmatites, granite intrusions, and fragmenting of the greenstones produced a high temperature, low pressure assembly of kyanite, andalusite, garnet and biotite within metasedimentary rocks (Van Eeden et al., 1939).

4.5 Mineralization

4.5.1 General

Numerous mineral showings and abandoned mines and several presently active mines attest to the variety of mineralization within the Murchison greenstone belt. This is fairly typical of greenstone belts throughout the world.

Six main types of mineralization are known to occur, two of which, antimony and emeralds, support active mines. Gold deposits have been worked in the past, and today gold is an important byproduct of the antimony production.

The six types are briefly described in order of probable decreasing age of formation.

1. Volcanogenic Fe-Zn-Cu massive sulphide deposits occur within the Rubbervale Subgroup, at the top of the pile of felsic volcanic rocks. Associated with these are zones of disseminated and vein-type sulphides.

2. Massive and disseminated antimony sulphides occur within calcareous and siliceous horizons at the top of the Gravelotte Subgroup sedimentary sequence. The mineralization, along a stratigraphic horizon termed the "Antimony Line" by Van Eeden et al. (1939), consists of stibnite with lesser berthierite, pyrite, arsenopyrite, gersdorfite and ullmanite (Muff, 1978). Later mobilization has concentrated the

sulphides into gash veins, and along fracture systems associated with second order splay faulting (Winter, 1975).

There are at present four working mines along the "Antimony Line". The orebodies occur at intervals of approximately 4 km in the central portion of the belt, with several prospects and showings at similar intervals east and west of these. The evidence for and against a syngenetic or epigenetic origin to the mineralization has been summarized by Viljoen et al. (1978), although Minnitt (1975) and the present writer prefer a syngenetic origin.

It is noteworthy that the vast majority of the antimony mineralization is found within carbonate and chert horizons in that part of the sedimentary sequence overlying the felsic volcanic rocks of the Rubbervale Subgroup.

3. Mercury is known from one locality in the Murchison Range, where it was mined during the second world war (Hammerbeck, 1976). Cinnabar-bearing cherty carbonate forms a stratigraphic horizon north of the "Antimony Line" at Monarch Kop. This horizon is similar to, but stratigraphically beneath, that hosting the antimony deposits (Hausman, 1959; Viljoen et al., 1978).

4. Copper-nickel sulphides occur within amphibolitic segregations and hornblende+magnetite horizons in the lower parts of the Rooiwater gabbro. The mineralization consists of disseminated chalcopyrite and nickeliferous pyrrhotite and is considered to have originated by magmatic segregation, possibly due to liquid immiscibility between oxide and sulphide phases. No economic deposits have been located.

5. Gold occurs, and has been exploited throughout the entire sequence of Murchison rocks. Indeed it was this that first attracted prospectors to the area (see chapter 1). The gold is mainly found within hydrothermal quartz veins containing chalcopyrite, pyrite, arsenopyrite and tetrahedrite, and as impregnations along shear zones with pyrite and pyrrhotite. These veins and shear zones generally follow the S_2 cleavage. The main concentration of auriferous vein deposits is in the sedimentary rocks around the town of Leysdorp.

Several gold deposits occur along the "Antimony Line" where they are associated with local banded iron formations and black shales (Merensky, 1905; Mellor, 1906; Mendelsohn, 1938). They are regarded as syngenetic, probably volcanic-exhalative in origin (Minnitt, 1975; Viljoen et al., 1978).

6. Emeralds and beryl are mined in the south of the Murchison greenstone belt where late-stage pegmatites intruded the granitic terrain which contains many ultramafic greenstone xenoliths. The emeralds are concentrated within the biotite-rich selvage to these xenoliths.

7. In addition to the above, showings of barite, asbestos, scheelite, and iron ore, have been reported (Van Eeden et al., 1939).

4.5.2 Fe-Zn-Cu Sulphide Deposits

Within the Murchison greenstone belt, four massive Fe-Zn-Cu sulphide deposits are known. These occur at the top of the felsic volcanic rocks belonging to the Rubbervale Subgroup where they form a horizon known as the "copper-zinc line" (Van Eeden et al., 1939). The deposits are, from east

to west, Mashawa coppers, Letaba coppers, Solomons Mine and J locality, and are spaced at intervals of 14 to 19 km along this line. The Solomons Mine and J deposits are described in detail in chapter 7.

Although not identical, the deposits have several similarities:

1. All occur at or near the major contact between volcanic and sedimentary rocks and appear to have formed during or immediately after the final volcanic episode prior to, or at the onset of, sedimentation.
2. The local volcanic environment varies from one of active volcanism with flows overlain by pyroclastic rocks near the centre of the volcanic pile, as at the J locality, to a quieter environment with lesser flows and thinner, bedded tuffs in the east of the Belt.
3. Underlying the lens of massive sulphides is a zone of altered volcanic rock containing varying amounts of disseminated and crosscutting veinlet sulphide. Siliceous tuffs and cherts in the hanging wall to the massive lens appear to be unaltered.
4. The massive sulphides exhibit compositional banding of pyrite and sphalerite, and chalcopyrite, and have a general zonation from a copper-rich base to a zinc-rich top. Laterally they grade into zinc-rich cherts.
5. The massive sulphide lenses tend to be zinc rich with respect to copper.

In most respects these deposits are similar to and can be classified with the "Archaean" or type I massive sulphide deposits of chapter 3.

4.6 Interpretation of Stratigraphy *

Hall, in 1912, was the first to group the schists of the Murchison Range into the Swaziland System, and correlate the prominent quartzite horizons with Moodies Group sediments of the Barberton Mountain Land.

On the basis of detailed field mapping, Van Eeden et al. (1939) divided the schistose rocks of the Murchison greenstone belt into three major divisions, those lying above, and those below a sequence of prominent quartzites, grits and rocks of sedimentary affiliation. These were all grouped within the Swaziland System, see fig. 3.

From the outcrops of the various quartzite horizons in the No.2 Division, Van Eeden et al. (1939) proposed that a tight syncline constituted the major structure running along the centre of the Belt, with a near horizontal fold axis. Quartzites of the Chloritoid Bar were repeated as the parallel Antimony Bar. However, rocks corresponding to the Quartz Porphyry Group of the No.3 Division were not repeated in the southern fold limb. Other quartzite horizons in the area around Leydsdorp, and in the east of the Belt, were interpreted as synclines plunging to the west and east respectively, with rocks of the No. 1 Division occupying their cores.

The Rooiwater Igneous Complex was found to be intrusive into the Quartz Porphyry Group along the northern flank of the Murchison greenstone belt. "Old Granite" is intrusive into all Divisions, and the Rooiwater Igneous Complex.

This stratigraphic and structural interpretation remained in use until the present, when Minnitt (1975) mapped in

*See section 4.6.1., Special note.

detail the eastern portion of the Murchison greenstone belt, where the sequence bifurcates around a tonalitic pluton.

The greenstone stratigraphy to the north and south of this pluton is similar and represented by a basal sequence of ultramafic meta-basalts containing interlayered aluminous schists. These are overlain by mafic basaltic lava with a variety of intercalated mafic tuffs, acid to intermediate tuffs, and chemical sediments. In the southern area the ultramafic and mafic basalts are overlain by an arenaceous sedimentary assemblage. Minnitt (1975) equated this stratigraphic sequence with that proposed by Viljoen and Viljoen (1969a) and An haeusser (1972) for the Barberton Mountain Land, see fig. 4.

In a report to the South African Committee for Stratigraphy, Jant ski (1978) proposed a new stratigraphic column and nomenclature to cover the Murchison greenstone belt. A similar report was later submitted by Viljoen et al. (1979). Although essentially the same, these two reports differ in their interpretation of the sequence of felsic tuffs and volcanics lying between the Rooiwater Igneous Complex to the north and the Chloritoid Bar to the south, i.e. the Quartz Porphyry Group of Van Eeden et al. (1939).

The present writer is in agreement with Jantski and has been able to observe the relationships between rocks of the proposed various sub-divisions with him in the field. Fig. 5 compares these two proposals with that of Van Eeden et al. (1939) and presents the stratigraphy adopted in this thesis.

From this, and other recent work, it is clear that the "Murchison syncline", as proposed by Van Eeden et al. (1939), does not exist, and that the Antimony Bar and Chloritoid Bar represent two parallel quartzite horizons separated by grits and "mafic metalavas" (Van Vuuren, 1975; Viljoen et al., 1978). Similarly the two plunging synclines in the east, and near Leydsdorp, have been re-interpreted as anticlinal structures (Viljoen et al., 1979; J. de Waal - personal communication, 1979).

Both Viljoen et al. (1979) and Jantski (1978) agree on the position and nature of the two lower subgroups, the Malati and Leydsdorp Subgroups. However, Viljoen et al. (1979), using geochemical evidence across the sequence, and younging directions from the lower subgroups, assume the entire sequence of Murchison rocks youngs to the north. Hence in their classification the Rubbervale Subgroup overlies the Gravelotte Subgroup and youngs to the NORTH.

The present writer and Jantski (1978) recognize, from abundant field observations, that the Rubbervale Subgroup youngs to the SOUTH and is overlain conformably by sediments belonging to the Gravelotte subgroup (see chapter 5).

There is an almost complete lack of exposure between the "Antimony Line" and the Spitzkop - La France line of hills in the south, fig.2, plate 1. This masks the relationship between the southern portion of the greenstone belt, containing magnesium-rich metalavas and metatholeiites overlain by clastic sediments, which youngs to the NORTH, and the northern portion of the belt which youngs to the SOUTH. It is suggested that these help define an isoclinal syncline along the central valley of the Belt.

In the extreme northeast of the Murchison greenstone belt, Minnitt (1975) mapped a sequence of siliceous cherty rocks and quartz-feldspar porphyries, and provisionally placed them above mafic basaltic lavas now equated to the Leydsdorp subgroup. From a reconnaissance in the area, the writer believes these quartz-feldspar porphyries to be a lateral continuation, or equivalent, of the felsic volcanic rocks of the Rubbervale subgroup. If this is correct, then the Rubbervale subgroup overlies the Leydsdorp subgroup. Nowhere, apart from the above ambiguous occurrence, do rocks of these two subgroups come into contact. Everywhere the base of the Rubbervale subgroup is intruded by the Rooiwater Igneous Complex. The Rubbervale and Leydsdorp subgroups are conformably overlain by clastic sediments of the Gravelotte subgroup.

It is proposed that the Rubbervale subgroup was deposited on top of mafic lavas belonging to the Leydsdorp subgroup, but was only formed along what is now the northern flank of the Murchison greenstone belt, as depicted in figs. 5 and 6.

4.6.1

*Special Note

Since completing the section on Stratigraphy, the writer has received a copy of part of the "official" stratigraphy of South Africa (South African Committee for Stratigraphy (SACS), 1980). Their interpretation of the stratigraphy of the Murchison Range is presented in the accompanying figure.

The entire volcanic and sedimentary sequence is now termed the Gravelotte Group, and is divided into six Formations. The order and nature of these is essentially that of Viljoen et al. (1979). The Mac Kop, Weigel, and La France Formations comprise the Gravelotte Subgroup of Viljoen et al. (1979) and this thesis, see fig. 5.

The criticisms levelled at Viljoen et al. (1979) in section 4.6 are still valid and apply equally to this interpretation. Although SACS (1980) acknowledge that the Rubbervale Formation youngs to the south, they still fail to accept that the sediments of their Weigel Formation overlie the Rubbervale Formation and young consistently south, i.e. the Antimony Bar is stratigraphically underlain by, and is younger than, the Chloritoid Bar.

The writer also does not accept the presence of mafic lavas in the Rubbervale and Weigel Formations. Rocks corresponding to these represent basic sills probably affiliated to the Rooiwater Igneous Complex. In the present study area they have been shown to post-date all units except the Rooiwater Igneous Complex.

Formation	Lithology	Approx. thickness (m)	Remarks
Rubbervale	Felsic porphyritic tuffs, mafic porphyritic tuffs and subordinate mafic lavas and sills	3 500	
Mac Mac	Quartzites, grits, with intercalated chlorite schists, minor sericite schists and conglomerates	1 500	Intrusive serpentinite bodies
Weigel	Quartz-chlorite schists (magnesiopelites), quartzite "bar", quartz-muscovite schists, variety of carbonate rocks Banded iron formation Mafic lavas including Mg- and Fe-rich varieties and alkali tholeiites Talc-chlorite schists (altered ultramafic lavas)	3 500	Castle Koppies bar Chloritoid bar Antimony bar Antimony line Louwskop bar Spitzkop bar
La France	Conglomerates, grits, quartzites, chlorite schists (high-alumina metamorphic minerals)	2 000	
Leydsdorp	Mafic lavas (metatholeiitic, Mg-metatholeiitic) with interlayered banded iron formation, quartz-chlorite schist and quartz porphyry; variously carbonatised	3 000	
Mulati	Mafic lavas (basaltic komatiites, Mg metatholeiitic) lesser ultramafic lavas (peridotitic komatiites) and felsic tuffs		

Figure to accompany Special Note. Lithostratigraphy of the Gravelotte Group according to SACS (1980).

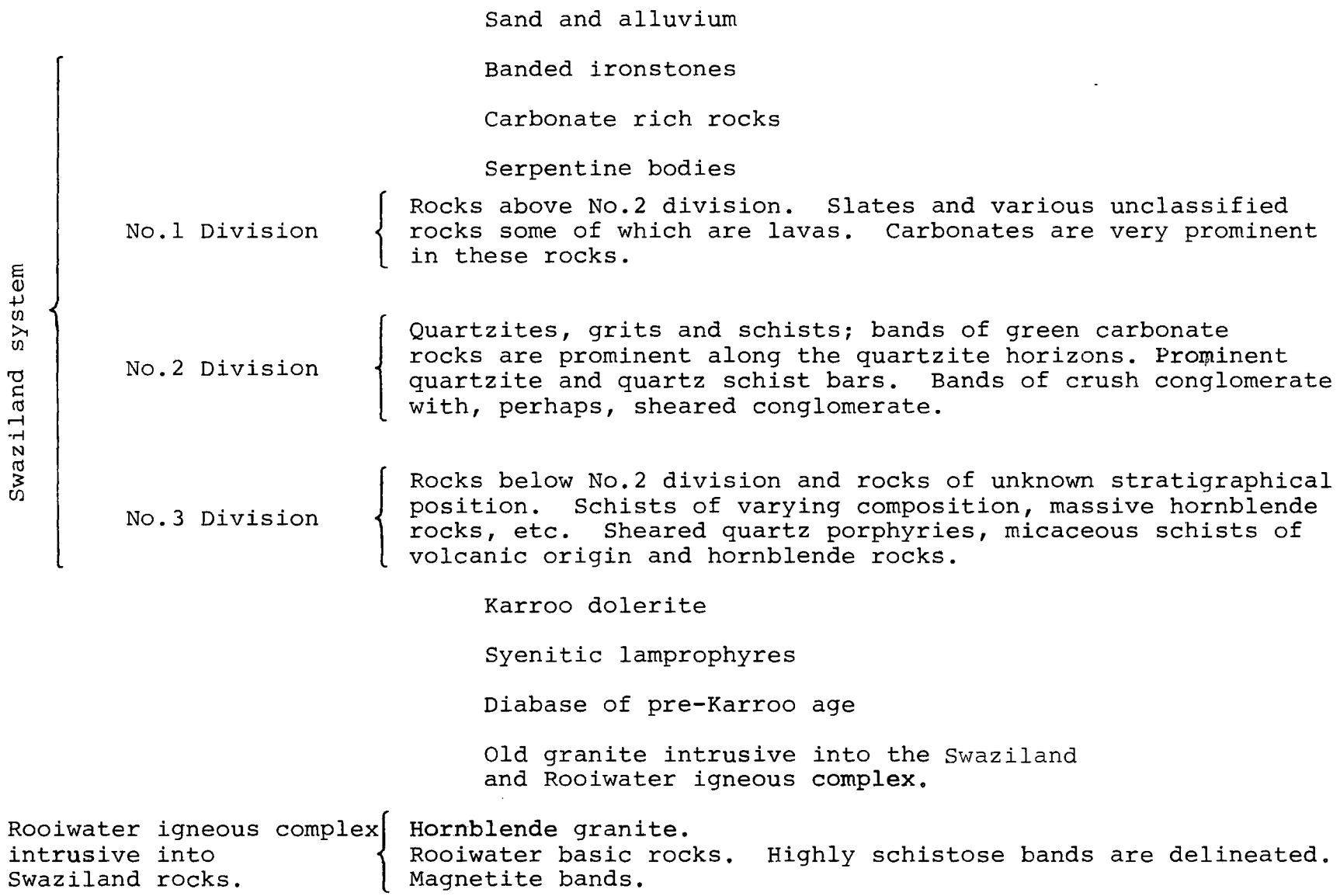

Fig.3. Stratigraphy of the Murchison Range according to Van Eeden et al. (1939).

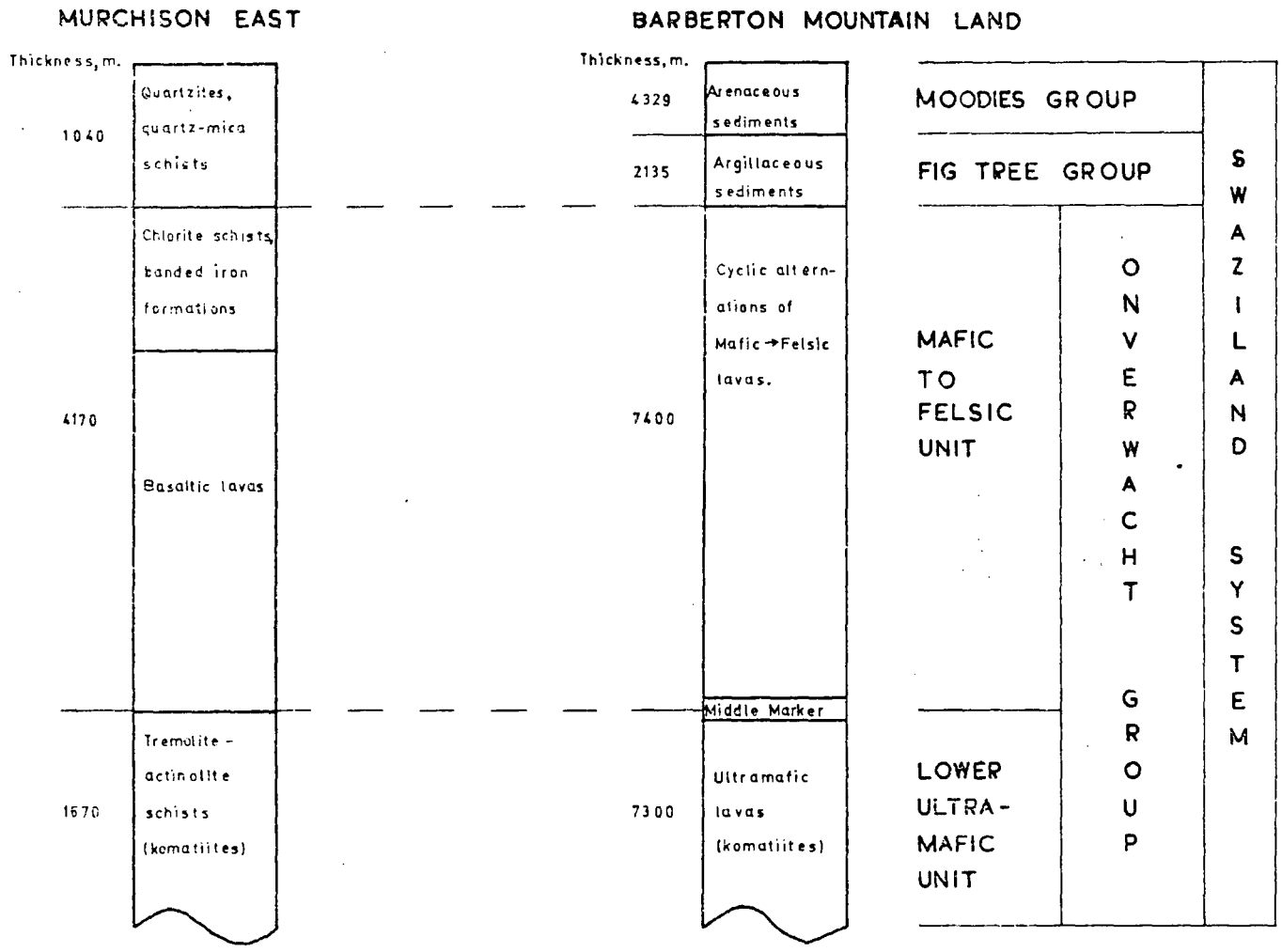

FIG 4

STRATIGRAPHY OF THE EASTERN PORTION OF THE MURCHISON RANGE COMPARED TO THE BARBERTON MOUNTAIN LAND.

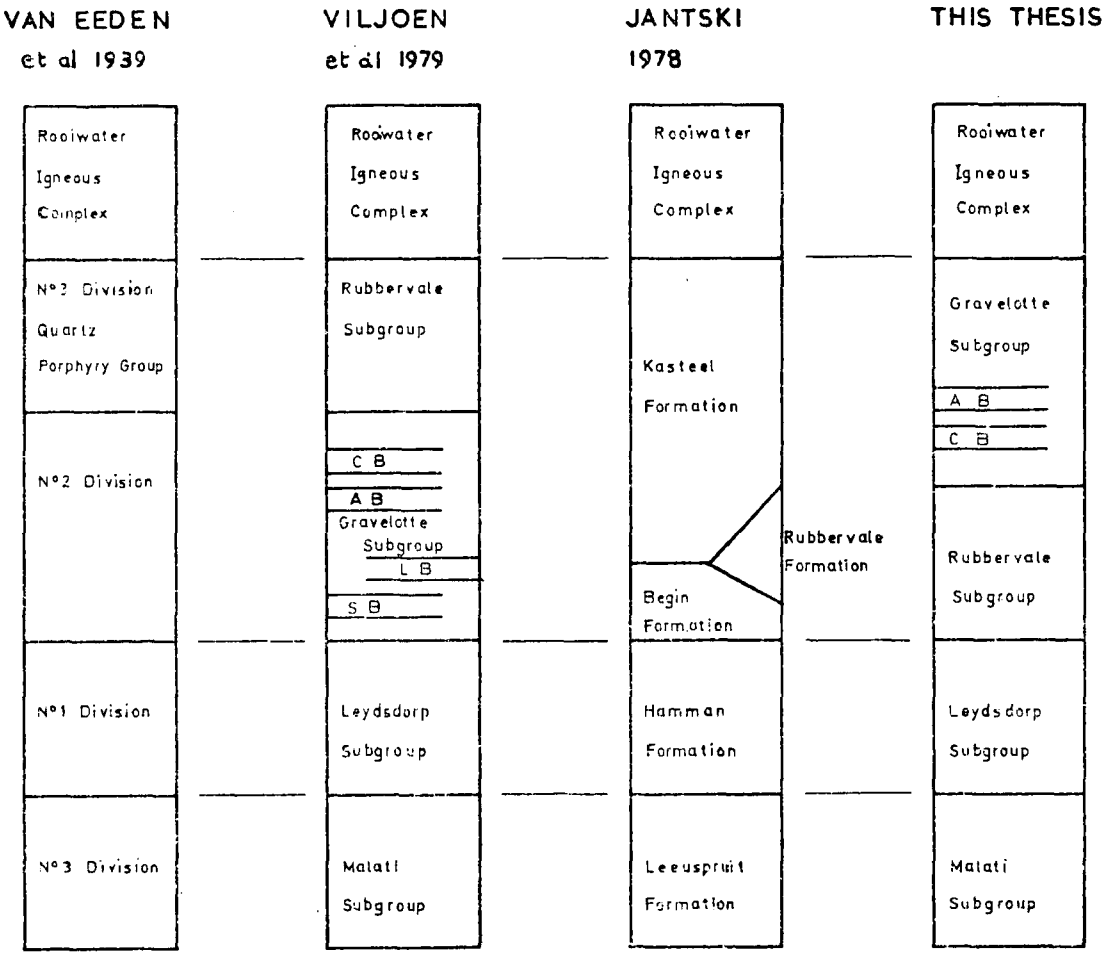

FIG 5

VARIOUS STRATIGRAPHIC PROPOSALS FOR THE MURCHISON RANGE.

QUARTZITE BARS

AB Antimony

CB Chloritoid

LB Louskop

SB Spitzkop

Fig. 6. North-South Section, and Development of the Murchison Greenstone Belt.

Stage I. Development of steepsided rift or trough in early crust, possibly in part of composition similar to ultramafic lavas of Malati Subgroup. Infill of rift with greenstone volcanic sequence and accumulation of pile of felsic volcanic rocks on north flank of trough. Overlain by clastic sediments as pile begins to sag. Emplacement of basic sills into all rocks (not shown), and finally the Rooiwater Igneous Complex.

Stage II. North-South section through present-day configuration of the Murchison greenstone belt in the Gravelotte area. Collapse of volcano-sedimentary pile, partial melting of greenstone "roots" and upwelling of tonalitic magma. Rooiwater Igneous Complex and felsic volcanic pile formed a massive block resulting in only minor tonalitic invasion and low grade metamorphism as compared to the southern part of the Belt.

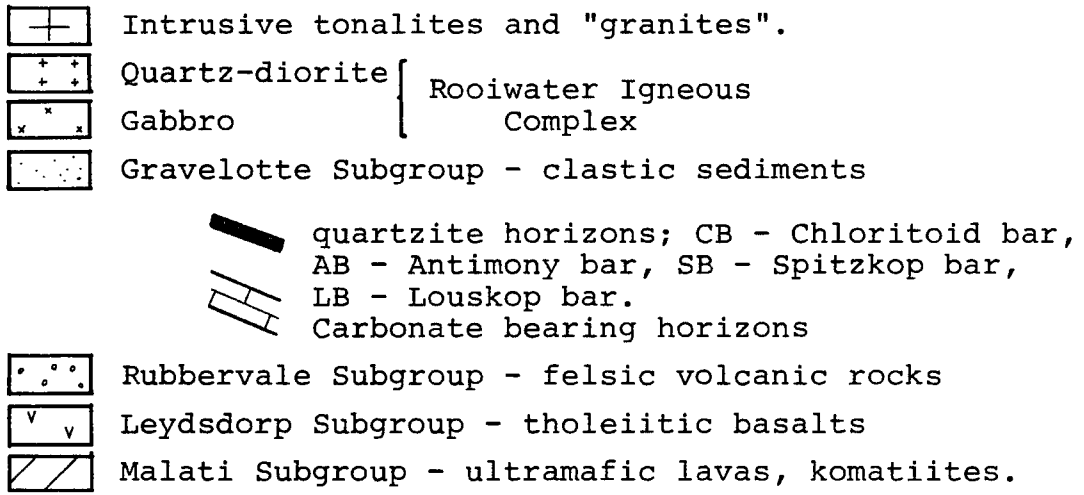

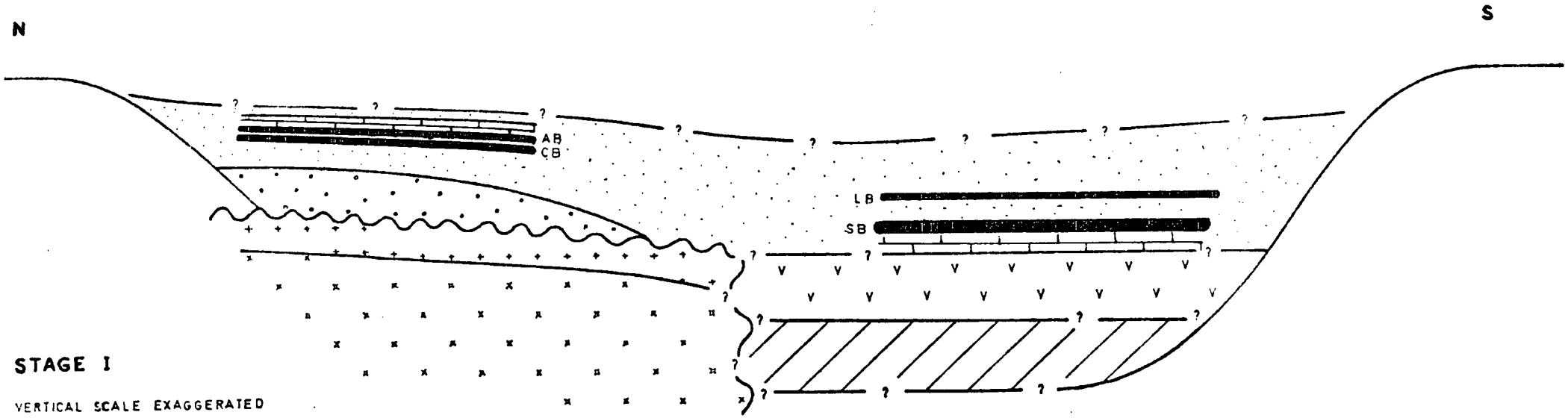

STAGE I

VERTICAL SCALE EXAGGERATED

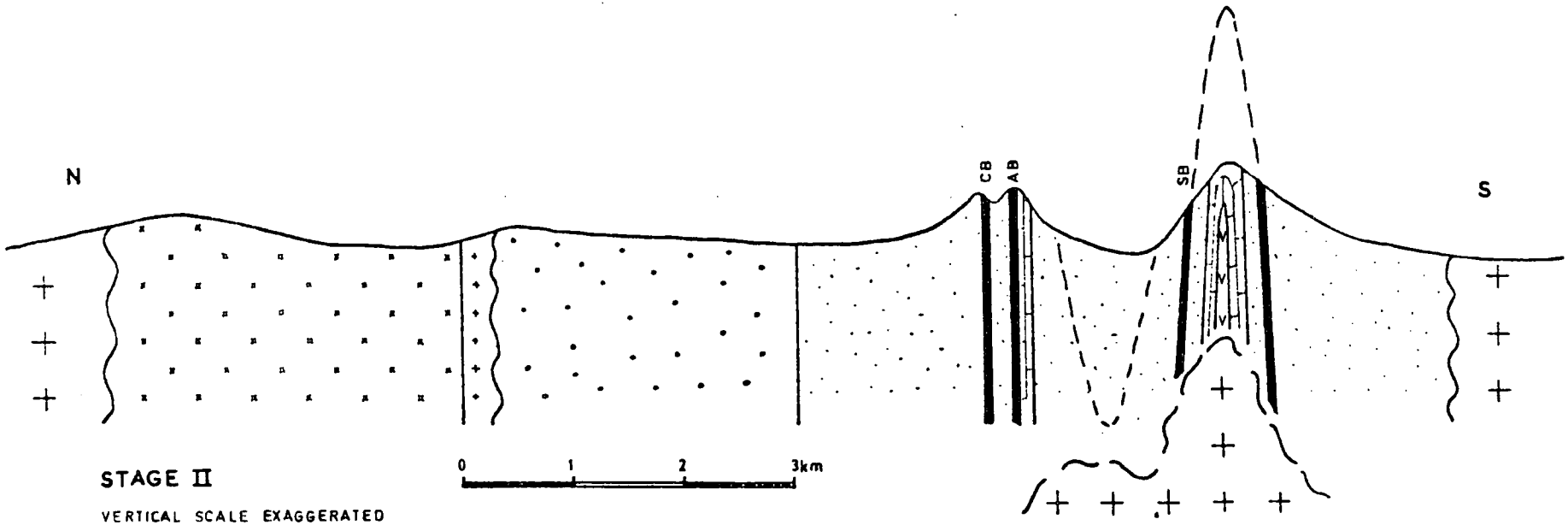

STAGE II

VERTICAL SCALE EXAGGERATED

CHAPTER V

DETAILED GEOLOGY OF STUDY AREA

5.1 Location

The area studied in the present investigation covers portions of eight adjacent farms in the central sector of the Murchison greenstone belt, near the town of Gravelotte; see fig. 2, also plates 1 and 2. This covers an area of 22 km parallel to strike, and a width of up to 4 km. For further information on these farms and the subsequent field techniques utilized refer to chapter 2.

5.2 Geology

5.2.1 Introduction

Within the study area, the main lithologies encountered are felsic tuffs and flows belonging to the Rubbervale Subgroup. These form an E-W trending series of vertical beds. They are overlain in the south by clastic sediments of the Gravelotte Subgroup, and are intruded in the north by the Rooiwater Igneous Complex; refer to map 1. Rocks belonging to the Leydsdorp and Malati Subgroups, as defined by Viljoen et al. (1979), are not present in the study area. Due to the irregular intrusive nature of the Rooiwater Igneous Complex, the preserved thickness of the volcanic pile varies from 1000 to 3700m,with the maximum thickness being on the farm Rubbervale. The lower 1000 m of the sedimentary sequence, and the upper 1000 m of the Rooiwater Igneous Complex are included in the study area.

At several localities way-up structures such as graded bedding, trough-cross bedding and flow-top breccias were observed. They all give a younging direction to the south.

Although the sequence has been subjected to a large amount of shearing, and metamorphism of the upper greenschist facies, sufficient textures and structures have been preserved to enable the original nature of the rocks to be determined early on in the investigation, e.g. tuffs, flows, intrusives, sediments etc. These original rock terms have been applied to the various lithologies; metamorphic terminology was only used where the original nature of the rock was uncertain.

As the investigation progressed, and more drill core became available, especially in the west of the area, this scheme of terminology was invaluable in aiding exploration.

5.2.2 Rubbervale Subgroup

There is a gradual change in the volcanic sequence from west to east within the study area. On the farm Maranda, thick felsic and siliceous flows, with abundant coarse tuff horizons, indicate proximity to the centre of vulcanism. Eastwards, on the farms Mon Desir and Solomons Mine, the sequence is represented by thinner, uniform bedded tuffs with minor intercalated sedimentary horizons. Flows here tend to be less persistent and thinner. The sequence in the east is indicative of a more distal volcanic environment compared to that in the west.

The base of the volcanic pile is everywhere intruded by the Rooiwater Igneous Complex.

Towards the base of the preserved extrusive sequence is a prominent horizon of coarse tuffs. These attain their thickest and coarsest development (30 mm clasts, 300 m thick)

on the farms Rooiwater and Cottondale where they form part of the Tshutshu-Carrolls Peak range of hills. Although disjointed by later faulting, this horizon can be traced from the west of the farm Rooiwater eastwards to Rubbervale farm where it is represented by a thin, 50 m, horizon of tuffs, coarse tuffs and a coarsely brecciated chert. The average size of clast decreases from 30 mm in the west to less than 5 mm in the east.

On the farms Mon Desir and Solomons Mine, at the base of the preserved volcanic sequence, is a 350 m thick, uniform, red-brown coloured tuff exposed as a series of low hills. These resemble the coarse tuffs on Rooiwater and Cottondale, but seldom do clasts, where preserved exceed 5 mm. The tuffs are capped by a 200 to 300 m thick sequence of massive siliceous flows with lesser tuff horizons.

The rest of the volcanic sequence comprises fairly uniform and monotonous fine grained felsic tuffs with minor coarser varieties. Locally flow material may dominate. At the surface the tuffs are characterized by a red-brown colouration and fissile nature, but when fresh they are blue-green in colour. Blue opalescent quartz "eyes" are abundant in these tuffs, and represent original high temperature quartz phenocrysts. In general the schistose fabric has obliterated original tuffaceous textures, but in rare instances rounded clasts or fragments were observed which graded laterally into more typical schistose rocks. With the exception of farms west of Rubbervale, lateral correlation within the tuffs is virtually impossible due to the lack of exposure, presence of basic sills, and subsequent faulting. However, thin flow horizons can be

used as local markers.

On the farm Rooiwater, and in the west of Maranda, the volcanic rocks overlying the coarse tuffs consist of a mixture of coarse tuffs, volcanic breccias and flow material. Individual horizons are laterally impersistent. Within this sequence a 400 m thick felsic unit has been traced for 2500 m along strike. This comprises a uniform, fine grained rock with hexagonal cooling joints perpendicular to the schistosity, plate 3. The unit has a tuffaceous or brecciated top.

The portion of the sequence exposed on Gravelotte farm is dominated by later basic sills with only thin wedges of volcanic rocks, mainly flows, between these.

In the east of Maranda farm, a 200 m thick sequence of felsic extrusives, with minor tuffs, forms a prominent ridge leading up to Carrolls Peak. The dominant rock type is a friable, pale coloured quartz+chlorite+feldspar schist within which flow banding and brecciated flow tops have been recognized, plate 4. This horizon contains sporadically disseminated sulphides and has given rise to several highly anomalous copper and zinc soil values. The horizon has been traced westwards for 2500 m from Carrolls Peak, to where the ridge ends. Further west these rocks are covered by thick loamy soil.

On the farm Solomons Mine, a 100 m thick sequence of flows and associated tuffs and breccias lies 300 m from the top of the volcanic pile. This horizon is continuous over 3500 m and contains minor amounts of disseminated sphalerite and pyrite. It is possible that this horizon and the flows around Carrolls Peak are lateral equivalents.

The top of the volcanic sequence is marked by localized areas of extrusive and explosive activity; plate 5. Siliceous flows and associated coarse tuffs and breccias occur at intervals of 4 to 5 km along strike. From west to east these centres occur at the western end of Maranda farm (the J locality), south of Carrolls Peak (the L-W area), the SE corner of Rubbervale farm, and in the east of Gravelotte farm. On Solomons Mine the top of the volcanic sequence comprises uniform tuffs. Exposure elsewhere is limited, but where examined by air-flush and diamond drilling, consists of fine tuffs, often bedded, with minor, thin flow material.

Associated with, and overlying these areas of localized vulcanicity are a massive sulphide deposit at the J locality, zones of disseminated zinc and copper sulphides in the L-W area, and a massive sulphide deposit, the MGZ, on Solomons Mine. Mineralization was not found on Gravelotte farm, and the locality in the SE of Rubbervale farm was not available for examination.

Frequent, small, syn-volcanic, felsic intrusives cross-cut the volcanic pile. They are considered to be an integral part of the sequence. Rarely hexagonal cooling joints are developed within the larger intrusives.

5.2.3 Rubbervale Subgroup - Transition Zone

The Transition Zone is a field term for the uppermost part of the Rubbervale Subgroup, during which a period of volcanic quiescence allowed the accumulation of banded cherts, and some reworking of the volcanic pile.

The lower portion of the Transition Zone is composed of fairly monotonous cherts, aluminous cherts, and thin sericite-rich layers. At the MGZ and J localities, massive sulphide lenses, grading laterally into thin mineralized chlorite schists, form the base of the sequence. At the L-W locality 30 m of chert and aluminous chert contain varying amounts of disseminated sphalerite and pyrite. The upper portion of the Transition Zone consists of a thick, rather uniform welded tuff, termed an "acid porphyry". This is best developed in the west where 175 m of acid porphyry is sharply conformable upon cherts overlying the sulphide deposit at the J locality. Above the acid porphyry are clastic sediments of the Gravelotte subgroup. The base of the Transition Zone is taken as the contact between "true volcanic rocks", i.e. flows and tuffs, with cherty and volcano-sedimentary horizons. The contact is remarkably sharp and persistent throughout the study area and is considered to represent a time/stratigraphic marker. Both the lower and upper contacts of the Transition Zone are easily identifiable.

Due to weathering rocks of the Transition Zone are rarely exposed, and are either covered by thick loamy soil or form the southern slopes of the Carrolls Peak - Tshutshu range where they are covered by extensive scree and detritus. South of Carrolls Peak, however, is a prominent E-W trending ridge comprised of cherts, and cherty tuffs overlying massive felsic flows and coarse tuffs. The ridge extends along strike for 1400 m. The cherts form the lower part of the Transition zone and here contain sporadic pyrite and

sphalerite mineralization at the L-W locality. The overlying acid porphyry unit occupies flat-lying, soil-covered ground to the south.

The distinction between the lower cherts and the upper acid porphyry is very distinct at the J locality, less so at L-W, and indistinct at the MGZ locality in the east. Here, the sequence commences with a massive sulphide lens grading laterally into a mineralized chlorite schist and overlain by 100 m of thinly bedded cherts, reworked felsic tuffs and reworked acid porphyry. The acid porphyry unit as seen in the west does not occur here, the rocks present represent lateral reworking of the porphyry unit. This would indicate a source for the acid porphyry to lie to the west of Maranda farm.

Soil geochemistry, photolineaments, minor geophysical anomaly patterns, and extensive air-flush drilling have traced the sub-outcrop of the Transition Zone throughout the study area. Details of the nature and stratigraphy of the Transition Zone have come from diamond-drill core from the J, L-W and MGZ localities.

A generalized section through the Zone can be seen in fig. 7.

5.2.4 Gravelotte Subgroup

An argillaceous and arenaceous sedimentary unit overlies the volcanic succession. The contact between the two is not exposed in the study area, but 25 km to the west, on Magoboya's Location, cherts and cherty tuffs are

conformably overlain by argillaceous sediments, or phyllites, which form the base of the sedimentary unit. Drilling south of the three main mineralized localities in the central sector of the Belt has intersected the contact and suggests a fairly abrupt and conformable change. Unfortunately there is an almost total lack of exposure of the sedimentary unit in the study area. Immediately south of the farms Solomons Mine, Mon Desir and Gravelotte, two quartzite horizons, the Chloritoid and Antimony Bars, form prominent parallel ridges traceable from west of the town of Gravelotte eastwards to Castle Koppies, a distance of 20 km (Van Eeden et al., 1939).

From drill information and traverses made to the south of the study area, the sequence in fig. 8 was deduced.

The sedimentary assemblage has been best examined on the farm Solomons Mine where it is approximately 1550 m thick to the top of the Antimony Line. The lower 1000 m are not exposed, but the upper 550 m are reasonably well exposed and lie to the south of the study area. Up to 20% of the total thickness is thought to be occupied by laterally extensive basic sills of Rooiwater age, see section 5.2.5.

The base of the sedimentary sequence is taken as the top of the acid porphyry or reworked acid porphyry. This coincides with the first appearance of fine grained chlorite, chlorite+sericite, and quartz+sericite schists characterized by inherently high nickel contents (range 200-700 ppm). They closely correlate with the $>$ 100 ppm Ni contour from the soil geochemical survey. Intercalated within the lower

part of the sequence are thin acid tuff horizons compositionally similar to the acid porphyry unit. Three hundred meters from the base of the sequence a diamond drill-hole intersected a succession of fine grained laminated chlorite, quartz+sericite+chlorite and quartz+sericite schists. Preserved structures include graded bedding from a quartz rich base to chlorite rich top, one bed grading from coarse quartz and chlorite schist to banded chert, plate 6. Truncated cross-bedding and trough cross-bedding are also present, all younging to the south. These rocks appear to represent a sequence of greywacke-turbidites suggestive of a relatively deepwater environment. Within these greywackes is a conformable horizon, 27 cm thick, of interlaced pyrrhotite with traces of chalcopyrite and pyrite in a chlorite gangue. This horizon was traced for 7 km along the surface during the PEM survey, and parallels the regional schistosity. Four such horizons were located within the sedimentary sequence.

In the east of the farm Solomons Mine, a thin quartzite horizon is exposed over 250 m. This quartzite contains small, 1-2 mm, oval, deformed, and compacted quartz grains in an intergranular matrix of quartz, zoisite and infrequent fuchsite mica. A chemical analysis of this rock is presented in table 3.

South of the farm boundary the two prominent quartzite horizons form an E-W trending series of hills. The northern horizon, the Chloroid Bar, is continuous, broken only by later NE trending dolerite dykes. The southern

horizon, the Antimony Bar, is more discontinuous appearing to pinch and swell along the length of the Murchison Range.

A section through the Chloritoid Bar was examined south of Mon Desir farm, and part of the Antimony Bar in an abandoned quarry north of the Gravelotte Antimony Mine, fig. 9.

The Chloritoid Bar comprises three quartzite horizons, locally fuchsitic and with pebble bands, separated by chloritic schists and carbonate bands. The sequence is approximately 230 m thick. Laterally the Chloritoid Bar includes interlayered iron formations and carbonaceous shales (Viljoen et al., 1978).

Separating the two Bars are 350 m of sheared chlorite and chlorite+quartz schists considered by Van Vuuren (1975) and Viljoen et al. (1978) to have been magnesium-rich basic lavas. Van Eden et al. (1939) describe these rocks as "...hornblende+quartz+clinozoisite rocks, which undoubtedly represent altered lavas." The present writer is of the opinion that this horizon is a sheared basic sill of Rooiwater age.

The Antimony Bar consists of a sequence of greywackes and cherts, with rare tuff horizons, thin pebble conglomerate horizons and increasingly towards the top, thin, nodular, pyrite bands. Sedimentary structures within the greywackes are well developed with graded bedding occurring as tightly packed conglomerate layers grading southwards into finer grained rock. Often the upper contact is marked by a thin ferruginous horizon; plate 7.

The conglomerate bands tend to contain angular to sub-

rounded clasts, dominantly quartzite but with some banded chert and chloritic clasts. Some layers contain deformed elongated pebbles while others have angular, undeformed, unoriented clasts.

South of the Antimony Bar an assemblage of carbonates, talcose, siliceous and cherty carbonates and talc schists is host to the important antimony mineralization of the area and which form a horizon known as the Antimony Line (Van Eeden et al., 1939). The best antimony mineralization occurs in areas where the carbonate and quartzites are thickest (Muff, 1978).

Rocks south of the Antimony Line are dominantly fissile chloritic phyllites (Van Vuuren, 1975).

South of the Antimony Line, exposure is virtually nil in the central valley of the Murchison greenstone belt. South of the Gravelotte to Palabora road the prominent ridges of Spitzkop and La France contain quartzite horizons similar to the Chloroid and Antimony Bars. According to Viljoen et al. (1979) the whole area is underlain by Gravelotte Subgroup sediments.

In the west of the study area, on the farm Maranda, exposure is limited to the Carrolls Peak-Tshutshu range where Rubbervale Subgroup volcanic rocks occur. Two and a half kilometers south of this, and forming the southern boundary of the farm, fuchsitic quartzites crop out in a series of hills and form part of the Leydsdorp anticline. South of this are metatholeiites belonging to the Leydsdorp Subgroup (Viljoen et al., 1979).

Exposure between the two ridges is nil, except for a thin granodiorite in a stream bed in the east-central portion of Maranda.

5.2.5 Basic Sills

The Rubbervale and Gravelotte Subgroups have been intruded by numerous sills of tholeiitic composition. It is estimated that these sills comprise approximately 20% of the volcanic and sedimentary sequence, although they are subject to preferential weathering and are rarely exposed.

The sills were intruded along bedding planes and occasionally crosscut the volcanic stratigraphy. They are often thick, 150 m being common, and in one instance have been traced along strike for 7 km before being lost under superficial cover. Rarely are irregular discordant intrusives seen.

Sills tend to be polyphase, with coarse grained, fine grained and porphyritic varieties. Intrusive contacts are generally sharp, marked by thin, 1 mm, quartz veins, and may be chilled against the host rock.

The thinner, less than 5 m, intrusives are fine grained, with thin, 1 cm, glassy chilled margins and may contain small feldspar phenocrysts. Shearing is common and later deformation generally imparts a strong schistosity.

Drill-core intersections of top and bottom contacts has confirmed their intrusive nature. Contacts tend to be sharp and clear, generally parallel to the volcanic layering although irregular, brecciated and split contacts do occur.

Upper and lower contacts of thick sills are generally sharp with margins of up to 4 m width, more usually 1 m. They were commonly chloritized and foliated parallel to the local schistosity during deformation.

The host volcanic rocks are baked and hardened up to 1 m from the contact. They may contain quartz and/or chlorite veins parallel to the contact. Where intruded into sulphide horizons, chalcopyrite has been remobilized along the contact and has been incorporated into the first few centimeters of the intrusive.

Sills were not observed to cross or cut the quartz-diorite (upper) phase of the Rooiwater Igneous Complex. However, on Gravelotte farm, a xenolith of basic rock was found to be entirely surrounded by quartz-diorite. This would seem to indicate that the sills pre-date the intrusion of the Rooiwater Igneous Complex.

5.2.6 Rooiwater Igneous Complex

5.2.6a Introduction

The name "Rooiwater Igneous Complex" was proposed by Van Eeden et al. (1939) for the rocks comprising the prominent range of hills lying to the north of the main Murchison Range. They distinguished a gabbro group, forming the hills, and a hornblende granite lying in flat land to the south between these hills and the main Murchison Range, a width of 3000 m.

The Rooiwater Igneous Complex occupies a wedge shaped area along the northern flank of the Murchison greenstone belt. It has been traced eastwards from the base of the Escarpment as a series of rugged, rather irregularly rounded

hills, to north of Rubbervale where they become less pronounced and finally form part of the monotonous plain extending north of the koppies of the Antimony Line. The Complex peters out to the west of Hartebees farm, its eastward extension being a series of closely spaced basic sills.

In the study area, only the southern portion of the gabbro, and most of the hornblende granite phase are present, occupying low ground in the north of the area.

The complex is best observed in the north of Solomons Mine and Mon Desir where frequent small rounded exposures of gabbro and granite can be seen. The hornblende granite is well exposed on the farm Gravelotte.

In the west of the study area, on Cottondale farm, small exposures of granite and gabbro occur adjacent to a large dolerite dyke immediately north of the Carrolls Peak-Tshutshu range of hills

5.2.6b Gabbro Phase

The gabbro phase consists of a variety of basic rocks ranging from coarse amphibole-rich "pegmatites" to quartz-free and quartz-bearing gabbros. The more mafic varieties tend to occur in the north, with quartz-bearing gabbros in the south, at the contact with the hornblende granite.

True gabbros, which are the dominant rock type, have a mafic component which varies from 30 to 70% of the rock. Melanocratic and leucocratic varieties commonly form impersistent, interfingering layers or bands, the layering being accentuated by thin mafic and felsic streaks within

the gabbro horizons. Anorthosite and amphibolite layers also occur although these are relatively minor. Occasional thin hornblende+magnetite horizons or layers can be traced for over 500 m and parallel the gabbroic layering.

Kingston (1976) reports on an amphibolite band containing 13% magnetite and 9% apatite, and magnetite+apatite zones are also reported by Van Eeden et al. (1939).

Sporadic, irregular amphibolite bodies occur within the gabbro, commonly containing disseminated magnetite, chalcopyrite and nickeliferous pyrrhotite.

Several areas of talc+actinolite schist were found to be parallel to local shear zones.

The contact with the hornblende granite phase is nowhere exposed, although small exposures of gabbro and granite were found within 50 m of each other. Van Eeden et al. (1939) report a gradational contact.

The northern contact of the gabbro phase is intruded by the surrounding Younger Granites (Van Eeden et al.. 1939). Borehole core from the farm Quagga, north of Rubbervale intersected tongues of this granite intrusive into the gabbro.

5.2.6c Hornblende Granite Phase

Although termed "hornblende granite" by Van Eeden et al. (1939), Jantski (1978), on the basis of chemical analyses, suggested the term diorite or quartz-diorite to be more accurate. The present writer prefers the term quartz-diorite.

The main outcrop is on the farms Free State, Solomons Mine, Mon Desir, Gravelotte and Rubbervale where thicknesses

of 1500 m are obtained. Some interfingering of quartz-diorite and gabbro occurs on Rubbervale and the adjacent farm Beesplaas.

West of Rubbervale the only exposure of quartz-diorite is on the farm Cottondale. The maximum thickness possible here is 1200 m. From photogeological interpretation, this exposure forms part of a narrow outcrop between volcanic rocks and the gabbro phase, possibly joining the main outcrop on the farm Beesplaas.

On surface, the quartz-diorite is a massive, pale grey to white rock containing occasional clots of mafic minerals, mainly chlorite. Mafic rich phases occur near the gabbro contact.

The southern margin of the quartz-diorite contains numerous xenoliths of felsic tuff, the largest being 50 m across. Rare basic xenoliths occur, the largest on the farm Gravelotte, and are similar in appearance to the numerous basic sills within the volcano-sedimentary pile.

The quartz-diorite is intrusive into the base of the Rubbervale Subgroup. At the contact, the quartz-diorite is very fine grained hard and siliceous and may contain rare blue quartz phenocrysts identical with, and probably derived from, the volcanic sequence.

Near the contact, the intruded volcanic rocks become more massive with the loss of textures, they are silicified, and contain local developments of green amphibole and colourless mica. In general, no distinct line can be drawn between the volcanic rocks and quartz-diorite over a zone of up to 50 m in width.

5.2.6d Summary

The Rooiwater Igneous Complex is intrusive into the Rubbervale Subgroup volcanic pile and is intruded by the surrounding Younger Granite. The quartz-diorite phase, lying to the south of the gabbro phase, has a higher mafic content near the gabbro contact. Adjacent to the quartz-diorite the gabbro contains free quartz. This leads to the conclusion that the two are comagmatic, also stated to be the case by Van Eeden et al. (1939). It is further suggested that the quartz-diorite is a differentiation phase of the Igneous Complex.

The gabbro phase comprises gabbro, with variable feldspar content, and amphibole+magnetite+apatite horizons. These give rise to a banding or impersistent layering with the more mafic and magnetite-bearing horizons in the north of the Complex. This layering is compositional, and is vertical and roughly parallel to the bedding and schistosity within the overlying volcanic and sedimentary pile. It is considered to have been caused by original differentiation processes within an essentially horizontal magma chamber. The quartz-diorite would have formed a roof over the gabbro phase.

The absence of crosscutting basic sills, and their rare presence as xenoliths within the quartz-diorite phase, indicate the emplacement of the Complex as a horizontal body within, possibly near the base of the volcanic pile of the Rubbervale Subgroup. Prior to emplacement, the pile was intruded by numerous basic sills. The emplacement of the Rooiwater Igneous Complex was the final phase of

greenstone development prior to deformation and metamorphism of the assemblage.

5.2.7 Post-Greenstone Intrusives

5.2.7a Younger Granites

Intrusive granites and tonalites are absent from the study area except for a thin granodiorite exposed in a stream bed in the east-central part of the farm Maranda. This outcrop is very weathered, but is considered to be an extension to the granite body cropping out on Crown Land to the east, at the western termination of the Antimony and Chloritoid Bars (Van Eeden et al., 1939; Coetzee, 1976).

5.2.7b Later Dolerites

Crosscutting the greenstone sequence are a number of roughly parallel dolerite dykes, trending 040° magnetic and following the major fault or fracture direction. In the west of Maranda farm one dolerite dyke trends 145°mag, and is cut by a later 040° dyke and faults. The main concentration of dykes is on the farms Gravelotte, Mon Desir and Solomons Mine where they occur at spacings of 400-500 m.

The dykes are dark, fine grained dolerite and have not been subjected to deformation or metamorphism. They are considered to be of Karroo age by Van Eeden et al. (1939).

5.3 Structure

5.3.1 Structures

Large scale folding is absent in the study area, the volcanic and sedimentary rocks forming a vertical E-W trending sequence younging to the south.

The most notable structural feature is a penetrative planar schistosity which is generally vertical and trends approximately E-W. Pole plots of this schistosity, termed S_1, on a lower hemispherical stereonet, show the trend to vary from 90/085 on the farms Solomons Mine and Mon Desir in the east, 90/080 on Gravelotte farm, 90/080 on the farms Rubbervale and Beesplaas, and 84/089N on the farms Maranda, Cottondale and Rooiwater. See fig. 10. The regional, greenschist facies, metamorphic fabric is developed along this S_1 plane.

Where observed, S_1 was found to be parallel to compositional and lithological banding and original bedding, termed S_0. However, in rare instances in drill core from the western farms, small rootless intrafolial folds were observed where folded S_0 was cut by an axial planar cleavage indistinguishable from and parallel to S_1 at that locality; plate 8.

Fold axes to these rootless folds, termed F_1 trend within the range 060° to 080° magnetic, plunging gently east or west. The trace of S_0 on S_1 plunges from 12 to 35°E, rarely up to 47°W. Within S_1 is a mineral lineation L_1 which appears to have developed at the same times as the S_1 metamorphic fabric. This lineation is present as an alignment, or streak, of minerals, and elongation of fragments within the tuffaceous units, plate 9. The orientations of these lineations has been plotted on fig. 10. L_1 lineations were recorded from borehole core at various localities. Unfortunately core orientation studies were not undertaken, but the local S_1 was in all cases found to be the same as that of the regional S_1 trend.

In figure 10, the mean plunge of several lineations at each locality has been plotted along the mean S_1 plane.

From this diagram it is obvious that the plunge of L_1 varies from vertical on the farms Solomons Mine and Mon Desir, to steep westerly on Rubbervale and Beesplaas, and on the farm Maranda plunges at 61-75°W in the Carrolls Peak area, and 55°W at the J locality in the extreme west of the farm.

This variation agrees with that noted by the writer over the length of the Murchison greenstone belt, where L_1 plunges 60°E in the east, is vertical in the Gravelotte area, and plunges at 40°W in the far west of the Belt.

In borehole core from three localities, steep easterly plunging lineations similar in appearance to L_1 were noted. The mean plunge is 78°E at J, 61°E at W and 68°E at the L localities. The absence of original spherical objects in the rocks meant that it was not possible to accurately measure the ratios of the three principal axes of the strain ellipsoid which produced S_1 (Ramsay, 1963, 1967; Hopwood, 1978). Measurements of the largest axis and two at right angles to this were made on fragments from several oriented tuff blocks. These however are suspect owing to the probable non-spherical nature of these fragments. The maximum ratio determined was 6.1:2:1 (maximum:intermediate:minimum strain direction) for 8 mm sized fragments on the farm Gravelotte. The average ratio was however 4:2:1.

Superimposed on S_1 is a non-penetrative cleavage S_2, similar to the shear cleavage of Ramsay (1967, p.388). This

is most noticeable within tuff horizons east of Rubbervale; plate 10. S_2 trends at approximately 112° magnetic and is generally vertical. Poles to S_2 are plotted on figure 10. Lineations formed by the S_1 - S_2 intersection are parallel to L_1 lineations. In thin sections, S_2 is formed by extension and shearing along the limbs of microfolds with re-alignment and bending of micaceous minerals parallel to this; plate 11. The deformed S_1 has a definite asymmetry which according to Ramsay (1967, p.390) is due to shearing asymmetric to layering, or in this case S_1. In a small quarry above the Gravelotte antimony mine a local buckle or intrafolial fold was observed within a bedded greywacke-carbonate sequence. Here the bedding, S_0, was observed to be parallel to S_1 and to strike 070°. The fold, F_2, has an axial plunge 75°W, parallel to the local L_1 lineation, and has an axial plane cleavage at 100° parallel to the local S_2 trend, plate 12.

5.3.2 Distribution of Schistosity

The S_1 fabric is developed throughout the study area and is virtually everywhere parallel to S_0, the original bedding. However, the degree of development of S_1, especially its penetrative nature and the associated amount of shearing, is not uniformly distributed.

On the farms east of Rubbervale the volcanic succession contains thin, uniform bedded tuffs with relatively few flows compared to the western area. Also the number of basic sills is greater. This results in the volcanic component readily accommodating the deformation and

shearing along S_1 and later S_2 trends with development of the penetrative S_1 - L_1 fabric i.e. the rocks are less competent in the east than in the west of the study area. Original volcanic textures are only locally preserved in small areas of relatively competent massive flows and siliceous tuffs; plate 13. S_2 is prominently developed, and original bedding is parallel to S_1.

West of Rubbervale, in the Carrolls Peak-Tshutshu range of hills, the felsic volcanic rocks contain a higher proportion of massive flows, coarser tuffs and lesser basic sills. Here original textures are frequently preserved. S_1 is present and is fairly penetrative, S_2 is rarely observed. Small rootless F_1 folds occur, but F_2 folds are absent. The volcanic rocks appear to have reacted to the deformation as a resistant mass.

5.3.3 Fracturing

During a much later stage of cooling or uplift, the area was subjected to fracturing and faulting. As before, eastern and western areas appear to have reacted in slightly different ways; fig. 12. In the east, i.e. east of the Rubbervale to Leydsdorp road, the main fracture trend is 035° magnetic with minor trends at 175° and 095°, although this latter trend is nearly parallel to S_1 and could be spurious.

West of Rubbervale, the main fracture trend is 045° within a zone varying from 030-060°, minor trends occur at 135° and 180°. Both sets of fracture pattern are similar, fig. 12, however the 135° trend is absent in the eastern area, but may be due to the relatively sparse exposure.

5.3.4 Dykes

Dolerite dykes of Karroo age cut the greenstone sequence. Their trends and relative lengths have been plotted on fig. 13. In the eastern area dykes are common, trending 035° and are spaced on average 400-500 m apart. These follow the prominent fracture trend of fig. 12.

In the west dolerite dykes are uncommon, three large and several small dykes being noted. These trend at 055° magnetic, within the broad trend of the main fracture zone. A single early dyke trends 146°, probably influenced by the 135° fracture trend.

5.3.5 Discussion

The sequence of deformation found within this area of the Murchison greenstone belt is similar to that mapped by Ramsay (1963) over an area in the north of the Barberton Mountain Land, and of the general model developed by Hopwood (1978).

From the stratigraphic younging directions in the north and south of the Belt, see chapter 4, it is suggested that the core of the Murchison Range is occupied by an E-W trending isoclinal syncline F_1. The axial plane of the syncline is vertical and the fold axis is subhorizontal.

A penetrative schistosity S_1 was developed as an axial plane cleavage to F_1. Increasing compression from north and south (Frip et al., 1980) resulted in tightening and deepening of F_1 and extension of the strain ellipsoid in the A-B plane, fig. 11, with the formation of prominent mineral lineations L_1 and elongation of tuff fragments parallel to the A strain direction. To accommodate the

north-south compression, bedding S_0 was rotated parallel to S_1 (Hopwood, 1978). Small rootless intrafolial F_1 folds attest to this. The main planar-linear metamorphic fabric was imposed on the rocks at this time.

Further extension of the strain ellipsoid along the B axis was prevented by lateral constraints on the greenstone assemblage, and the rocks deformed by buckling and the development of a shear cleavage S_2 at 22^{o} south of S_1. Large scale buckle folds are rare, and develop as intrafolial F_2 folds with fold axes parallel to the L_1 lineation direction (Ramsay, 1963; Hopwood, 1978). Lineations produced during this phase were still under the influence of the A strain axis. It is possible that the non-parallellism of S_1 and S_2 is due to slightly asymmetric shear (Ramsay, 1967).

The S_2 cleavage was produced prior to, and influenced the emplacement of, tonalitic diapirs along the margins of the Belt (Viljoen et al., 1978; Jantski - personal communication, 1979; see also chapter 4). A low grade thermal metamorphic event was overprinted on the S_1 - S_2 fabric.

According to Ramsay (1963) and Hopwood (1978) these deformations probably belong to one continuous evolving "orogenic" phase. Variations in the L_1 plunge direction are probably a result of slight bending of the Belt about a vertical axis (Cilliers, 1975). A much later event caused brittle fracture and subsequent dolerite intrusion along the dominant fracture trend.

5.4 Metamorphic Petrology

5.4.1 Introduction

Two distinct periods of metamorphic mineral growth can be identified. An early phase accompanied, or followed,

the formation of the S_1 - L_1 planar-linear fabric. A later, post-tectonic thermal event took place under static conditions resulting in the growth of coarse metamorphic minerals. This latter event is probably related to intrusion and subsequent cooling of granitic plutons (Anhaeusser, 1973; Minnitt, 1975). Both mineral assemblages belong to the middle to upper greenschist facies (Turner, 1968) or Low Grade of metamorphism of Winkler (1974). See fig. 14 for a summary.

5.4.2 Pre-Metamorphic Minerals

The volcanic tuffs and flows of the Rubbervale Subgroup are characterized by the presence of opalescent, blue quartz "eyes" (Van Eeden et al., 1939). In thin section these "eyes" are seen as low quartz pseudomorphs after high temperature quartz phenocrysts, commonly having a bipyramidal outline, although angular and rounded varieties are common. Their size is generally in the range 1 to 5 mm, and frequently their margins are embayed and corroded, indicating partial resorption by the liquid. During the deformation, these quartz phenocrysts have been subjected to strain, with sub-grain polygonal recrystallization. Examples of all stages from fresh bipyramids to lenses of recrystallized quartz were observed, plate 14.

In certain flow units, and also towards the centre of the acid porphyry unit, there are small euhedra of albite. These may be fresh, crushed, rounded, broken or corroded and are considered to be albitized alkali feldspar phenocrysts of igneous origin, plate 15.

Within the acid porphyry unit, especially from the J locality, patches and radial aggregates, or spherulites, of finely intergrown quartz and alkali feldspar represent devitrification of glassy siliceous rock (Hatch et al., 1961, fig. 92); plate 16. Possible snowflake texture, as described by Anderson (1969), was also observed, suggesting that the porphyry unit was originally a welded tuff.

Small, < 0.5 mm, rounded quartz grains, containing numerous minute inclusions, were found within some of the more sheared tuff horizons. These quartz grains probably represent modified, recrystallized spherulites, plate 17.

Basic sills are massive, relatively coarse grained rocks comprising amphibole and feldspar with minor interstitial quartz, epidote, chlorite and opaques; plate 18. Some opaques have a skeletal appearance and elongate apatite crystals were also recorded. Hunter (1980) has argued that these represent a rapid phase of growth in quickly cooled dolerites.

5.4.3 Metamorphic Petrology

5.4.3a Regional Dynamothermal Metamorphism

Fabrics

The metamorphic fabric follows and outlines S_1 and L_1. Platy minerals, e.g. chlorite and muscovite, lie within the S_1 plane, and tend to form streaks along the L_1 trend. In the uniform tuff horizons these micaceous minerals impart a braided schistose texture to the rocks, typical of this kind of low-grade metamorphism (Hopwood, 1978); plate 19.

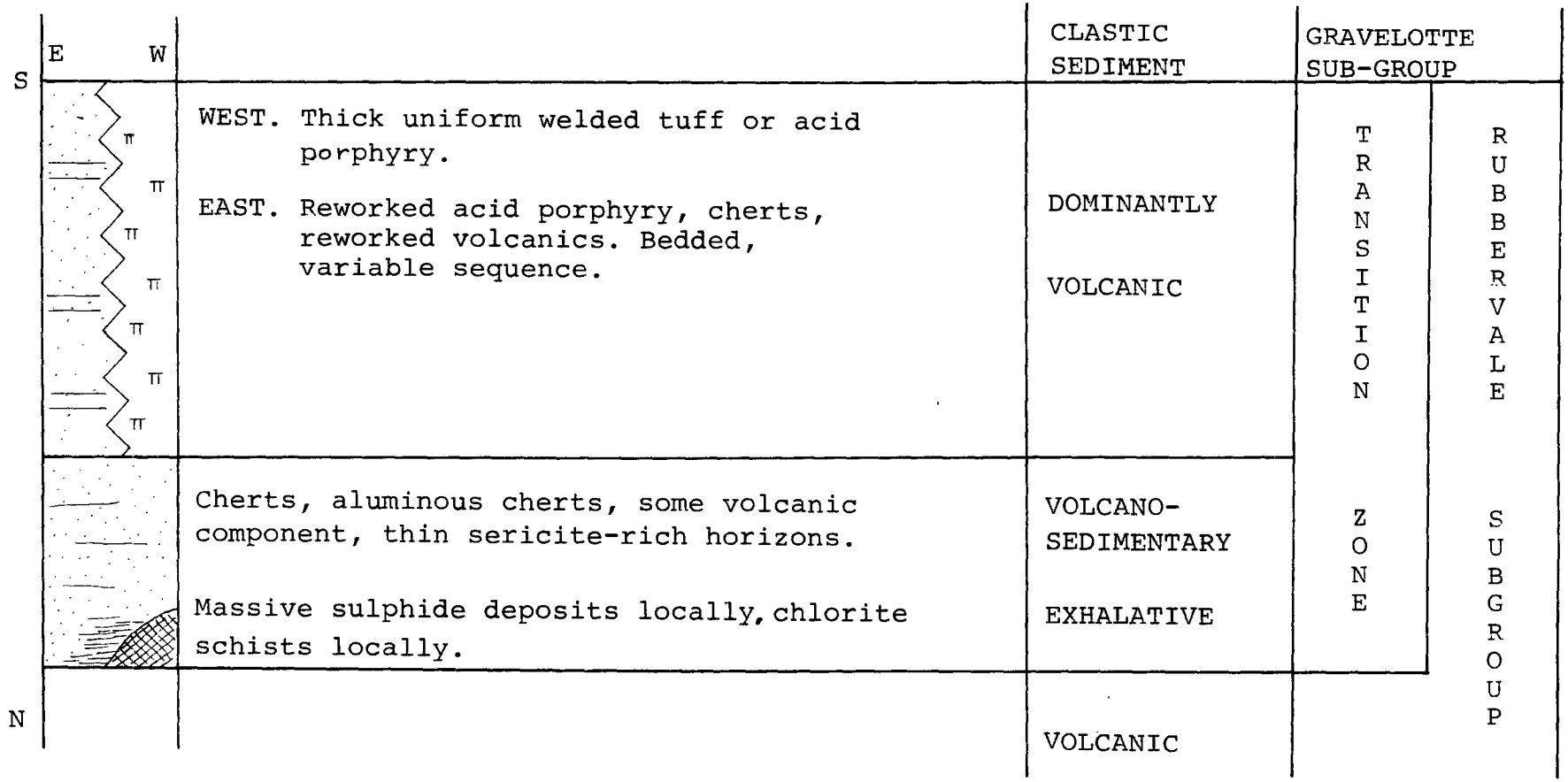

Fig.7. Generalized Stratigraphic Section through the Transition Zone.

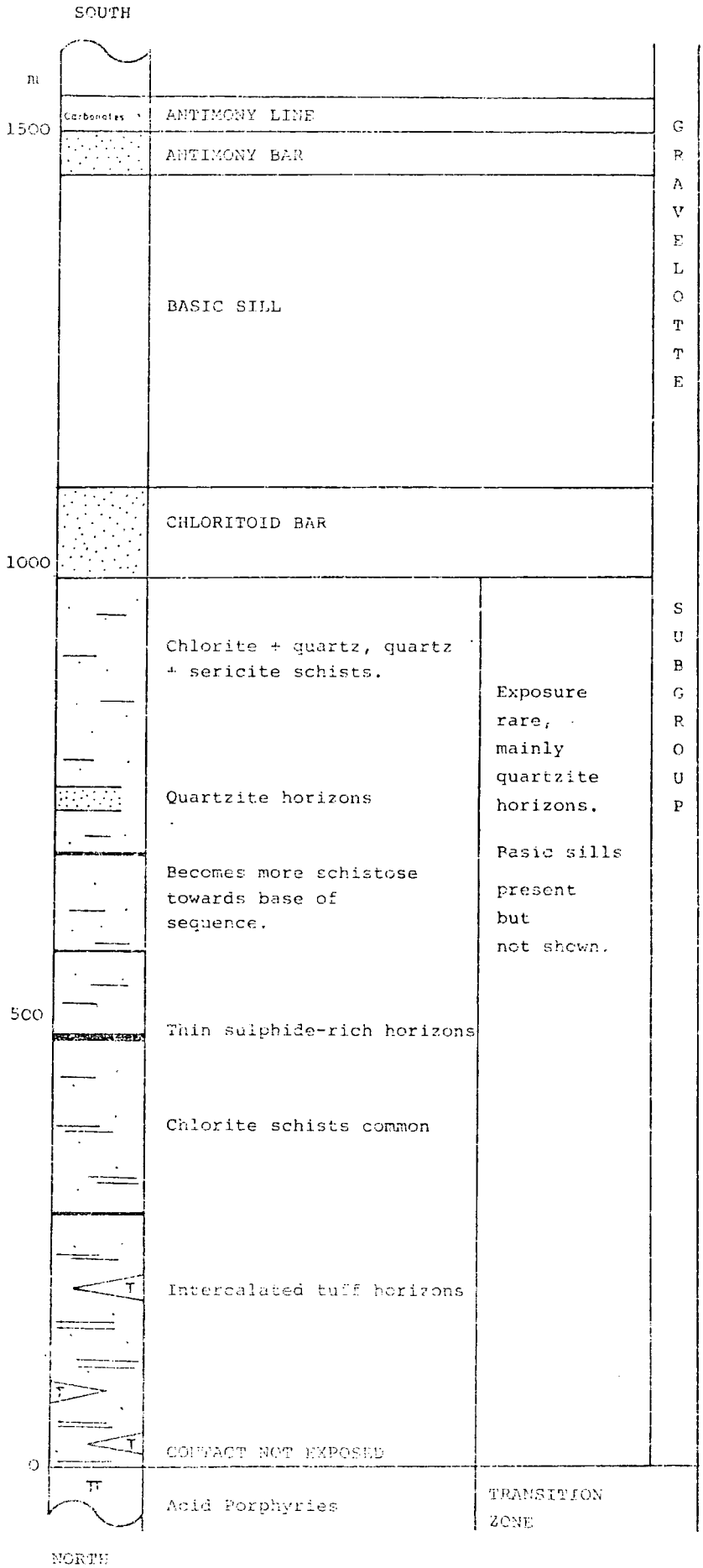

Fig.3. Stratigraphic section through the Gravelotte Subgroup on the farm Solomons Mine.

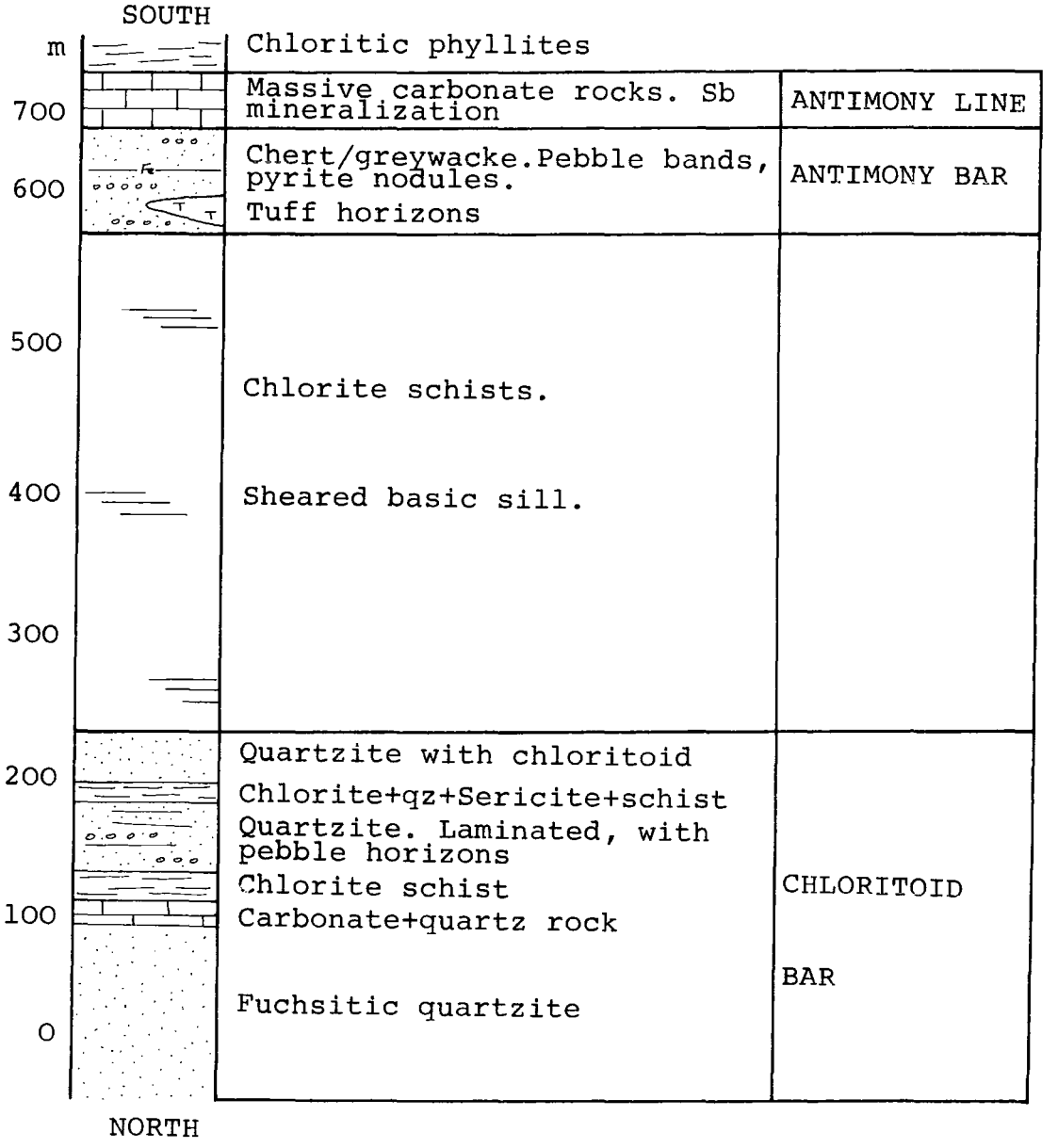

Fig.9. Stratigraphic sequence through the Chloritoid and Antimony Bars.

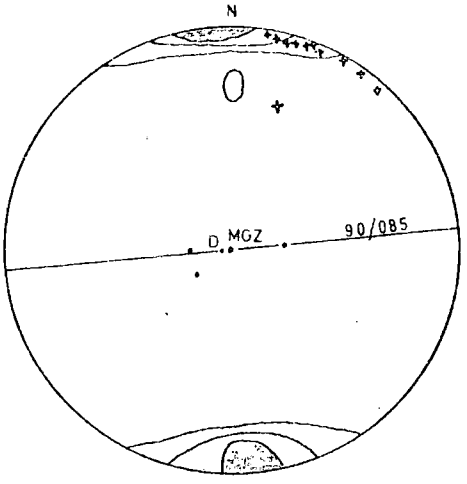

SOLOMONS MINE, MON DESIR

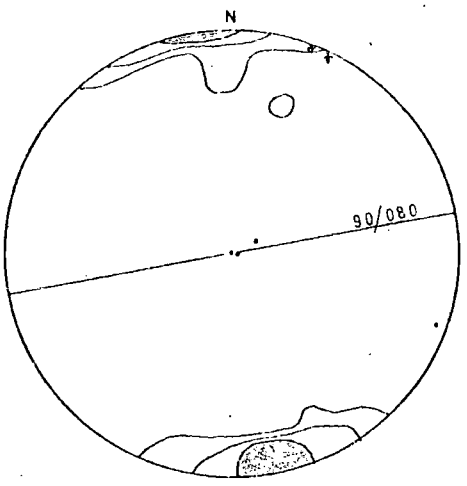

GRAVELOTTE

CONTOURS:

2% per 1% area

8 "

20 "

+ S_2 POLE PLOTS

• L_4 PLOTS

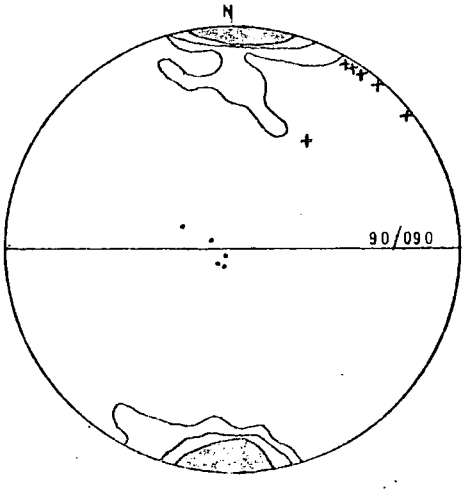

RUBBERVALE, BEESPLAAS

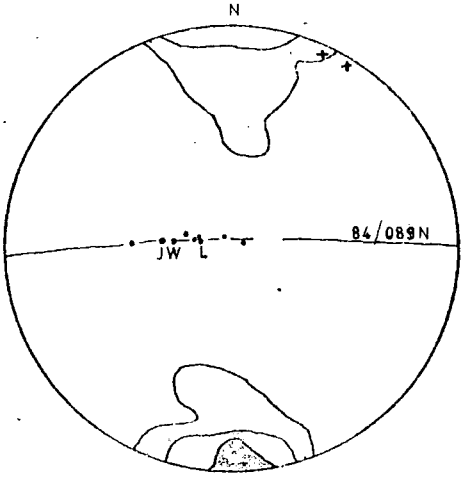

MARANDA, COTTONDALE, ROOIWATER

FIG 10: S_1 POLE PLOTS

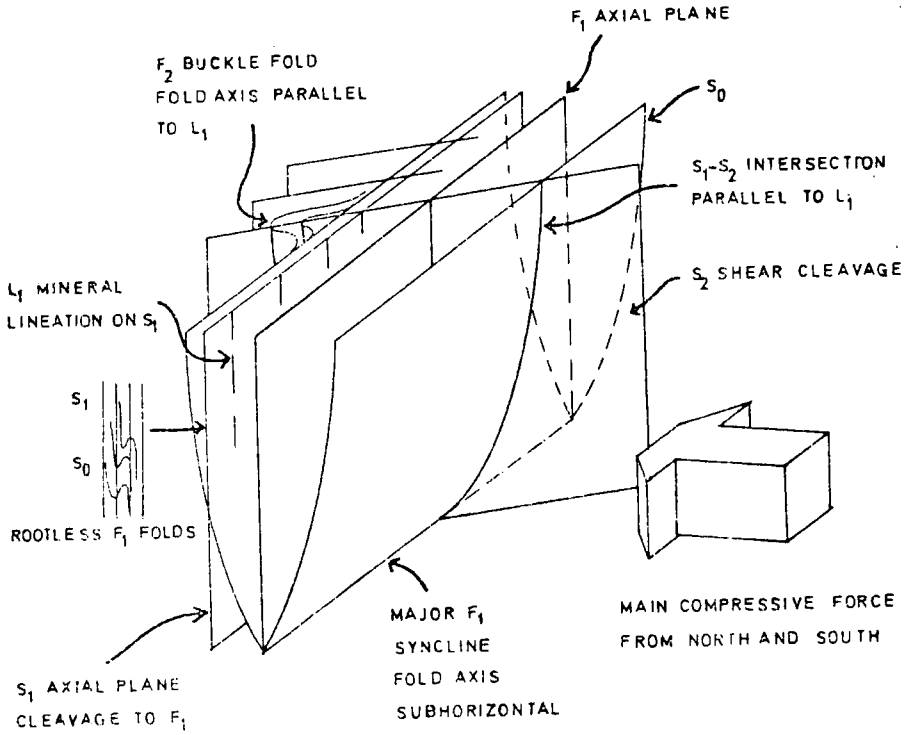

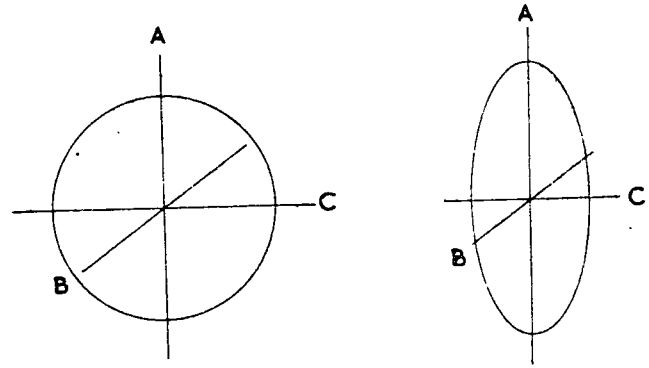

ORIGINAL STRAIN ELLIPSOID

STRAIN ELLIPSOID DURING S_1

PRINCIPAL STRAIN AXES AFTER HOPWOOD (1978)

FIG 11

SCHEMATIC INTERPRETATION OF THE STRUCTURE OF THE MURCHISON RANGE

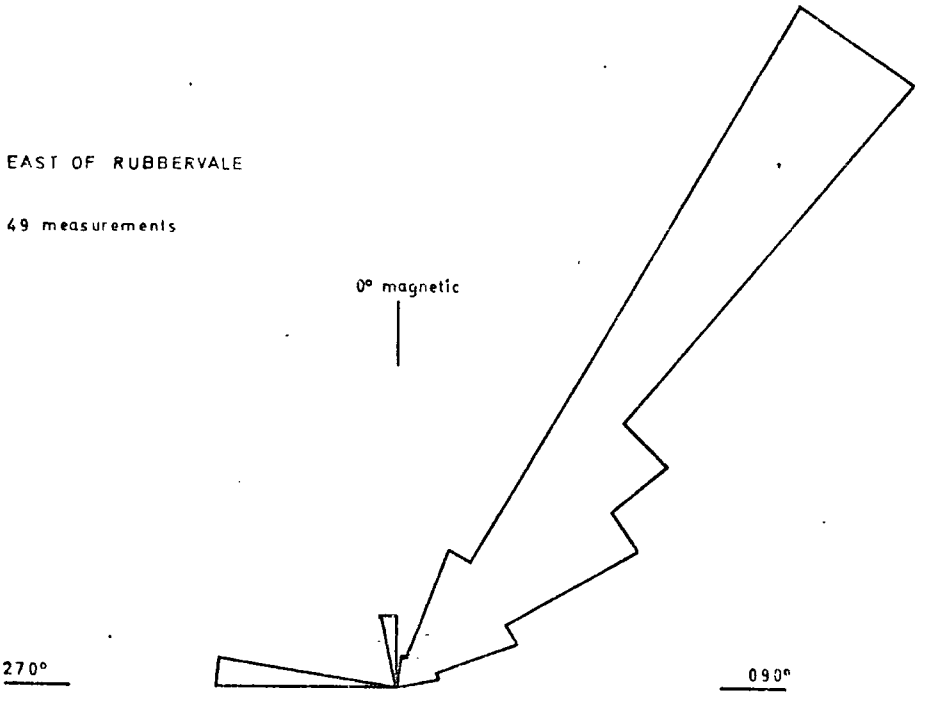

FIG 12 : FRACTURE TRENDS (PLOTTED AS UNIT LENGTH OF FRACTURE TRACE)

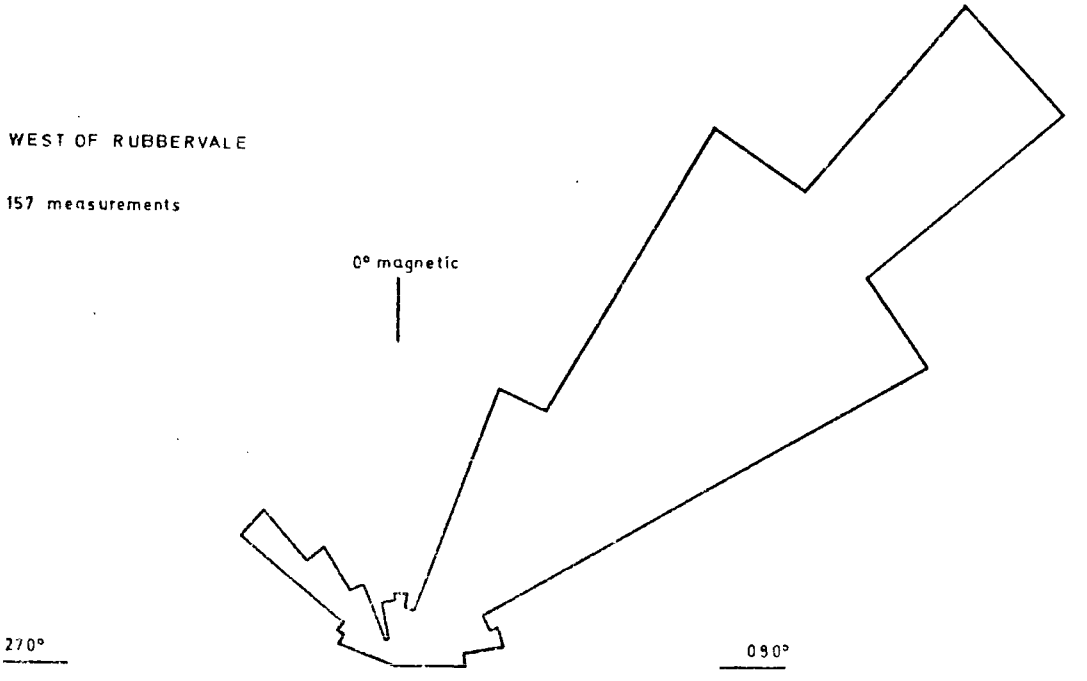

EAST OF RUBBERVALE

16 measurements

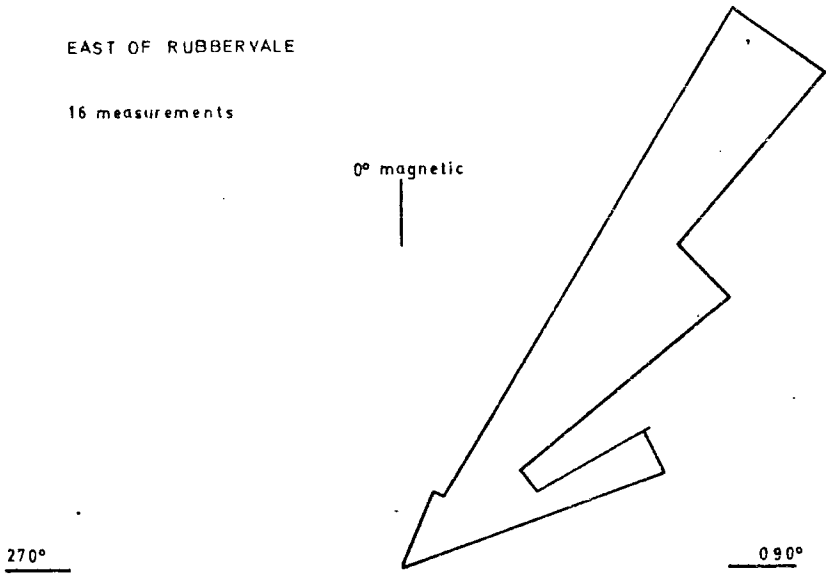

FIG 13: DYKE TRENDS (PLOTTED AS UNIT LENGTH OF SURFACE TRACE)

WEST OF RUBBERVALE

8 measurements

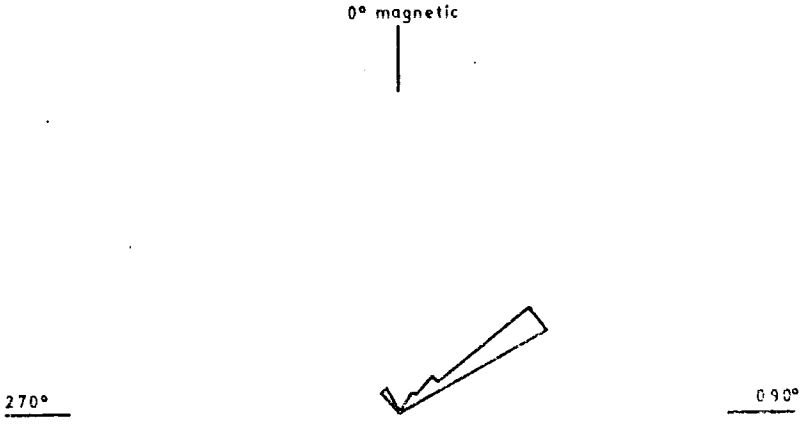

Plate 3. Hexagonal cooling joints (dashed) in felsic intrusive on Rooiwater.

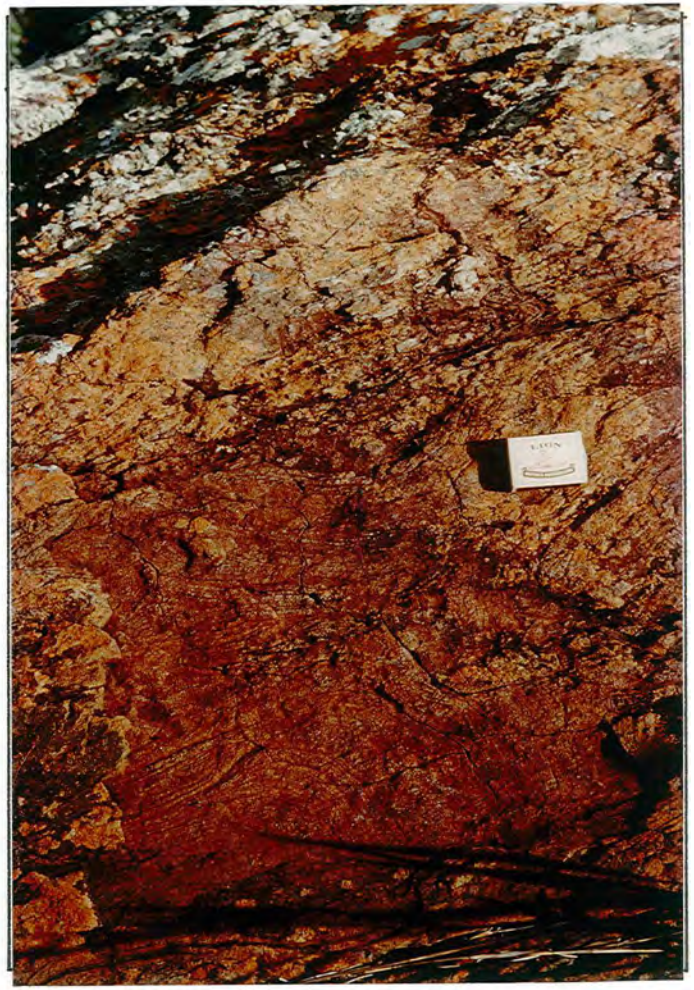

Plate 4. Flow banding and flow-breccia in rhyolites, Maranda.

Plate 5. Coarse felsic pyroclastic rocks, Maranda.

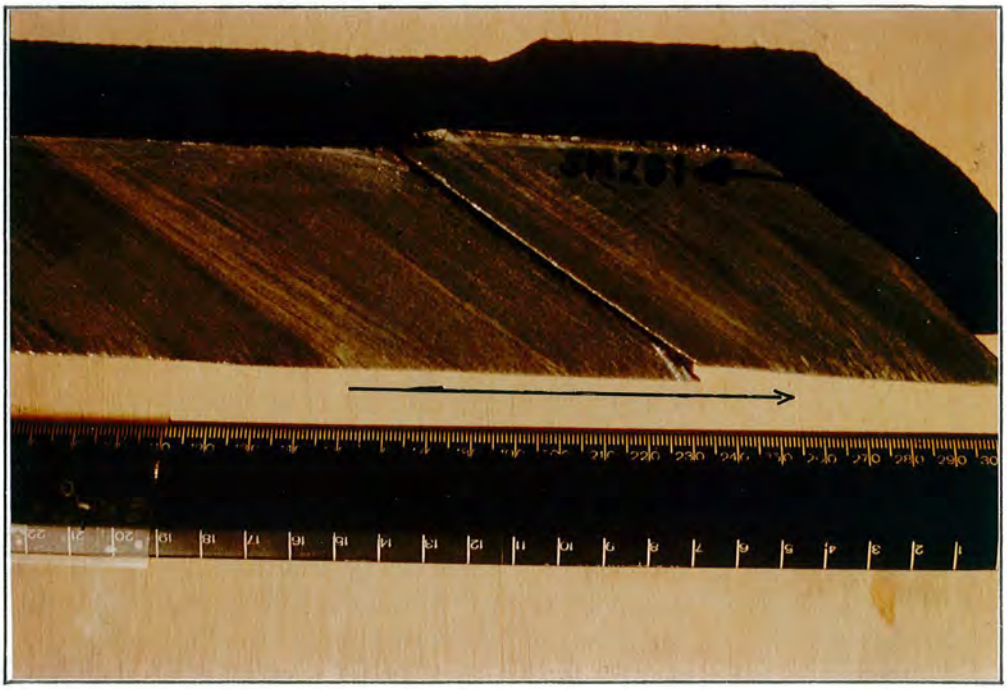

Plate 6. Graded bedding; greywackes from Gravelotte Subgroup, Solomons Mine. Arrow points from base to top of one bed.

Plate 7. Graded bedding; greywackes from the Antimony Bar. Top of bed marked by a thin, dark, pyritic layer. Note diffraction of S_2 in finer grained horizon. Arrow points to top of bed.

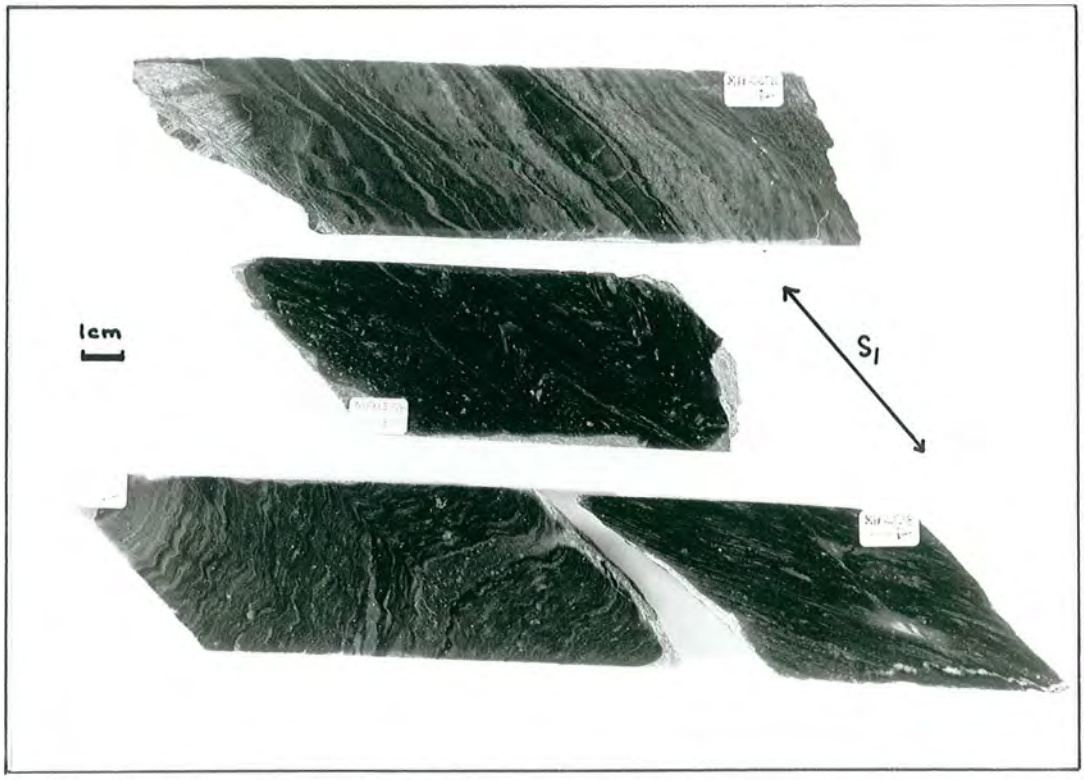

Plate 8. Original bedding, S_0, folded and cut by an axial plane cleavage, S_1. Transition Zone sequence, Maranda.

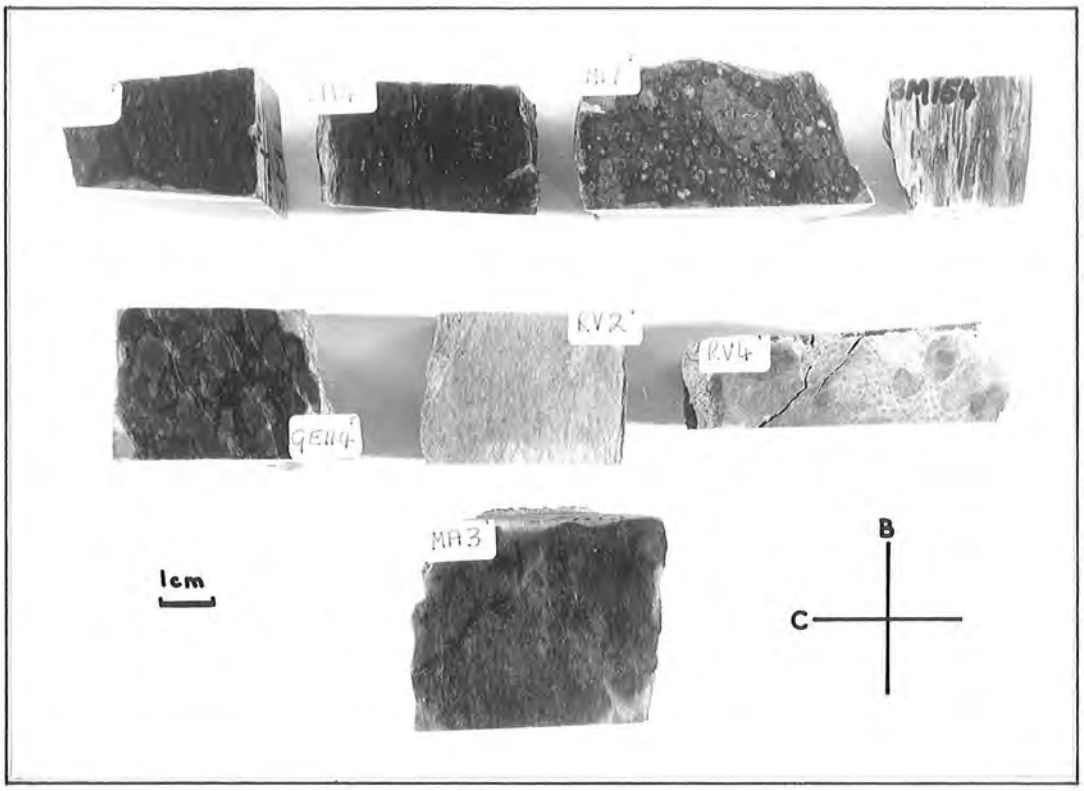

A: viewed in the B-C plane.

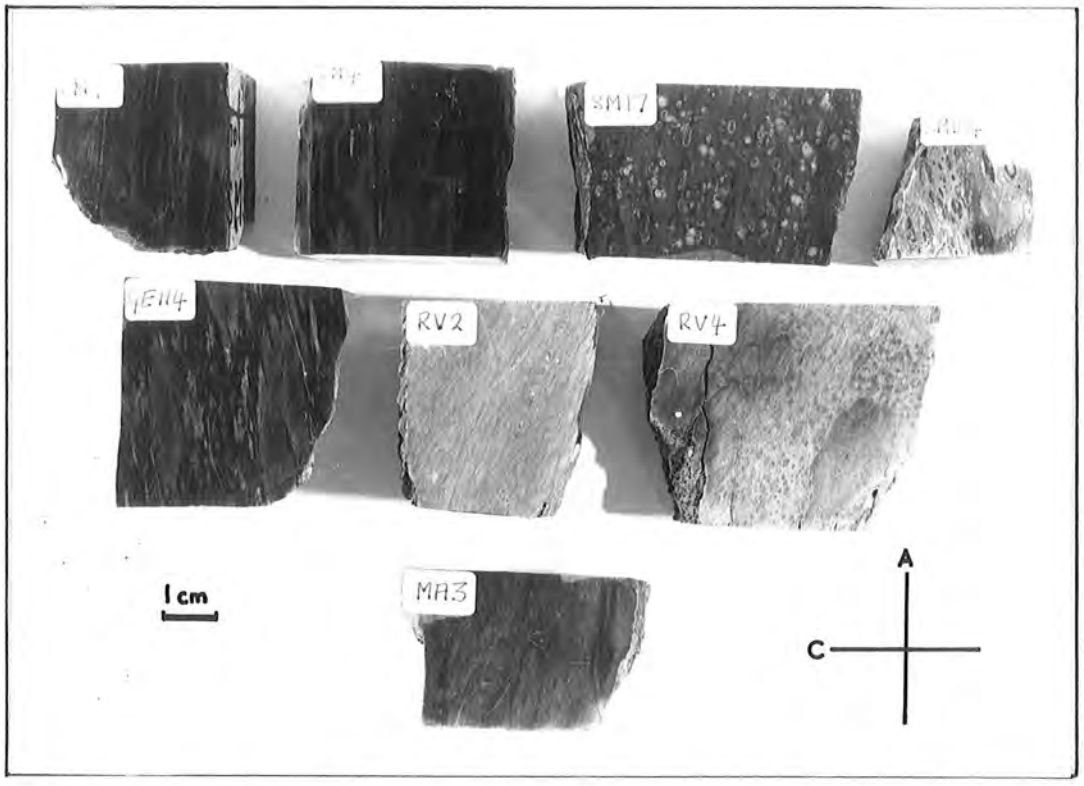

B: viewed in the A-C plane.

Plate 9. Blocks of coarse tuff from the Rubbervale Sub-group. Also refer to fig. 11.
N.B. Sample SM154 transposed on plates A and B.

Plate 10. S_1 and S_2 in tuffs from the Rubbervale Subgroup, Solomons Mine.

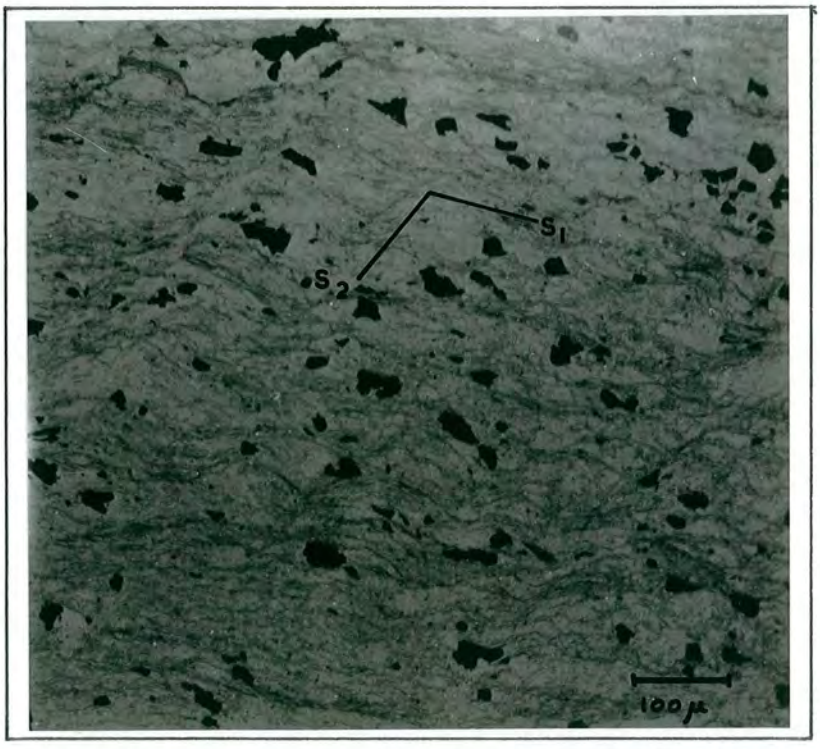

Plate 11. S_1 and S_2 in thin section. Micaceous schists, Transition Zone sequence. Sample MA28W2. Plane polarised light.

Plate 12. F_2 fold in greywackes of the Antimony Bar. S_2 axial plane cleavage parallel to pen. S_1 is parallel to compositional layering/bedding.

Plate 13. Flow banded rhyolite from Rubbervale Sub-group, Solomons Mine.

Table 3. Gravelotte Subgroup: Sediments, compared with similar rocks from the Barberton Mountain Land.

	1	2	3	4	5
Sample	SM16	MD3	SM501		
(wt%)					
SiO_2	87.55	74.08	56.61	66.20	59.80
Al_2O_3	5.24	15.05	19.78	10.20	12.90
Fe_2O_3	1.89	4.46	8.13	7.01	6.56
MgO	2.34	2.64	9.81	4.50	4.44
CaO	2.62	0.00	1.16	1.97	3.18
Na_2O	0.01	0.38	1.70	1.80	2.83
K_2O	0.07	2.33	1.95	1.58	2.23
TiO_2	0.22	0.93	0.62	0.52	0.55
MnO	0.03	0.03	0.11	0.08	0.07
S	0.00	0.01	0.07		
P_2O_5	0.04	0.10	0.06		
Total	100.01	100.01	100.00		
ppm					
Ba	19	266	398	319	626
Nb	5	12	11		
Zr	141	312	139	134	184
Y	12	41	17		
Sr	132	36	85	98	354
Rb	3	45	63	54	90
Zn	15	158	131		
Cu	9	30	23		
Ni	126	94	406	290	160
Cr	565	3164	1112		
La	15	23	15		
Ce	58	40	50		

1. Quartzite

2. Fuchsite-bearing quartzite; Chloritoid Bar.

3. Greywacke-turbidite.

4 & 5. Average greywackes from Fig Tree Group, Barberton Mountsin Land (Condie et al., 1970).

The later S_2 cleavage is superimposed on the planar fabric and is evident as banding and reorientation of micaceous minerals along the S_2 direction, plate 11.

The S_1 schistosity "bends around" and envelopes relict phenocrysts, and outlines deformed fragments. Pressure shadows at the ends of these "obstructions" are filled with coarse grained, randomly oriented metamorphic minerals, plate 20.

Mineral Assemblages

Tuff horizons have an equilibrium mineral assemblage of quartz+sericite+chlorite with minor epidote. Flows have assemblages of quartz+sericite+chlorite, quartz+chlorite+albite+sericite, quartz+sericite+biotite+albite, and quartz+sericite+biotite+calcite. Biotite and chlorite were not observed together. Albite is present as relict feldspar phenocrysts.

Volcanic-sediments of the Transition Zone sequence have a rather varied mineral assemblage dependent on the original chemical composition of the particular horizon. The most common rock type, an aluminous chert, contains quartz+sericite+chlorite$\pm$calcite$\pm$epidote, and quartz+sericite+albite$\pm$chlorite. The acid porphyry horizons contain quartz+sericite+chlorite+albite$\pm$calcite. Within the sedimentary sequence the greywacke-turbidites are now represented by quartz+sericite+chlorite+sphene, quartz+sericite+epidote, and quartz+sericite+albite+chlorite+sphene. Quartzites consist mainly of quartz with minor fuchsite mica and clinozoisite. Chloritoid has been reported from the Chloritoid Bar (Van Eeden et al., 1939).

Basic sills comprise albite+epidote+actinolite+ clinozoisite+chlorite+quartz+calcite.

Electron Microprobe Analysis

Electron microprobe analysis of representatives from the various mineral species was undertaken. The results are discussed below. For details of analytical techniques and full, tabulated results, refer to Appendix B.

a. Chlorite

Analyses of chlorites from tuffs in the volcanic pile plot within a small area of fig. 15 and have a mean Fe^{2+}:Mg ratio of 0.7 within the range 0.6 to 0.9. Thus their composition falls into the field of ripidolite (Hey, 1954, in Deer et al., 1971, p.233).

b. Feldspar

Relic feldspar phenocrysts have compositions of albite, An <3% with two analyses of An 5.5 and An 6.8. Potash content is generally less than 0.1 wt %. Fig. 17.

c. Micas

Sample RV1, a lava, contains green iron-rich biotite with an Fe^{2+}:Mg ratio of 4.0, and sample SM4 contains orange biotite with Fe^{2+}:Mg of 1.04. Sericites have variable ratios, presumably due to variations in the original bulk rock composition; fig. 20. Two micas from sample SM16, a quartzite within the sedimentary sequence, contain 1.24 and 0.58 wt % Cr_2O_3. Fuchsite is a common mineral in the sediments.

d. Epidote

Epidote group minerals were analysed from basic intrusives, volcanic rocks and sediments. In the volcanic and intrusive rocks, Fe_2O_3 content was found to be in the range 12-14 wt %; fig. 16. Iron poor epidote occurs in sample SM16.

Interpretation

These mineral assemblages are characteristic of the Low Grade of metamorphism of Winkler (1974). Chlorite is not in equilibrium with biotite, and the plagioclase composition is less than An 7. Biotite+muscovite is stable, and stilpnomelane was not observed. This would suggest the temperature to be in the range 450-480^{o}C at relatively moderate pressures (Myashiro, 1973; Winkler, 1974); see fig. 14. The metamorphic pressure could not be derived from the above mineral assemblages, but is expected to be greater than 2 kbar (Turner, 1968). Use of the sphalerite geobarometer (see chapter 8) gives a mean tectonic pressure of 5.6 kbar in a range of 4.4 to 7.1 kbar. Minnitt (1975) suggests that the maximum pressure that could have been operative during metamorphism in the eastern part of the Murchison Range was 6 kbar.

5.4.3b Thermal Metamorphism

Following the regional deformation and production of the schistose, Low Grade, metamorphic mineral assemblage, rocks of the Murchison greenstone belt were subjected to a further, thermal event, most probably as a result of intrusion and cooling of the surrounding granite plutons (Annhaeusser, 1973). This resulted in the growth of homotropic, poikiloblastic and porphyroblastic minerals in

rocks of appropriate chemical composition.

In tuffs and sediments biotite (±muscovite) may develop as a replacement of chlorite. The footwall alteration zones to the MGZ and J massive sulphide deposits sometimes contain the assemblage amphibole±biotite±albite, and in one sample coarse chlorite developed, partially replaced by biotite at a later stage. The minerals spessartine garnet±biotite± albite are present in Mn-rich mineralized zones.

Biotite

Orange biotite is common in quartz+chlorite±sericite schists of the Transition Zone sequence, in the footwall alteration zone to the J deposit, and more rarely in flows, sediments and acid porphyries.

The biotite is pleochroic from orange-brown to colourless, and forms homotropic porphyroblasts up to 1 mm in size, replacing chlorite. Traces of the original schistosity can be observed to continue undeformed through the biotites; plate 21. In some instances partial regression to green chlorite has taken place along cleavage planes and grain margins, and in one sample orange biotite is rimmed, and replaced, by green iron-rich biotite.

A plot of the microprobe analyses of several of these biotites is given in fig. 20 in terms of end-member molecular percentages of Al_2O_3, FeO (total), and MgO.

Chlorite

In sample SM8S2 from the footwall alteration zone to the MGZ deposit, coarse porphyroblastic chlorites were observed in the "chlorite schist". These chlorites are up to 1 mm in length and have a composition similar to chlorites in the

surrounding matrix, and chlorites of the regional or dynamic metamorphic event, fig. 15. In places they are replaced by orange biotite.

Garnet

The Transition Zone assemblage at the L-W mineralized locality is of a different chemistry to that at the MGZ where post-tectonic biotite is common. Although biotite does occur, it is subordinate to spessartine garnet and/or porphyroblastic albite. These minerals are common along certain horizons below and within the mineralized zones. Garnet and albite tend to occur separately, but where adjacent appear to be in mutual equilibrium.

The garnets are typically up to 3 mm in size and their poikiloblastic texture allows the earlier metamorphic record to be traced. They are best developed within, or adjacent to sphalerite+phyrite bearing bands and horizons, and appear to have been formed at the expense of pre-existing msucovite; plate 22.

Electron microprobe analyses of several garnets show a zonation from a Mn-rich core to Fe-rich margin; the maximum variation observed was from 21.4 wt % MnO + 15.4 wt % FeO (total iron) to 15.6 wt % MnO + 20.3 wt % FeO.

In sample MA23W2, garnet core compositions approximate to the margin compositions of the above mentioned garnets, and the margins are Ca-rich. Both the MnO and FeO content decrease slightly with increasing CaO. See fig. 21.

Garnets with an MnO content of 6-8 wt % occur in thin cherty horizons associated with minor sulphide mineralization encountered in a drill core from an area 650 m north

of the MGZ locality, on the farm Solomons Mine. Zonation within these garnets is minor, although two garnets contain Fe-rich and Ca-rich margins respectively; fig. 21.

Amphibole

The development of unambiguous post-tectonic amphibole is limited to the footwall alteration zones of the MGZ and J massive sulphide deposits. Tabular and needle-like crystals of pale green amphibole occur randomly within the mineralized "chlorite schist" horizons immediately beneath the massive sulphide bodies. In several cases the original schistosity continues unaltered through the amphibole crystal implying conditions of static growth; plate 23.

Chemical zonation of the amphiboles was not encountered either from optical observations or from microprobe analyses. Electron microprobe analyses of several amphiboles indicates them to be actinolite with Fe^{2+}:Mg ratios of 0.2 at the MGZ and 0.3 at the J locality. The Al_2O_3 contact is less than 3 wt %, fig. 22. In sample SM1S2 from the MGZ locality, amphibole analyses have Al_2O_3 contents of up to 8.6 wt % and plot along a trend towards the hornblende composition on fig. 22. Zonation was not observed within these amphiboles.

Coarse, euhedral amphiboles occur as part of the gangue mineral assemblage in the massive sulphide bodies. At the MGZ deposit these are of actinolite composition, with Fe^{2+}:Mg ratio of 0.2 although they are Mg rich, and Fe (total)poor, with respect to the amphiboles in the footwall. However, it is unclear as to which metamorphic event these amphiboles belong.

The numerous basic sills and intrusives within the volcanic and sedimentary pile contain amphibole as a major component with feldspar. Within the sills, the amphibole occurs as coarse interlocking prisms and tabular crystals often with imperfect margins. Where the rock is foliated the amphiboles generally follow the foliation, but in the more common massive sills amphibole is randomly interlocked with feldspar.

Optically the amphiboles may be zoned with cores and patches of light green actinolite having a poikiloblastic texture with quartz inclusions, plate 24. The margins and rims are dark hornblende and free from inclusions.

From this it is concluded that the original actinolite is being replaced by or changed to hornblende, from the grain boundaries inwards. Each crystal is continuous in that the hornblende does not form overgrowths and the light green-dark green boundary is somewhat diffuse. It is believed, therefore that actinolite was the stable amphibole during the regional metamorphism, forming poikiloblastic laths and prismatic crystals, which, during the subsequent thermal event, were replaced, albeit partially, by hornblende with expulsion or loss of inclusions.

Microprobe analyses of the light green (core) and dark green (margin) illustrate this change. The maximum Fe^{2+}:Mg ratio change is from 0.6 at Al_2O_3 of 2.6 wt % to 1.4 at Al_2O_3 of 14.6 wt%, fig.23.

In sample MA4K1 several small amphiboles have compositions between the two extremes suggesting a solid solution series rather than a compositional "jump".

It is noted that the actinolite to hornblende trend of fig. 23 is paralleled by amphibole compositions from sample SM1S2 in fig. 22.

Albite

Post-tectonic feldspar is limited to the aluminous cherts of the Transition Zone at the L-W and J localities and the footwall alteration zones to the MGZ and J sulphide deposits. It occurs as rounded porphyroblasts, usually 1 mm in diameter, as irregular, interlocking masses and as euhedral grains with albite twinning. Optically it is albite with composition An < 10%. Traces of the earlier schistosity can be seen running undeformed through the crystals; plate 25.

Microprobe analyses give compositions of An<6% although one sample, MA6J4, recorded compositions of between An 11.5 and An 18.3. The K_2O content is less than 0.1 wt % most probably due to the general low K_2O content in the host rock (fig. 18).

Interpretation

The original bulk chemistry of the rocks has, to a large degree, determined the type and amount of minerals developed during this later thermal event. Biotite developed by replacement of chlorite where potash was available. Spessartine-rich garnet developed in rocks rich in manganese and which also happen to contain disseminated sulphides. Albite was formed in rocks where soda was available and which did not already contain feldspar.

Development of amphibole rather than, and in some cases as well as, biotite as a replacement of chlorite in the alteration zones to the massive sulphide deposits may be due to the relative lack of potash and generally "basic" chemistry of the rocks. A relative lack of alumina may also account for the lack of hornblende, with the exception of sample SM1S2 referred to above.

The compositional changes from core to margin in garnet and amphibole are indicative of prograde metamorphism (Sturt, 1962; Engel and Engel, 1962; Winkler, 1967, 1974). According to Winkler (1974) the actinolite-hornblende transition in mafic rocks occurs at 500°C virtually irrespective of pressure. The plagioclase composition of An<6% would suggest temperatures of less than 500°C. The presence of at least one instance of An 11.5 - 18.3 is probably due to chemical control. The presence of spessartine-rich garnet is indicative of low temperature and pressure, becoming iron-rich with increasing temperature. Biotite forming from chlorite at these relatively low temperatures is indicative of low pressure metamorphism (Myashiro, 1973).

From these various mineralogical indications it is postulated that the second metamorphic event was thermal with temperatures rising from 480°C to at least 500°C at pressures of less than 3 kbar. Static mineral growth is indicated by the lack of deformation of schistosity relicts within the new mineral grains. See also fig. 14.

5.4.3c Rooiwater Igneous Complex

General

The Rooiwater Igneous Complex has been subjected to the same deformation and metamorphism as the overlying

volcanic and sedimentary sequences. However, due to its massive nature, the Complex acted as a resistant block with only partial development of a cataclastic S_1 plane, and virtual absence of S_2.

In thin section, rocks of the Complex exhibit crush or mortar texture, with thin streaks and patches of fine grained recrystallized metamorphic minerals separating areas or large crystals of original, partially altered igneous minerals, plate 26. These streaks are vaguely parallel and on surface form the S_1 planar trend.

The mineral assemblage of quartz+albite (An 1.4) in the quartz-diorite phase is suggestive of Low Grade regional metamorphism (Winkler, 1974), but the assemblage in the gabbros, whilst having a fabric characteristic of regional, dynamic metamorphism, has a plagioclase component of An $>$ 18 with hornblende stable. It is probable that the later thermal event influenced the composition of these mineral assemblages without alteration to the fabric.

Gabbro Phase

In hand specimen the gabbros comprise varying amounts of coarse, interlocking amphibole and feldspar, with lesser opaque spinels. In thin section the amphibole is seen to be composed of aligned aggregates of fine grained hornblende pseudomorphing an original stumpy mafic mineral. Feldspars are very heavily altered and pseudomorphed by epidote-group minerals although relicts of the original feldspar can be observed. Microprobe analyses of one of these feldspars indicates the original composition to have been plagioclase of An 42, now progressively and patchily albitized, the

lowest composition being An 18; fig. 19. There is no evidence of original compositional zonation within these feldspars. The thin streaks and patches comprising the mortar or crush texture consist of fine grained quartz+ hornblende+epidote+oligoclase(An 18)+chlorite.

Sample QA1A, from an amphibolite horizon near the northern edge of the "gabbro", contains coarse interlocking amphiboles which are optically and compositionally zoned from pale green cores to dark green margins similar to amphiboles from basic intrusives; see section 5.4.3b. The dark green margins are hornblendic with compositions similar to those in the basic intrusives, fig. 23. However, the cores, possible relict original amphiboles, are hornblendic with a higher Al_2O_3 content and slightly lower Fe^{2+}:Mg ratios than the margins.

Quartz-Diorite Phase

This is essentially an albite+quartz rock with very minor amounts of epidote, muscovite and hornblende. In thin section the texture consists of coarse albite and quartz crystals and anhedral grains in a fine grained matrix of quartz+albite+accessories. Granophyric texture is common, plate 27. Large grains exhibit strain extinction, partial sub-grain recrystallization, deformation twin lamellae and bent, kinked albite twins. Grain boundaries tend to be sutured and interpenetrant. The relationship between the matrix and the coarse grains is one of crush or mortar texture, plate 26. This crush texture has a vague planar fabric.

Microprobe analyses of the feldspars give an albite composition of An < 1.4 and a potash content < 0.15 wt %. One crystal was optically zoned with a large core area full of minute inclusions, surrounded by a clear rim. The crystal was overgrown by optically continuous albite. Analyses of the core area showed it to have Ca:Na:K ratios of 3.1:92.9:4.0; the margin was almost pure albite of ratios 1.5:97.9:0.6, fig. 19. Small anhedral grains of feldspar with well developed polysynthetic crosshatched twinning were originally thought to be microcline. Subsequent analyses showed these to be almost pure albite. The twinning is probably the result of deformation.

5.4.3d Summary

Two distinct periods of metamorphism have affected the Murchison greenstone belt; see fig. 14. The earlier phase accompanied the general deformation with development of a planar and linear metamorphic fabric. In rocks that were originally rhyolite flows and tuffs, the new mineral assemblage is quartz+sericite+biotite/chlorite±albite, and in sediments quartz+sericite±chlorite±sphene±epidote. Basic sills comprise albite+epidote+actinolite+clinozoisite+ chlorite+quartz+calcite. Albites have compositions of An < 7 wt % and chlorite lies in the field of ripidolite. These are characteristic of the Low Grade of metamorphism of Winkler (1974) with temperatures in the range 450-480^{o}C at pressures of up to 5.6 kbar.

This was followed by a static event characterized by the sporadic development of homotropic, poikiloblastic chlorite, biotite, albite, hornblende and garnet in rocks

of appropriate chemical compositions. As temperatures rose, chlorite crystallized initially but was subsequently replaced by orange biotite. Garnet composition changed from a Mn-rich core to Fe or Ca-rich margin. Hornblende partially replaces actinolite and the composition of albite does not exceed An 6. These observations suggest final temperatures of around 500^{o}C (Winkler, 1974). The metamorphic pressure was < 3 kbar. Retrograde effects are limited to minor chlorite replacement of biotite.

The Rooiwater Igneous Complex tended to resist deformation and a crush or mortar texture developed. Within these crush zones the mineral assemblage is quartz+actinolite+ chlorite+albite, characteristic of the first metamorphic event. Feldspars are partially albitized to An 18 from an original composition of An 42, and hornblendes have rims with lower Al_2O_3 content and lower Fe^{2+}:Mg ratios, similar to the hornblendes developed in basic sills during thermal metamorphism.

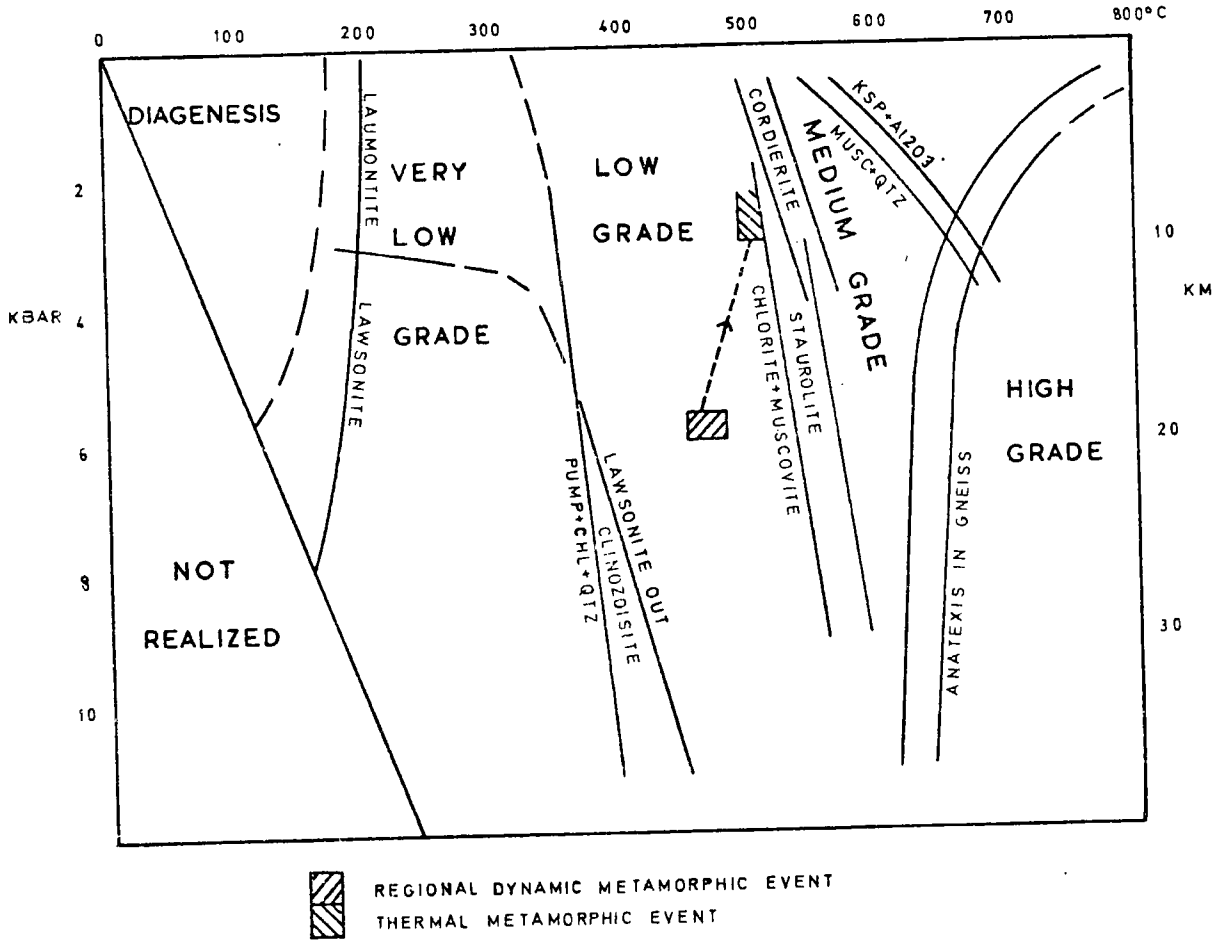

FIG 14 PRESSURE-TEMPERATURE DIAGRAM, AFTER WINKLER (1974)

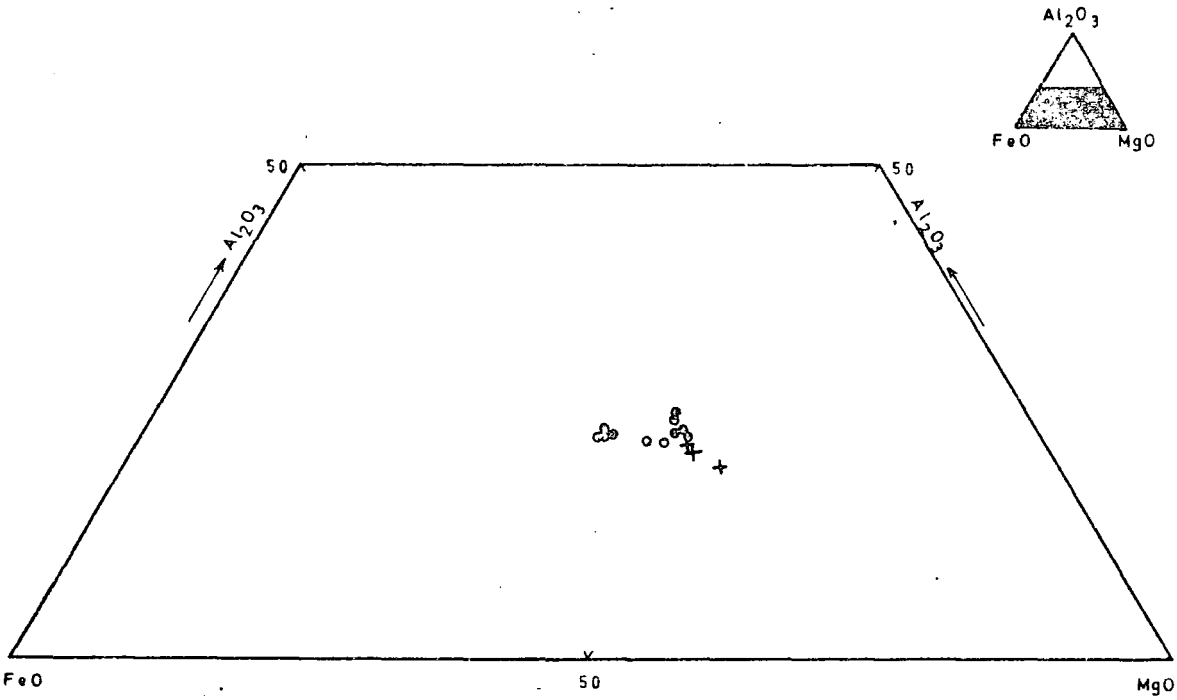

o REGIONAL METAMORPHISM + THERMAL METAMORPHISM (SM8S2)

FIG 15 CHLORITE COMPOSITIONS

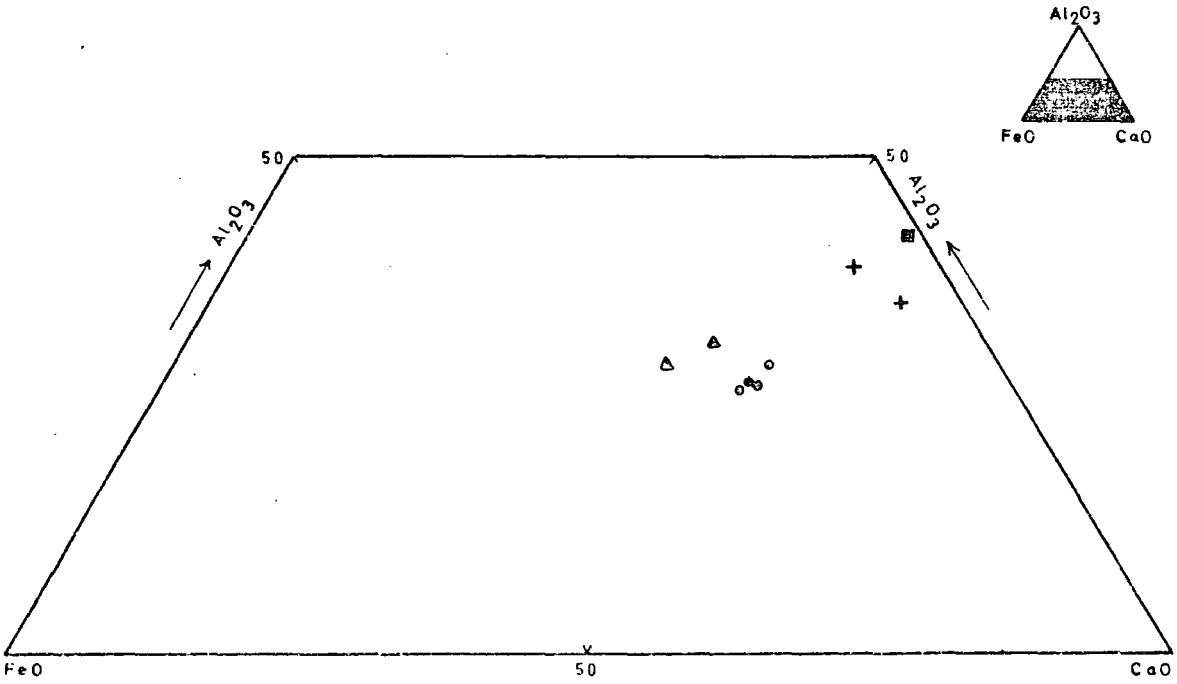

⊕ BASIC SILL (MA4K1) △ TUFF (MA6J4)

+ GABBRO (MD1) ▣ SEDIMENT (SM16)

FIG 16 EPIDOTE COMPOSITIONS

VALUES IN MOLECULAR PERCENTAGE END MEMBERS.

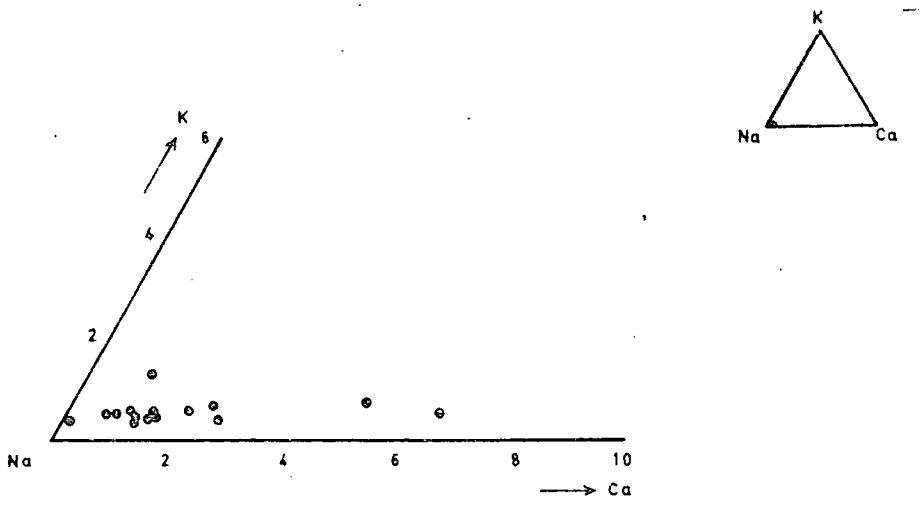

FIG 17 FELDSPAR COMPOSITION: REGIONAL METAMORPHISM

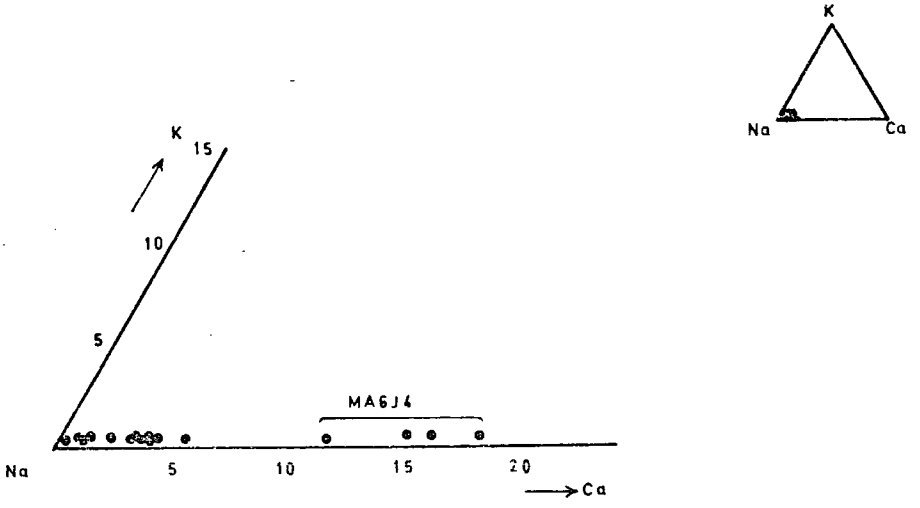

FIG 18 FELDSPAR COMPOSITION: THERMAL METAMORPHISM

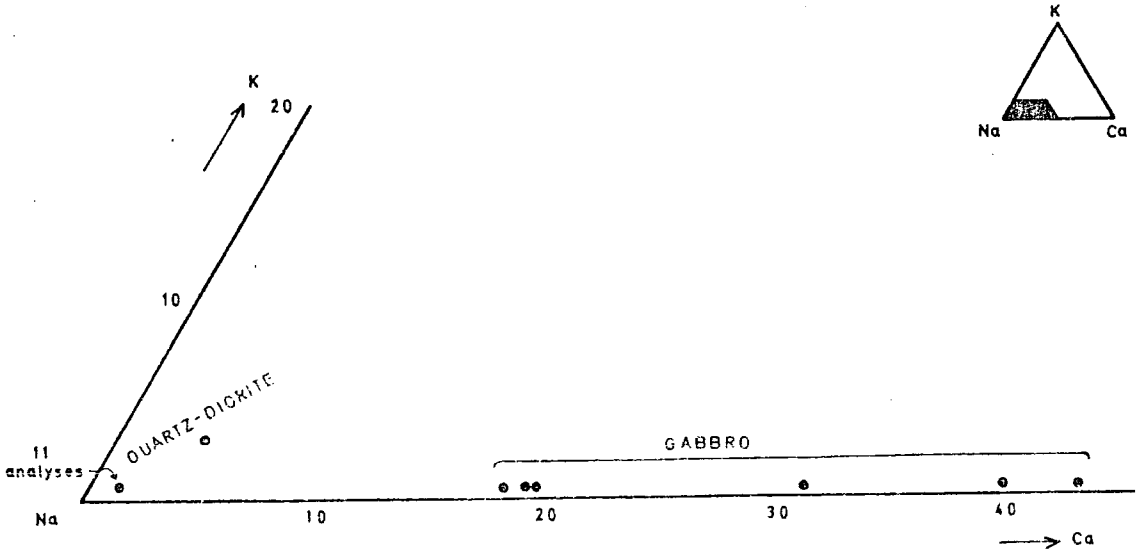

FIG 19 FELDSPAR COMPOSITION: ROOIWATER IGNEOUS COMPLEX

VALUES IN WT.%

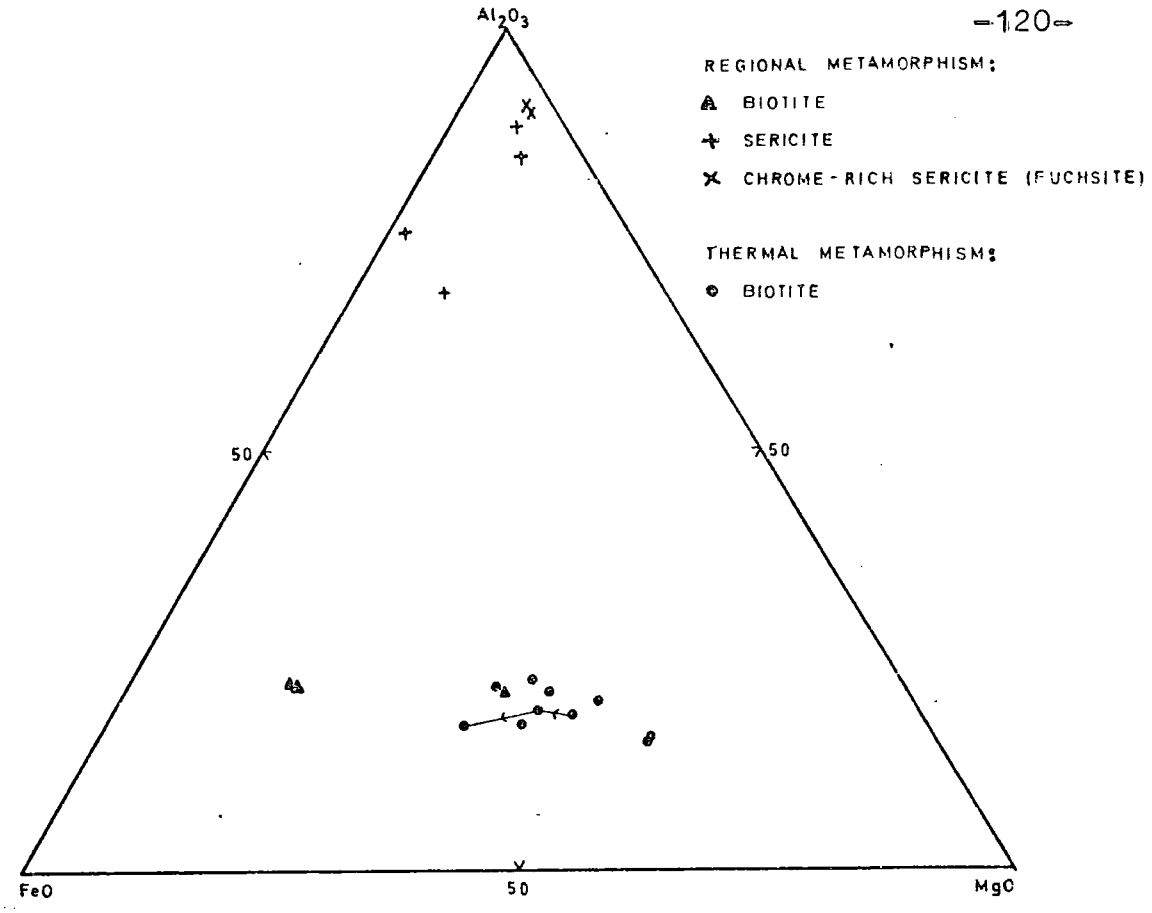

FIG 20 MICA COMPOSITIONS

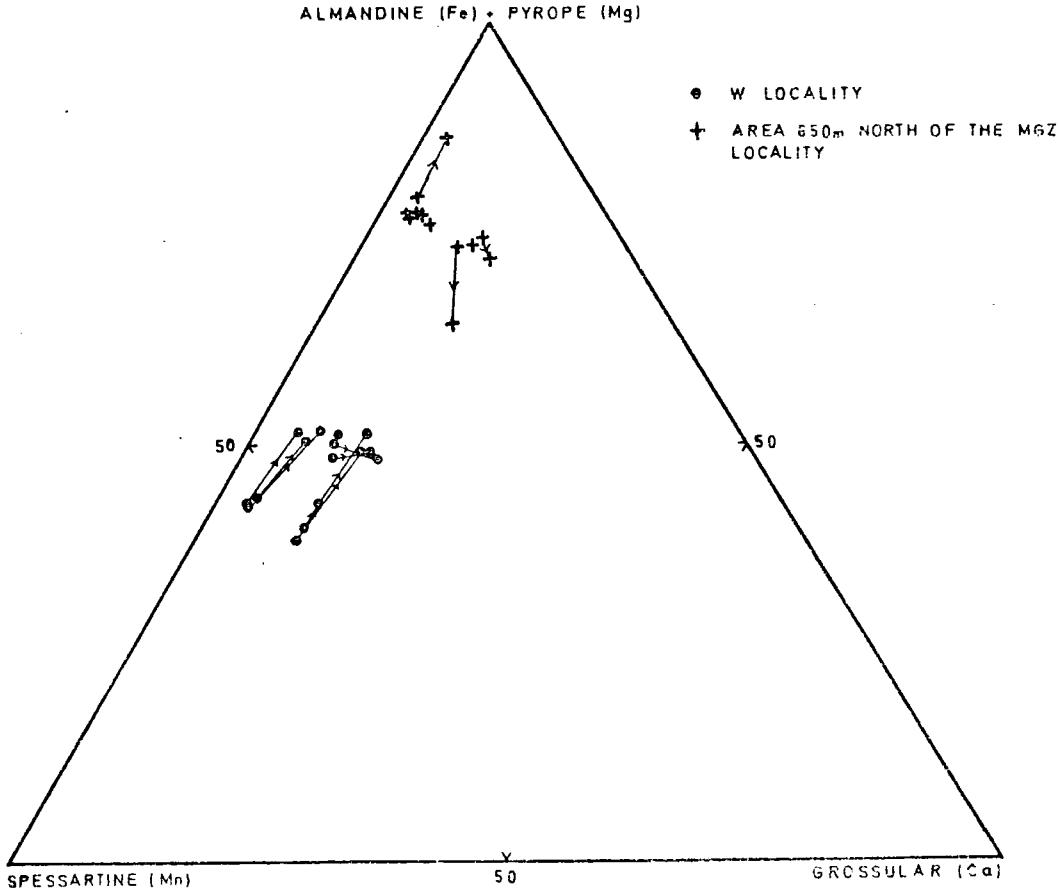

FIG 21 GARNET COMPOSITIONS : THERMAL METAMORPHISM

VALUES IN MOLECULAR PERCENTAGE END MEMBERS

TIE LINES JOIN SINGLE CRYSTAL. ARROW POINTS FROM CORE TO MARGIN

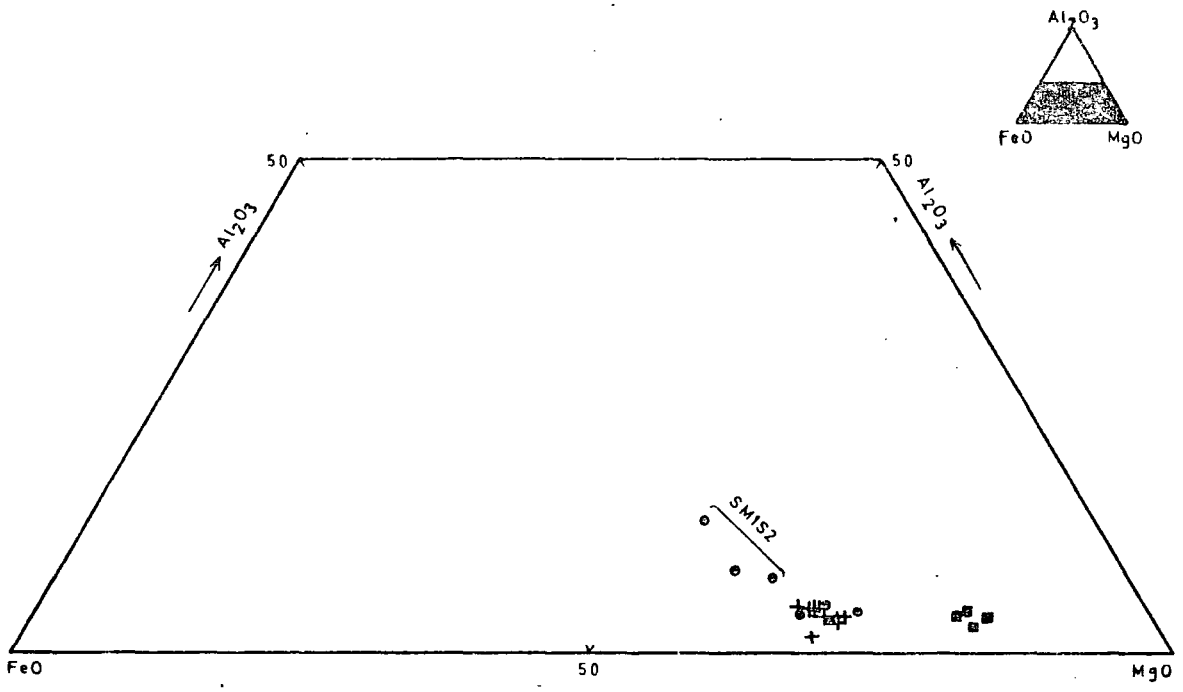

● MGZ CHLORITE SCHIST UNIT (UNMINERALIZED)

+ J FOOTWALL ALTERATION ZONE ■ MGZ MINERALIZED CHERT UNIT

FIG 22 AMPHIBOLE COMPOSITIONS: THERMAL METAMORPHISM

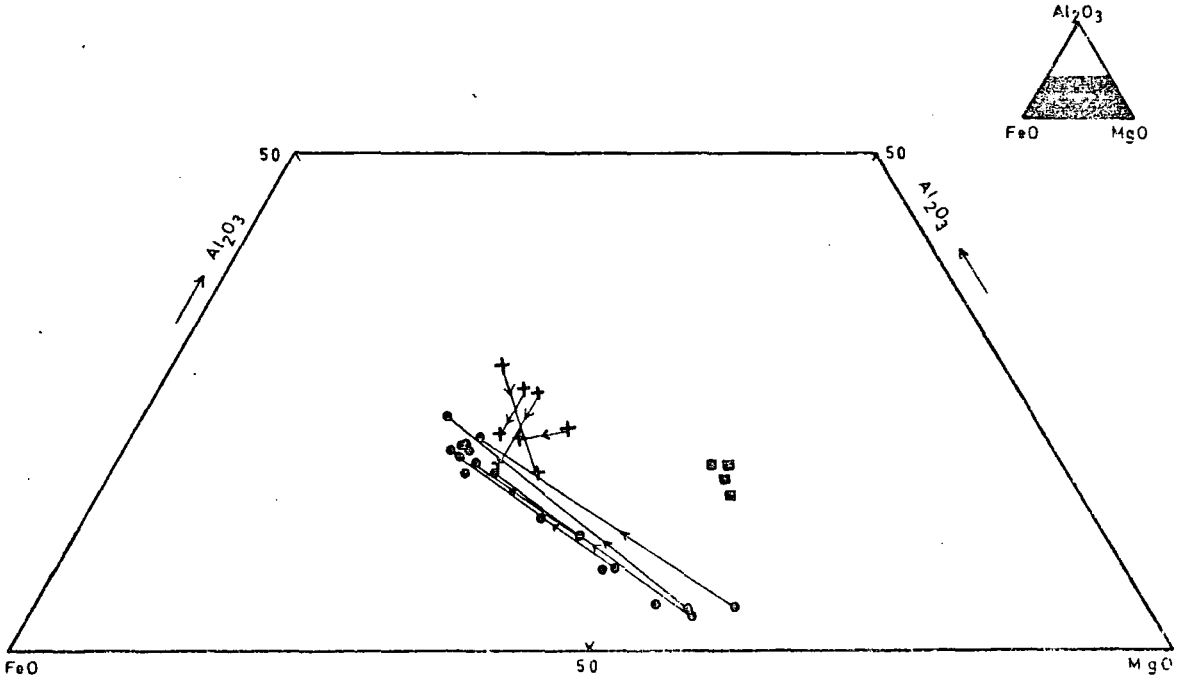

● BASIC SILLS

+ BASE (QA1A) } OF GABBRO

▨ TOP (MD1) }

TIE LINES JOIN SINGLE CRYSTAL. ARROW POINTS FROM CORE TO MARGIN.

FIG 23 AMPHIBOLE COMPOSITIONS: BASIC SILLS & GABBRO

VALUES IN MOLECULAR PERCENTAGE END MEMBERS

Plate 14. Stages in recrystallization of quartz phenocrysts. Scale bar on plates A, B and D, is 100 microns, or 0.1 mm.

A: relatively fresh phenocrysts with deep embayment. Sample RV3, crossed polars.

B: phenocryst with overgrowth, now fractured with incipient granular recrystallization. Sample RV7, crossed polars.

C: increased, granular recrystallization and streaking out of quartz. Sample SM204, crossed polars.

D: final stage. Lens of recrystallized quartz. Sample SM204, crossed polars.

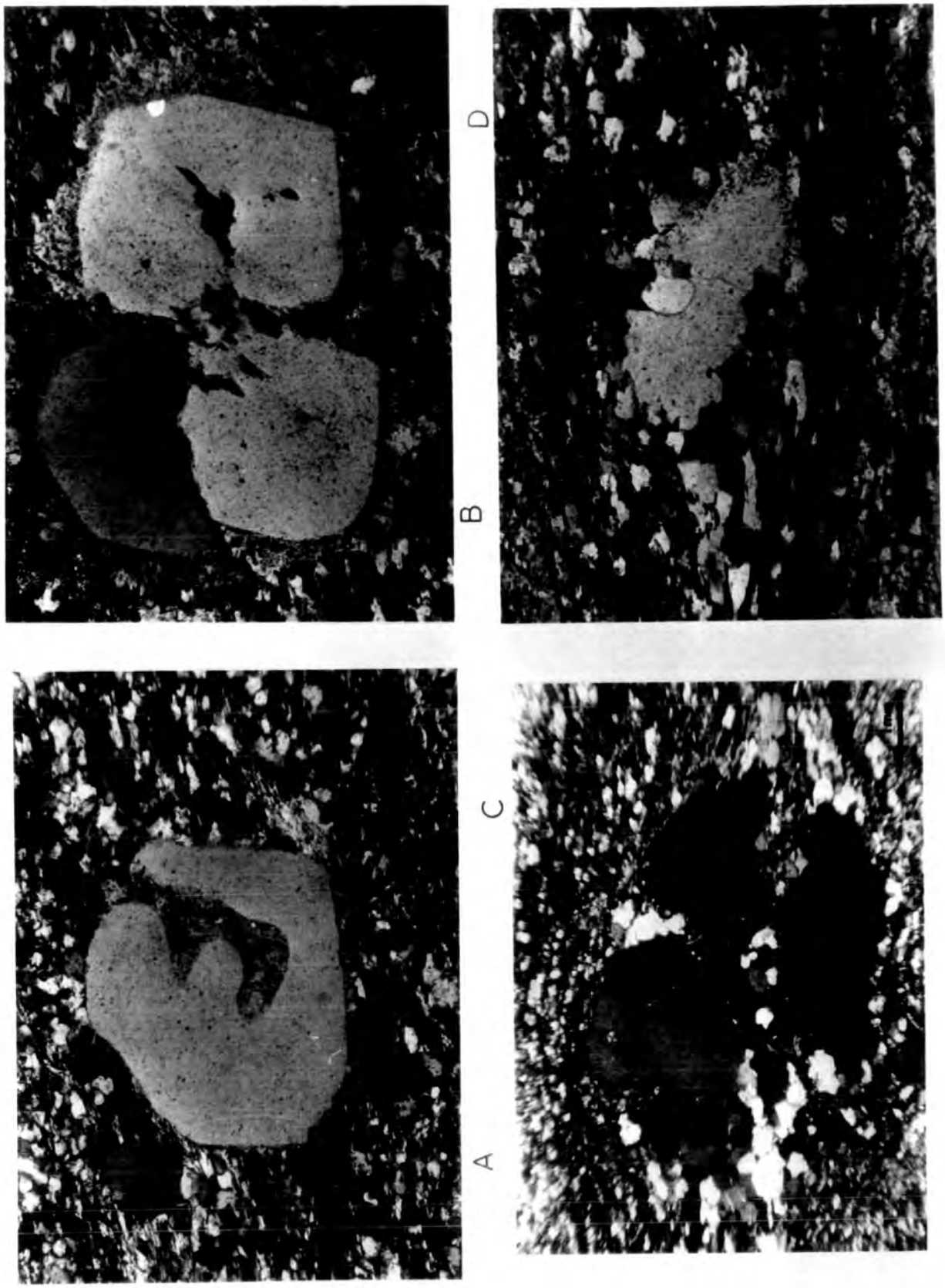
B
D
A
C

Plate 15. Original, twinned, feldspar phenocryst; now almost pure albite. Sample SM204, crossed polars.

Plate 16. Devitrification spherulites of quartz and alkali feldspar in acid porphyry, W locality. Sample MA18W2, crossed polars.

Plate 17. Quartz grain with inclusions; representing an original, devitrification spherulite. Sheared tuff, sample SM11S1, crossed polars.

Plate 18. Typical basic sill. Opaque spinels - white; amphibole - grey; feldspar - dark. Sample MA4K1. Print of thin section.

16

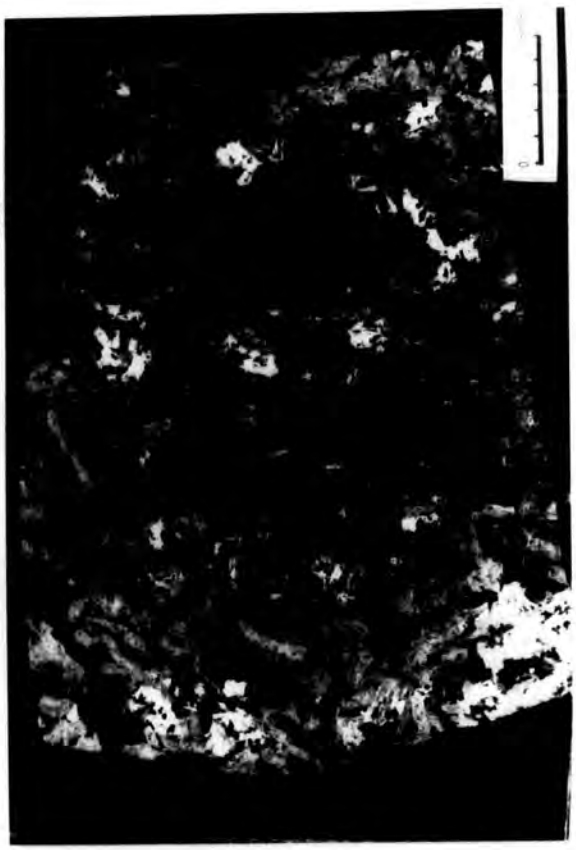

18

15

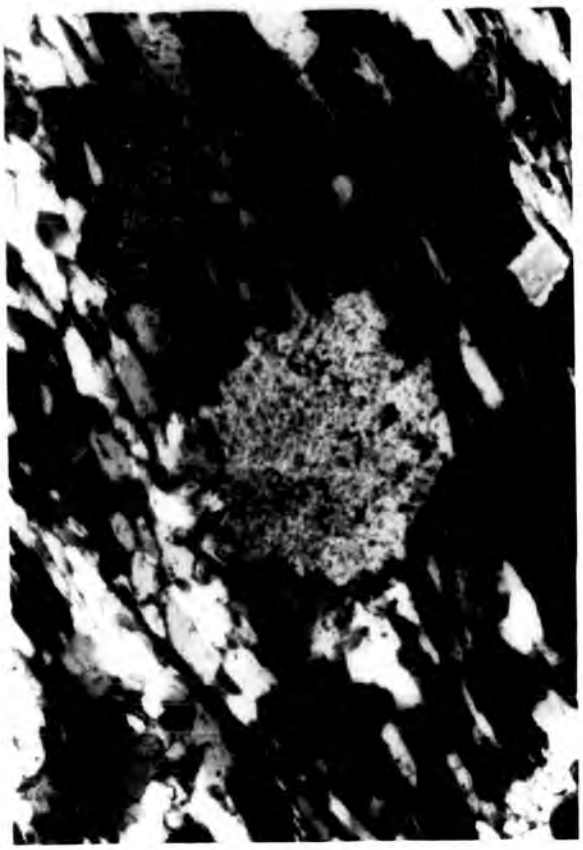

17

Plate 19. Typical braided, metamorphic texture in quartz+chlorite+sericite schist. Sample MA28W2, plane polarised light.

Plate 20. Coarse biotite and quartz in pressure shadow to quartz phenocryst. Sample MS7/4, plane polarised light.

Plate 21. Homotropic biotite with relict S_1. Sample MA28W2, plane polarised light.

Plate 22. Poikiloblastic garnets, W locality. Sample MA9W2, plane polarised light.

20

22

19

21

Plate 23. Coarse amphibole with relict S_1. Sample MA4J4, plane polarised light.

Plate 24. Zoned amphibole from basic sill. Dark, hornblende, margin; and light, actinolite, core. Sample SM401, plane polarised light.

Plate 25. Porphyroblastic albite with S_1 relicts. Sample MA16W2, crossed polars.

Plate 26. Crush texture in quartz diorite phase of the Rooiwater Igneous Complex. Sample SM12, crossed polars.

24

26

23

25

Plate 27. Granophyric texture in quartz diorite phase of the Rooiwater Igneous Complex. Sample CD21, crossed polars.

CHAPTER VI

GEOCHEMISTRY

6.1 Introduction

Samples from the Rubbervale and Gravelotte Subgroups, and the basic intrusives, were analysed for major and trace elements. Drill core was selected where possible, otherwise the freshest available surface material was used; refer to Appendix A. The major elements Si, Al, Fe, Mg, Ca, Na, K, Ti, Mn, P and S, and trace elements Ba, Nb, Zr, Y, Sr, Rb, Zn, Cu, Ni, Cr, La and Ce were determined.

Analyses were performed on pressed powder briquettes using a Philips PW1400 X-ray fluorescence spectrometer. International standards G1, G2, GSP1, GR, SY1, BCR1, BOB1 and BR were used for direct calibration of major elements; and ratios of peak to background for trace elements. Data was reduced using the University's IBM 360-37 computer. For details of the analytical techniques used, and tabulated whole rock analyses please refer to Appendix C.

6.2 Results

The extensive alteration prevalent in metamorphosed volcanic rocks invalidates classification schemes based on major element oxides, especially alkalies, and immobile trace elements such as Ti, Zr, Y and Nb must be used instead (Winchester and Floyd, 1977; Floyd and Winchester, 1978; Davies et al., 1979; MacGeehan and MacLean, 1980a).

Volcanic rocks from the Rubbervale Subgroup are discussed fully below. Quartzites and a greywacke from

the Gravelotte Subgroup were found to contain high Cr, Ni, Sr and Zr trace element contents indicating derivation from a mixed granite-ultramafic source, as suggested by Condie et al. (1970) for similar rocks from the Fig Tree and Moodies Groups of the Barberton Mountain Land; table 3.

Basic sills intrusive into the volcanic and sedimentary rocks are post-mineralization and have been completely albitized. On the basis of trace element data they are of tholeiitic composition, figs. 27 and 28, table 4.

6.2.1 Rubbervale Subgroup

6.2.1a Flows

Analyses of the extrusive rocks are presented in table 4. These have SiO_2 > 70 wt % and variable Na_2O and K_2O contents, being either K_2O or Na_2O rich, a feature noted by Wilson et al. (1965) but subsequently disputed by Spitz and Darling (1975).

Plots of alkali, and alkali vs. alumina are presented in figs. 24 and 25, with unaltered rhyolites for comparison. In fig. 25 the flows fall into two groups outside the "igneous spectrum" of Hughes (1973). The first group is depleted in alkalies, has a high K/K+Na ratio and is enriched in alumina with respect to unaltered rhyolites; see also fig. 24. Rocks from this group have normative corundum values of > 10 mol %, indicative of extreme alumina oversaturation (Cornell, 1977). The second group is more scattered but is slightly depleted in alkalies and alumina and has a generally low K/K+Na ratio. This group contains < 3 mol % normative corundum.

Of the trace elements Ba and Rb correlate with K; Sr, and to some extent, Y correlates with Na, fig. 26. In the case of Y, the correlation is more notable in the flows than in tuffs, and care must be exercised when considering Y as an immobile trace element.

Fig. 27 is a plot of Zr/TiO_2 vs. Nb/Y after Floyd and Winchester (1978). The flows fall into two groups, one scattered within the rhyolite field, and another inside the rhyodacite+dacite field. This latter group consists of three samples from the farm Gravelotte.

6.2.1b Tuffs

Compared with flow material, tuffs contain lower silica and higher alumina and MgO contents; table 4. This is probably due to a higher proportion of chlorite in the tuffs. The three analyses with high Na_2O and low K_2O contain albite phenocrysts.

On fig. 24 the tuffs follow the same trends as the flows, though with greater scatter. There is a notable group containing alumina > 17 wt % and a K/K+Na ratio of > 0.88.

Using the trace element plot of fig.27 , most tuffs fall, with the flows, in the rhyolite field. Exceptions are one example from Gravelotte farm, which plots with flows from there, and four samples in the middle of the dacite field. These latter were taken from the top of the tuff pile on the farm Solomons Mine.

It can be seen that, with the above exceptions, on the basis of trace element data, the tuffs and the flows were originally of similar composition.

6.2.1c Transition Zone

Chemical analyses of the cherty, sericite-bearing rocks between the mineralization and the acid porphyries at the W and J localities bear close similarities to the tuffs and flows in the underlying volcanic pile, table 4. Silica, alumina and K_2O are relatively high and Na_2O is generally depleted, and the informal name "aluminous cherts" was given to these rocks.

In fig. 27 these aluminous cherts lie in a restricted area within the rhyolite field occupied by tuffs and flows. Cr, Ni and Sr values are low and thus not characteristic of sediments from the Gravelotte Subgroup.

The acid porphyries or welded tuffs were only observed in drill core at the L-W and J localities. The mean and range of analyses from the J locality appear in table 4. From fig.24 it can be seen that the porphyries have undergone minor alteration and are closely associated with the second group of flows though trending towards unaltered rhyolites.

On fig. 27 these porphyries occupy the rhyodacite+ dacite field, despite the relatively high silica content. They plot, with one exception, adjacent to the flows from Gravelotte farm.

6.3 Summary and Discussion

Major and trace element analyses were undertaken on the various lithologies present in the study area. Alkali and alumina contents of the felsic volcanic rocks have been significantly modified with respect to unaltered rhyolite, separating into two groups. One is characterized by low

total alkalies, high alumina and a high K/K+Na ratio, and a second group contains slightly depleted alkalies and alumina and a relatively low K/K+Na ratio. The acid porphyries occur with the second group but trend more towards unaltered rhyolite. This alteration is shown in fig. 24.

The mineralogy of the first group consists of quartz+ sericite+chlorite, and that of the second is quartz+sericite+ albite+chlorite; the albite present as albitized original phenocrysts with compositions of An < 7 wt %.

A possible mechanism for this alteration is the break-down of original feldspar releasing Na, K and Al. Rocks originally having a high albite content or containing large feldspar phenocrysts appear to have lost K and retained, or gained, Na to form albite, whilst others have lost Na, some K, and gained Al to form sericite. In basic intrusives the plagioclase is now albite of composition An < 7 wt %.

This type of alteration is akin to the formation of spilites from basic intrusives, and keratophyres from felsic volcanic rocks (Hughes, 1973). The basic intrusives would have acted as a sink for Na liberated from the flows and tuffs which appear to have redistributed K and Al among themselves. The timing of this would therefore be post-intrusive and post-mineralization, and would seem to ignore the role of circulating groundwaters associated with the process of massive sulphide formation. MacGeehan and MacLean (1980b), from a study of similar rocks in the Matagami greenstone belt in Canada, suggest this type of alteration to be caused by sub sea-floor geothermal activity related to the formation of massive sulphide deposits.

Despite this alteration, immobile trace elements such as Ti, Zr, Nb, Y and Cr can be used to classify the various rocks (Floyd and Winchester, 1978; Davies et al., 1979). Ba and Rb were found to correlate with K, and Sr and Y with Na. The correlation between Y and Na, although somewhat scattered, could affect the use of Y as an "immobile" trace element. However, a plot of Nb against Y for use in fig. 27 showed no significant abnormalities.

From fig. 27, flows and tuffs can be classified as rhyolites, with a group of flows from the farm Gravelotte lying in the dacite field. Tuffs from the top of the volcanic pile on the farm Solomons Mine also plot as dacites. Acid porphyries from the J locality are dacite, similar to the flows from Gravelotte farm. The compositions of flows and tuffs are similar, suggesting a common origin from rhyolitic magma, with localized areas of dacite composition.

Aluminous cherts from the W and J localities have trace element compositions which suggest derivation from the underlying pile of tuffs and flows.

6.4 Conclusions

The lowermost subgroup in the Murchison greenstone belt is the Malati Subgroup which consists of komatiite basalts and tholeiitic basalts, with Mg-tholeiites (Minnitt, 1975). Overlying this is the Leydsdorp Subgroup comprising tholeiites, Mg-tholeiites and some komatiite basalts (Viljoen et al., 1979). Minor andesitic lavas have been reported in the east of the Belt (Minnitt, 1975). From the present work, the upper volcanic unit, the Rubbervale Subgroup, comprises rhyolite flows and tuffs

with subordinate dacites. Overlying thin cherts were derived from these. Basic sills intruding the entire sequence are iron-rich tholeiites with minor andesitic varieties.

The entire greenstone volcanic sequence is thus dominantly tholeiitic. Sediments from the Gravelotte Subgroup are similar to those of the Fig Tree and Moodies Group sediments from the Barberton Mountain Land, and were derived from a mixed granite-ultramafic terrain.

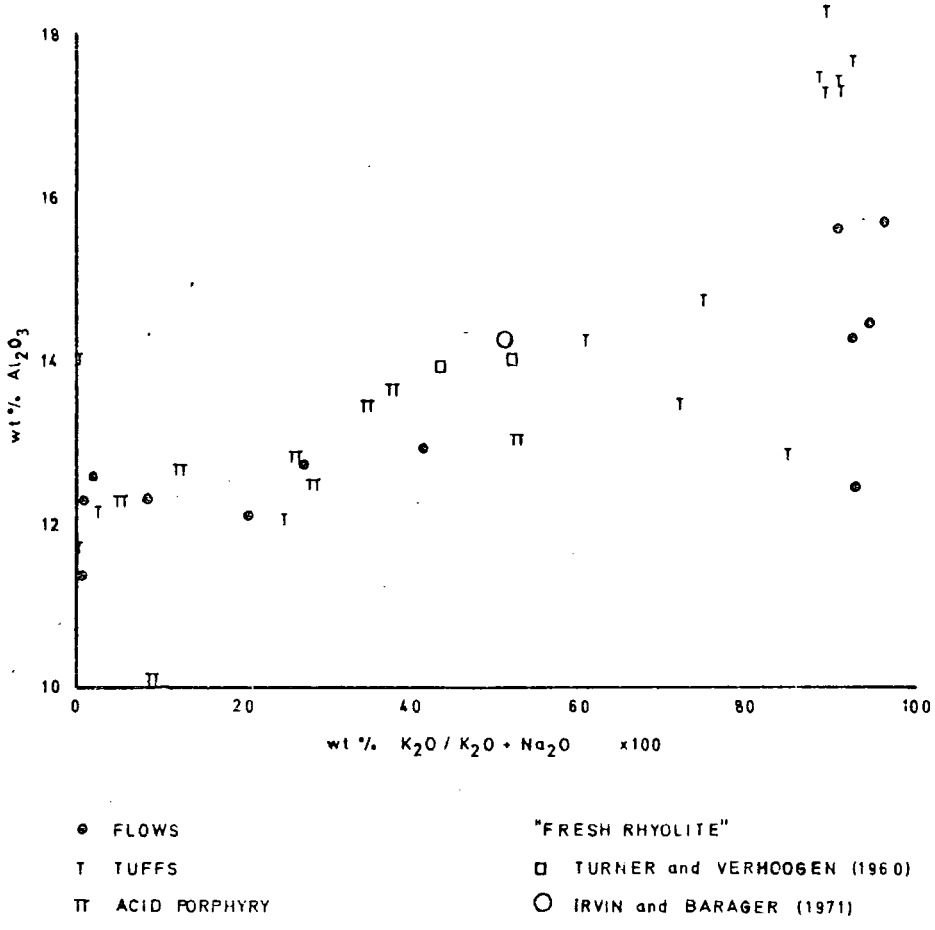

FIG 24 PLOT OF ALUMINA VERSUS ALKALIES FOR RUBBERVALE SUBGROUP

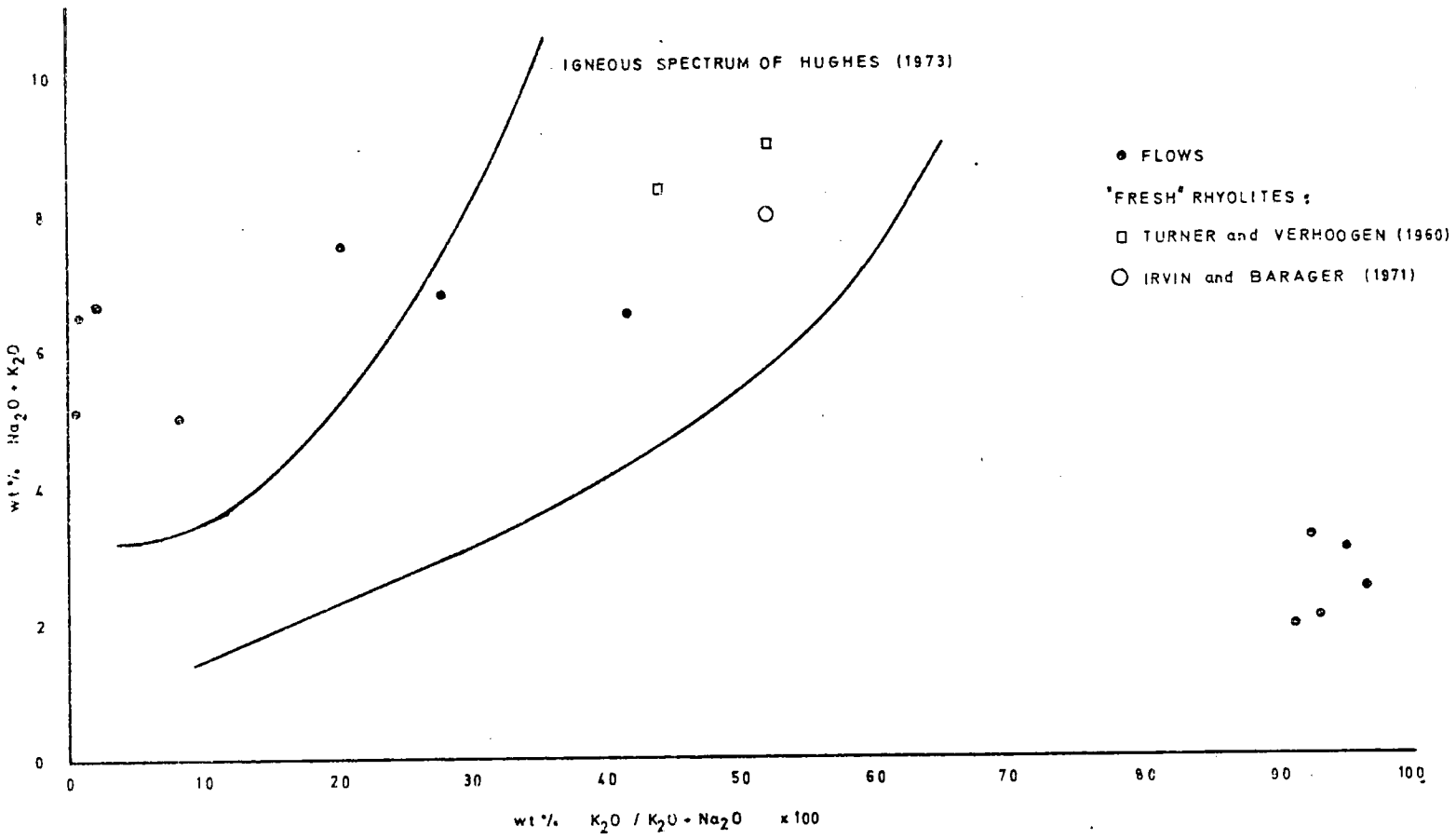

FIG 25 ALKALI PLOT OF RUBBERVALE SUBGROUP

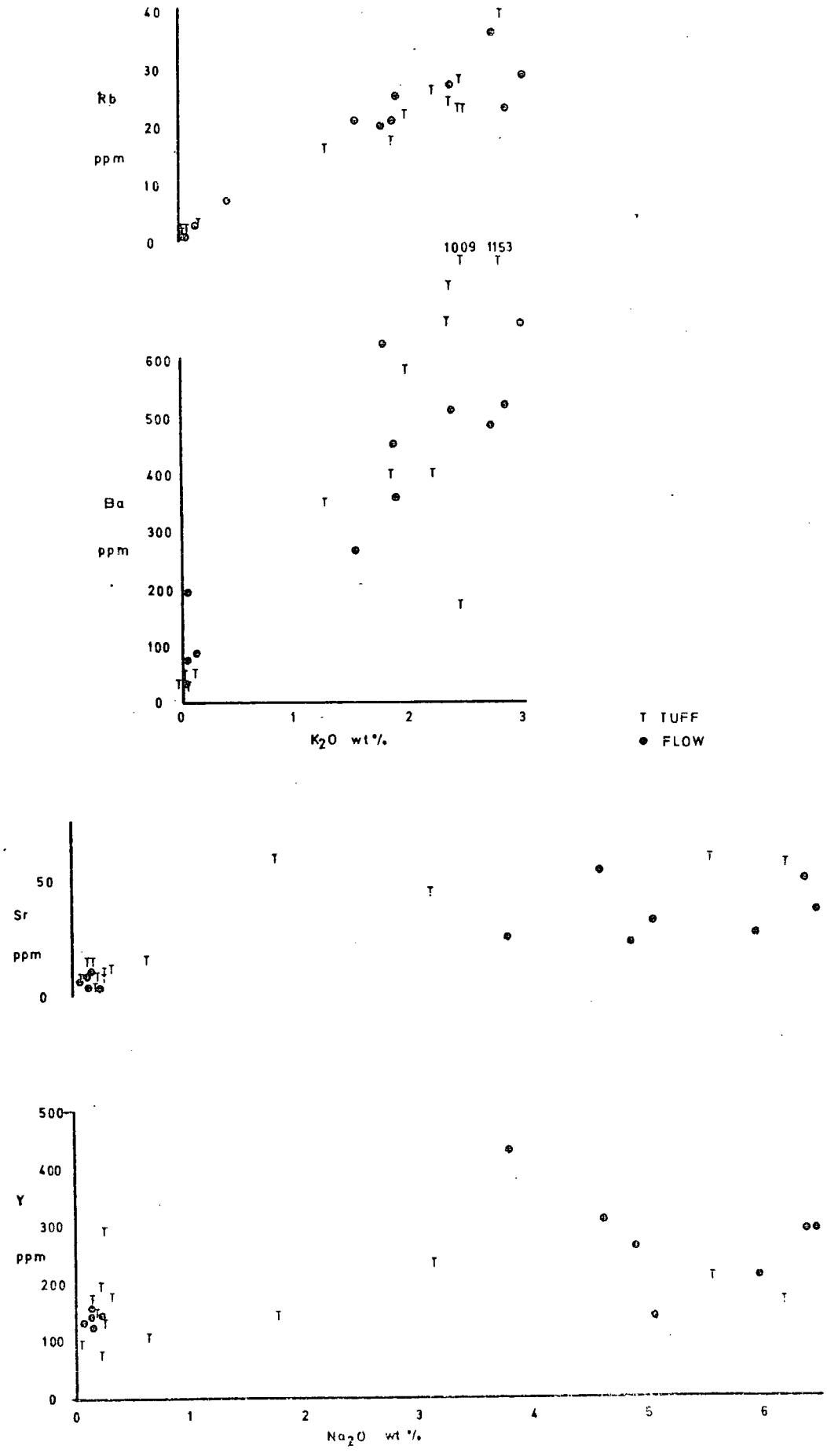

FIG 26 PLOTS OF K_2O VERSUS Ba & Rb; AND Na_2O VERSES Sr & Y FOR RUBBERVALE SUBGROUP

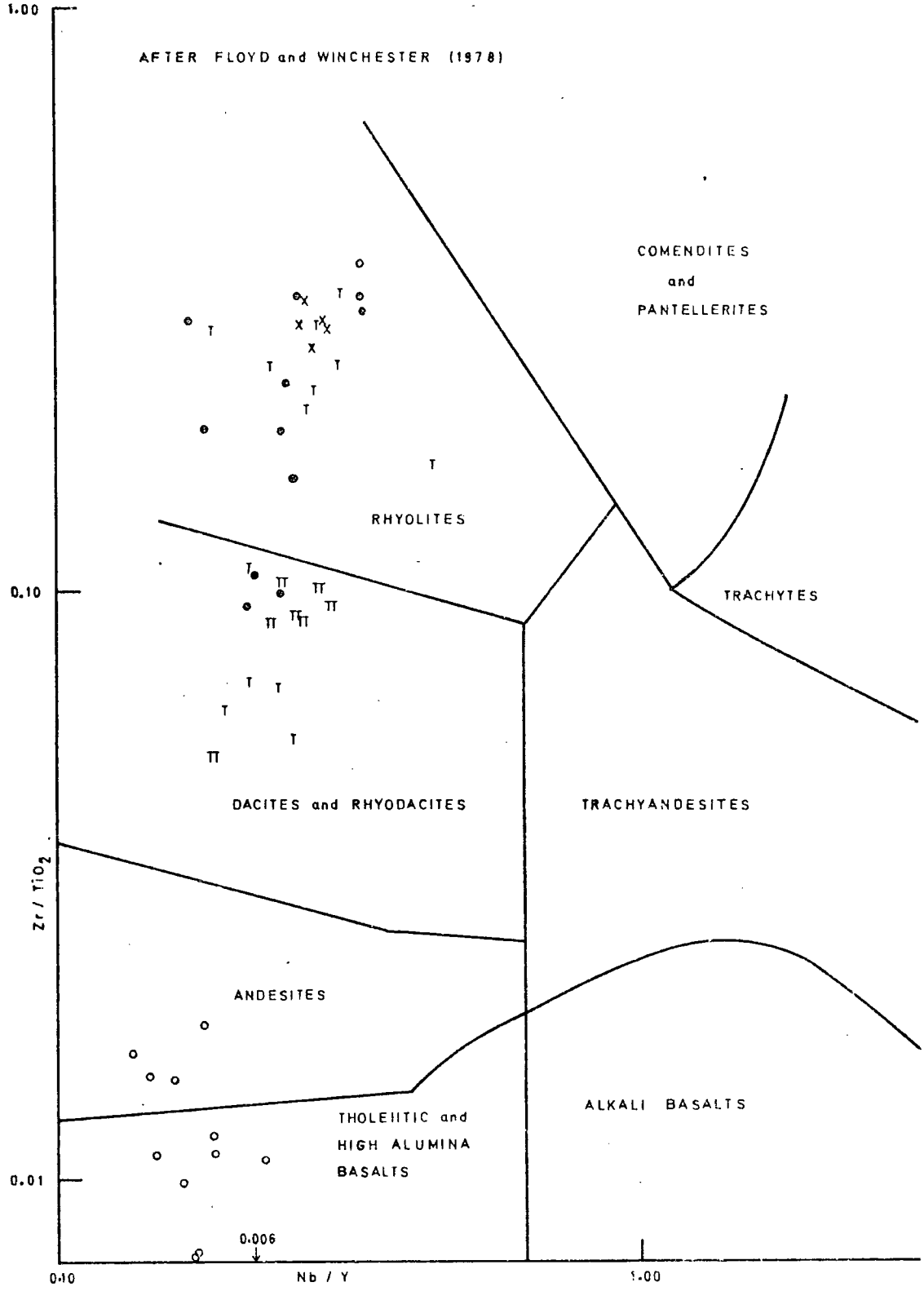

X ALUMINOUS CHERTS - W LOCALITY (selected analyses)

TT ACID PORPHYRIES - J LOCALITY (selected analyses)

o FLOWS T TUFFS

o BASIC INTRUSIVES

FIG 27 PLOT OF Zr/TiO_2 VERSUS Nb/Y FOR RUBBERVALE SUBGROUP

● BASIC INTRUSIVES PLOTTING IN THOLEIITE FIELD OF FIG 27

TREND LINES AFTER DAVIES et. al. (1979)

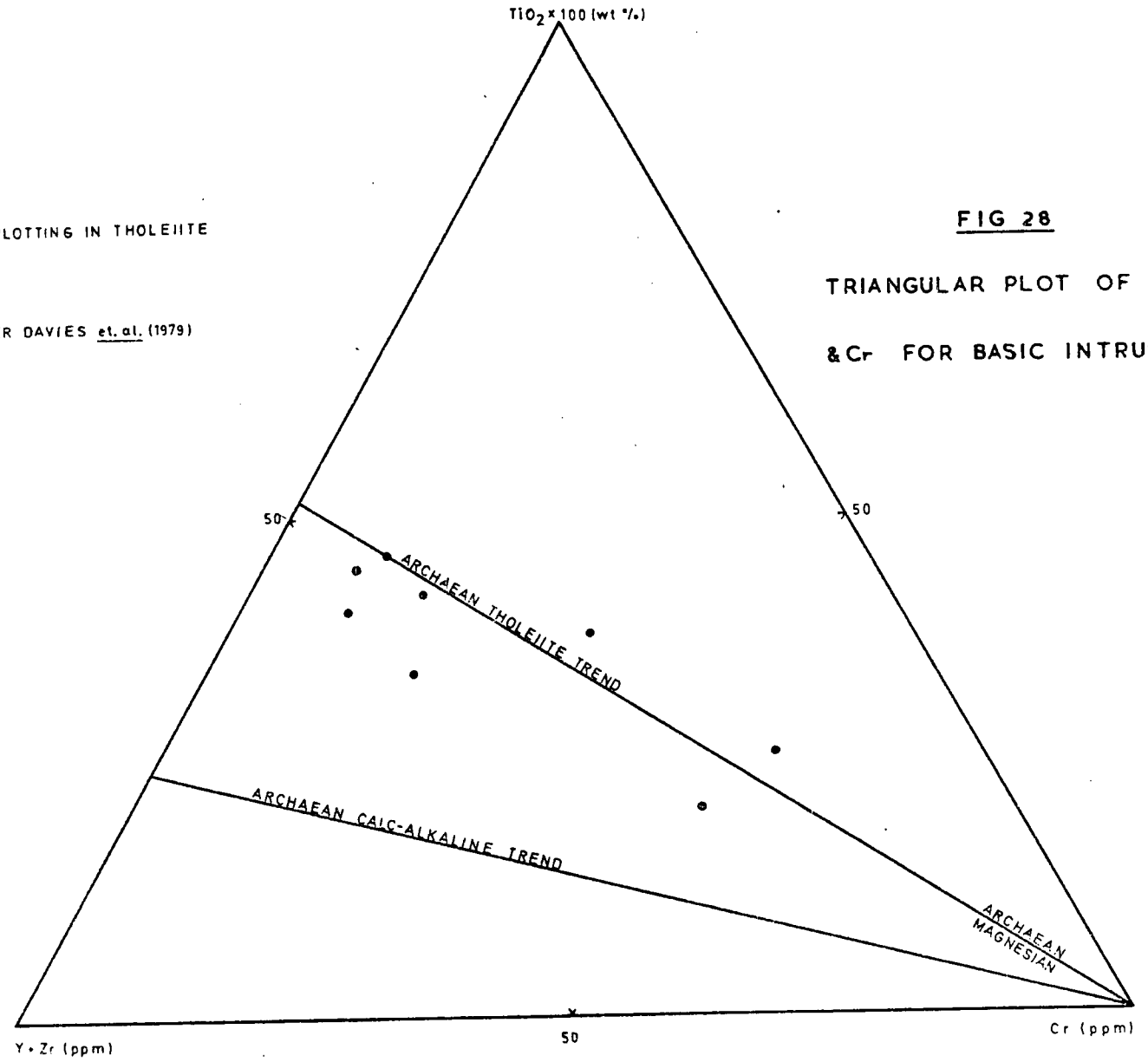

FIG 28

TRIANGULAR PLOT OF TiO_2, Y+Zr, & Cr FOR BASIC INTRUSIVES

Table 4. Mean and range of chemical analyses of the various rock types.

	FLOWS: high Na, low K/K+Na		FLOWS: low Na, high K/K+Na		TUFFS	
wt%	mean	range	mean	range	mean	range
SiO_2	73.87	71.87-77.14	72.29	67.29-76.48	69.45	61.39-77.79
Al_2O_3	12.33	11.39-12.95	14.54	12.41-15.71	15.07	11.77-18.31
Fe_2O_3*	4.66	4.20-6.19	6.86	4.09-8.71	5.93	2.37-8.95
MgO	1.36	0.55-2.34	3.41	0.78-5.93	5.20	1.14-10.80
CaO	0.78	0.00-2.20	0.00	0.00	0.64	0.00-2.50
Na_2O	5.34	3.81-6.51	0.16	0.09-0.24	1.41	0.07-6.22
K_2O	0.97	0.03-2.72	2.38	1.77-2.85	1.55	0.00-2.80
TiO_2	0.50	0.24-0.81	0.27	0.18-0.41	0.50	0.22-0.98
MnO	0.07	0.03-0.10	0.06	0.02-0.16	0.04	0.01-0.11
S	0.04	0.00-0.16	0.01	0.00-0.01	0.07	0.00-0.59
P_2O_5	0.09	0.02-0.18	0.04	0.01-0.09	0.12	0.03-0.26
Total	100.01		100.02		99.98	
ppm						
Ba	228	33-493	536	359-661	431	26-1153
Nb	61	30-74	41	24-53	41	25-68
Zr	760	701-900	673	569-789	693	521-985
Y	277	122-313	140	123-158	161	79-295
Sr	35	22-56	7	4-11	24	4-59
Rb	13	1-36	25	20-29	17	2-39
Zn	116	46-190	169	22-443	76	0-227
Cu	11	3-24	29	5-46	7	0-21
Ni	17	13-24	11	8-15	16	0-53
Cr	32	13-46	43	28-61	49	10-198
La	77	39-129	41	3-88	32	1-75
Ce	185	147-221	98	41-180	105	14-201

*total iron as Fe_2O_3

Table 4. Mean and range of chemical analyses of the various rock types (continued).

	ALUMINOUS CHERTS W locality		ACID PORPHYRIES J locality		BASIC SILLS	
wt%	mean	range	mean	range	mean	range
SiO_2	70.65	68.40-74.19	71.34	69.32-73.87	47.60	44.52-49.68
Al_2O_3	15.77	14.33-18.20	12.70	10.33-14.06	12.84	11.34-13.77
Fe_2O_3*	6.29	1.68-8.46	5.78	3.94-6.92	17.46	14.86-19.17
MgO	1.76	0.46-3.19	3.06	1.65-5.14	7.74	6.40-11.09
CaO	0.00	0.00-0.80	1.14	0.00-2.86	9.38	7.79-11.72
Na_2O	0.78	0.20-3.54	3.43	1.10-5.37	2.39	1.59-3.53
K_2O	3.25	2.81-4.29	1.09	0.10-2.18	0.06	0.00-0.15
TiO_2	0.29	0.25-0.33	0.65	0.51-0.85	1.68	1.04-2.63
MnO	0.15	0.03-0.26	0.06	0.03-0.09	0.20	0.17-0.24
S	1.03	0.03-2.80	0.60	0.04-1.61	0.18	0.01-1.02
P_2O_5	0.03	0.01-0.05	0.13	0.09-0.40	0.47	0.19-0.62
Total	100.00		99.98		100.00	
ppm						
Ba	518	406-873	275	31-492	48	4-239
Nb	55	47-65	52	31-65	7	4-12
Zr	836	725-1022	658	444-850	183	102 269
Y	205	157-253	210	167-261	40	27-65
Sr	14	8-24	36	16-80	121	67-156
Rb	43	31-57	19	6-31	1	0-4
Zn	5931	160-38000	1083	0-3896	147	107-283
Cu	94	16-256	40	3-98	91	44-168
Ni	15	7-19	15	9-23	93	56-174
Cr	25	15-45	21	7-83	106	42-296
La	67	12-105	64	44-85	8	0-16
Ce	179	70-238	148	97-191	47	33-69

CHAPTER VII

MINERALIZATION IN THE RUBBERVALE SUBGROUP

7.1 General

7.1.1 Introduction

The Rubbervale Subgroup comprises a thick pile of extrusive felsic volcanic rocks, mainly tuffs with lesser flows and coarse pyroclastic material. These are overlain by a relatively thin unit, the Transition Zone, consisting of aluminous cherts, reworked volcanic rocks and acid porphyries or welded tuffs. These are in turn overlain by thick, clastic, deep-water sediments belonging to the Gravelotte Subgroup.

According to Sangster (1972), Hutchinson (1973) and Sangster and Scott (1976) volcanic and sedimentary sequences in Archaean greenstone belts are likely to host massive Fe-Zn-Cu sulphide deposits. Such deposits are present in the Murchison greenstone belt at the base of the Transition Zone, along a recognizable stratigraphic horizon termed the "copper-zinc line" by Van Eeden et al. (1939).

7.1.2 Previous Investigations

The first recorded reference to copper-zinc deposits in the Murchison Range was in 1939 by Van Eeden et al. who described three sets of Ancient Workings where copper and zinc oxides had been mined. These are, from east to west, on the farms Mashawa, Vlaklaagte and Platveld (later known as the Letaba Copper Mine), and Solomons Mine. Despite some interest by mining companies in the 1950's, no additional discoveries were made.

In 1959, Hausman conducted a mineralogical investigation of the Letaba copper-zinc ores which he considered to have formed as vein deposits along a fault zone. The Solomons Mine deposit, and its geological setting, was briefly described in a B.Sc. thesis by Kingston (1976). Viljoen et al. (1978) discussed mineralization in general in the Murchison Range, and considered the copper-zinc deposits to be of probable volcanogenic origin, but did not elaborate on this.

The geological setting and nature of copper-zinc deposits of the Murchison Range had not been examined in detail prior to the present investigation, despite attempts at mining the Mashawa and Letaba deposits (Hammerbeck,1976).

7.1.3 Present Investigation

The present investigation has examined the mineralization and setting of the Solomons Mine deposit and two other previously unknown massive sulphide deposits occuring along the so-called "copper-zinc line". Details of the field techniques employed are given in chapter 2.

The three copper-zinc deposits are, from east to west, the Ancient Working on the farm Solomons Mine (known as the MGZ deposit) and associated D massive sulphide deposit, the L-W locality consisting of disseminated sulphides, and the J massive sulphide deposit in the far west of the study area. The MGZ and J deposits are separated by a distance of 19 km.

All three deposits occur at the same stratigraphic horizon, at the base of the Transition Zone. Volcanic rocks in the footwall of the J and L-W localities are dominated by flows and coarse tuffs, and at the MGZ

locality by finer grained, more uniform tuffs with minor flows. This reflects the change in volcanism from west to east. Metamorphism and deformation have affected all deposits, although those at J and L-W have suffered less than the MGZ deposit and retain many depositional textures.

The J deposit is the most complete and least altered of the three, and consists of a massive lens of banded, sphalerite, pyrite, chalcopyrite and pyrrhotite overlying a zone of altered footwall tuffs. Textures in the sulphides and host rocks indicate that the massive sulphides were deposited as unconsolidated sediments in an aqueous environment. The alteration in the footwall results from the upward passage of the mineralized fluids which formed the overlying massive sulphide lens.

Disseminated sulphides, mainly sphalerite, occur in cherts at the base of the Transition Zone at L, and following the deposition of 20m of aluminous cherts, at W some 800 m to the west. The mineralization at L is pyrite-dominated, and has chlorite as a gangue mineral, while that at W is sphalerite-dominated, and is associated with Mn-rich garnets. The W mineralization is inferred to be a later, manganese and zinc-rich phase of the L mineralization, the disseminated nature of the sulphides being due to rather high sedimentation rates of the host rock. As at the J locality, textures indicate a sedimentary, aqueous environment for sulphide deposition.

The MGZ deposit consists of an upper pod of massive pyrrhotite+sphalerite+chalcopyrite overlying pyrite+ chalcopyrite bearing chert and chlorite schist. These lie

directly upon volcanic tuffs. A footwall alteration zone is absent.

7.2 J Locality

7.2.1 Introduction

The J locality is situated near the northwest corner of the farm Maranda, occupying an area of flat ground south of Tshutshu peak, see map 1. Exposure is limited to a low range of hills in the eastern part of the locality with surrounding flat areas covered by up to 10 m of red-brown, loamy soil.

Prominent zinc and copper soil geochemical anomalies (> 100 ppm Cu and > 200 ppm Zn in a background of 70 ppm) along the southern slopes of the hills were traced to veins and patches of sugary quartz, brown goethite and limonite-infilled cubic cavities after pyrite, in exposures of quartz+sericite+chlorite schists representing felsic tuffs and flows. Geochemical analysis of this material revealed anomalous concentrations of up to 1760 ppm copper and 1550 ppm zinc. The presence of stockwork-type sulphide mineralization associated with the tuffs was considered to be a favourable indicator for massive sulphides.

During an extensive ground PEM survey a bedrock conductor was located immediately to the west of these hills. Detailed surveying indicated the presence of a good conductor at a depth of 60 m, and having a strike length in excess of 200 m. The depth to the top of the conductor was later shown to be that of the water table, i.e. base of the oxidation zone. Subsequent air-flush

and diamond-drilling outlined a small, <1 m.tonnes, lens of massive sulphides overlying a zone of stockwork sulphides within hydrothermally altered felsic tuffs and breccias.

7.2.2 Geology

The geological sequence in the eastern part of the area as determined from borehole core, can be seen on figs. 29 and 30, and on map 2.

In the west of the locality, the entire sequence is dissected by at least one large, irregular, basic intrusive similar to the large sills found elsewhere in the volcanic and sedimentary pile. Despite this the footwall tuffs and breccias and associated stockwork sulphides thin out and disappear westwards.

7.2.2a Footwall Flows

These are generally massive, fine grained siliceous rocks, rather textureless, although flow banding has been observed in exposures to the east of the J locality. In borehole core, several thin fragmented and tuffaceous horizons are intercalated with the flows.

7.2.2b Footwall Tuffs

Overlying the massive flows is a sequence of fairly uniform tuffs, siliceous coarse fragmental horizons and chlorite-schists. The contact with the underlying flows is gradational with an increase in tuffaceous bands and the disappearance of massive horizons. The footwall tuffs are approximately 50 m thick in the area east of line 220E, map 2, and although cut by basic intrusives, appear to be virtually absent on line 20E where massive felsic rocks were intersected in drillholes. In a small exposure 200 m west of the boundary fence, on the adjacent farm

Harmony, massive felsic flows are overlain by a thin banded and mineralized cherty rock which is in turn overlain by acid porphyries.

The average fragment size from each drillhole intersection has been plotted on fig. 31 , which is a longitudinal section in the plane of the orebody. This shows that fragments of > 4 mm diameter extend as a narrow zone from -70 m on line 550E to -180 m on line 200E, east of which the basic intrusive obscures the geology. Below this, and to the west, the general fragment size is < 3 mm.

The tuffs contain small rounded fragments or clasts of quartz+sericite rock set in a fine grained, schistose matrix of quartz+chlorite+sericite. In the zone of oxidation, i.e. above the -60 m level, prominent foliation planes have become iron-stained giving the rock a stripey texture.

The upper 15 m of the footwall tuffs contain horizons of fine grained, dark green, chlorite schist. These schists frequently contain small siliceous fragments or bands of quatz-rich rock and horizons of euhedral, zoned pyrite, considered to be of diagenetic origin, see chapter 8, plate 42.

7.2.2c Footwall Alteration Zone

Within the footwall tuffs is a well defined alteration zone marked by the fairly abrupt decrease and disappearance of sericite, and increase in dark green platy chlorite. This corresponds to a decrease in Al_2O_3 and K_2O and an increase in the total iron content of the rocks. For details refer to chapter 9.

This pervasive mineralogical change is accompanied by the appearance of irregular veinlets containing chlorite+biotite, or less frequently, quartz+biotite, and often accompanied by sulphides. These veinlets crosscut the tuff producing a pseudo-breccia texture and, with increasing alteration, the "blocks" of host rock become progressively rounded. The amount and width of the chloritic veining increases upwards through the tuffs (plate 28).

Sulphides occur within the chlorite alteration as separate veinlets of quartz+pyrite+pyrrhotite+chalcopyrite+ sphalerite either crosscutting or contained within earlier chlorite veins. Varying amounts of pyrite+chalcopyrite, pyrrhotite, pyrrhotite+pyrite+chalcopyrite, chalcopyrite+ sphalerite also occur disseminated within chlorite schist horizons.

Quartz+sulphide veinlets continue below the chlorite alteration zone into the unaltered tuffs, diminishing in amount with depth into the sequence.

It was originally thought that sulphide-bearing chlorite schist horizons represented intense silicate and sulphide alteration. They are now considered to have been original clay layers along which mineralizing solutions penetrated. These clay layers produced a silicate mineralogy now appearing as dark green chlorite with varying amounts of quartz, carbonate, albite, coarse actinolite needles and chlorite+biotite "clots", with sulphides forming braided or mesh textures of pyrite$\pm$ chalcopyrite$\pm$pyrrhotite$\pm$sphalerite; plate 46. Crosscutting

quartz+sulphide veinlets are absent or rare.

Separating these chlorite schist horizons from the massive sulphide lens is a "barren zone" varying in width from a few centimeters to over one meter. Both upper and lower contacts are conformable and parallel to schistosity and layering. The rock is very siliceous, contains large patches of pale green, fine grained, massive chlorite and is characterized by the presence of frequent blue quartz phenocrysts, often with white overgrowths. A vague banding is often discernable. Sulphides are confined to minor disseminations of pyrite, chalcopyrite and sphalerite. In several drill-holes to the west of line 26OE, the "barren zone" is a pale grey chert containing much finely disseminated granular sphalerite and is fractured and crosscut by quartz+sphalerite±pyrite veins; plate 29.

Massive sulphides directly overlie the tuffs and "barren zone" with a sharp lower contact conformable to local schistosity and layering in the host rocks. The footwall alteration zone has an asymmetrical distribution. Everywhere it is overlain by massive sulphides except in the far east where the sulphides are replaced by a pyrite+sphalerite bearing chert. Alteration is best developed in the area between lines 14OE and 55OE. On surface, gossanous and chloritic tuffs and coarse tuffs have been traced eastwards for 6OO m before they die out. West of line 14OE a basic intrusive disrupts the sequence, but where observed, alteration is absent.

The best development of "stringer sulphide" mineralization within the footwall, taken as a combination of sulphide content and width and divided arbitrarily into good, fair, poor or absent, has been plotted on fig. 32 . Good alteration with a high copper and zinc content forms a narrow zone extending in depth from the oxidation level at -80 m, to -160 m between lines 440E and 140E, west of which is a basic intrusive. This zone corresponds to the zone of coarsest tuff fragments of fig. 31 . It is also useful to compare these with the distribution of the various sulphide species as in fig. 33 .

It is apparent that the footwall tuffs provide a suitable, porous conduit for the sulphide-bearing solutions, more altered tuffs presumably allowing a greater flow rate.

7.2.2d Massive Sulphides

Directly overlying the footwall sequence is a thin lens of massive Fe-Zn-Cu sulphides, plate 30. On surface the lens strikes westwards for over 400 m from line 460E, although between lines 20E and 180E a basic intrusive disrupts the sequence; map 2. On line 500E a NE trending fault terminates the massive sulphides and their easterly equivalent is a pyrite+sphalerite bearing aluminous chert. Fig. 34 is a longitudinal section in the plane of the massive sulphide lens on which the true thickness of each borehole intersection has been plotted. Holes 7, 8, 15 and 19 are disrupted by thin intrusives and the thicknesses shown are minimum. From this it can be seen that the massive sulphide lens has a westerly plunge of approximately 30^{o} and thickens westwards roughly parallel to this. The

lower extremity of the lens is coincident with the zone of good development of footwall alteration, but continues downplunge from the termination of this alteration; compare with fig. 32.

The sulphide lens is composed of varying amounts of sphalerite, pyrite, pyrrhotite and chalcopyrite with traces of other sulphides, and an average of 15% gangue minerals, mainly quartz. Sphalerite is the dominant sulphide and can locally form up to 60% of the rock; plate 30. These sulphides impart a compositional banding to the rock, the most common being small pyrite euhedra forming thin impersistant bands and parallel horizons set in a massive red-brown sphalerite matrix, plate 31. Some of these pyrite bands are contorted with features akin to slumping, plates 32 and 47. Other common textures are granular, rather irregular and network intergrowths of chalcopyrite+sphalerite+pyrrhotite, some of which may be very finely banded, and coarsely banded chalcopyrite-rich and sphalerite-rich horizons, plate 33. Many horizons contain round silicate inclusions, and at the base of the lens, frequent "chlorite schist" fragments occur within a horizon of randomly oriented large pyrite cubes in a sphalerite matrix, plate 48. These "chlorite schist" fragments are considered to have been derived from the footwall sequence; see also chapter 8. An upper massive sphalerite horizon is present in several boreholes, and in hole 18 the top of the sulphide lens is a thin banded sulphide and silicate rock, plate 32.

Correlation of the banding between drill holes is

difficult if not impossible, although bands of sphalerite+ pyrite are dominant in the west, and towards the top, of the sulphide lens.

Textures indicative of an original sulphide layering or banding are rare and consist of slump banding, observed in several places. The presence of fragments from the footwall may imply brecciation and redeposition coincident with sulphide formation, but could equally be caused by tectonic brecciation. However the absence of a brecciated, tectonised footwall contact would suggest the former. Sulphide bands were found to be parallel to lithological layering in the footwall and hangingwall sequences. Fractured pyritic horizons and pyrite "balls" are indicative of movement during metamorphism (Sarker et al., 1980).

Both hangingwall and footwall contacts are sharp and parallel to banding, layering and schistosity in the host rocks. In several places the upper contact is marked by a shear zone, represented by contorted quartz veins, displaced and fragmented cherts, and local remobilization of sulphides.

Within the massive sulphide lens, mineral zonation across the width varies with some intersections having a well developed zonation from a copper-rich, zinc-poor base to a copper-poor, zinc-rich top while others have no obvious pattern or display a reverse zonation. Parallel to the layering there are no obvious distribution patterns for copper or zinc and it is notable that the zinc content is high and relatively uniform.

Where the massive sulphide is not present in the

sequence, and where there is no intrusive interference, its place is taken by a pyrite+sphalerite bearing aluminous chert, in which the zinc content decreases away from the massive sulphide lens. This chert passes upwards into, and is indistinguishable from the hangingwall sequence.

In hole 9, an early F_1, intrafolial fold has folded a sulphide-bearing layer within these aluminous cherts, indicating the sulphides to be pre-metamorphic in origin.

7.2.2e Hangingwall Aluminous Cherts

Stratigraphically and conformably overlying the massive sulphides is a sequence of fine grained siliceous and cherty rocks containing abundant sericite. Due to their relatively high alumina content, these rocks are informally termed "aluminous cherts". These are well foliated, with chlorite and quartz-rich bands, and in places contain abundant fine grained chlorite. Minor, thin horizons of quartz+sphalerite+pyrite and lenses and segregations of quartz with sphalerite+pyrite are present, although these decrease upwards through the cherts. Alteration similar to that in the footwall has not been observed. This unit is commonly <5 m thick.

7.2.2f Acid Porphyries

Conformably overlying the hangingwall aluminous cherts, and forming a 175 m thick unit, is a sequence of acid porphyries or welded tuffs. The porphyries are very susceptable to weathering and are not exposed anywhere within the study area. They form the low ground immediately to the south of the ridge of felsic tuffs extending eastwards from the J locality.

In drill core the porphyries comprise a rather massive, pale grey, siliceous, uniform rock. Squashed siliceous fragments are common and the unit is characterized by the presence of abundant blue phenocrysts of inverted high temperature quartz, which may reach 5 mm in diameter. Spherulitic devitrification structures are common in thin section; see chapter 5, and plate 16.

At its base the porphyry unit is fairly fine grained, contains small fragments, and has interlayered chlorite and pyrite horizons. Towards the centre the rock becomes coarser grained with the appearance of albite and quartz phenocrysts, and the absence of intercalated chloritic horizons.

The porphyries have a high sulphide content, as thin veins and patchy disseminations of pyrite and sphalerite. Zinc values are generally in the range 0.1 to 0.2%.

7.2.2g Sediments

In the far south of the J locality, air-flush drilling intersected chlorite and chlorite+sericite schists containing inherently high nickel values. These are correlated with Gravelotte Subgroup sediments and overlie the porphyry unit.

7.2.2h Intrusives

Syn-Volcanic Intrusives

Numerous thin felsic dykes and sills cut the pile of tuffs and flows. None of these cut or occur within the massive sulphides or the hangingwall sequence, and they are considered to be contemporaneous with, and form an integral part of, the volcanic rocks.

Post-Volcanic Intrusives

In the western half of the J locality, a large polyphase basic or gabbroic intrusive disrupts the volcanic and sedimentary sequence. The intrusive varies from massive to highly sheared, has an irregular cross-cutting nature, and is similar to the basic sills described in chapter 5. The main intrusive body cuts the volcanic sequence in a NE direction and dips moderately to the NW. Tongues and protruberances from the margins interfere with, and fragment, the host rocks at different vertical levels, i.e. at a decreasing vertical depth from line 20E to line 260E, east of which the sulphide horizon is unaffected.

In the oxidized zone, between 10 m and 80 m in depth, the intrusive is extremely decomposed with development of clay and micaceous minerals. Copper and zinc, released by oxidation of the sulphide zone have become fixed within these clays producing anomalously high copper and zinc assay results in the pulp from air-flush drilling.

7.2.3 Summary and Discussion

At the J locality a lens of banded, massive sulphides occurs on the contact between felsic flows and tuffs in the north, and thin aluminous cherts overlain by thick acid porphyries in the south. The flows and tuffs form the top of the large, thick, volcanic part of the Rubbervale Subgroup, with the Transition Zone sequence here comprising aluminous cherts and acid porphyries. Sediments belonging to the Gravelotte Subgroup overlie

the porphyries in the extreme south of the locality.

Tuffs forming the upper part of the footwall, and underlying the massive sulphide lens, were altered during the passage of mineralizing solutions, and this alteration increases towards the sulphide lens. No such alteration was observed in the hangingwall rocks. Three different styles of alteration have been determined, and were probably forming at the same time;

a. Diffuse alteration of the rock with a depletion in Al_2O_3 and K_2O, and enrichment in iron, resulting in the disappearance of sericite and an increase in the amount of dark green, iron-rich chlorite. Minor disseminated sulphides may accompany this.

b. Discrete irregular veins of dark chlorite with minor interstitial sulphides, generally sphalerite and pyrite.

c. Irregular crosscutting veinlets of quartz containing various amounts of pyrite, chalcopyrite, sphalerite and pyrrhotite. Pyrite, chalcopyrite and pyrrhotite are the dominant sulphides becoming more abundant with increasing alteration.

Horizons and bands of "chlorite schist" were originally thought to be zones of intense alteration, but are now considered to represent original chloritic or clay-rich layers intercalated within the upper parts of the pile of tuffs. Later ascending mineralized fluids replaced and penetrated these layers depositing sulphides.

Studies of fragment size distribution in the tuffs, and the degree of visible alteration, indicate that the most intense alteration coincides with the area of coarsest

fragments; figs. 31 and 32 The coarser tuffs, being the most porous, would facilitate passage of the mineralized fluids.

Although the alteration zone crosscuts the tuffs, both have been subjected to the same metamorphic and deformational events.

Separating the alteration zone from the base of the massive sulphides is a thin siliceous horizon. This is sparsely mineralized and altered, and possibly acted as a barrier to the ascending solutions forcing them to permeate the tuffs. An explosive break through is indicated by fracturing of this horizon, plate 29, and fragments of footwall tuff in the lower horizons of the massive sulphide lens, plate 48.

Textures within the sulphide lens, such as slumped layering and fragments of underlying rocks are indicative of deposition as unconsolidated sediments in an aqueous environment. The absence of alteration in the overlying aluminous cherts suggests that they were deposited after the sulphides had been formed. A longitudinal plot of the thickness of the sulphide lens shows the eastern extremity to form a line plunging at approximately 30^{o} to the west, fig. 34. The sulphides thicken westwards parallel to this line, and any continuation of the sulphide lens in this direction has been eroded away.

7.3 Main Gossan Zone

7.3.1 Introduction

The farm Solomons Mine derives its name from the presence of an Ancient or pre-European Working. This

Fig. 29. Generalized Stratigraphic Sequence at the J Locality.

	Thickness m.			
SOUTH		Chlorite+sericite, chlorite+quartz schist. Sediments.		GRAVELOTTE SUBGROUP
	175	Acid porphyry	TRANSITION	RUBBERVALE SUBGROUP
	<5	Chert, aluminous chert		
	0-5	Massive sulphides	ZONE	
	0-10	Chlorite schist, and altered tuff with stock-work sulphides	VOLCANICS	
	50	Felsic tuffs and breccias		
NORTH		Felsic flows with minor tuffs		

Thin dykes of acid and intermediate composition cut the volcanic sequence, and the whole is crosscut by thin, < 5m, basic intrusives.

The entire sequence dips at approximately 80° to the north and is stratigraphically overturned.

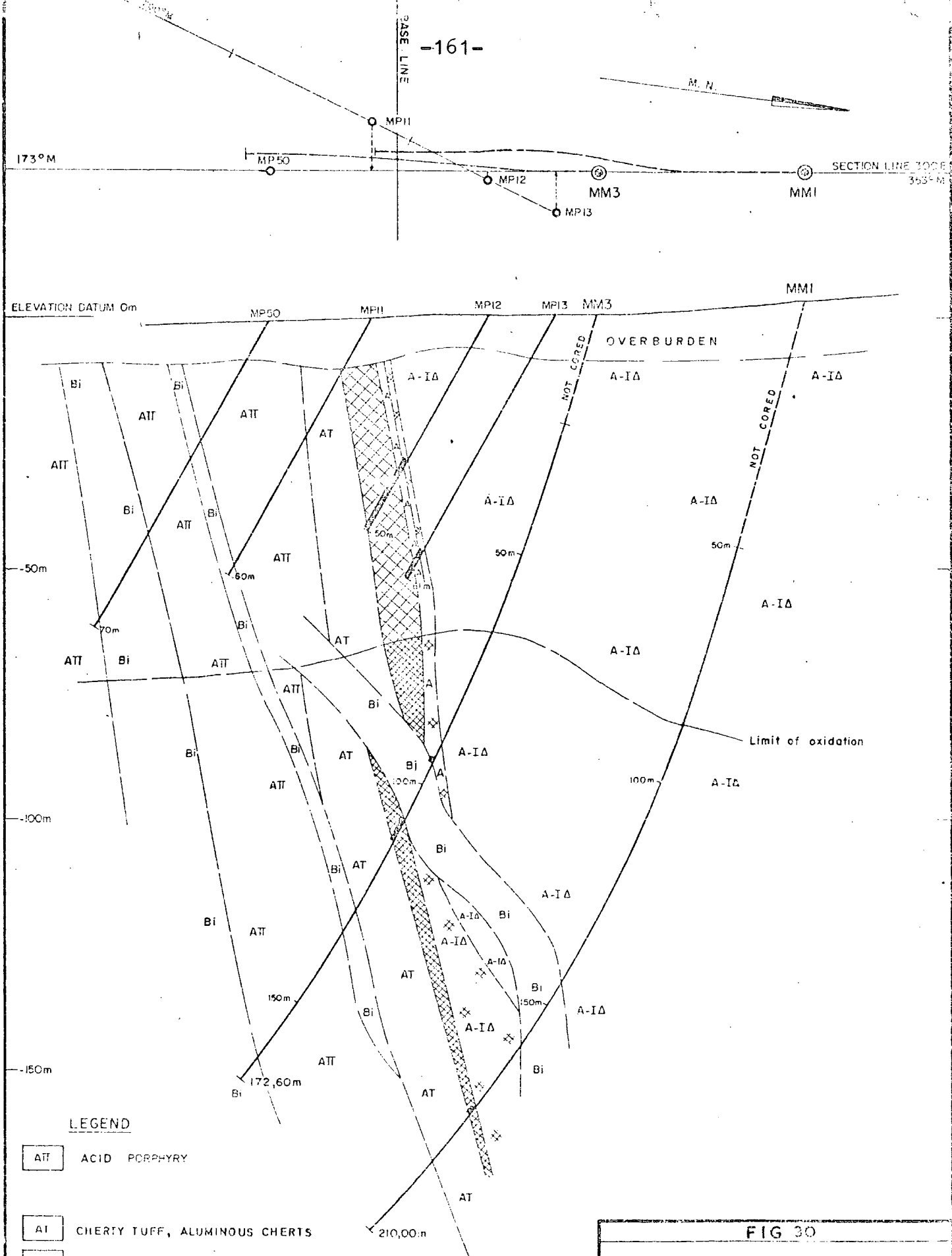

FIG 30

MURCHISON AREA

MARANDA

TARGET J

DIAMOND DRILL SECTION 300E

HOLES MM1 and MM3

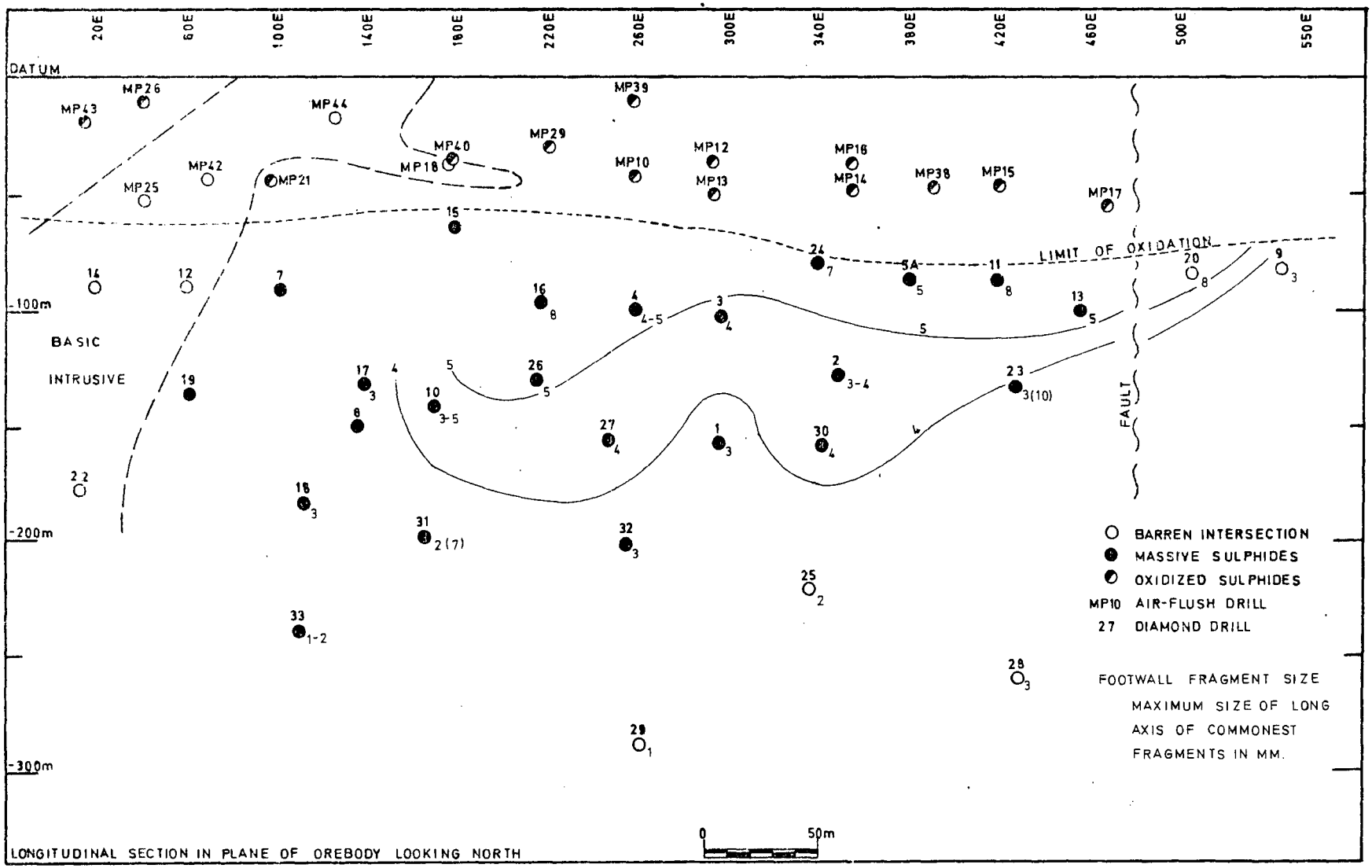

FIG 31 FRAGMENT SIZE IN FOOTWALL TUFFS AT THE J LOCALITY

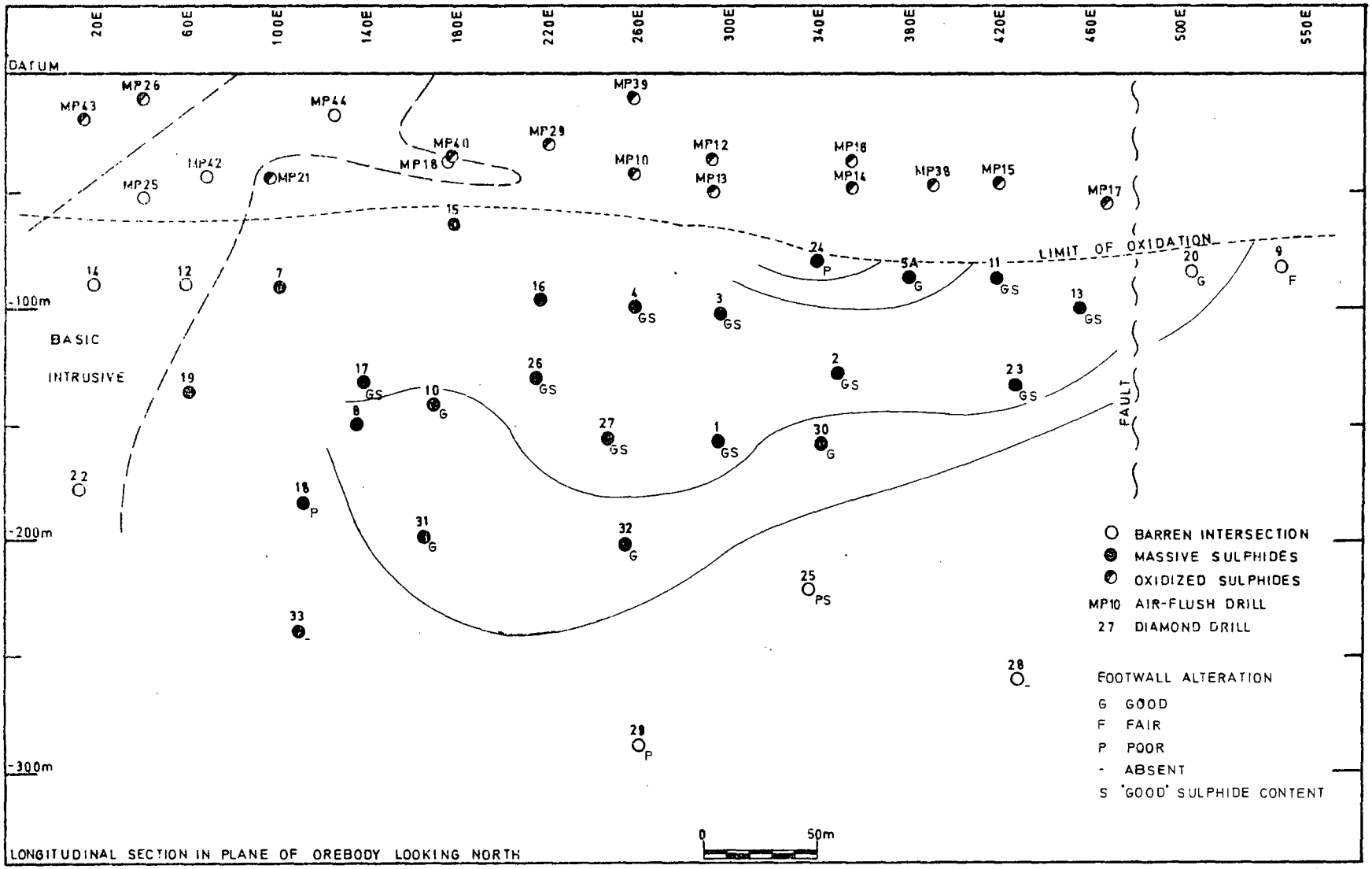

FIG 32 ALTERATION IN FOOTWALL TUFFS AT THE J LOCALITY

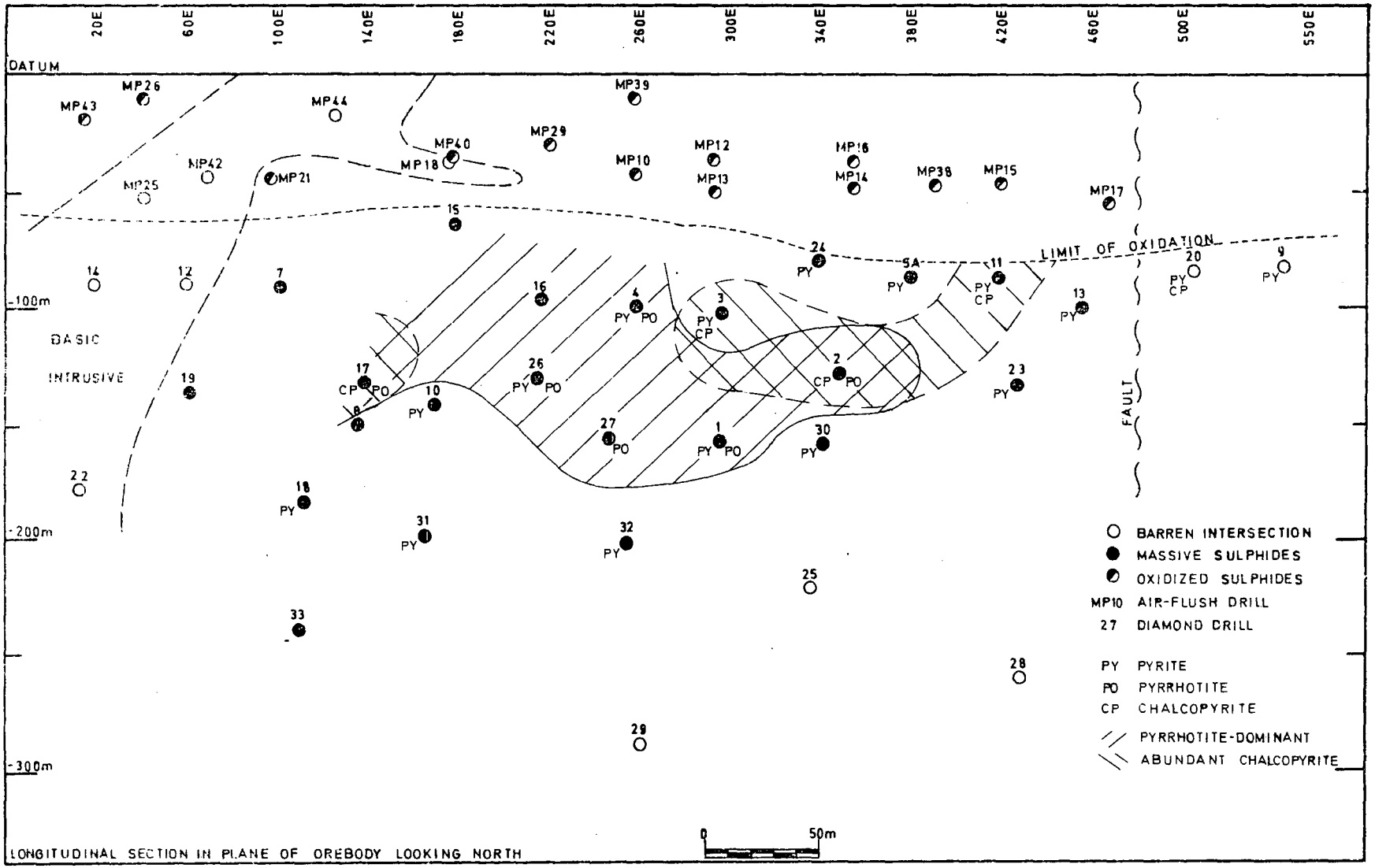

FIG 33 SULPHIDE DISTRIBUTION IN FOOTWALL ALTERATION ZONE AT THE J LOCALITY

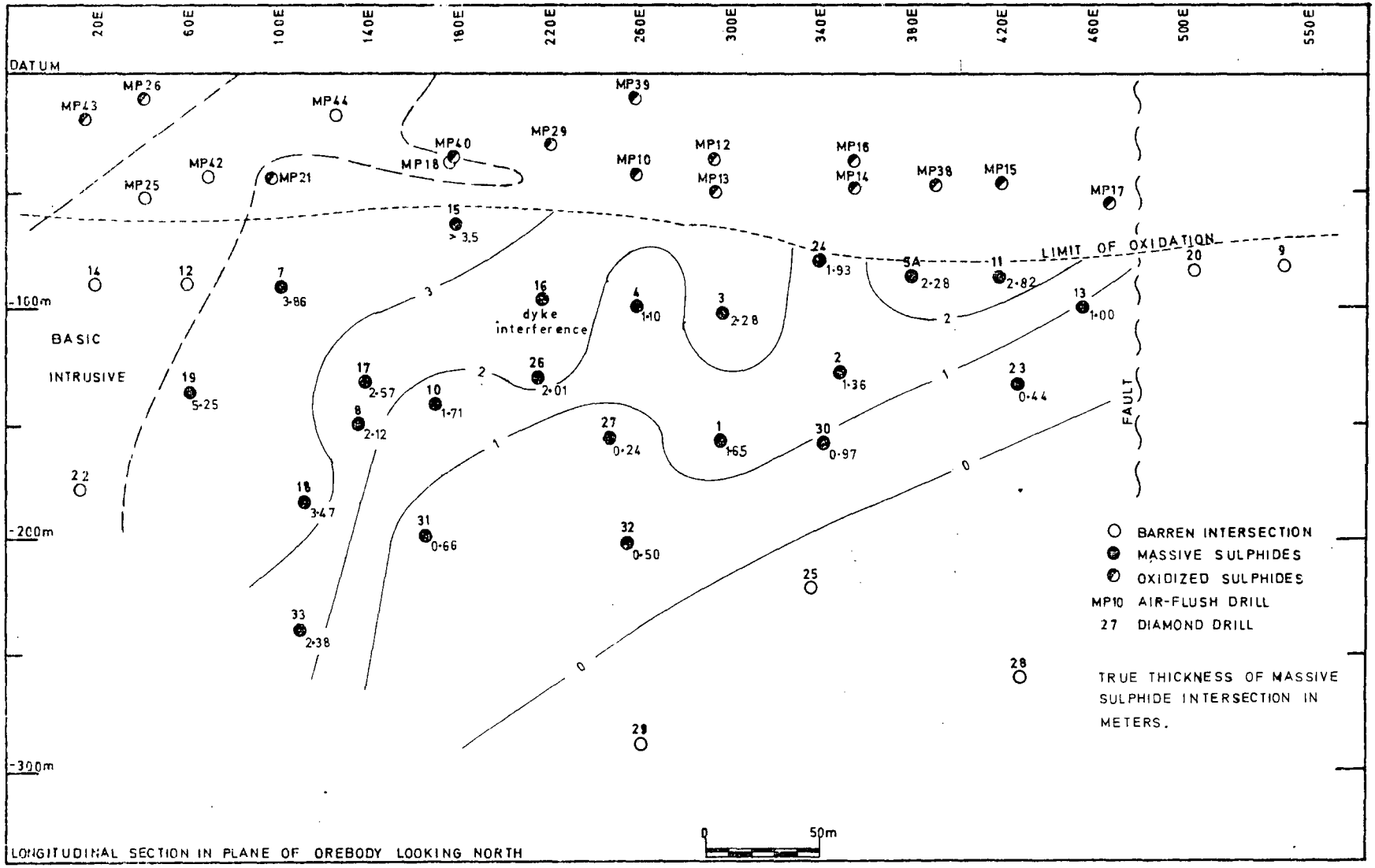

FIG 34 TRUE THICKNESS OF MASSIVE SULPHIDE LENS AT THE J LOCALITY

Plate 28. Typical alteration in footwall to the J massive sulphide deposit. White areas are original tuff.

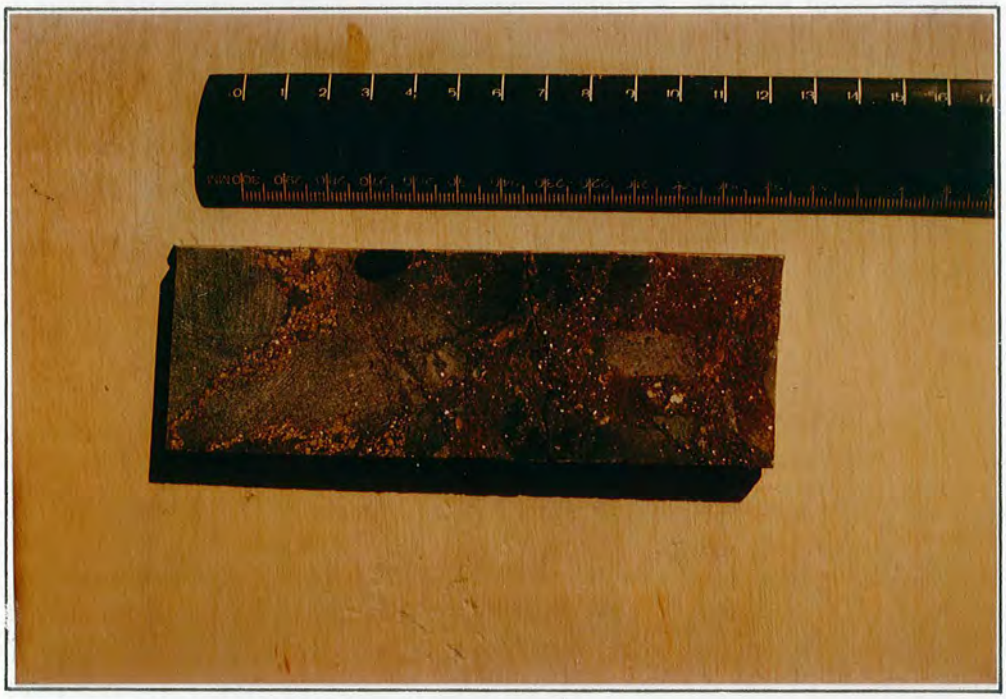

Plate 29. Chert horizon in the footwall of the J massive sulphide deposit. Brecciated and cut by sphalerite and pyrite veins. S_1 and S_0

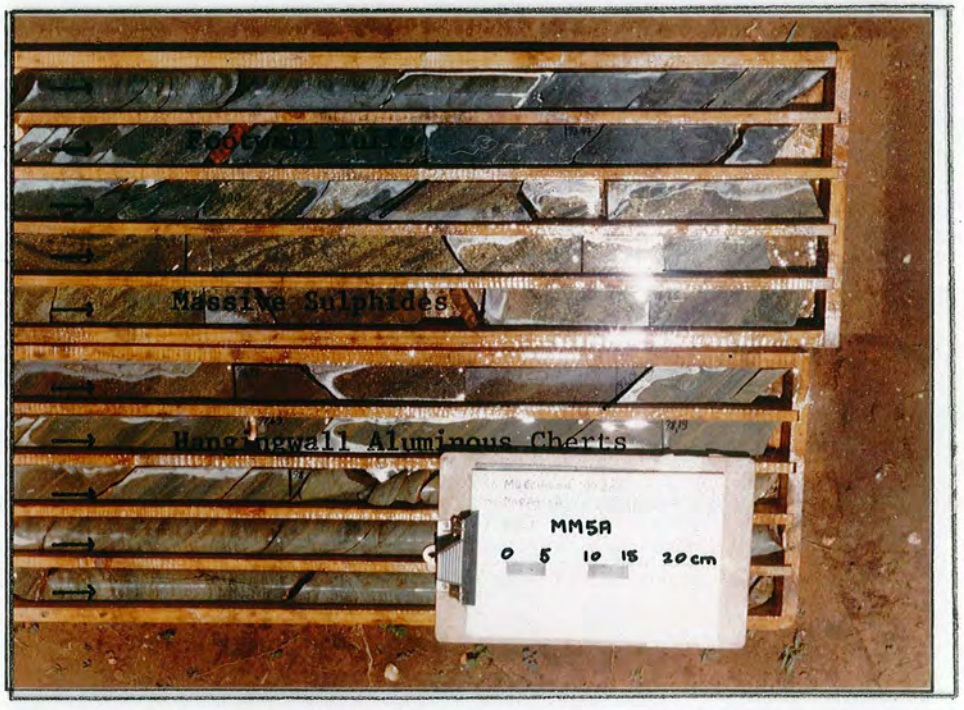

Plate 30. Massive sulphide intersection from hole MM5A, J locality. Arrow points from base to top of each run.

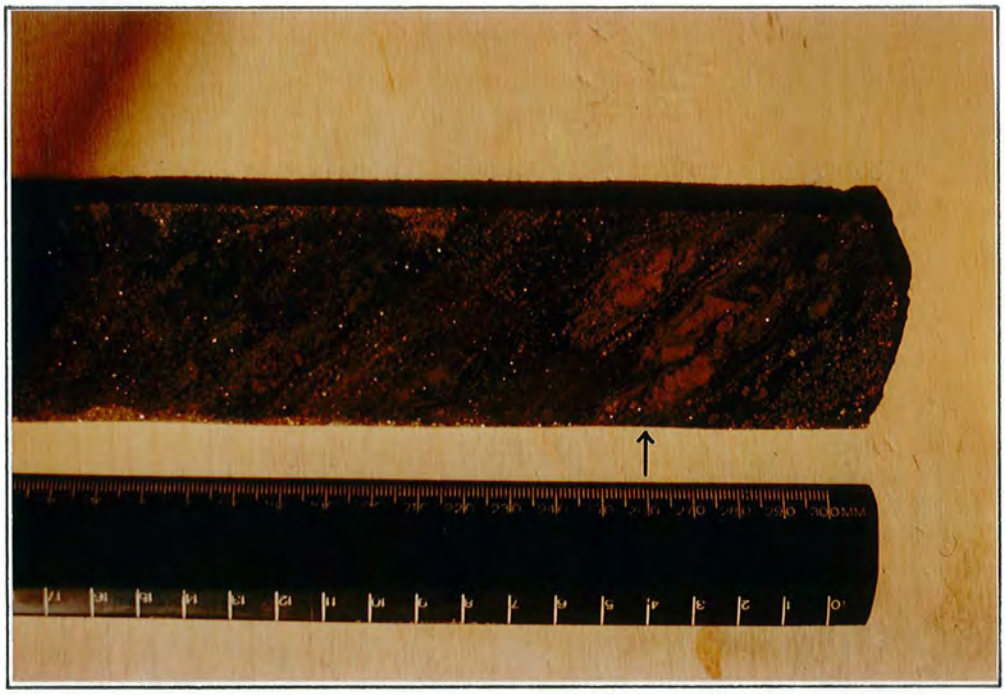

Plate 31. Banded pyrite+sphalerite ore, J massive sulphide deposit. Fragmented pyrite horizon arrowed.

Plate 32. Slump structures in banded silicate-sulphide horizon, J massive sulphide deposit.

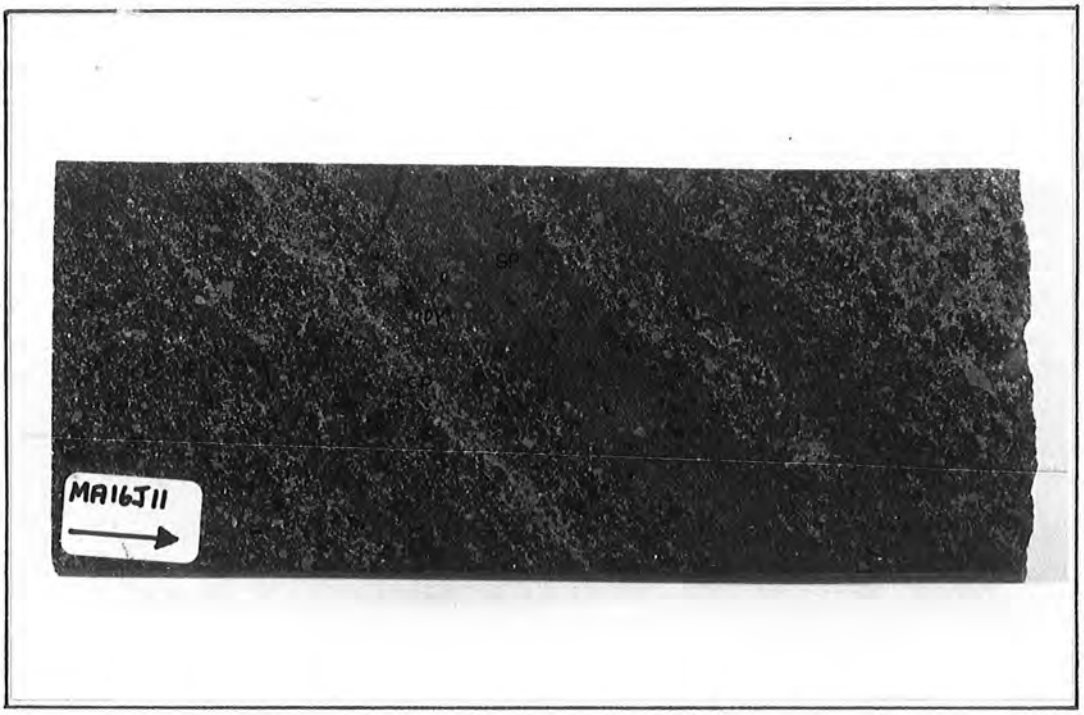

Plate 33. Banded massive sulphides, J massive sulphide deposit. Py - pyrite; sp - sphalerite; cp - chalcopyrite; po - pyrrhotite. Natural size.

working consists of a 100 m long trench, parallel to the geological strike, 5 m in width and, originally, probably 20 m in depth, which has been backfilled to within 3 m of the present surface. At the western end of the trench a pillar of massive goethite and limonite gossan was left; plate 34. Material from the surrounding dumps indicates that malachite was quarried, although the high zinc content would produce a brass-like alloy on smelting. Mining ceased when the oxide-sulphide boundary, and water table, was reached.

This Ancient Working appears to have been first mentioned by Van Eeden et al. (1939), and subsequent workers have recognized it as the surface expression of a massive sulphide deposit. Drilling of the deposit in the 1950's outlined a pod of massive Fe-Zn-Cu sulphides extending below the surface working, but failed to fully explore below the -100 m level.

The writer examined and worked on this deposit, here termed the MGZ or Main Gossan Zone, as part of the present investigation.

7.3.2 Geology

The geology at the MGZ locality was outlined from surface mapping, air-flush and diamond drilling, and is presented on fig. 35 and as a section in figs. 36 and 37

Intrusive into the sequence are three large basic sills, and a thin porphyritic "dolerite" which crosscuts the sulphide horizon. A later NE trending dolerite dyke occupies a fault, having an apparent horizontal displacement of 30 m dextrally. With the exception of the NE

dolerite dyke, the rocks have undergone regional deformation and metamorphism. The resultant schistosity S_1 is pervasive and parallel to S_0 the original bedding.

Original depositional textures have been largely destroyed and are preserved only in the cherty, hangingwall sequence. Three hundred meters north of the Ancient Working, flow-banding and flow-breccia textures were observed in an exposure of felsic extrusives; plate 13.

7.3.2a Footwall Sequence

The footwall sequence comprises uniform, fine grained quartz+chlorite+sericite schists containing rounded quartz "eyes" and lenses of fine grained quartz. These schists are identical to the uniform tuffs forming the majority of the volcanic pile elsewhere, and it is concluded that they were originally felsic tuffs. The quartz "eyes" represent relic high-temperature quartz phenocrysts, and the lenses either recrystallized phenocrysts or original siliceous fragments.

Diamond-drill hole MS1 provided a detailed section through the footwall immediately below the mineralization. The tuffs are grey-green, fine grained, with micaceous minerals forming a braided, schistose texture enclosing small lenses of fine, polygonally-granular quartz and/or quartz phenocrysts in various stages of re-crystallization. The chlorite content tends to vary but there is a general upwards increase through the sequence, with the appearance of thin, fine grained chlorite-rich horizons towards the top of the tuffs.

Fifty meters to the east, in drill hole MS6, footwall tuffs are identical to those in MS1 but contain more banded

chloritic horizons, and appear to be finer grained, more "sedimentary" in nature.

On surface, the footwall tuffs are exposed in and immediately north of the Ancient Working.

7.3.2b Mineralized Zone

When fully developed, the Mineralized Zone consists of three separate lithologies each with its own characteristic sulphide content, fig. 36 and plate 35. From bottom to top these are: a chlorite schist containing up to 20% vein and disseminated pyrite, pyrrhotite and chalcopyrite, overlain by mineralized chert with vague horizons of pyrite, chalcopyrite and pyrrhotite and finally massive pyrrhotite, sphalerite and chalcopyrite Contacts between each unit are sharp, although the lower chlorite schist grades into "normal footwall tuff" over 3 m.

The Mineralized Zone has been traced over a strike length of 120 m, the entire length of the Ancient Working, and in depth to over 200 m, although the massive sulphide unit only extends to a vertical depth of 100 m. Laterally to the west, the zone peters out to be replaced by a thin, 1 m wide, chlorite schist containing carbonate, quartz, sericite and variable amounts of pyrite and sphalerite. At the limits of the Mineralized Zone the chlorite schist is notably enriched in sphalerite.

In the east the zone is terminated by a large NE trending dolerite dyke, east of which only a thin chloritic schist marks the Mineralized Zone.

Chlorite Schist

The top of the footwall tuffs is marked by an increase in bands or layers of chlorite, and grades from a braided, schistose rock containing quartz "eyes" and lenses to a more laminated chloritic rock with patches or bands rich in quartz. This gradation is considered to be due to an increase in fine grained volcanic or volcano-sedimentary components during the last stages of tuff deposition. Over a 3 m interval this merges into a soft, dark green, chlorite schist.

Within this chlorite schist, occasional "ghosts" can be seen, in outline resembling quartz lenses, but composed of fine grained green chlorite.

Sulphides form thin veinlets and disseminations of pyrite, chalcopyrite and pyrrhotite. Pyrite also forms large porphyroclasts with pressure shadows containing chalcopyrite and pyrrhotite, plate 69. Sphalerite is present as small grains in the chalcopyrite. Total sulphide content increases towards the upper contact where it may constitute up to 20% by volume of the rock. The chalcopyrite+pyrite component increases relative to the pyrrhotite.

The contact with the upper mineralized chert is sharp and conformable with schistosity and banding within the footwall sequences.

Mineralized Chert

This forms a prominent, well mineralized horizon. On surface, and to a vertical depth of 100 m, it is overlain by massive sulphides. Below this depth the

massive sulphide horizon is absent and the chert is directly overlain by the hangingwall sequence.

The rock is pale grey to white, consisting of coarsely recrystallized quartz with minor chlorite, sericite and actinolite, and is considered to represent a recrystallized chert or quartzose rock. The informal term "mineralized chert" was applied to this unit. Sulphides form crude parallel horizons of semi-massive, coarse, 5 mm, cubic pyrite with interstitial chalcopyrite and pyrrhotite. The pyrite is commonly fractured and broken with infills of pyrrhotite, plate 70. Sphalerite is present as minute grains in the other sulphides. Chalcopyrite tends to have an antipathetic relationship with the pyrite, being concentrated in pyrite-poor horizons. Overall, the sulphide content is estimated at 40% pyrite, 6% chalcopyrite, 5% pyrrhotite, and traces of sphalerite. In one diamond-drill hole and several air-flush holes, two mineralized chert horizons were intersected, separated by unmineralized actinolite+ chlorite+quartz+magnetite schist.

Massive Sulphides

In the surface Ancient Working, the mineralized chert unit is overlain by up to 2 m of massive goethitic and limonitic gossan, plate 34. Air-flush drilling immediately beneath this gossan intersected massive pyrrhotite+sphalerite+chalcopyrite in a quartz+chlorite gangue. Pyrrhotite is the dominant sulphide, pyrite being virtually absent, and sphalerite+chalcopyrite together form approximately 10% of the total. This

massive sulphide unit only extends to 100 m vertical depth. Its limited extent would suggest that the original occurrence was a small, pod-like body.

Unfortunately only small chips, less than 5 mm in diameter, of fresh sulphide were available for study, and sulphide-sulphide textures could not be observed. However the sulphides do appear to be coarsely granular and recrystallized.

7.3.2c Hangingwall Sequence

Surface exposure of hangingwall rocks is limited to a chlorite+quartz+epidote schist along the southern wall of the Ancient Working, and small exposures of "cherty tuff" 80 m to the south. The lower 100 m of the hanging-wall sequence, or Transition Zone, has been examined in borehole core.

Immediately above the massive sulphides or mineralized chert is a 1 m thick chlorite+quartz+epidote schist. Some coarse quartz grains and granular lenses are also present within this, and laths of ilmenite are disseminated throughout, and may locally constitute up to 15% of the rock. Sulphide mineralization is confined to minor amounts of disseminated pyrite. There is no visible alteration nor are there crosscutting sulphide veinlets.

This schist is similar to, though more uniform than, other thin bands of chlorite+quartz+epidote schist within the hangingwall succession.

The remainder of the sequence comprises a varied assemblage of thinly banded and layered, pale green siliceous rocks with finely laminated chloritic horizons

and coarser, siliceous bands containing frequent rounded, corroded and broken albite and quartz grains, and fragments of a medium to fine grained acid rock. Banded cherts have also been recorded.

Horizons containing rock fragments, feldspar and quartz grains, chert "lenses", banded cherts, graded bedding, and a well developed compositional and textural layering would suggest that the sequence was derived by the reworking of volcanic rocks with intercalated cherts and muddy or clay-rich horizons. These reworked volcanic rocks bear many similarities to, and occupy the same stratigraphic interval as, the acid porphyries of the L-W and J localities to the west.

Pyrite is fairly abundant as fine bands of disseminated cubes parallel to the schistosity, often in thin quartz-rich laminae. Some pyrite occurs in small crosscutting quartz veinlets which may be caused by metamorphic remobilization. Minor amounts of pyrrhotite and sphalerite are also present.

Air-flush drilling intersected the top of the Transition Zone sequence approximately 150 m south of the Ancient Working. Here finely laminated chlorite+ sericite and quartz+sericite schists contain inherently high nickel values, > 300 ppm, and mark the beginning of the overlying sedimentary sequence. This contact is not exposed on the surface.

7.3.2d Intrusives

In the immediate area of the MGZ deposit, three large basic sills intrude the sequence, figs. 35 and 36

one in the footwall and two in the hangingwall. In appearance and mineralogy they are identical to sills elsewhere in the study area, see chapter 5.

The sill in the footwall is slightly transgressive in the original vertical plane, being 40 m north of, and hence below, the mineralized zone on surface but intersecting this zone at a vertical depth of 250 m in drill hole MS4.

A thin, 4 m wide, porphyritic "dolerite" was intersected near the surface 15 m south of the Ancient Working. The same intrusive cuts the mineralized zone at approximately the -150 m level, winding in and out of the sulphide horizon. This intrusive is a fine grained chlorite+quartz+actinolite rock with albitized plagioclase phenocrysts, and is essentially a fine grained version of the sills mentioned above.

7.3.2e Metamorphism and Deformation

Both sulphide and silicate horizons have undergone metamorphism. Definite depositional textures could still be observed in the hangingwall sequence, but these have been obliterated in other rocks.

The S_1 schistosity is universally developed, being parallel to bedding as defined by compositional and lithological layering. Small intrafolial folds were not observed, nor was the S_2 cleavege in the immediate vicinity. The L_1 lineation is present on surface exposures of footwall schists and is vertical. Similar vertical lineations are present in the massive gossan pillar, in the Ancient Working, suggesting that the sulphide lens

has undergone the same deformation; plate 36.

Fig. 38 is a vertical section in the plane of the mineralization. This clearly shows the limited extent of the massive sulphide unit, and the vertical elongation of the mineralized chert parallel to surface L_1 lineations.

7.3.3 Summary

The MGZ sulphide deposit consists of chloritic and cherty mineralized horizons overlain by massive sulphides. These three units, forming the Mineralized Zone, lie on the contact between "true volcanic tuffs" to the north, and cherts, chloritic horizons and reworked acid porphyry to the south. The mineralized zone is laterally impersistent, grading rather abruptly through a zinc-rich halo, into a thin, sporadically mineralized chloritic horizon which elsewhere in the area marks this important contact.

The lower two units, the chlorite schist and mineralized chert, contain disseminated to semi-massive sulphides. These are dominantly pyrite with significant chalcopyrite and pyrrhotite. Sphalerite occurs in trace amounts only. Within the chlorite schist the copper content increases stratigraphically upwards.

In the overlying massive sulphide unit, pyrrhotite is the dominant sulphide with sphalerite and lesser chalcopyrite. Pyrite is virtually absent. A cross-cutting alteration zone was not observed in the footwall sequence. However geochemical studies suggest that chemical alteration has taken place in the footwall, see chapter 9.

Later metamorphism and deformation have recrystallized the sulphide assemblage, elongating the original sulphide pod in the vertical axis parallel to local L_1 lineations.

Evidence on the origin of the deposit is not conclusive, but the following points suggest a syn-sedimentary or volcanogenic origin:

1. Sharp layering of the mineralized units conformable with the bedding of the hangingwall sequence.
2. Asymmetry of the mineralization in the stratigraphic vertical sense.
3. Absence of alteration in the hangingwall.
4. Occurrence at the same stratigraphic level as the J and L-W deposits.

7.4 D Locality

7.4.1 Introduction

One kilometer along strike to the west of the MGZ deposit a diffuse, low amplitude soil geochemical anomaly of 288 ppm zinc, in a background of 108 ppm, was found to be associated with a weak PEM anomaly in an area of no exposure. Subsequent drilling outlined a small pod of massive sphalerite, associated with felsic tuffs, and sandwiched between basic sills.

7.4.2 Geology

The volcanic sequence is complicated by the presence of four large basic sills. These apart, the sequence consists of various siliceous, felsic, and cherty tuffs with a prominent white chert horizon; fig. 39 . Within these tuffs a pod of massive sphalerite, with minor pyrite and chalcopyrite, is underlain by a thin chlorite schist containing metamorphic amphiboles, magnetite blebs

FIG 35

GEOLOGICAL MAP OF THE MGZ LOCALITY

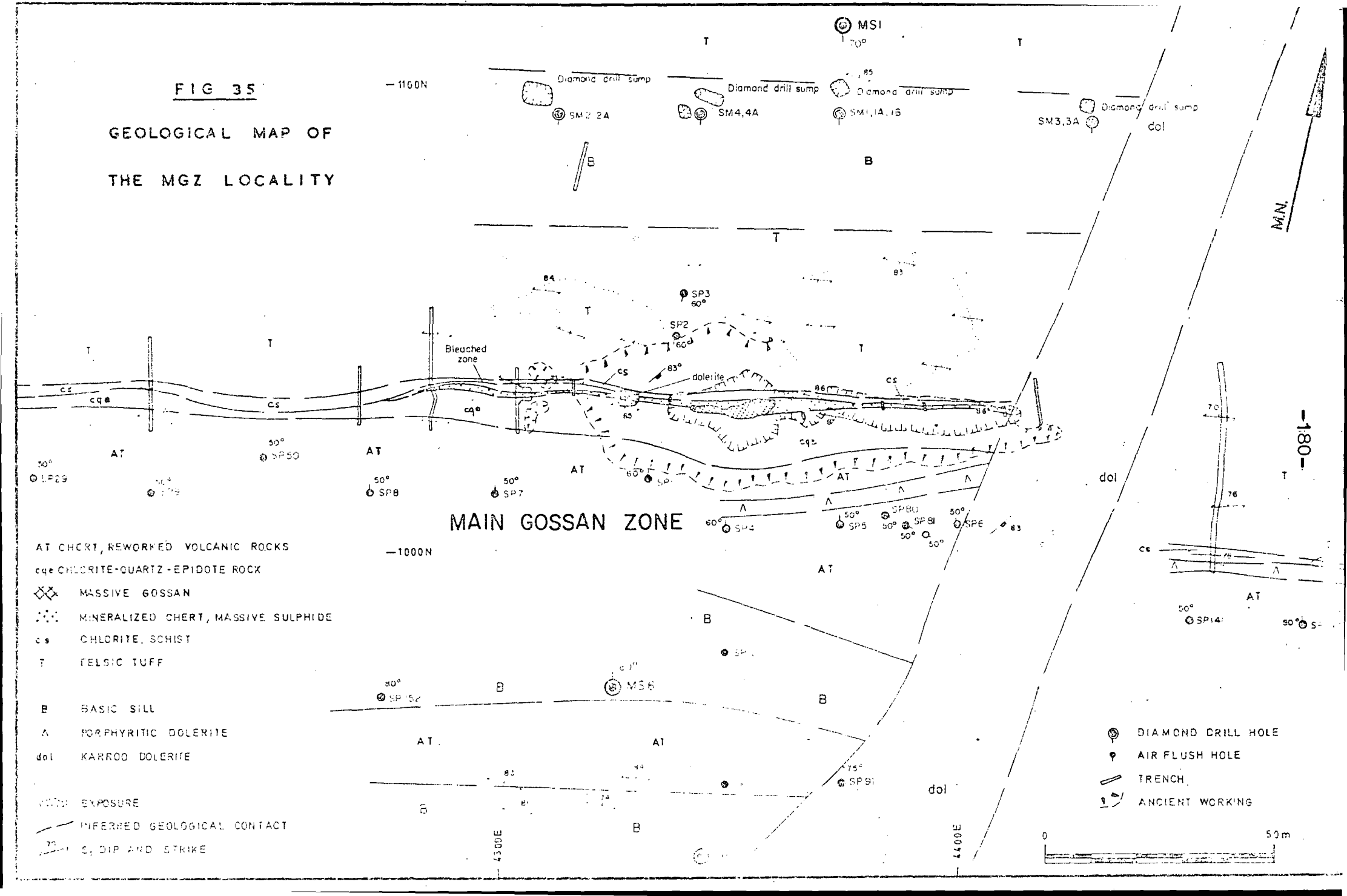

AT CHERT, REWORKED VOLCANIC ROCKS

cqe CHLORITE-QUARTZ-EPIDOTE ROCK

MASSIVE GOSSAN

MINERALIZED CHERT, MASSIVE SULPHIDE

cs CHLORITE. SCHIST

T FELSIC TUFF

B BASIC SILL

Λ PORPHYRITIC DOLERITE

dol KARROO DOLERITE

EXPOSURE

INFERRED GEOLOGICAL CONTACT

DIP AND STRIKE

DIAMOND DRILL HOLE

AIR FLUSH HOLE

TRENCH

ANCIENT WORKING

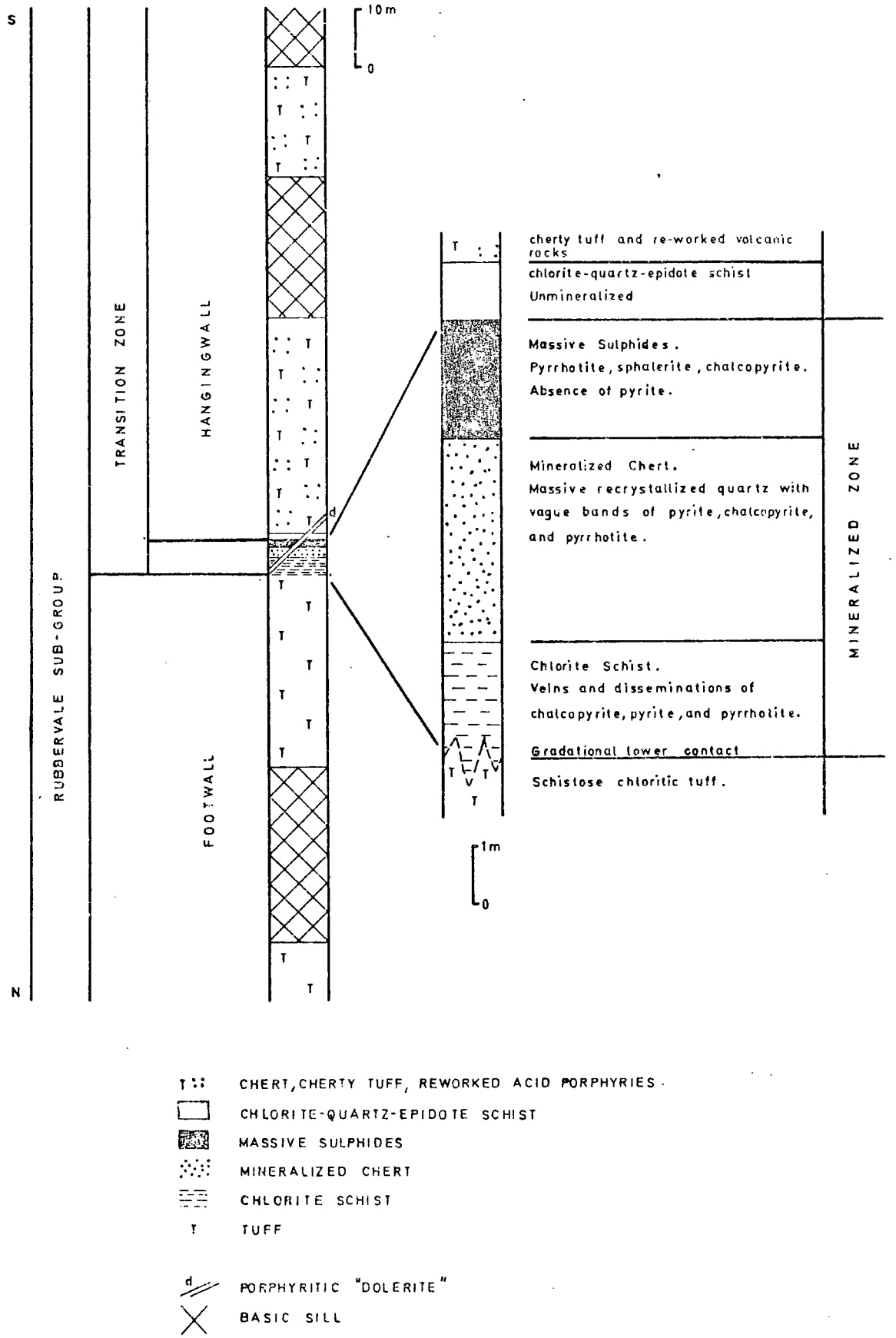

FIG 36 STRATIGRAPHIC SEQUENCE AT THE MGZ LOCALITY

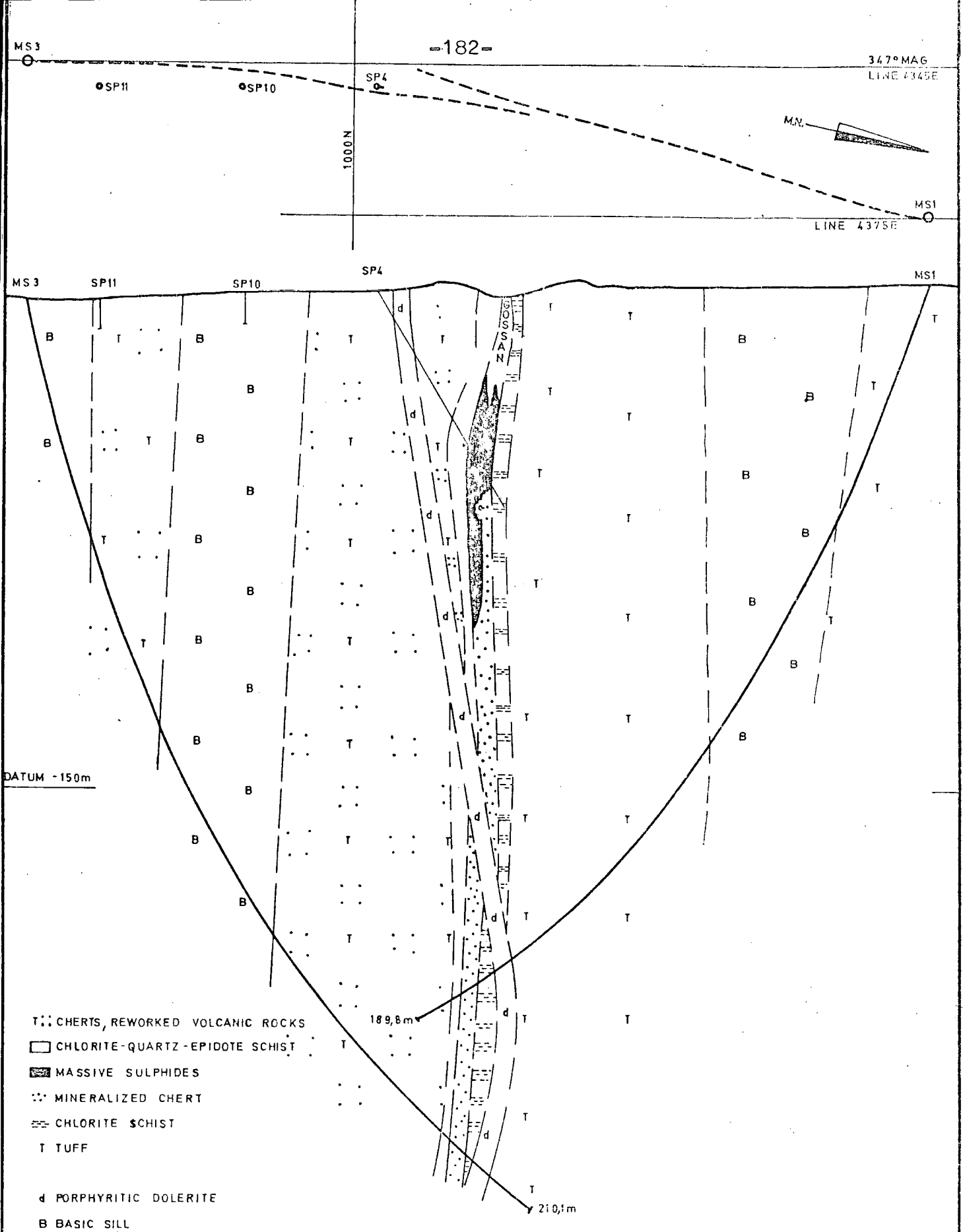

FIG 37 DIAMOND DRILL SECTION

4345E. HOLES MS1 & MS3.

MGZ LOCALITY

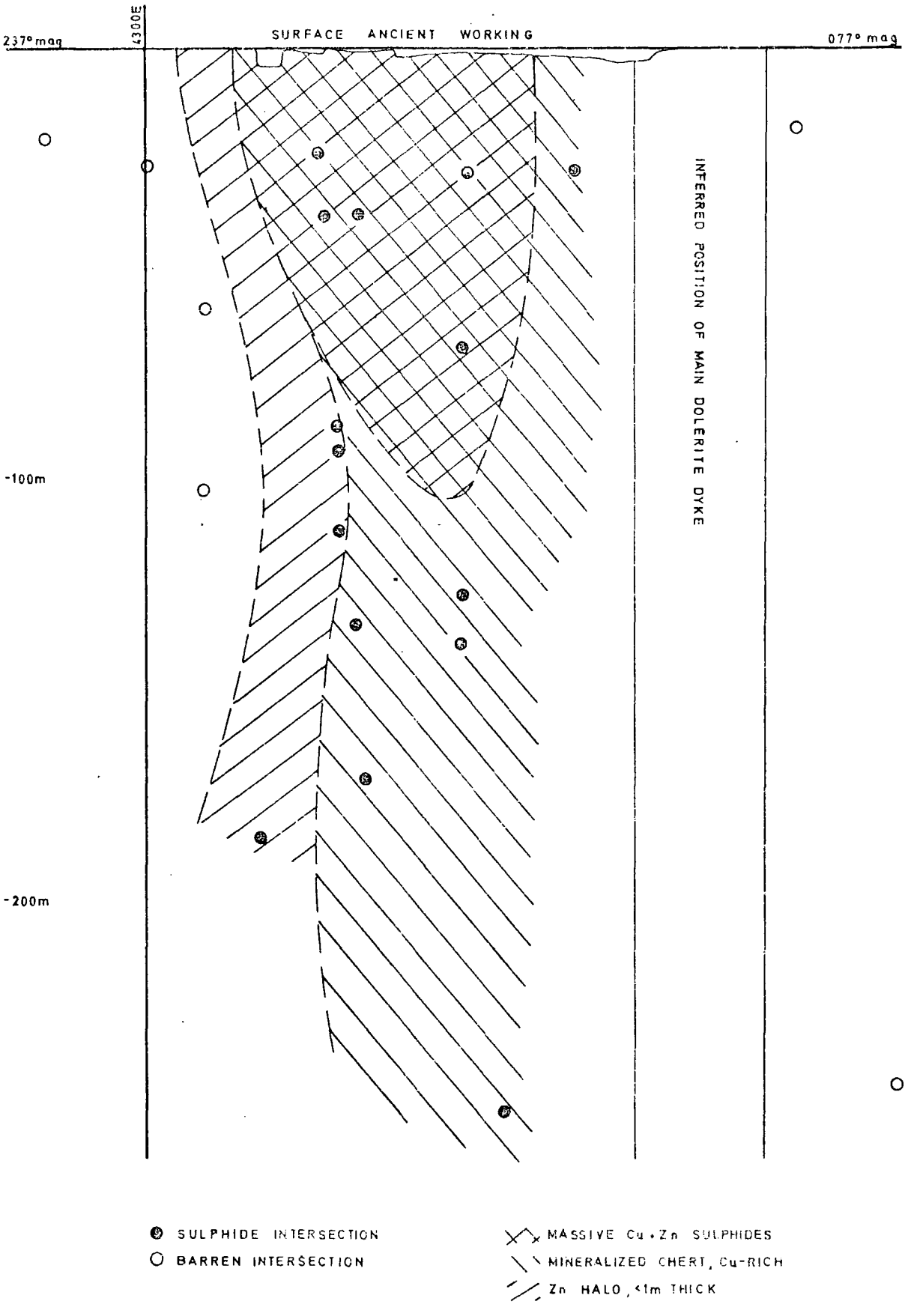

FIG 38 LONGITUDINAL SECTION IN THE PLANE OF MINERALIZATION, MGZ LOCALITY

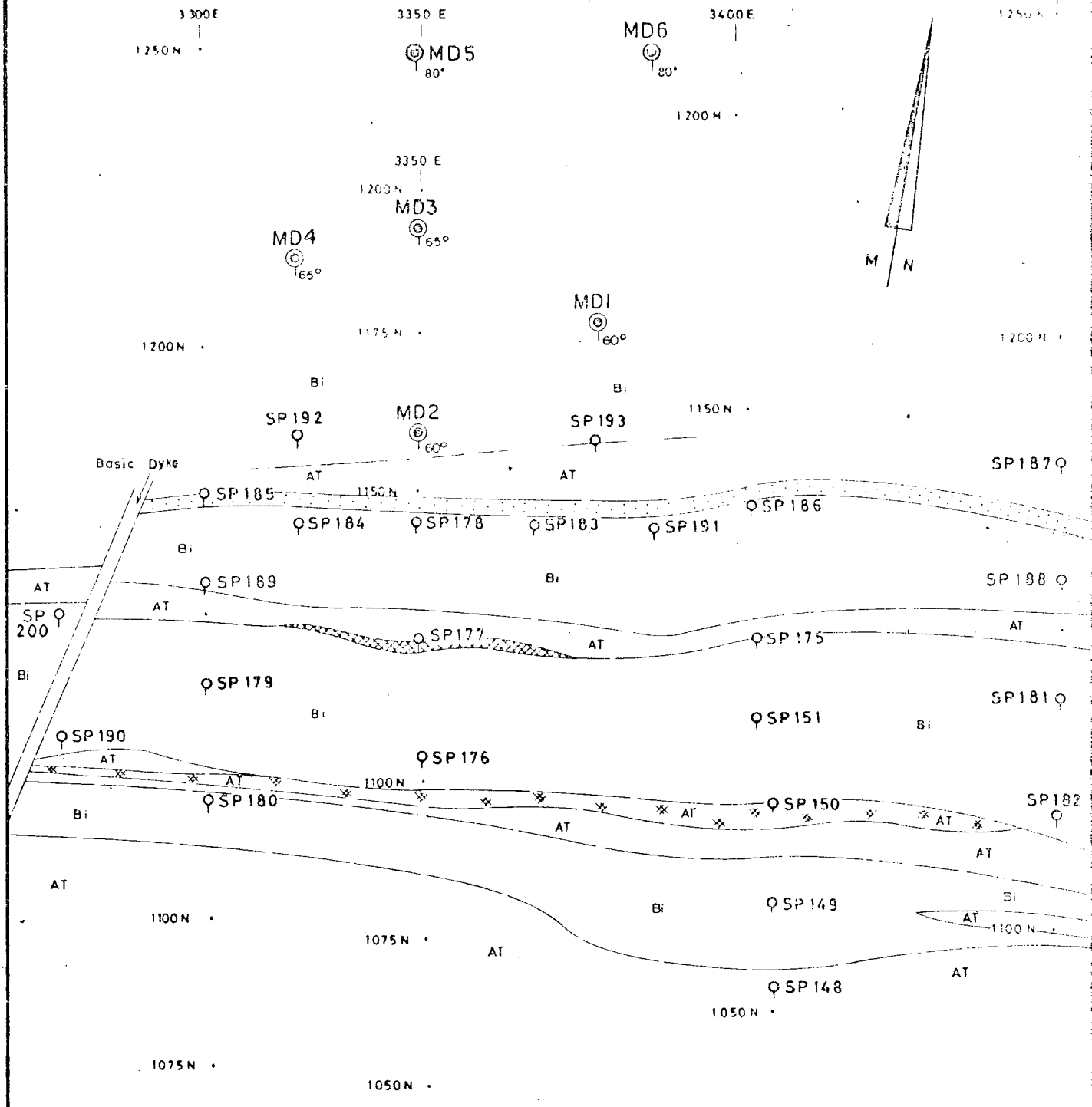

NOTE: ALL PERCUSSION HOLES DRILLED AT 60° INCLINATION

LEGEND

- AT — ACID TUFF
- CHERT
- Bi — BASIC INTRUSIVE
- MASSIVE GOSSAN
- DISSEMINATED GOSSAN
- DIAMOND DRILL HOLE COLLAR
- PERCUSSION DRILL HOLE COLLAR
- INFERRED GEOLOGICAL CONTACT

10 0 10 20 30 40 50 m

SCALE

FIG 39

MURCHISON AREA

MON DESIR

TARGET D

GEOLOGY

SCALE 1 INCH

Plate 34. Pillar of gossan (G) in the Ancient Working at the MGZ deposit, Solomons Mine. Hangingwall sequence (HW) is immediately to the left of the gossan.

Plate 35. Sulphide intersection from hole MS1, MGZ locality. Massive sulphide unit is absent.
Arrow Points from base to top of each run.

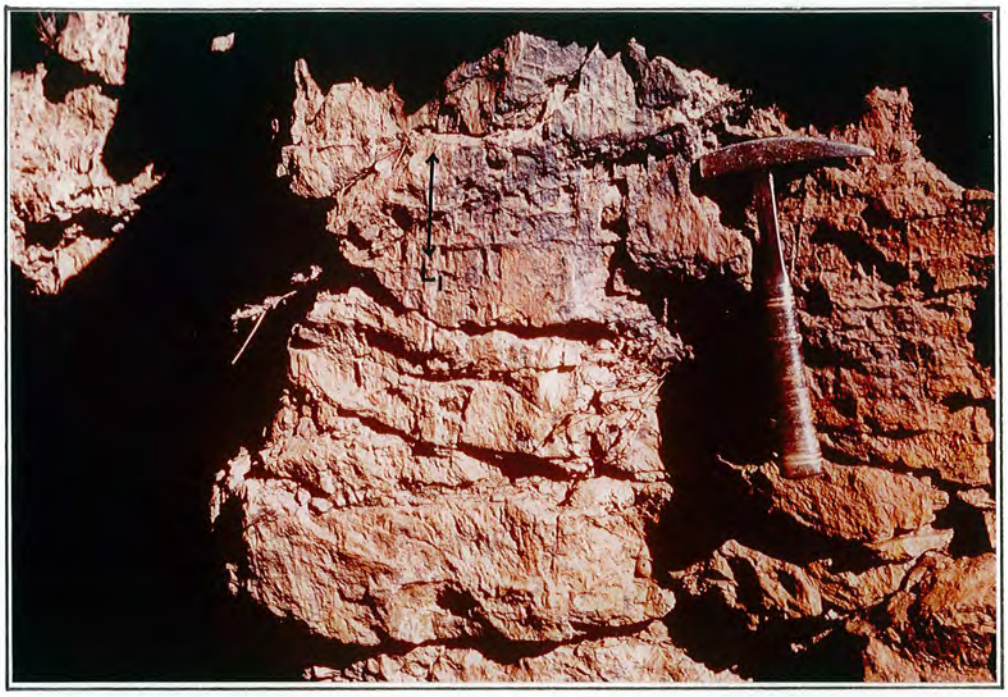

Plate 36. Vertical L_1 lineations on gossan pillar in the Ancient Working at the MGZ locality, Solomons Mine. Horizontal lines are caused by weathering.

Plate 37. Massive sulphide intersection from hole MMD2 D locality. Cs- chlorite schist with sphalerite bands (brown); MS - massive sulphide, mainly sphalerite; BI - basic intrusive.

and minor chalcopyrite and pyrite. The pod is now everywhere in direct contact with a basic sill, plate 37. A footwall alteration zone or disseminated sulphide zone was not located, although veinlets of pyrite and sphalerite occur laterally to the massive sulphides.

The sulphide pod is 50 m long, 2 m maximum thickness and has been traced vertically for 100 m. The lower part is banded with layers of chlorite+quartz and sphalerite+quartz+carbonate; the sphalerite content increases up the sequence. This part is overlain by coarse to finely crystalline, dark red-brown sphalerite with occasional bands of chlorite+quartz+carbonate. The top of the sulphide pod is in sharp contact with a basic sill, although the contact is marked by a thin zone of carbonate; plate 37. Some inclusions and grains of sphalerite occur within the sill.

The banded nature of the sulphide pod and its occurrence at a chloritic, mineralized stratigraphic horizon would suggest an original massive sulphide lens. Later basic sills possibly partially remobilized the sulphides.

7.5 The L and W Localities

7.5.1 Introduction

Approximately 100 m south of Carrolls Peak, in the northeast of the farm Maranda, a prominent ridge trends for 1000 m westwards from the farm boundary, terminating abruptly in flat-lying ground, plate 2. Exposure is limited to the crest of the ridge; the slopes being covered by extensive scree, and the surrounding flat

areas by thick, loamy soil.

Surface prospecting located gossanous and limonitic float which was traced to two areas of mineralized outcrop. The eastern area, designated the L locality, consists of flow banded and brecciated felsic lavas and cherty schists containing limonite as spots and in veins. Eight hundred meters to the west, at the termination of the ridge, limonite spots and thin goethite veins were observed in cherty, tuffaceous-looking rocks, and this area was termed the W locality. Both areas are associated with copper and zinc soil geochemical anomalies, but these are displaced downslope to the south of the surface exposures. Mineralization was not observed in the area between the two targets.

7.5.2 Geology

The geology, style and amount of mineralization were elucidated from surface mapping, air-flush and diamond drilling at each locality. Both areas cover the same stratigraphic horizon and the mineralization is confined to a 30 m thick sequence of "cherts" occurring between felsic flows to the north and acid porphyries to the south. This is the same interval in which the massive sulphide deposits at J, 5 km to the west and MGZ 14 km to the east, are located. A generalized sequence comprises:

SOUTH	Acid porphyry	Hangingwall	Volcanic Transition Zone	Rubbervale Subgroup
	Cherts, aluminous cherts, re-worked volcanics. Mineralized	Mineralized Zone		
NORTH	Flows, tuffs, breccias	Footwall		

See also fig. 41 and map 3.

7.5.2a Footwall Sequence

The footwall volcanic rocks consist of a series of thin, 2-13 m thick, pale grey, massive, siliceous flows, separated by up to 1 m of coarse breccia or tuff. Within the flows laminar or contorted flow banding and areas or lines of quartz-filled amygdales were observed. The bases of individual flows tend to be very fine grained and often silicified, although this may be secondary. The tops tend to show contorted flow banding and amygdales. They may show occasional fragments, or grade into breccia horizons. An imperfect planar fabric, parallel to the local S_1 plane, is outlined by prominent chlorite-filled fractures, the alignment of fine grained chlorite in the rock, and the elongation of quartz+chlorite-filled amygdales.

Partial weathering along fractures gives rise to pseudo-breccia textures, which are absent below the oxidation level in borehole core.

Intercalated with the flows are thin, 45 cm thick, coarse breccias, often having irregular lower contacts with flow banded and brecciated lavas. The upper contacts are sharp; plate 38. The breccias consist of unsorted lava fragments up to 80 mm in length, usually with their long axes parallel to the flow banding in the lava, set in a fine grained groundmass of quartz and chlorite. Occasionally thin tuff horizons were observed with slump structures and graded bedding younging to the south; plate 39. They are indicative of sub-aqueous deposition. The contact with the Transition Zone is marked by 1 m of reworked volcanic rocks.

Mineralization in the footwall is common at the L locality where minor amounts of pyrite, sphalerite, pyrrhotite and

chalcopyrite occur in quartz stringers within flows, and as matrix disseminations with diffuse chlorite in the tuff horizons. Locally up to 10% sulphides may occur in the tuffs.

7.5.2b Mineralized Zone

The lower part of the Transition Zone at L and W, is composed of a varied, largely cherty, assemblage up to 30 m thick and grading rather abruptly into the overlying acid porphyries or welded tuffs, fig. 40. Mineralization, in the form of finely disseminated sphalerite with minor pyrite, chalcopyrite and pyrrhotite, is confined to the base of the sequence at the L locality but occurs near the top at W; see also fig. 40. In both cases the host rock to the best mineralization is a pale grey chert.

The L Locality

The succession through the mineralized zone was studied in detail in drillhole ML2; fig. 40. This hole was drilled at an inclination of 60^{o} from the horizontal, towards the south; frontispiece. All depths given are depths down the hole.

From the surface to 44 m acid flows with flow-top breccias and tuff horizons were intersected. Sulphides are disseminated within the matrix of the tuffs, and occur as veins of pyrite+ chalcopyrite+sphalerite. The interval between 34 and 44 m was logged as a flow although the rock is fine grained, massive and siliceous, and contains minor sericite and abundant fine, diffuse,dark green chlorite. Frequent, 1 mm thick quartz veins and lenses often carry chalcopyrite and sphalerite. The base of the Transition Zone is at 44 m, and from here to 60 m the rock consists of a pale grey, very fine grained chert containing thin sericite bands. Frequent thin irregular quartz+sphalerite+ +chalcopyrite veinlets and disseminated red-brown sphalerite

grains are concentrated between 44 and 46 m, although the total sulphide content rarely exceeds 10% of the rock. In the interval 48-53 m, fine siliceous fragments occur in a chloritic and siliceous matrix giving the rock a blotchy, banded appearance. Between 5 and 10% sulphides, mainly pyrite, form veins, fracture infills and are associated with chlorite clots in the matrix.

From 60 to 78 m is a cherty tuff containing 50% siliceous fragments set in a groundmass of fine grained quartz+chlorite+ sericite. Distribution of sulphides is patchy. Above 66 m there is an abrupt decrease in total sulphide content, being confined to minor disseminations of pyrite, and rare quartz+ sphalerite veinlets.

Closely packed siliceous fragments in a cherty matrix form tuff horizons from 78-80 m.

A basic sill was intersected between 80 and 84 m baking the tuffs on either side for a distance of 60 cm.

From 84 to 90 m further tuffs contain elongate siliceous fragments, of 1-2 mm and 5 mm sizes, and these often form thin bands with chlorite partings. This horizon has a more banded or laminated appearance. Conformably overlying this are quartz porphyries. The hole was terminated at a depth of 137 m.

The following interpretation is proposed for the sequence described above.

Pure cherts account for a relatively minor proportion of the lower part of the Transition Zone which here contains a high proportion of cherty tuffs or volcanic fragments set in a very fine grained quartz-rich matrix. The presence of

fragments of volcanic rock and the trace element chemistry of these cherts, see chapter 6, suggests that they are reworked felsic volcanic rocks. Rounded fragments, fine sericite banding and interlayered tuff and cherty rock suggest a subaqueous depositional environment.

The majority of the sulphide mineralization is patchily distributed throughout the upper 3 m of the flows and the lower 22 m of the cherts and cherty tuffs, with the higher zinc values occurring between 44 and 46 m down the hole. The dominant sulphide is pyrite with lesser amounts of sphalerite and traces of chalcopyrite and pyrrhotite, and these occur in quartz veinlets or in the groundmass to the tuffs. These quartz veinlets are possibly later segregations from the tuffs or cherts. Dark green chlorite and clear quartz are the immediate gangue minerals.

The W Locality

Here the mineralization is confined to cherts and aluminous cherts within the Transition Zone. On surface there appear to be two mineralized horizons coalescing in the west. Diamond drilling however only intersected one horizon. See map 3. The geological sequence at W was studied in detail in drillhole MW2 which was drilled at an inclination of 75° towards the south.

This hole passed through 37 m of basic intrusive, followed by 66 m of felsic flows containing several breccia and tuff horizons. The Transition Zone sequence consists of 75 m of cherts, aluminous cherts, thin volcanic sediments and cherty tuffs. The majority of the sphalerite mineralization is contained within a 19 m wide band towards the top

of this sequence, fig. 40. The hole was terminated, after intersecting 9 m of acid porphyry, at a final depth of 187.80 m. The top of the footwall volcanic sequence, from 102-103 m, is marked by a 1 m thick horizon of coarsely fragmented lava, re-worked volcanic rocks and thin tuff bands. This is overlain by a fairly uniform, fine grained, siliceous rock with a variable sericite and chlorite content which imposes a fine braided schistosity and micaceous banding to the rock. The banding is possibly derived from an original compositional banding or layering. In an earlier section this sequence was interpreted as banded, impure cherts, and is referred to as aluminous cherts; see also chapter 6.

From 103 to 106 m numerous homotropic, porphyroblastic biotites are scattered throughout the aluminous cherts. Pink, poikiloblastic, Mn-rich garnets appear between 109 and 122.5 m, occurring within or adjacent to sulphide-bearing horizons. Garnets reappear at 143 m as scattered, coarse, 2 mm diameter, crystals in a fine uniform, micaceous chert, dissappearing again at 149 m. They are also present in the interval 155 to 170 m when they finally disappear. Here they occur as scattered poikiloblasts in sulphide-rich bands.

Above 149 m the rock is fairly uniform with rare layers of pyrite+sphalerite in quartz-rich or cherty horizons. A thin chlorite+quartz+epidote schist horizon resembles those at the MGZ locality and could represent a clay-rich sediment.

Below 161 m mineralization is minimal and confined to impersistent bands of sphalerite and lesser pyrite, especially in the more quartz-rich or cherty horizons. Local remobilization into crosscutting fractures has occurred during

metamorphism.

Porphyroblastic albites of composition An < 7, are common within the interval 161 to 174 m, where they form 0.4 mm untwinned grains and larger granular aggregates confined to sericitic layers and bands. Below 161 m albites are rare. A similar banded cherty and sericitic rock occurs above 175 m but neither albites nor garnets were observed.

Above 161 m the rock becomes progressively more cherty with development of 5 mm lenses and thin, 1 mm, horizons of clear quartz, often containing sulphide grains. The chlorite and sericite content decreases. From 168 to 171 m mineralization is fairly abundant and consists of banded pyrite with lesser pyrrhotite+chalcopyrite+sphalerite. Sphalerite-rich horizons occur where the rock is very cherty. These sulphide bands and horizons are aligned and parallel to the compositional and lithological banding of the host rock.

Above 171 m the sequence consists of creamy to grey, massive, very fine grained chert containing fine bands of sericite and chlorite, commonly sheared. Lenses and droplets of clear quartz are common and often contain sulphide grains. The rock is heavily mineralized with sphalerite in thin layers and in quartz-rich bands. Sphalerite also occurs as finely disseminated crystals and in crosscutting, remobilized veinlets. A small, intrafolial F_1 fold containing a quartz+sphalerite band is shown in plate 40. Thickening of the sphalerite has taken place along the fold limb. The mineralization ends abruptly at 174.2 m although the chert continues for a further 50 cm.

The sequence from 174.7 to 178.2 m is similar to the banded aluminous cherts below the heavily mineralized horizons, and is also similar to the hangingwall aluminous cherts of the

J locality. Fine grained quartz and sericite form bands and layers 1-3 mm, rarely 10 mm in width. Minor intrafolial folding was observed in these, plate 8.

The overlying acid porphyries are conformable with the aluminous cherts, the contact being fairly abrupt and parallel to compositional banding within the cherts and porphyries.

The following interpretation of this sequence is offered.

The top of the flow unit is marked by the reworking of lavas and associated debris and marks the end of vulcanism. It is followed by a quiescent period during which deposition of sedimentary and volcanically derived cherts, impure cherts and volcanic-sediments produced a rather uniform, banded sequence. Slight changes in chemistry have, during metamorphism produced bands or zones rich in chlorite, biotite, garnet and/or albite.

The close association of sulphides and bands and lenses of clear quartz suggests a common origin. It is further suggested that the quartz represents original lenses and bands of volcanically derived silica containing zinc, iron and sulphur, later recrystallized to produce the present assemblage. The common occurrence of garnets in close proximity to the sulphides also suggests a sulphide-associated source for the manganese.

The rather rapid increase in sulphide content, and its abrupt termination, suggest a peak period of mineralization which coincides with the formation of a massive chert layer; chert deposition continuing after the cessation of sulphide mineralization. The two may have a common origin. Sedimentary conditions do not appear to have changed before or after this mineralization.

Sulphide horizons, garnet-bearing horizons and chert+ quartz horizons are parallel to compositional banding and tuff layers. This implies that they are original depositional features. Both sulphide+quartz bands and banded aluminous cherts were found as intrafolial folds, indicating them to be pre-deformation in origin.

Overlying the aluminous chert sequence are fairly uniform acid porphyries, considered to represent welded tuffs, with a total thickness probably greater than 100 m. This indicates renewed volcanism prior to clastic sedimentation. It is not clear whether this vulcanism was subaerial or subaqueous.

7.5.2c The Hangingwall Acid Porphyries

Acid porphyries or welded tuffs conformably overlie the aluminous cherts. These porphyries characteristically contain phenocrysts and fragments of inverted high temperature quartz, and albite, and abundant devitrification spherulites. The porphyries form a rather massive unit, siliceous and cherty in appearance, with a tuffaceous texture of small, < 1 mm, often densely packed, rounded fragments, set in a fine grained matrix. Slight changes in the amount of sericite and chlorite present give the appearance of banding. Occasional, thin pyritic layers contain quartz, carbonate and sphalerite.

The top of the porphyries was not intersected in the drill holes, and is not exposed on surface.

7.5.3 Summary

At the L and W localities, felsic volcanic rocks are overlain by the Transition Zone which comprises a lower portion of aluminous cherts and reworked volcanics at L, and aluminous cherts only at W, and an upper portion of

uniform acid porphyries. The economically important, lower portion of the Transition Zone was found to be mineralized.

At the L locality in the east, pyrite and sphalerite are disseminated throughout a chert layer forming the base of the Transition Zone. Mineralization at W, 800 m along strike to the west, is sphalerite-dominated with lesser pyrite, and is associated with the development of manganese-rich garnets. As at L, the sulphides occur as disseminations and layers within a massive grey chert, which occurs towards the top of the lower Transition Zone.

Textures within the volcanic rocks, cherty tuffs and aluminous cherts indicate that they were deposited sub-aqueously, although similar evidence from the porphyry is lacking. The intimate association of sulphides with quartz and/or chert horizons, and the parallelism of sulphide layers and sedimentary layering suggests that they were formed and deposited along with their host rocks.

The following sequence of events is considered to have taken place:

Following a period of extensive, extrusive volcanism, aluminous cherts and reworked volcanic horizons were deposited to form the lower portion of the Transition Zone. At the L locality mineralization took place immediately following the volcanism with the formation of an iron+sulphur bearing fine grained siliceous rock, now seen as a mineralized chert. Chlorite was formed as a gangue mineral. At W, 20 m of aluminous chert but no reworked volcanic rocks, were accumulated prior to a period of mineralization. The aluminous cherts grade upwards into a sphalerite+pyrite bearing siliceous rock or chert. Manganese associated with

the mineralization was, during metamorphism, taken up to form spessartine garnets, but these were not observed at the L locality. Renewed explosive activity, centered to the west of the study area, see chapter 5, deposited a thick, fairly uniform sequence of acid porphyries or welded tuffs.

The Transition Zone sequence below the porphyries is thicker than at the J locality which may indicate conditions of fairly rapid sedimentation and concomitant dilution of the mineralization. It is interesting to note that the thickness of barren aluminous cherts above the main mineralization at W, 3.3 m, is approximately the same as that above the massive sulphide deposit at J.

Crosscutting footwall alteration zones, containing silicates and/or sulphides, were not observed at either the L or W localities.

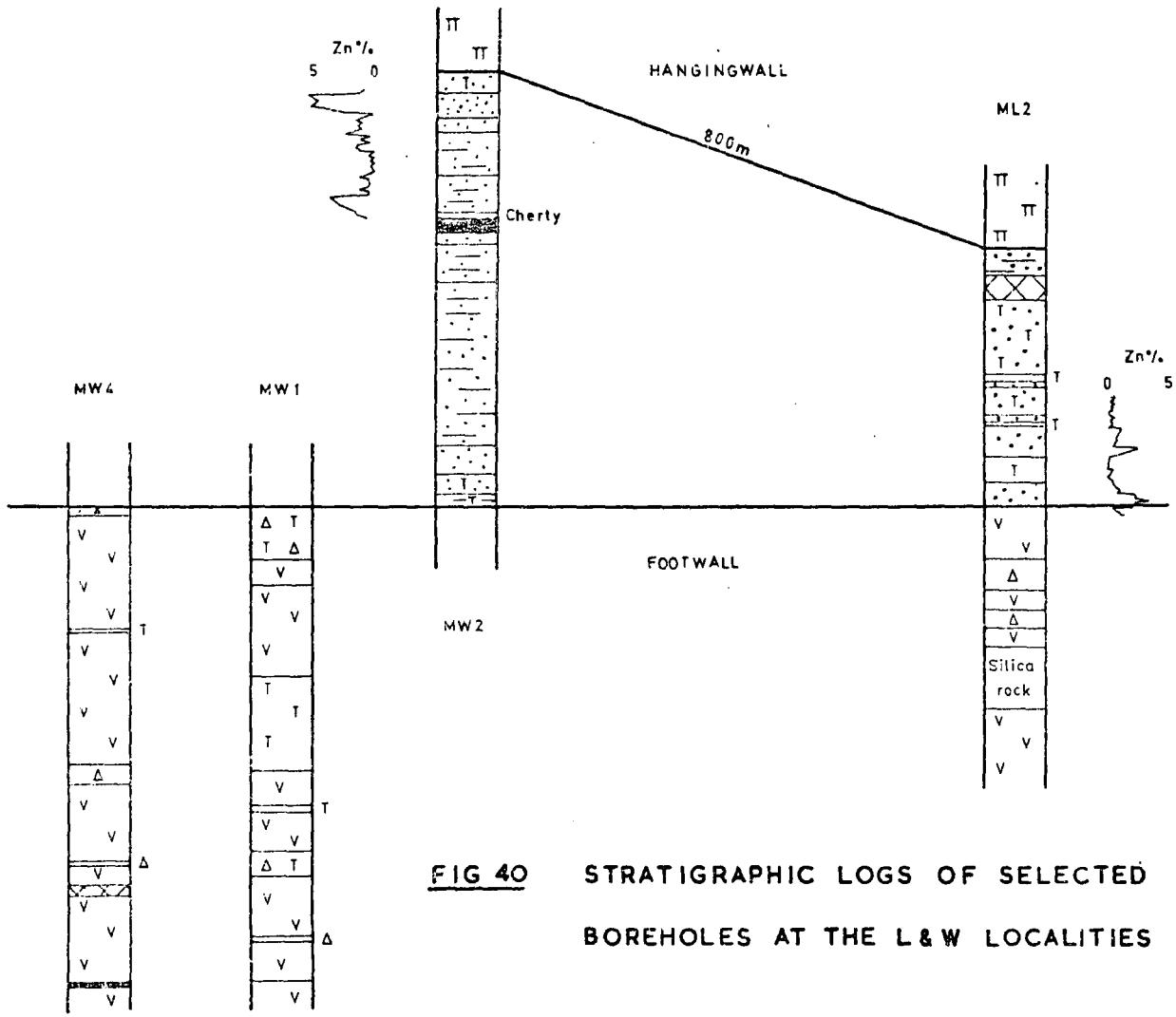

FIG 40 STRATIGRAPHIC LOGS OF SELECTED BOREHOLES AT THE L&W LOCALITIES

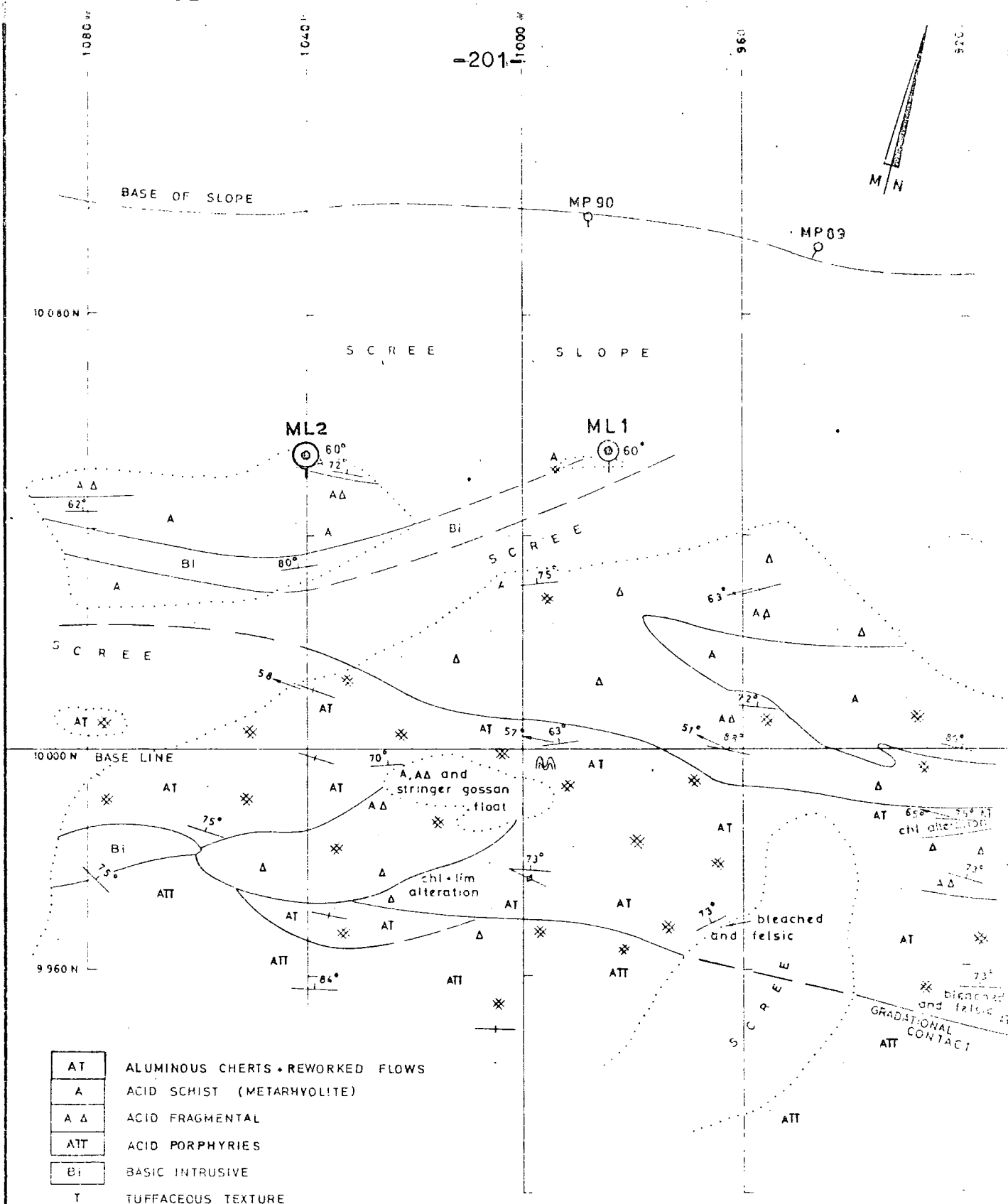

AT	ALUMINOUS CHERTS + REWORKED FLOWS
A	ACID SCHIST (METARHYOLITE)
A Δ	ACID FRAGMENTAL
ATT	ACID PORPHYRIES
Bi	BASIC INTRUSIVE
T	TUFFACEOUS TEXTURE
	STRINGER GOSSAN
	FLOW BANDING
	LIMIT OF OUTCROP
	GEOLOGICAL CONTACT
	INFERRED GEOLOGICAL CONTACT
	FOLIATION, DIP AND STRIKE S_1
	LINEATION, PLUNGE L_1
	SECONDARY FOLIATION (VERTICAL) S_2
	DIAMOND DRILL HOLE COLLAR
	PERCUSSION DRILL HOLE COLLAR

10 0 10 20 30 40 50 m

SCALE

FIG 41

MURCHISON AREA

MARANDA

TARGET L

GEOLOGY

Base of rhyolite flow, showing sharp contact with underlying breccia horizon.

Top of same flow showing vague flow banding (arrowed) and overlying breccia.

Plate 38

Brecciation and flow banding in rhyolites from the W locality. Drillhole MW4. Drawn from streak print (see Morris and Ewers (1978)).

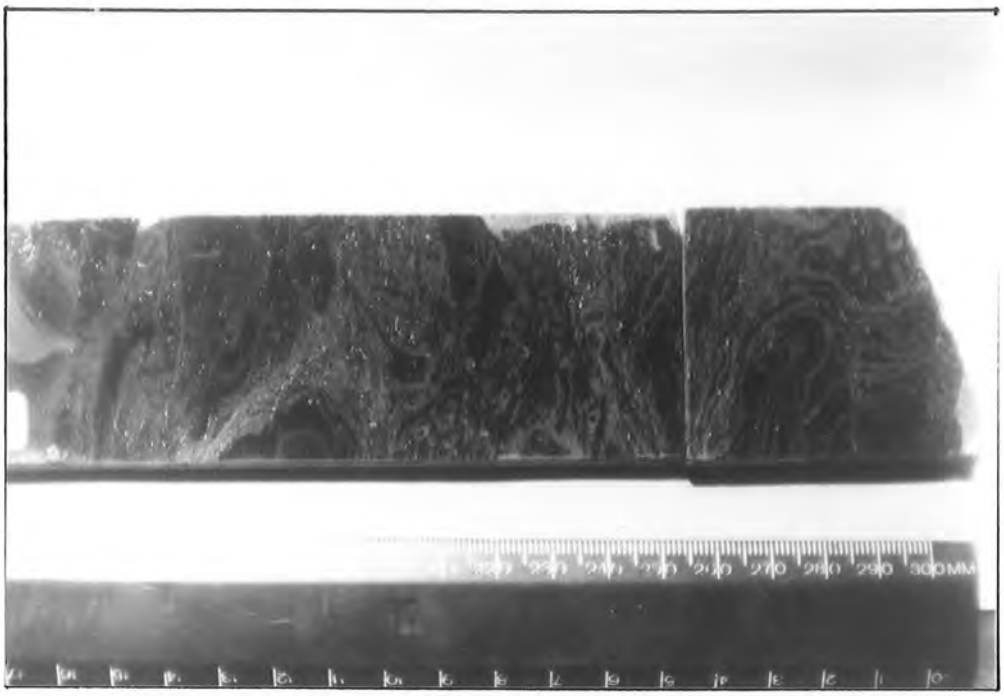

Plate 39. Slump structures in tuff horizon from the footwall volcanic rocks at the W locality.

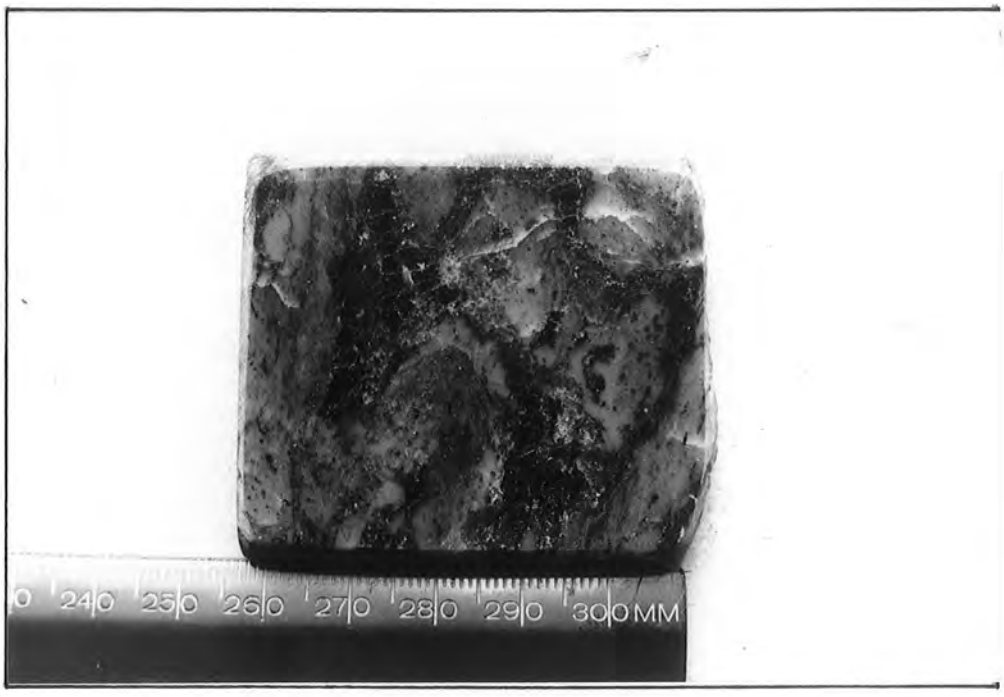

Plate 40. F_1 fold in quartz+sphalerite layer from the W locality.

CHAPTER VIII

ORE MINERALOGY

8.1 Introduction

Polished specimens were prepared from selected samples of sulphide assemblages obtained from borehole core from the four mineralized localities. For the massive sulphide pod of the MGZ deposit, only small chips were available and these were mounted in clear plastic for polishing.

Mineralogy and texture were examined using a Leitz reflected light microscope. Structure etching was carried out using the techniques and reagents described in Appendix D. Several samples were subjected to electron microprobe analysis and the results are discussed below in the relevant section. For analytical techniques and tabulated results refer to Appendix B.

8.2 J Locality

8.2.1 Pyrite in Footwall Tuffs

The tuffaceous volcanic pile forming the footwall sequence to the massive sulphide lens, contains chlorite schist horizons within which disseminated pyrite forms thin bands and horizons. This pyrite is not associated with veining or products of hydrothermal alteration and, however it originated, continued to grow in situ in the sediment. The most common forms are fine grains and granular aggregates, zoned euhedra, and fragmented banded masses.

8.2.1a Fine Granular Pyrite

These form thin horizons of fine grained, <0.05 mm, subhedral and granular pyrite, which may be clear or contain blebby inclusions of chalcopyrite, pyrrhotite or silica. Areas of irregular, "sieve textured" pyrite may also be present.

Pyrite aggregates develop by growth and impingment of small grains and subhedra. Within these aggregates, an irregular distribution of silicate inclusions is produced by preservation of original inclusions within individual grains and further intergranular entrapment during aggregation. Later, during metamorphism, these aggregates have been recrystallized into an optically continuous mass, some of which have formed euhedral outlines with inclusion-free margins: see plates 41a-d. These clear margins are due to partial self-purification of the pyrite during recrystallization (Anger, 1971; Shadlun, 1971).

8.2.1b Zoned Euhedra

Coarse pyrite cubes, up to 3 mm in size, occur in separate horizons as single euhedra or clusters of separate euhedra. In these horizons this is the only form of pyrite present. Within these euhedra, minute silica inclusions form a regular cubic zonation; see plate 42.

8.2.1c Fragmented, Banded Masses

These are rare, but consist of separate horizons containing clusters of coarse, >2 mm, irregular pyrite fragments. The fragments are angular, and were originally part of a continuous layer. Individual fragments are partially zoned with alternating bands of clear and

inclusion-ridden pyrite around a central core which may contain blebby inclusions of silica and, rarely, chalcopyrite. The boundary between pyrite and host rock may be undulose and embayed suggesting partial solution of pyrite. Radial lines or fractures filled with silica have been observed within some of the zoned fragments; plate 43.

Rarely there is an optically continuous overgrowth of euhedral pyrite, the shape and width of which bears no relationship to the zonation. Sphalerite and chalcopyrite may be associated with this; plate 44.

8.2.1d Interpretation

Zoned and banded pyrite form in an unconsolidated sedimentary environment, or as open-space growths. Metamorphic recrystallization and growth of pyrite tends to produce clear euhedra or subhedra. Inclusions within original sedimentary pyrite would be expelled during metamorphism, or assume a rounded shape, the state of lowest surface free-energy (Stanton, 1972). During recrystallization unoriented, granular aggregates form large optically continuous grains with partial or total loss of internal texture.

The three varieties of pyrite described above have features which imply original growth in an unrestricted or unconsolidated environment. Superimposed on these features are the effects of metamorphism and deformation which can be seen as partial recrystallization, notable in the fine granular aggregates, and lesser external grain growth. Original pyritic layers have been fragmented and individual fragments rotated. The margins of several

pyrites are embayed, with caries-texture suggestive of partial solution of the pyrite. In fragments of layered pyrite, radial lines of silicate cut across the zonation. These are similar to shrinkage cracks described and illustrated by Anger (1971, fig.32), and were produced by diagenesis and recrystallization of an original gel.

The origin of the pyrite is problematic. However the pyrite nucleated, either in the sediment or around small crystals deposited with the sediment, it is obvious that they continued to grow in situ. This also implies that the host chlorite schists are derived from an original, possibly muddy, sediment.

8.2.2 Footwall Stringer Sulphide Zone

8.2.2a Introduction

Underlying the massive sulphide lens is a zone of hydrothermally altered tuff, within which sulphides occur as crosscutting veins and disseminations, and increase in amount upwards with increasing alteration of the tuffs. Pyrite is the most abundant sulphide followed by pyrrhotite, chalcopyrite and sphalerite. Pyrite is present where the alteration is poorly developed, being restricted to occasional veins and patches usually containing traces of chalcopyrite and sphalerite. As the alteration increases, pyrrhotite, chalcopyrite and sphalerite become more prominent being abundant in chlorite schist horizons towards the top of the altered tuffs.

Sulphide variation within the alteration zone has been referred to in chapter 7, and can be seen in fig. 33. There is a central area of pyrrhotite$\pm$chalcopyrite coinciding

with the strongly developed alteration, and peripheral to this pyrite is the dominant sulphide.

8.2.2b Pyrite

Pyrite is found within veins and patches, commonly associated with other sulphides, where it forms anhedral to subhedral grains, often with rounded edges, and which may be clear or contain inclusions. Pyrite is also present as scattered anhedral grains.

Pyrite in veins and patches

Pyrite forms grains of up to 2 mm in size, and granular aggregates in small quartz veinlets. Euhedral faces occur against other sulphides, with irregular boundaries against silicate. Minute silicate inclusions were observed in the core areas of some pyrite grains.

Scattered pyrite

Pyrite as single grains, or aggregates occurs in the tuffs, without associated quartz or sulphide. This pyrite generally forms partially developed cubes or sieve-textured masses. The cubic pyrite is commonly < 0.5 mm in size and is either clear, or contains zones of silicate inclusions. The sieve-textured variety has no regular internal structure, but contains inclusions of silica.

It is not clear whether, and how much of, this pyrite was present in the rock prior to the passage of mineralizing solutions.

8.2.2c Other Sulphides

Pyrrhotite, chalcopyrite and sphalerite occur in varying amounts within the footwall alteration zone, generally comprising $< 20\%$ of the rocks.

More massive sulphides are found within chlorite schist horizons at the top of the alteration zone. All these sulphides have been recrystallized during metamorphism and form polygonally granular aggregates, or coarse mutual boundary textured intergrowths. Individual grain size is in the range 0.1 to 0.3 mm.

The sulphides occur as irregular veins and network patterns with a quartz+chlorite+amphibole gangue. There is a tendency for segregation into sphalerite, pyrrhotite or chalcopyrite-rich bands and these tend to be aligned parallel to the local S_1 plane. Sulphide-quartz contacts tend to be cuspate and rounded, with quartz forming blebs and round patches in sulphide. Amphibole and chlorite form needles and long tabular crystals which penetrate into, and are euhedral against, the sulphides. Where these gangue minerals dominate, the sulphides occupy angular interstices. Some amphibole needles have been broken and the fractures infilled with chalcopyrite and/or pyrrhotite; plate 45.

Host rock fragments were occasionally observed within sulphide-rich areas. In the chlorite schists, rafting and lifting of silicate slabs occurs; plate 46.

8.2.3 Massive Sulphides

8.2.3a Introduction

The J deposit consists of a stratiform lens of massive sulphides overlying an extensive alteration zone containing stockwork or stringer-type sulphides. The massive sulphide lens has an average thickness of 2 m and present vertical and horizontal dimensions of 100 m and 400 m respectively; see map 2 and fig.34. From assay values and visual

estimation, the overall sulphide content is 37% pyrite, 30% sphalerite, 8% chalcopyrite, 7% pyrrhotite, 3% other sulphides and magnetite, and 15% gangue.

Pyrite and sphalerite are the most abundant sulphide minerals and commonly form banded sequences containing only minor amounts of the other sulphides; plate 53 . Chalcopyrite is present as thin bands with pyrrhotite and sphalerite, and also within certain pyrite+sphalerite horizons; plate 48. Pyrrhotite is found in the east and centre of the deposit.

The different minerals and their textures are described in detail below:

8.2.3b Pyrite

Three varieties of pyrite have been found; these are sieve-textured, thin bands and horizons of small euhedra, and large subhedra.

All pyrite is weakly anisotropic, blue to orange-brown. Bayliss (1977) has postulated a triclinic structure for pyrite to account for this.

Sieve-Textured Pyrite

The term "sieve-texture" is applied to pyrite which forms rather irregular masses of generally optically continuous pyrite whose internal texture is sieve-like, though commonly with no apparent structure or orientation, plate 49. The "holes" are occupied by other sulphides or silica. Variations in the internal and external appearance and shape of this "sieve-texture" pyrite has resulted in three common forms:

a) Isolated Forms

These occur as rounded or angular pyrite, up to 5 mm diameter, with a well-developed sieve-texture. In some cases this sieve-texture has no regular pattern, but in others radial or feathery patterns develop which suggest directed growth; plates 49 and 50. This pyrite only forms a small percentage of particular horizons where it is the only type developed.

b) Fragmented Forms

Occasionally pyrite masses are strung out along one horizon and have clearly originally formed part of a continuous layer, which was later fragmented. Most fragments do not appear to have been rotated and remain parallel to the original horizon. The internal sieve-texture is highly irregular and contorted, with inclusions of silica and sphalerite. Many of these inclusions are linear, approximately perpendicular to the original horizon, and represent fracture-infills from mechanical fragmentation, plate 51. Banding may be observed within the pyrite fragments, which is not related to brecciation and is parallel to the original horizon. This may take the form of massive pyrite, very finely intergrown pyrite+sphalerite, and layering of pyrite with radial and concentric-type structures; plate 52. Sphalerite is the dominant sulphide within the pyrite, even where the fragments are enclosed by other sulphides.

c) Pyrite Balls

Round lenses or spheres of pyrite are common in the banded sphalerite+pyrite ore, and less so in chalcopyrite+ pyrrhotite+sphalerite horizons. In the banded ore these

may form as swellings and rotations of pyritic horizons, or separate lenses, but are found as entirely separate, rounded masses in chalcopyrite+pyrrhotite+sphalerite horizons. The size of the balls varies, with 20 mm diameter being the maximum observed. The balls are aggregates of irregular sieve-textured pyrite, often enclosing small pyrite enhedra, and granular pyrite, which together constitute 50-75% of the ball. Silica and other sulphides comprise the remainder; plates 47 and 48.

Small Euhedral Pyrites

Small, i.e. < 0.3 mm, euhedral pyrite forms the majority of pyrite in the banded sphalerite+pyrite ore. The banding is imparted by alterations of pyrite-rich and pyrite-poor layers, ranging from 1 to 5 mm in thickness, with sphalerite as the major matrix mineral. The bands are fairly sharply defined and tend to be undulose, pinching and swelling along their length, and laterally impersistent; plate 53.

Pyrite constitutes up to 50% of individual bands, generally as separate, or touching, cubic crystals in three grain sizes, 0.05 mm, 0.1-0.2 mm, and > 0.3 mm in diameter. Occasionally patches of sieve-textured pyrite enclose, or form aggregates with, these euhedra; plate 54. The smaller grains, those ≤ 0.05 mm, occur as single grains and in small aggregates, generally with a sub-idiomorphic outline. In some horizons, inclusions of sphalerite and silica are common within and between the pyrite. In others, especially those containing a higher proportion of pyrite which has a more irregular shape, silica and chalcopyrite are common, sphalerite being absent,

even though it forms the matrix where chalcopyrite and silica are absent. Coarse pyrite euhedra, > 0.3 mm, develop in horizons where sieve-textured pyrite is now absent or very rare, and are probably a result of metamorphic recrystallization.

Massive Pyrite in Bands

Bands of massive pyrite were found to be composed of a granular mosaic or aggregate of anhedral, irregular grains, 0.07 to 0.15 mm in diameter. Triple junctions are common but angles only occasionally reach 120°, being generally more irregular. Some coarse grains have a vague cubic shape, but with irregular margins; plate 56.

In etched samples, several grains were found to be internally zoned, with cubically oriented, etched and unetched bands surrounding a relatively clear core. These zones are not related to the present grain boundary, plate 58, and rare examples were observed where this zoning extends across two or more grains.

Some large grains have cores containing minute silica and sulphide inclusions. These occasionally form chains outlining round, clear areas of pyrite, plate 57. Sphalerite inclusions are rare. By comparison with pyrite textures observed in the footwall tuffs, it is suggested that these massive pyrite bands originally consisted of zoned euhedra and granular aggregates. During metamorphism, recrystallization produced the granular mosaic pattern but did not develop fully annealed textures (Stanton, 1972). Silica and sulphide inclusions represent former inter- and intra-granular minerals.

Coarse Pyrite Subhedra

Coarse subhedral pyrite occurs in horizons which are dominated by sphalerite and contain chalcopyrite and pyrrhotite. All sulphides are relatively coarse grained, and banded textures are absent. The pyrite is randomly oriented, from 0.4 to 1.0 mm in size, and tends to form cubes though with only 1, 2 or 3, rarely 4 faces, fully developed. The shape is occasionally interrupted by deep, rounded embayments, and large, rounded to oval inclusions, plate 59. In some horizons the cubic shape is rounded. This shape and mode of occurrence is identical to that described by Stanton (1964), and Vokes (1969) as being produced by metamorphic recrystallization of a poly-sulphide aggregate.

Electron microprobe analysis of cores and margins of this pyrite reveal a cobalt-rich margin, or clear over-growth, with respect to the core area. Nickel appears to have generally lower values in the margins compared to the core, see table 5.

As in the case of the massive pyrite, several of these subhedra contain minute inclusions of silica, chalcopyrite, pyrrhotite and rarely sphalerite, in their cores, plate 60. The origin of these is considered to be similar to that in the footwall pyrite described in section 8.2.1a. These subhedra have undergone a more thorough recrystallization and loss of internal texture.

Interpretation

Under conditions of increasing pressure and temperature, sulphide-rich assemblages tend to recrystallize, becoming

progressively coarser grained and eventually developing annealed textures (Stanton, 1964; McDonald, 1967; Shadlun, 1971). Pyrite tends to form idioblasts against "softer" sulphides such as pyrrhotite, chalcopyrite and sphalerite. These form mutual boundary textures with each other (Stanton, 1964; Ramdohr, 1980).

Under shear or load stress, pyrite will deform by fracture and cleavage (Gill, 1969; Stanton, 1972). Sphalerite, pyrrhotite and chalcopyrite deform by twinning, slip and plastic deformation and where pyrite is present they flow around the relatively competent pyrite grains (Gill, 1969; Clark and Kelly, 1973). In these circumstances, original depositional or growth textures tend to be obliterated with increasing metamorphism. Obliteration of the original textures will be completed earlier for the "softer" sulphides than for pyrite (Shadlun, 1971).

At the J locality, the grade of metamorphism is similar to elsewhere in the study area, i.e. upper greenschist facies or Low Grade, see chapter 5, although the amount of deformation is less, with preservation of many original textures. The low grade and possible short duration of metamorphism has produced an inhomogenous recrystallization of the sulphides. This is most notable in pyrite, which varies from coarse recrystallized subhedra to virtually unaltered grains and granular aggregates, often in the same or adjacent horizons.

In section 8.2.1a it was observed that small inclusions within cores of large pyrite subhedra are the result of inter- and intra-

granular entrapment during growth and aggregation of granular or euhedral pyrite. Thus these inclusions represent the original matrix in which the pyrite formed during sedimentation or diagenesis. It has also been noted that these inclusions are dominated by silica, with minor chalcopyrite and pyrrhotite and only rare sphalerite. Pyrite euhedra are only well developed in banded sphalerite+ pyrite ore where the pyrite content of a particular horizon is $< 50\%$. Etching has not revealed any internal zonation. The association of the smaller euhedra with irregular, sieve-textured pyrite, see plate 54, is very similar to that observed by the writer in samples taken from presently active massive sulphide deposits forming in the 21^{o} North area of the East Pacific Rise, by direct precipitation from metalliferous fluids emerging from vents on the sea-floor (RISE Project Group, 1980). Here, small euhedral pyrite crystals, often containing silica and sulphide inclusions, are surrounded by, or in aggregates with, irregular masses of marcasite having a "sieve-texture". The matrix to these modern deposits is fine grained silica.

Electron microprobe analysis of euhedral and adjacent, sieve-textured pyrite from the J deposit are presented in table 5. The only observable trace element variation is in the Co content which is slightly higher in the euhedral pyrite than in the sieve-textured variety.

Zinc values of up to 0.9 wt% were recorded but these are considered to be due to minute sphalerite inclusions. Sieve-textured pyrite is considered to indicate open-spaced growth, with the spaces now occupied by sphalerite,

chalcopyrite, silica and rare pyrrhotite. In some cases there is a suggestion of sphalerite replacing pyrite.

According to Anger (1971) and Sarkar et al. (1980) pyrite balls are the result of boudinage and brecciation of an originally continuous or impersistent pyritic horizon. However several examples were found where the pyrite apparently formed as a result of concretionary growth or slumping of a pyrite layer, leaving the neighbouring horizons unaffected, plate 47.

8.2.3c Sphalerite

Sphalerite is the dominant sulphide mineral, forming 30% of the massive sulphide lens. Sphalerite-rich horizons are common towards the top of, and in the west of, the sulphide lens. Textures observed within these horizons are generally imparted by variations in the amount of other sulphides. Textures within a seemingly massive sphalerite band were revealed by etching.

The form and grain size of the sphalerite in any particular horizon is dependent on the amount and texture of other sulphides present. In bands containing coarse subhedral pyrite with chalcopyrite and pyrrhotite, the chalcopyrite+pyrrhotite+sphalerite have a coarse, mutual boundary texture, with sphalerite to sphalerite grains being roughly polygonal, 0.2 to 1.0 mm in size, and often outlined by blebs of chalcopyrite, plate 61.

In banded pyrite+sphalerite ore, sphalerite occurs in pyrite-rich horizons as rather angular, roughly equigranular grains, 0.2 mm in diameter, and in sphalerite-rich horizons as generally coarser grains of >0.3 mm

diameter; plate 55.

In fine grained chalcopyrite+pyrrhotite+sphalerite bands the sulphides have complex mutual boundaries with a chain or string-like fabric, plate 63. Sphalerite forms small, 0.02 mm diameter granules with occasional large, 0.5 mm diameter, roundish or oval shaped areas of coarse, 0.1 mm diameter, angular, interlocking grains, devoid of other sulphides, plate 64.

Sphalerite, in copper-rich horizons, contains minute, roundish, chalcopyrite grains which form chains or blebs along sphalerite grain boundaries, plate 61. Very rarely is chalcopyrite found within sphalerite grains. This is the result of the expulsion of exsolved chalcopyrite during metamorphic recrystallization. Most sphalerite grains show deformation twin lamellae, which, in rare cases, are bent or deformed, plate 62.

All the sphalerite observed has presumably undergone metamorphic recrystallization with complete obliteration of any pre-metamorphic texture. Grain size appears to be dependent on the amount of, and texture of, other sulphides present in the particular horizon; the coarser sphalerite occurring in monomineralic bands.

Where finely intergrown with other sulphides, sphalerite appears to have started to segregate into roundish areas of coarser grained sphalerite, with expulsion of the other sulphides. Microprobe analyses give an FeS content of between 11 and 15 mol%, table 6. Other trace elements, where analysed, are low.

8.2.3d Chalcopyrite

Chalcopyrite is a relatively minor, though economically important, constituent of the sulphide lens, amounting to approximately 8% of the whole. Its distribution is greatest in the east where it is commonly found in thin horizons containing sphalerite, pyrite and pyrrhotite. It is generally absent from banded sphalerite+ pyrite ore.

Chalcopyrite forms mutual boundary intergrowths with sphalerite and/or pyrrhotite along well defined horizons, fine grained, complex intergrowths and lesser, more irregular growths in sphalerite-rich horizons. It is also present as exsolution blebs in, and granular films around, sphalerite grains, and as rounded and angular inclusions in euhedral pyrite.

Within the intergrowths, the chalcopyrite is granular, with a possible annealed texture, plate 65. It commonly contains spindle shaped deformation twin lamellae. Within individual grains, exsolved "worms" of mackinawite and elongate blebs of pyrrhotite were observed. The mackinawite is generally aligned in 2 or 3 directions, which are different from the orientation of the twin planes. Sphalerite exsolution is notably absent.

Where basic intrusives cut the massive sulphide lens, chalcopyrite has been mobilized along the contacts.

Chalcopyrite grains in contact with, and apparently in equilibrium with, pyrite and pyrrhotite were examined by Electron Microprobe Analysis; table 6. Copper, iron and sulphur contents approximate the stoichiometric composition of 34.63 wt%, 30.43 wt% and 34.94 wt%

respectively although Fe tends to be high. This produces the formula $Cu_{0.99}Fe_{1.04}S_2$. According to Deer et al. (1963, vol.V) excess iron may be due to minute iron sulphide inclusions. The zinc content of approx. 0.1 wt% is probably due to sphalerite inclusions. Cobalt is generally low, although one analysis, number 325, has a content of 0.14 wt% Co. Nickel is below the limits of detection. Silver is low, < 0.07 wt%.

8.2.3e Pyrrhotite

This has a more limited distribution than chalcopyrite, and is confined to thin bands and horizons with sphalerite and chalcopyrite in the east of the deposit, and in drill holes 10 and 17 in the west. Textures suggest annealing of the pyrrhotite with the formation of polygonally granular aggregates. When associated with chalcopyrite and sphalerite, pyrrhotite forms mutual boundary textures, plates 63 and 64. Pyrrhotite, together with chalcopyrite, is found along the contacts of basic intrusives, and may have been produced by the desulphurization of pyrite. Treatment with a magnetic colloid solution revealed that most pyrrhotite is hexagonal, with monoclinic, magnetic pyrrhotite forming replacements along cracks and grain boundaries, plate 66.

Pyrrhotite very rarely forms inclusions in sieve-textured pyrite masses, but is common as inclusions within pyrite euhedra. It may, however, infill later fractures in pyrite. Samples from drill hole 15 show partial oxidation of pyrrhotite with the formation of "birds eye" textured pyrite, plate 67. This is a recent

weathering phenomenon.

From microprobe analyses, pyrrhotite was found to be non-nickeliferous, the highest recorded Ni value being 0.01 wt%. Cobalt, on the other hand, is generally in the range 0.1-0.2 wt%, table 6. The mean Fe content determined was 60.23 wt%, giving a formula of $Fe_{0.89}S$.

8.2.3f Magnetite

Magnetite is sporadically distributed throughout the orebody as small rounded grains, often clear, but which may contain occasional, rounded, sulphide inclusions. These grains are from 0.1 to 0.2 mm in size, and are commonly found within a sphalerite matrix. Coarser, up to 1 mm diameter, euhedra and anhedra occur in the coarser grained sulphide horizons. These are generally fractured and may be corroded and embayed, and contain zonally arranged sulphide inclusions. These coarse magnetites are considered to have been recrystallized, plate 68.

Within the coarse magnetites, trace element concentrations are low, TiO_2 only reaching 0.13 wt%, table 6.

8.2.3g Miscellaneous Sulphides

Minor sulphides, present in amounts of less than 1% include bismuth-lead selenides, mackinawite, marcasite, and several unknown sulphosalts. Ilmenite and rutile are present as small corroded laths within chlorite fragments, mainly in the base of the sulphide horizon. These are considered to be pieces of footwall, brecciated and caught up with initial sulphide deposition.

In sample MA9J15, dominantly sphalerite with large euhedral pyrite and minor chalcopyrite, small blebs and

splashes of a blue-grey, anisotropic mineral were seen. These blebs consist of complex interlocking laths and grains of at least three different mineral phases, C, D, & E in table 7. Microprobe analyses indicate two bismuth selenides and one lead selenide to be present.

8.2.3h Silicates

Silicate minerals comprise, on average, 15% of the massive sulphide lens. They are dominated by quartz, with lesser amounts of chlorite, epidote and calcite. Amphibole was not observed, and albite was only recorded from the banded sphalerite+silicate horizon at the top of the orebody.

In general the silicates do not impart a fabric to the rock but occur as scattered crystals and grains throughout the sulphide horizons. Quartz forms coarse, up to 5 mm diameter, polygonally granular aggregates, with individual grains showing strain extinction; fine granular aggregates are rare. Chlorite is pale green, pleochroic, and generally exhibits anomalous purple interference colours. It forms flaky and prismatic crystals intergrown with sulphides, and, in rare instances, is replaced by an orange-brown biotite.

The basal sulphide horizons commonly contain fragments of silicate rock, plate 48, comprising aggregates of fine to coarse grained chlorite with small epidote crystals and coarse, anhedral or rhomb shaped calcite grains. The fragments frequently contain small, corroded ilmenite laths, and in this respect are identical to, and equated with, chlorite schist horizons from the footwall sequence.

Small quartz grains commonly rim these chlorite fragments. Sample MA2J18 from the top of the sulphide lens consists of thin alternating bands of sphalerite+pyrite+coarse, granular quartz with minor chlorite, albite (optically, An 7) and biotite, and fine granular quartz+chlorite+ albite.

8.2.4 Summary and Discussion

The J deposit consists of a lens of massive, banded sulphides overlying a zone of altered tuffs. The alteration zone contains veins of sulphides, and cuts across lithological layering in the tuffs. It is therefore of epigenetic origin. Textures within the massive sulphide lens indicate formation as a layered sulphide sediment in an aqueous environment. It is therefore of syngenetic origin. The sulphides and enclosing rocks have undergone Low Grade metamorphism and associated deformation, although many original sedimentary and volcanic textures are preserved. Sphalerite, chalcopyrite and pyrrhotite have been recrystallized, developing polygonally granular and mutual boundary textures, while pyrite has behaved as a brittle sulphide with patchy and incomplete recrystallization. Fragmentation of originally continuous pyrite horizons is a result of strain and shear parallel to the layering, with flowage of the less competent sulphides around the pyrite boudins. Pyrite is thus the only sulphide within which original textures can be observed.

In the footwall volcanic rocks, thin chlorite schist horizons contain pyrite which is considered to have grown in situ. Bands of small enhedral pyrite exhibit growth and aggregation with resulting entrapment of small, mainly silica, inclusions within and between the grains. Meta-

morphic recrystallization of these aggregates has produced optically continuous pyrite containing random and oriented chains of inclusions, which through later growth and/or purification of the margin, are now found only towards the centre of the large grain, plate 41 a-d.

Within the massive sulphide lens, the end result of this process can be observed as large pyrite subhedra whose cores contain minute, rounded inclusions of silica, pyrrhotite and chalcopyrite, occasionally forming chains outlining small patches of clear pyrite, plate 60. This pyrite is most common in the bottom layers of the sulphide lens.

Sieve-textured pyrite has either grown as, or been recrystallized into, an optically continuous mass without change in form. The spaces within this pyrite are filled with sphalerite which also forms the surrounding matrix. This pyrite is considered to have grown within the zinc-rich sulphide sediment. Fracturing and physical separation occurred during metamorphism.

The similarity between sulphide textures from the East Pacific Rise deposits and the banded sphalerite+pyrite ore from the J locality has been noted. In the former, silica, pyrite, chalcopyrite and sphalerite can be observed precipitating directly from hydrothermal fluids entering the sea-water. These precipitates then "rain down" onto the sea bed forming a sulphide+silica sediment, or layer. Within this, directly precipitated pyrite is enclosed by porous or unstructured marcasite which has formed in situ with amorphous silica.

In a previous section, it was suggested that sieve-textured pyrite from the J deposit was the result of in situ growth in the sulphide layers, and that the larger euhedral and subhedral pyrites are probably produced by metamorphic recrystallization. The evidence for formation of the small euhedra, often associated with porous pyrite, by a process of either in situ growth, metamorphic recrystallization, or accumulation of pre-formed euhedra, is not conclusive.

The composition of inclusions contained within the various types of pyrite is of interest. In the coarse subhedral pyrite, and bands of massive pyrite, these consist of silica with lesser pyrrhotite and chalcopyrite. There is a notable absence of sphalerite, even though sphalerite may dominate the surrounding matrix. These inclusions represent minerals that were originally present in, and adjacent to, the pyrite prior to, or during, crystal growth or granular aggregation. Silica must therefore have been present in far greater amounts than is now the case. By this reasoning sphalerite, if present, would have formed a minor component. Bands containing coarse subhedral pyrite show no obvious internal layering, but consist of an unsorted mass of pyrite, silicate fragments and coarse recrystallized sphalerite+pyrrhotite+chalcopyrite, plate 48. Pyrite from banded sphalerite+pyrite ore contains sphalerite inclusions indicating this to have been present during pyrite deposition or growth.

It is suggested that some of the sphalerite present in the massive sulphide lens was formed by replacement of an amorphous silica-rich matrix in pyritic horizons containing pyrrhotite and chalcopyrite, though possibly not in

their present form. The metastability of amorphous silica and its ease of replacement has been discussed by Siever (1962). The absence of replacement sphalerite, or any form of alteration, in the hangingwall rocks, and the occurrence of sphalerite-dominated inclusions in the upper sulphide horizons, indicates that the replacement took place after the initial deposition and formation of silica, pyrite, chalcopyrite and pyrrhotite layers, during accumulation of the upper, sphalerite and pyrite horizons.

8.2.5 Paragenetic Sequence

From the above discussion, the following sequence of sulphide deposition is considered to have taken place:

1. Growth of pyrite in unconsolidated clay-rich layers.
2. Ascension of mineral-bearing fluids altering the rock and precipitating pyrite, pyrrhotite, chalcopyrite and sphalerite in crosscutting veins.
3. Expulsion of fluids onto the sea floor and formation of, initially, silica, pyrite, chalcopyrite and pyrrhotite rich layers.
4. Possible changes in the physical conditions of the fluid to deposit sphalerite, pyrite and chalcopyrite on top of previous layers, with replacement of original silica by sphalerite

8.3 Main Gossan Zone

8.3.1 Introduction

Base metal sulphide mineralization at the MGZ is confined to three lithological units; a chlorite schist which grades downwards into unmineralized tuffs, a coarse quartz rock or recrystallized chert, and at the top of the

Plate 41. Successive stages in the growth, aggregation and metamorphic recrystallization of pyrite (white) in chlorite schist horizon in the footwall to the J massive sulphide deposit. Sample MA14J11. Scale bar is 100 microns, or 0.1 mm.

A: initial stage with small, subhedral pyrites, either clear, or containing inclusions. Beginning of aggregation.

B: pyrite aggregate with trapped silica.

C: large pyrite aggregate. Recrystallized into an optically continuous mass with loss of original grain boundaries.

D: final stage. Metamorphic recrystallization has produced a euhedral, clear, margin or overgrowth.

B

D

A

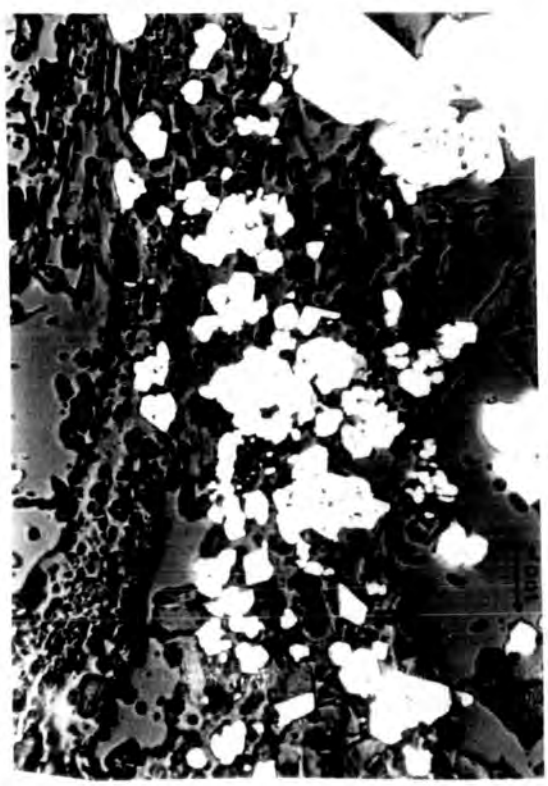

C

Plate 42. Zoned pyrite euhedron from a chlorite schist horizon in the footwall to the J massive sulphide deposit. Sample MA9J11b.

Plate 43. Fragment of zoned pyrite. Lines of inclusions, arrowed, perpendicular to zonation. Chlorite schist horizon, footwall to the J massive sulphide deposit. Sample MA9J11b.

Plate 44. Fragment of zoned pyrite, with overgrowth of pyrite, sphalerite, and chalcopyrite. Sample MA9J11b.

Plate 45. Rare, fractured, amphibole crystal (arrowed) healed with pyrrhotite. Sulphide mineralization in the footwall alteration zone to the J massive sulphide deposit. Sample MA4J4.

Scale bar is 100 microns, or 0.1 mm. Py - pyrite; sp - sphalerite; cp- chalcopyrite; po - pyrrhotite.

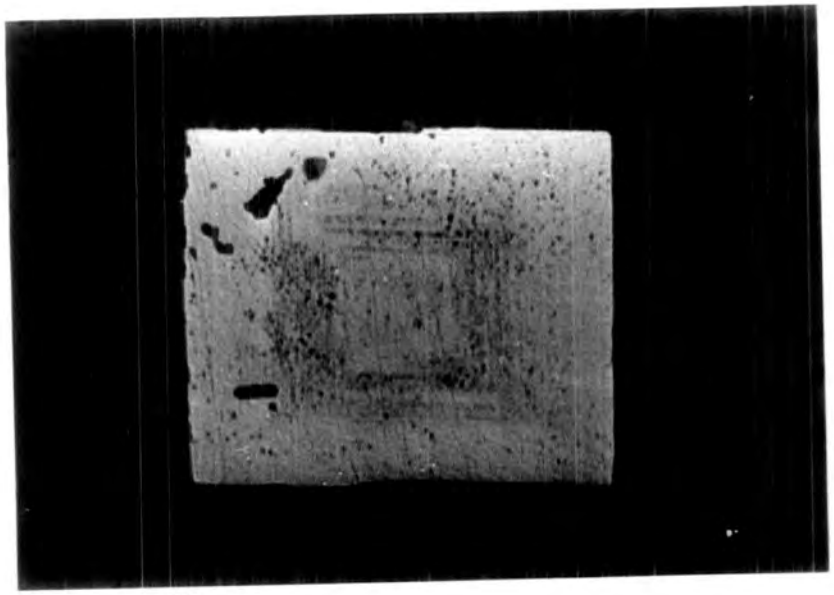

42

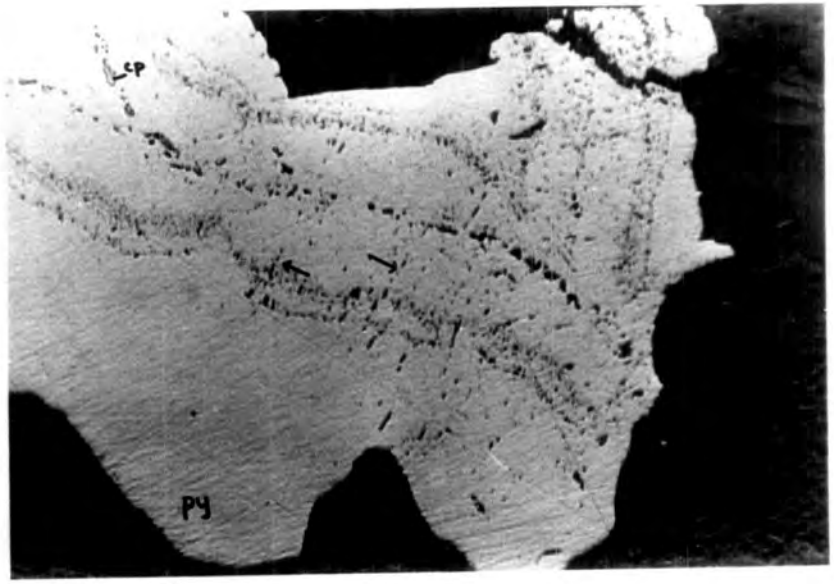

43

44

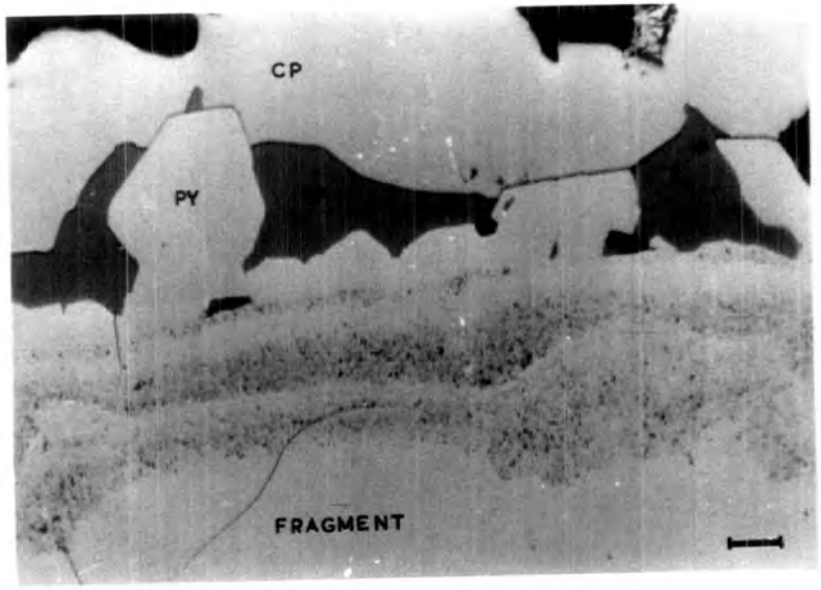

45

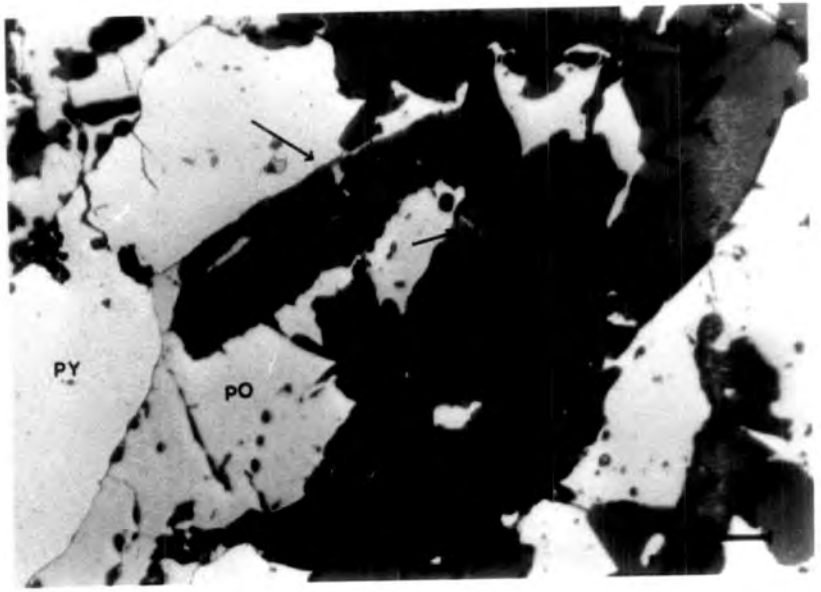

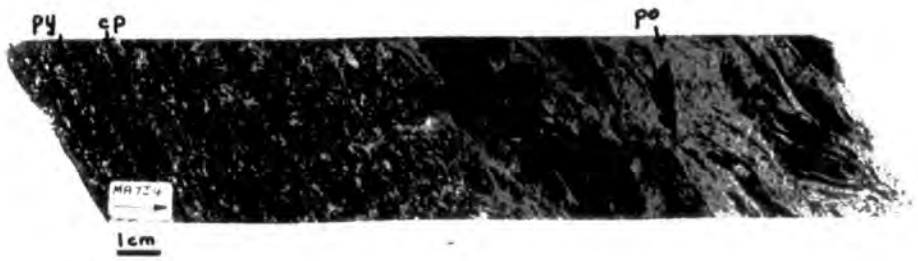

Plate 46. Chlorite schist horizon from footwall tuffs, J deposit. Typical mode of occurrence of sulphides in these horizons. Note apparent "rafting" of schist in pyrrhotite-rich layer.

Plate 47. Banded pyrite+sphalerite ore. Possible slump structures, pyrite balls and concretions.

Plate 48. Layered sulphides. Basal horizon of pyrite+ sphalerite+chalcopyrite with fragments of chlorite schist; finely intergrown chalcopyrite+ sphalerite+pyrrhotite with pyrite balls; and upper horizon of coarser chalcopyrite+ pyrrhotite+sphalerite.

py - pyrite; cp - chalcopyrite; po - pyrrhotite; sp - sphalerite.

Arrow points to the top of the sequence.

Plate 49. Unstructured, sieve-textured pyrite. Massive sulphides, J locality. Sample MA17J11.

Plate 50. Radial, sieve-textured pyrite. Massive sulphides, J locality. Sample MA17J11.

Plate 51. Fragmented, sieve-textured pyrite. Mechanical fractures with sphalerite infillings are arrowed. Massive sulphides, J locality. Sample MA18J11b.

Plate 52. Fragment of sieve-textured pyrite with concentric zonation. Massive sulphides, J locality. Sample MA18J11b.

Scale bar is 100 microns, or 0.1 mm. Py - pyrite; sp - sphalerite; cp - chalcopyrite.

49

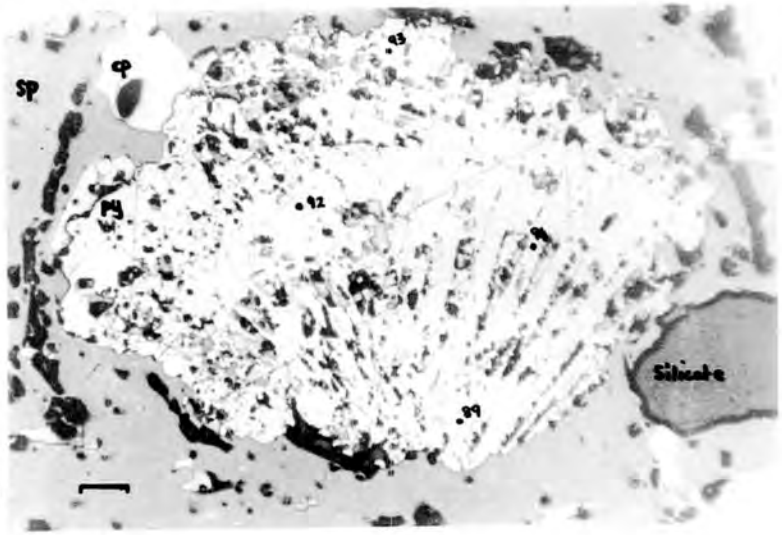

50

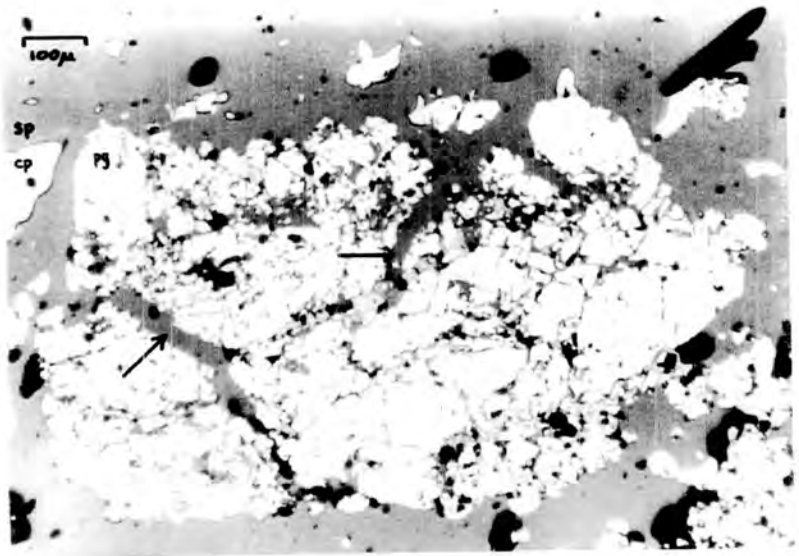

51

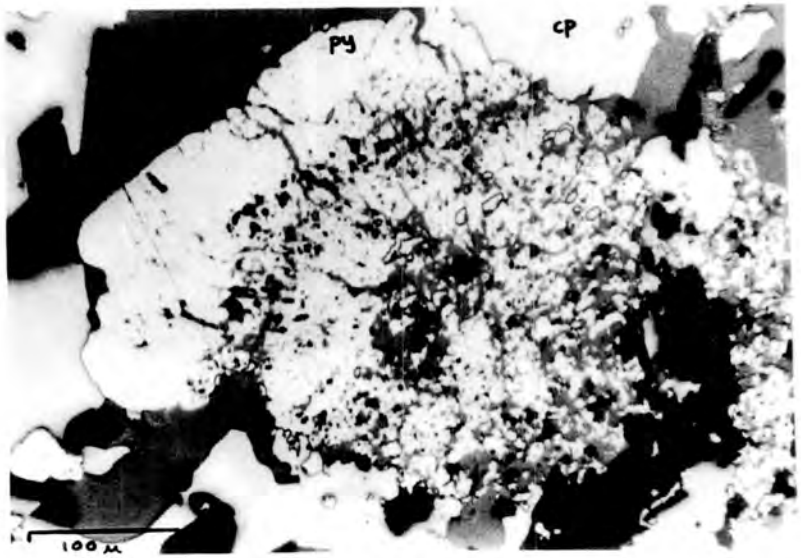

52

Plate 53. Banded sphalerite+pyrite ore. Etched for sphalerite. Massive sulphides, J locality. Sample MA6J15a.

Plate 54. Banded sphalerite+pyrite ore. Euhedral (E) and sieve-textured (S) pyrite. Etched for sphalerite. Massive sulphides, J locality. Sample MA6J15a.

Plate 55. Banded sphalerite+pyrite ore. Etched for sphalerite. Massive sulphides, J locality. Sample MA6J15a.

Scale bar for plates 54 and 55 is 100 microns, or 0.1 mm. Py - pyrite; sp - sphalerite.

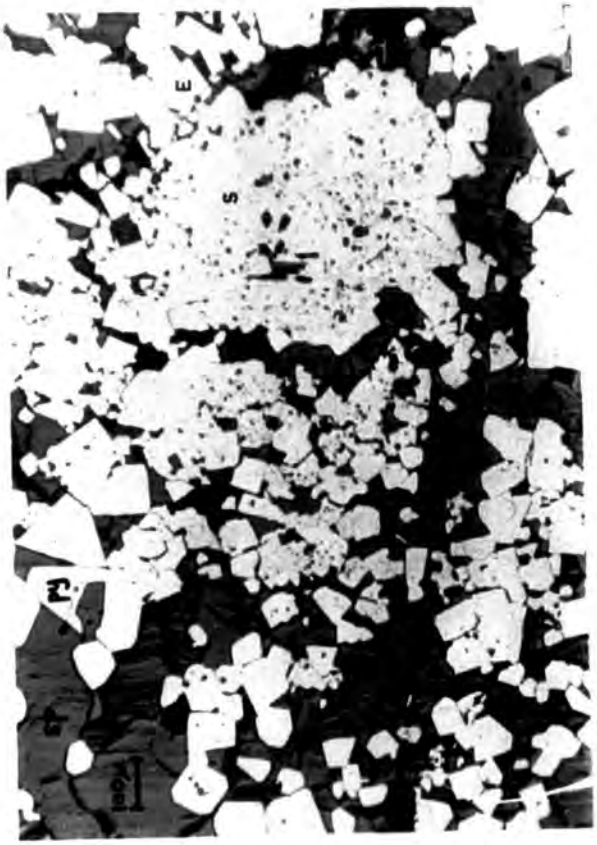

54

55

53

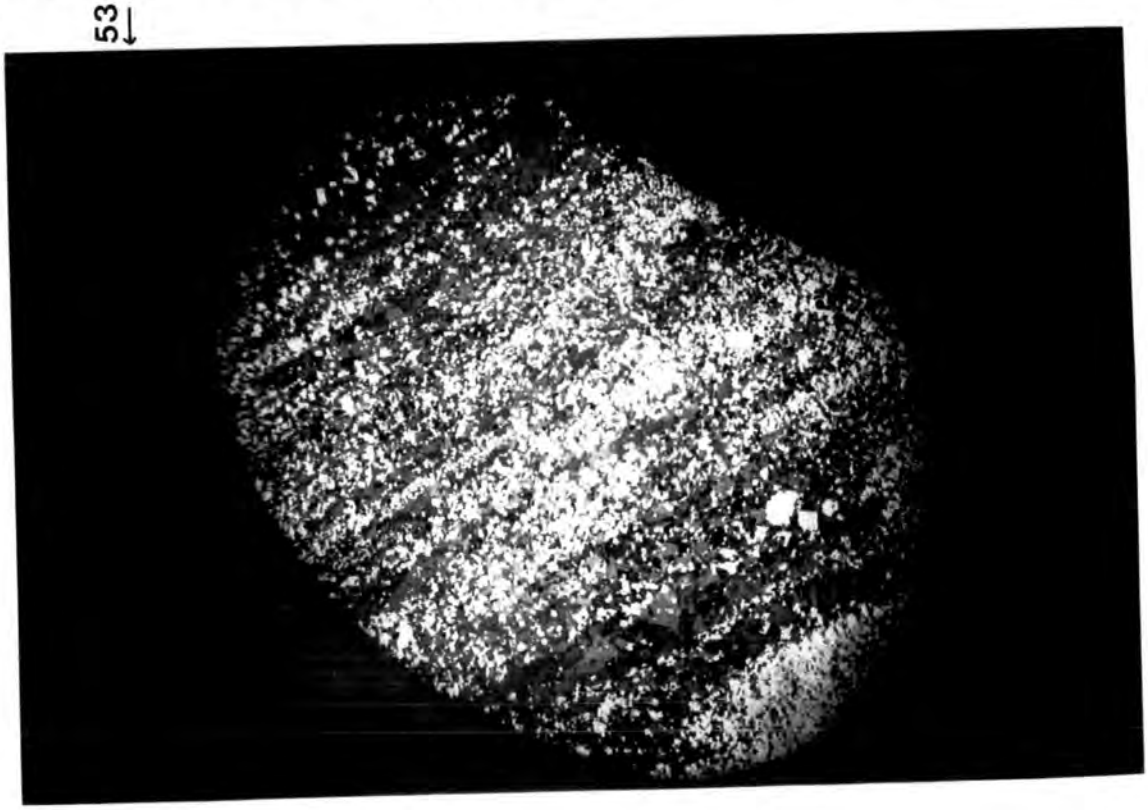

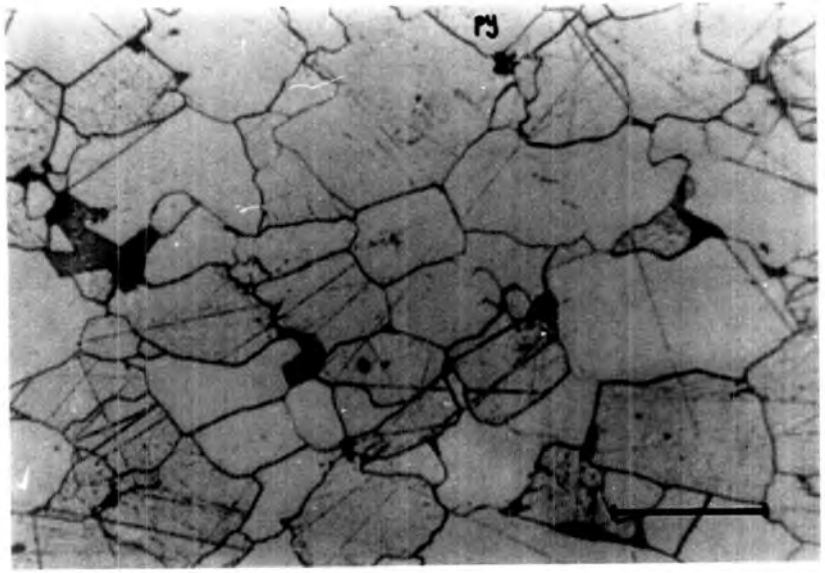

56

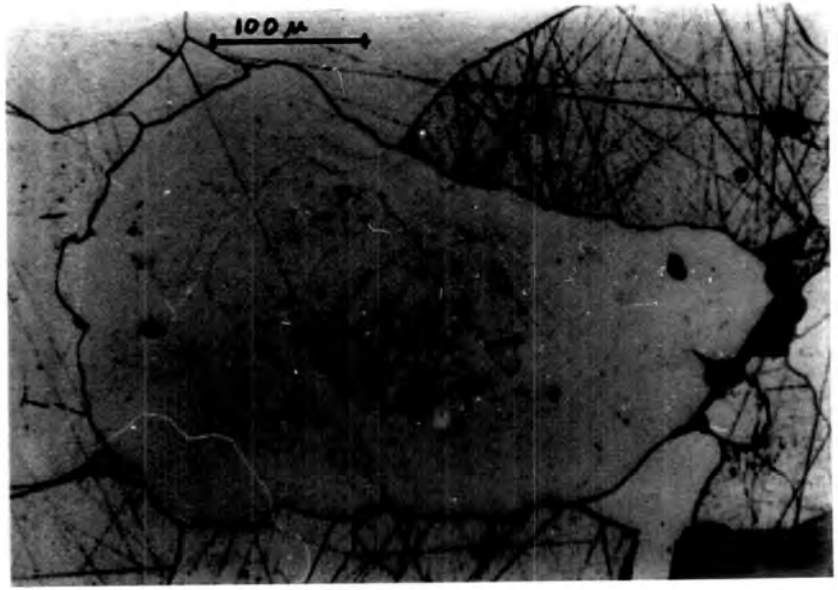

57

58

Plate 56. Massive pyrite, etched. Typical aggregate. Massive sulphides, J locality. Sample MA1J15.

Plate 57. Massive pyrite, etched. Grain with silica inclusions (dark) in core, some outlining round areas of clear pyrite (arrowed). Massive sulphides, J locality. Sample MA2J15.

Plate 58. Massive pyrite, etched. Zoned pyrite with irregular grain boundary. Massive sulphides, J locality. Sample MA1J15.

Pyrite is pale grey, silica is dark grey. Scale bar is 100 microns, or 0.1 mm.

Plate 59. Coarse, subhedral pyrite, with embayments. Massive sulphides, J locality. Sample MA15J11a.

Plate 60. Coarse, subhedral pyrite, with embayments, and silica inclusions in centre of grain. Some of these outline clear, round areas of pyrite (arrowed). Massive sulphides, J locality. Sample MA15J11a.

Plate 61. Chalcopyrite blebs outlining sphalerite grains. Massive sulphides, J locality. Sample MA2J18.

Plate 62. Etched sphalerite grains, with bent twin lamellae. Massive sulphides, J locality. Sample MA20J11.

Scale bar is 100 microns, or 0.1 mm. Py - pyrite; sp - sphalerite; cp - chalcopyrite.

60

62

59

61

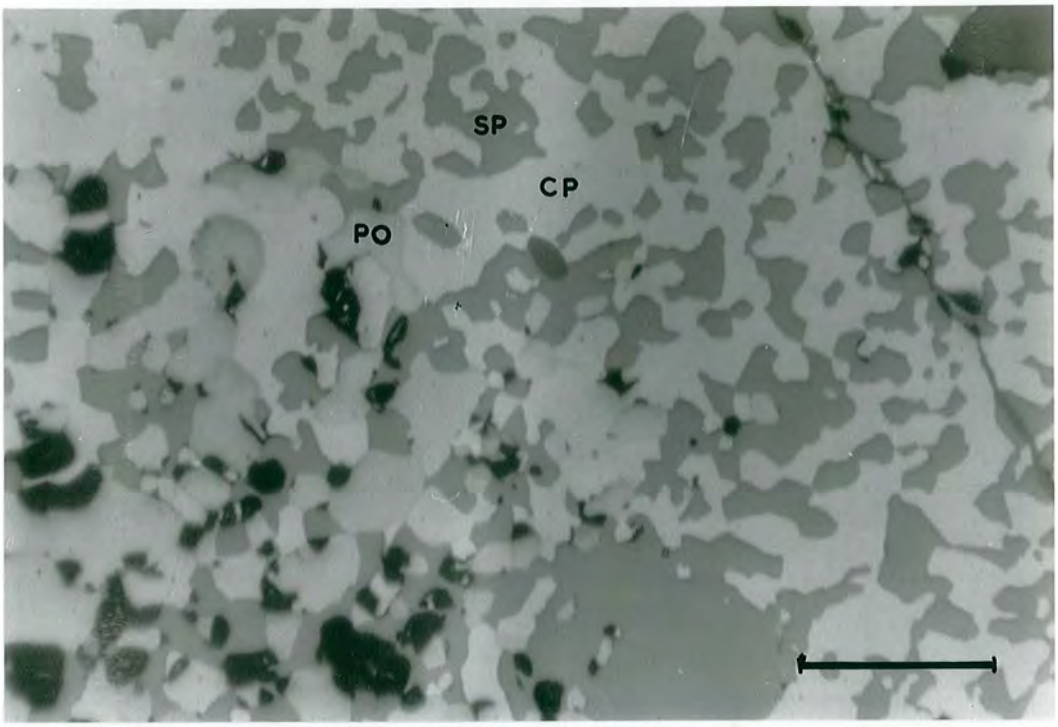

Plate 63. Mutual boundary textures in sphalerite - pyrrhotite - chalcopyrite horizon. Massive sulphides, J locality. Sample MA15J11c.

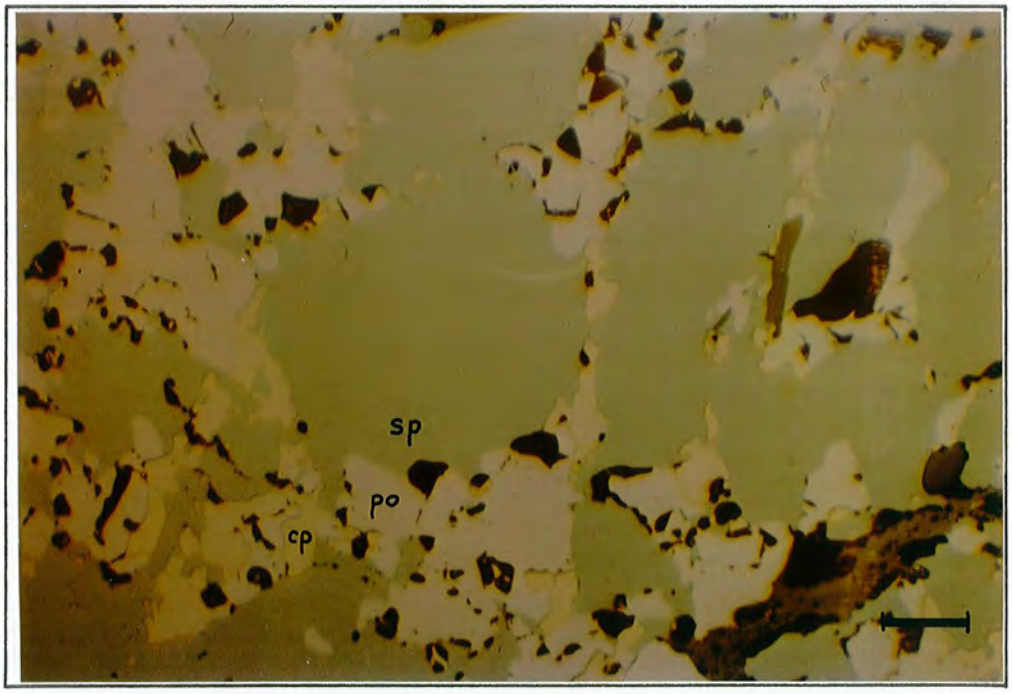

Plate 64. Oval "domains" of sphalerite in mutual boundary textured massive sulphides, J locality. Sample MA16J11c.

Scale bar is 100 microns, or 0.1 mm. Sp - sphalerite; cp - chalcopyrite; po - pyrrhotite.

Plate 65. Etched chalcopyrite showing granular texture and twin lamellae. Massive sulphides, J locality. Sample MA15J11c.

Plate 66. Hexagonal pyrrhotite replaced by magnetic, monoclinic pyrrhotite. Footwall stringer sulphides, J locality. Treated with magnetic colloid. Sample MA4J4.

Plate 67. Pyrite (arrowed), probably replacing pyrrhotite. Massive sulphides, J locality. Sample MA9J15.

Plate 68. Poikiloblastic(?), magnetite with chalcopyrite inclusions. Massive sulphides, J locality. Sample MA15J11d.

Scale bar is 100 microns, or 0.1 mm. Py - pyrite; sp - sphalerite; cp - chalcopyrite; po - pyrrhotite; mag - magnetite.

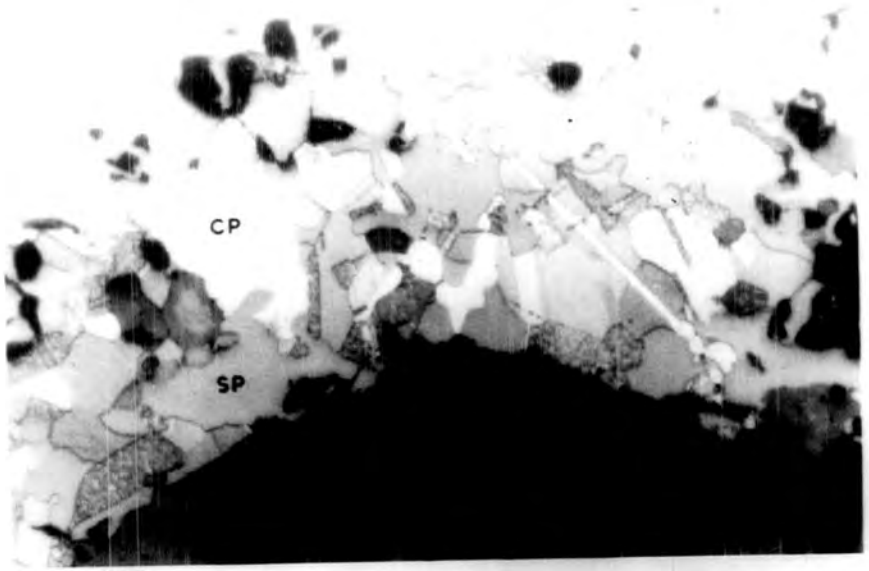

65

66

67

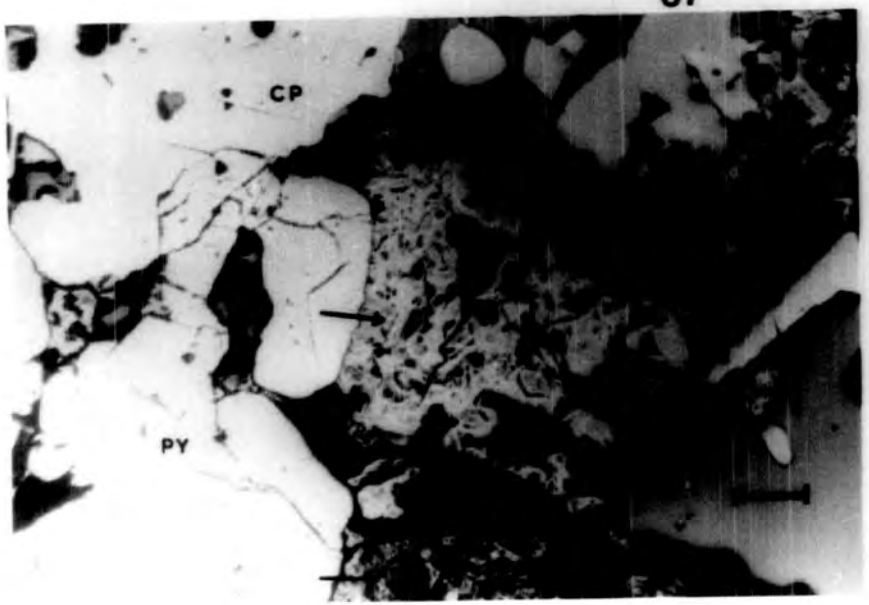

68

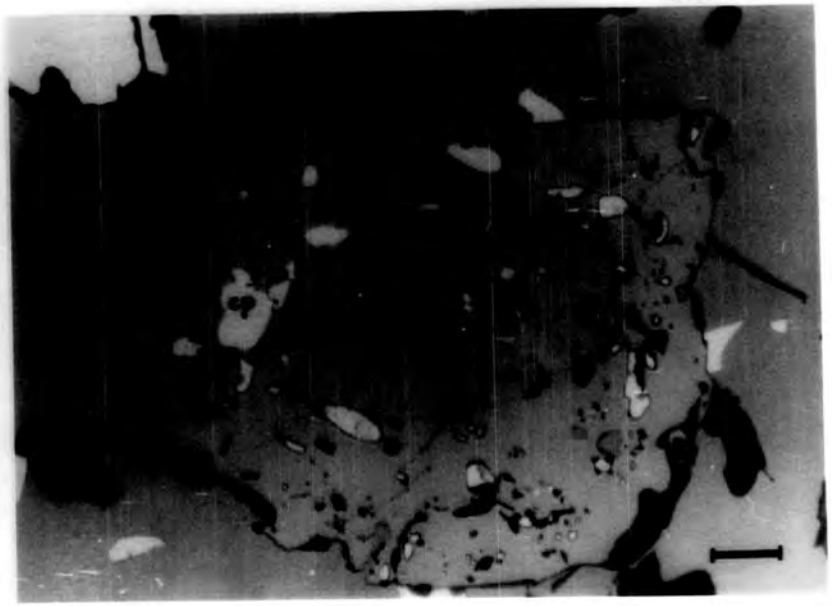

Table 5. J locality. Pyrite analyses from the massive sulphides.

	Coarse subhedral pyrite				Fine euhedral pyrite		Sieve-textured pyrite associated with fine euhedral pyrite.	
	core		margin					
	mean	range	mean	range	mean	range	mean	range
S	53.22	52.64-53.75	53.06	52.49-53.66	52.90	52.35-53.16	52.76	52.13-53.08
Mn	0.00	0.00-0.02	0.00	0.00-0.01	0.01	0.00-0.02	0.00	0.00-0.02
Fe	46.77	45.93-47.15	46.78	46.16-47.38	46.75	46.41-47.33	46.77	46.50-47.02
Co	0.12	0.01-0.36	0.19	0.11-0.36	0.25	0.14-0.41	0.15	0.06-0.27
Ni	0.03	0.00-0.06	0.01	0.00-0.04	0.01	0.00-0.04	0.00	0.00-0.03
Cu	0.04	0.00-0.06	0.08	0.01-0.20	0.05	0.00-0.26	0.01	0.00-0.02
Zn	0.02	0.00-0.09	0.09	0.00-0.50	0.35	0.03-0.98	0.09	0.00-0.19
Se	0.00	0.00	0.01	0.00-0.03	0.05	0.00-0.08	0.03	0.00-0.07
Ag	0.00	0.00	0.00	0.00-0.02	0.01	0.00-0.02	0.01	0.00-0.03
Total	100.20		100.22		100.38		99.82	

values in wt%

Table 6. J locality. Massive sulphides

	sphalerite		chalcopyrite		pyrrhotite		magnetite		
	mean	range	mean	range	mean	range		mean	range
S	32.88	32.14-33.63	34.41	34.09-34.68	38.63	38.16-38.84	SiO_2	0.02	0.01-0.03
Mn	na		0.00	0.00-0.02	0.02	0.00-0.04	TiO_2	0.09	0.06-0.13
Fe	7.99	6.44-9.24	31.12	30.54-31.67	60.23	59.75-60.90	Al_2O_3	0.04	0.00-0.09
Co	na		0.06	0.00-0.14	0.14	0.10-0.19	V_2O_3	0.02	0.00-0.05
Ni	na		0.00	0.00	0.00	0.00-0.01	Cr_2O_3	0.03	0.00-0.08
Cu	na		33.91	33.67-34.25	0.56	0.06-1.26	Fe_2O_3	68.69	67.89-69.42
Zn	58.99	57.54-60.95	0.18	0.09-0.48	0.13	0.00-0.55	FeO	31.14	30.77-31.52
Ag	na		0.05	0.03-0.07	0.03	0.01-0.04	MnO	0.00	0.00-0.01
							MgO	0.01	0.00-0.02
Total	99.86		99.73		99.74		Total	100.04	

Table 7. Unknown phases in sample MA9J15 from massive sulphides, J locality.

Phase	C	D	E
Colour in oil		Pale cream	Pale blue
Bireflectance in oil	Creamy yellow ⟶ Lt. Grey. Very strong	None	None
Anistropy in oil	Creamy yellow ⟶ Grey. Neutral grey	isotropic	isotropic(?)
Int. Refl.	None	None	None
R %	? 40	55	~50
H	<sp, <cp	<cp,= phase C, <phase E	<cp(just); >phase D, >phase C
Misc.	Thin laths & prisms. Single or multiple grains		Irreg. patches in cp. Interstitial to phase C
Probe Results	1	2	
Fe	0.359	0.143	0.237	1.567
Cu	0.00	0.148	0.144	1.207
Zn	3.332	0.447	1.665	3.657
Sb	0.333	0.156	0.216	0.00
Te	0.759	0.729	0.713	0.00
S	0.952	0.663	0.537	3.299
Bi	70.155	75.260	76.554	1.290
Ag	0.022	0.079	0.026	0.777
Pb	2.786	2.959	2.025	65.889
Cd	0.00	0.00	0.00	0.00
As	0.00	0.00	0.00	0.254
Se	19.600	19.863	19.377	21.386
Total	98.298	100.446	101.496	99.325

values in wt%

sequence a lens of massive sulphides. Each unit has a characteristic sulphide assemblage. In the chlorite schists, pyrite, pyrrhotite and chalcopyrite form irregular patches and bands comprising up to 25% of the rock. The recrystallized chert contains crude bands of pyrite with minor pyrrhotite and chalcopyrite. Pyrrhotite dominates in the massive sulphide lens with lesser amounts of sphalerite and chalcopyrite, and pyrite is virtually absent.

8.3.2 Pyrite

Pyrite forms large, up to 10 mm diameter, porphyroblasts. The crystals are cube-shaped with the development of (110) faces, although in the chlorite schist diamond-shaped crystals develop, with their long axes parallel to the schistosity and having pressure shadows of chalcopyrite and pyrrhotite, plate 69. The porphyroblasts are commonly intensely fractured and cleaved, with infills of pyrrhotite and rarely chalcopyrite. In many cases increased fragmentation has produced a breccia-textured pyrite set in pyrrhotite. Some of the fragments are rounded suggesting replacement of pyrite by pyrrhotite, plates 70 & 71. Frequently a thin film of pyrrhotite and/or chalcopyrite separates the margin of the pyrite from silicate gangue or host rock, plate 72.

Within the recrystallized chert, pyrite is idioblastic, and is rarely fractured. Most contain cores of inclusions, mainly chalcopyrite and pyrrhotite, but also silica, plate 73c. In sample SM5S3 an area of fine grained pyrite records the sequence of growth and recrystallization whereby

aggregates are formed by the impingement of adjacent grains to produce larger, optically continuous grains trapping silica and sulphides during growth. The final products are large, optically continuous euhedra containing areas of rounded sulphide and silica inclusions. Some of these euhedra have been fractured and cleaved at a later stage, plates 73 a-d.

8.3.3 Pyrrhotite

The distribution of pyrrhotite in the three units is the inverse to pyrite. In the chlorite schist pyrite and pyrrhotite are roughly equal in amount, in the chert pyrite dominates, and in the massive sulphides pyrite is virtually absent and pyrrhotite is the major sulphide mineral.

Pyrrhotite occurs as polygonally granular aggregates with triple junctions approaching 120°. The coarser grains show strain anisotropy and the development of polygonal subgrain boundaries. Pyrrhotite preferentially infills fractured pyrite, even when set in chalcopyrite, and commonly replaces the pyrite.

In the chert, pyrrhotite, although a minor component, forms crude granular rims around quartz and pyrite and along chalcopyrite-silicate contacts. Radial, elongate grains form around pyrite, plate 74. Sphalerite inclusions are fairly common as blebs within individual pyrrhotite grains.

Treatment with magnetic colloid shows the pyrrhotite to be hexagonal with thin replacement rims of the magnetic, monoclinic variety, plate 75.

Electron microprobe analyses of pyrrhotite from the massive sulphide unit show them to have an iron content of 61.32 wt% giving a formula of $Fe_{0.92}S$; table 8.

8.3.4 Chalcopyrite

Chalcopyrite is fairly abundant as a matrix to the large pyrite crystals and, in the chert, as intergranular films in the quartz-rich bands. In large areas, chalcopyrite comprises polygonally granular aggregates, each containing well developed spindle-shaped deformation twin lamellae in two directions. Exsolution "worms" of mackinawite occur along these twin planes, and stars of sphalerite are found throughout. Blebs of sphalerite are common along grain boundaries.

Electron microprobe analyses correspond to a formula of $Cu_{0.98}Fe_{1.02}S_2$, and are presented in table 8.

8.3.5 Sphalerite

Sphalerite forms $<1\%$ of the chlorite schist and chert units, occurring with chalcopyrite, as described above. It is a major component in the massive sulphides and appears to form granular, or coarse mutual boundary textures with pyrrhotite and chalcopyrite.

In the massive sulphide unit the sphalerite was found to have an iron content of 6.78 wt%, table 8.

8.3.6 Silicates

Quartz, chlorite and actinolite are the major silicates, or gangue minerals, in the sulphide assemblage. Quartz is present as round blebs or granular aggregates, often rimmed by pyrrhotite. Chlorite and amphibole form euhedral needles and prismatic crystal in chalcopyrite

and pyrrhotite, and chlorite has been observed within pyrite. Coarse actinolite is occasionally fractured and healed by pyrrhotite or chalcopyrite, plates 76 and 77.

From the results of electron microprobe analyses, the actinolite is magnesium-rich compared to similar minerals in the barren tuffs, fig. 22.

8.3.7 Summary and Discussion

Sulphides and silicates have been extensively re-crystallized during metamorphism, with near total obliteration of original textures. Pyrite in the chert unit contains inclusions of sulphide and silica, and in one rare example the origin of these can be traced to the growth, aggregation and recrystallization of small pyrite euhedra with entrapment of inter-granular impurities.

The crude distribution of sulphides into bands, and along parallel horizons, probably reflects an original depositional feature. The formation of idioblastic pyrite, with elongate axes parallel to schistosity, and the formation of pressure shadows, indicates growth in a stress field. The random orientation of chlorite and amphibole are the result of post-stress growth of these minerals. Later movement caused fracturing and subsequent healing of pyrite and amphibole, and some, possibly most, of the replacement of pyrite by pyrrhotite dates from this.

The inverse relationship between pyrite and pyrrhotite, and the localized increase in pyrrhotite with chlorite and amphibole, both of which are magnesium-rich, suggests that extensive de-sulphurization of pyrite has occurred (Mallio and Gheith, 1972):

$$\text{Fe, Mg chlorite/amphibole} + \underset{\text{from } FeS_2}{S} = FeS + \underset{\text{chlorite/amphibole}}{Mg}$$

The transformation of pyrite to pyrrhotite plus liquid takes place at 743°C in the presence of excess sulphur, rising by 14°C per kilobar (Kullerud and Yoder, 1959). The upper stability curve of pyrite, however, decreases with decreasing partial pressure of sulphur. Anger (1971) points to the conversion of pyrite to pyrrhotite at lower temperatures (unspecified) in the presence of surplus C and H_2O.

At the MGZ locality the maximum metamorphic temperature was approximately 500°C at a pressure of 5.6 kbar, see chapter 5. Pyrite has been converted to pyrrhotite in those rock units where iron was available from silicates and/or other sulphides and where the partial pressure of sulphur was low. This would explain the presence of magnesium-rich gangue minerals, their intimate relationship with pyrrhotite, and the replacement of pyrite by pyrrhotite. The abundance of pyrite with only minor pyrrhotite, and lack of replacement textures within the chert, can be explained by the paucity of chlorite and actinolite and the sealing effect of the chert retaining a high partial pressure of sulphur.

8.4 L-W Locality

8.4.1 Introduction

At both the L and W localities the sulphides are dominated by sphalerite. They occur as disseminations and within quartz bands in cherts and aluminous cherts of the Transition Zone sequence below the acid porphyries. The main mineralization occurs at the base of the

Plate 69. Large, porphyroblastic, pyrites with feathery chalcopyrite in pressure shadows (arrowed). Chlorite schist unit, MGZ locality.

Plate 70. Large, fractured, pyrite with infilling pyrrhotite. Mineralized chert unit, MGZ locality. Sample SM3S2.

Plate 71. Large, fractured, pyrite, partially replaced by pyrrhotite. Mineralized chert unit, MGZ locality. Sample SM5S3.

Plate 72. Large, fractured, pyrite, set in silicate, with a thin pyrrhotite and chalcopyrite rim. Chlorite schist unit, MGZ locality. Sample SM1S2a.

Py - pyrite; cp - chalcopyrite; po - pyrrhotite.

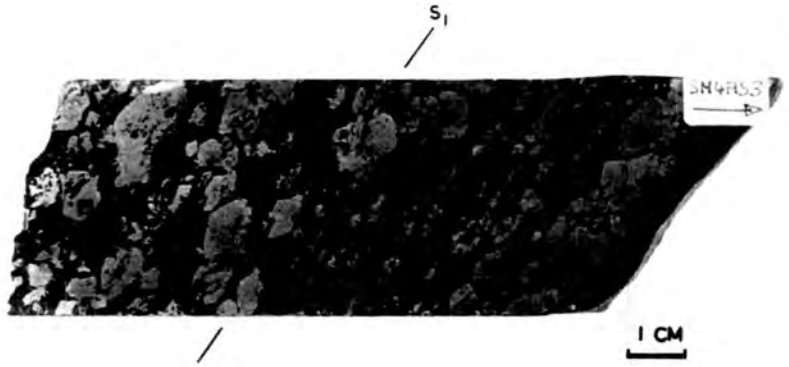

69

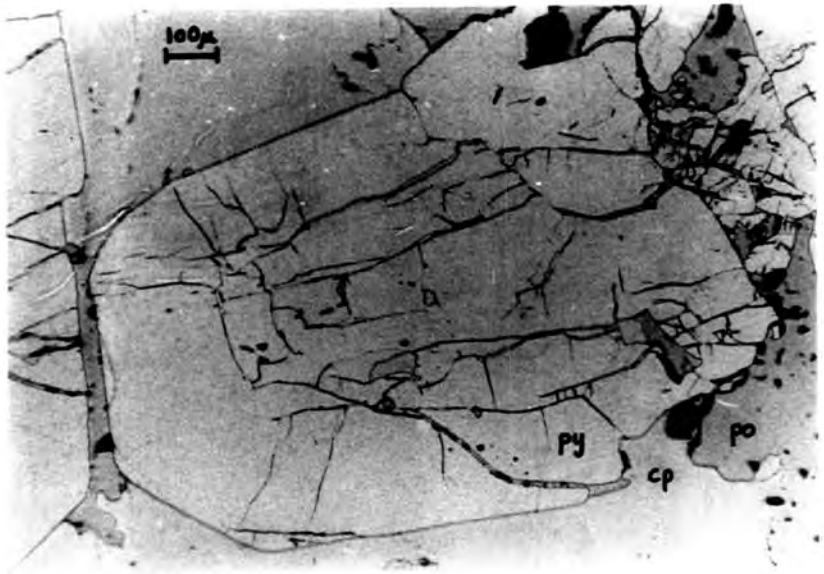

70

71

72

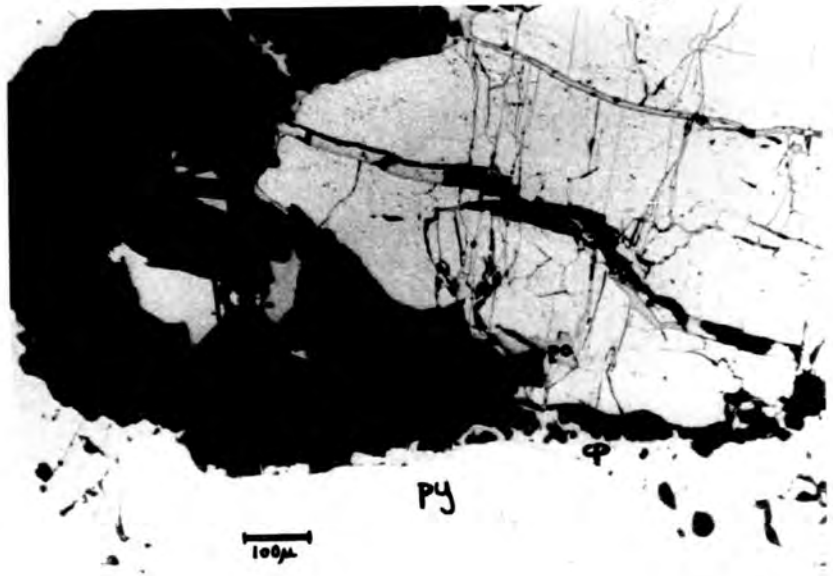

Plate 73. Stages in the growth, aggregation, and metamorphic recrystallization of pyrite, with entrapment of silica. Mineralized chert unit, MGZ locality. Sample SM3S2. Scale bar is 100 microns, or 0.1 mm.
Py - pyrite; cp - chalcopyrite; po - pyrrhotite.
A: initial stage. Small pyrite grains, beginnings of aggregation and entrapment of silica and chalcopyrite.
B: formation of larger aggregates, partial loss of original grain boundaries.
C: metamorphic recrystallization into large porphyroblast. Inclusions become rounded.
D: later fracturing and healing with pyrrhotite.

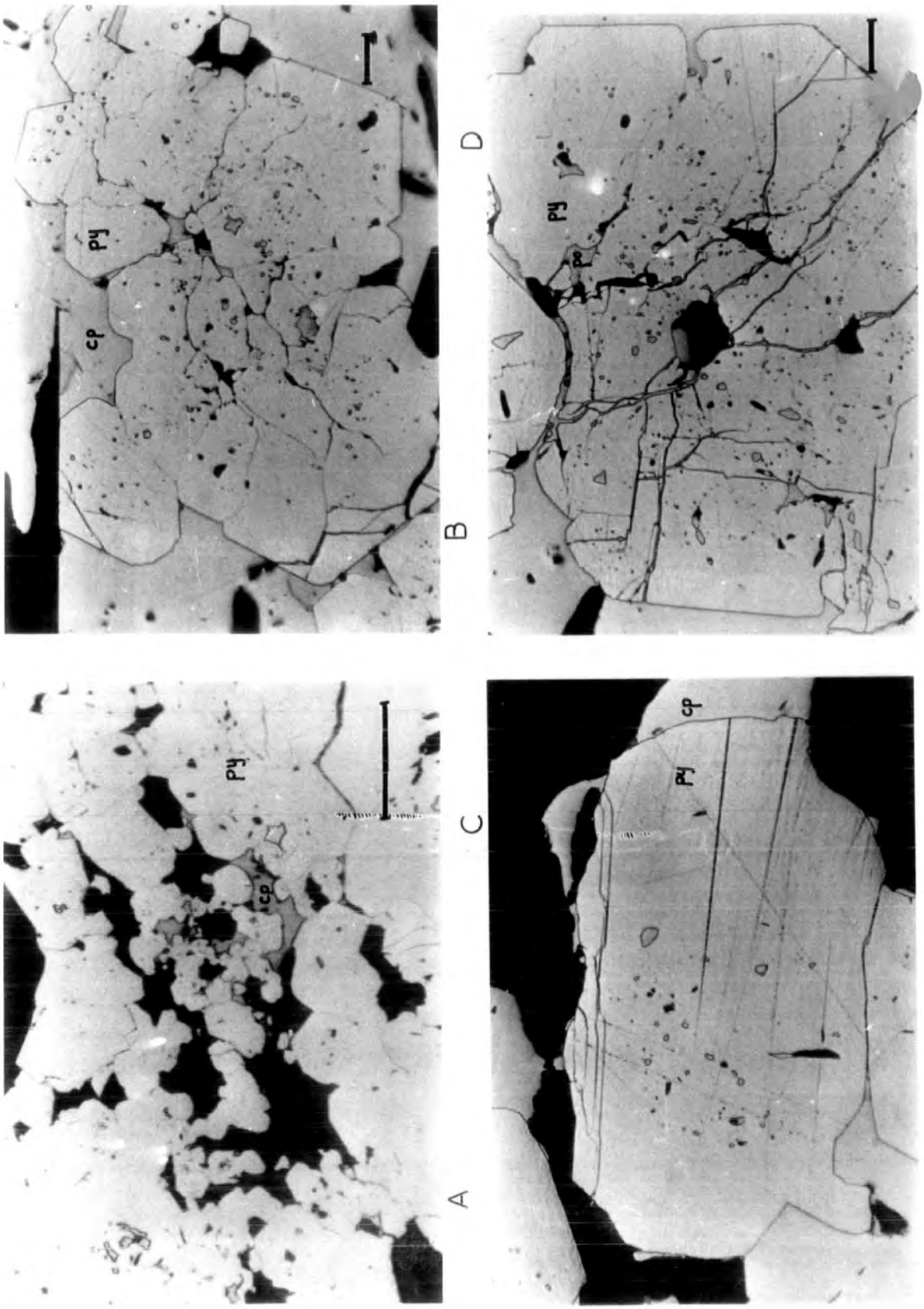
A
py
cp
B
py
cp
C
py
cp
D
py
cp

Plate 74. Pyrrhotite radially overgrowing pyrite. Partially crossed nicols. Mineralized chert unit, MGZ locality. Sample SM5S3.

Plate 75. Hexagonal pyrrhotite partially replaced by magnetic, monoclinic pyrrhotite. Treated with magnetic colloid. Mineralized chert unit, MGZ locality. Sample SM4S2b.

Plate 76. Intergrown pyrrhotite and Mg-chlorite. Chlorite schist unit, MGZ locality. Sample SM4AS3.

Plate 77. Fractured amphibole crystal, healed with pyrrhotite. Chlorite schist unit, MGZ locality. Sample SM4AS3.

Scale bar is 100 microns, or 0.1 mm. Py - pyrite; cp - chalcopyrite; po - pyrrhotite.

75

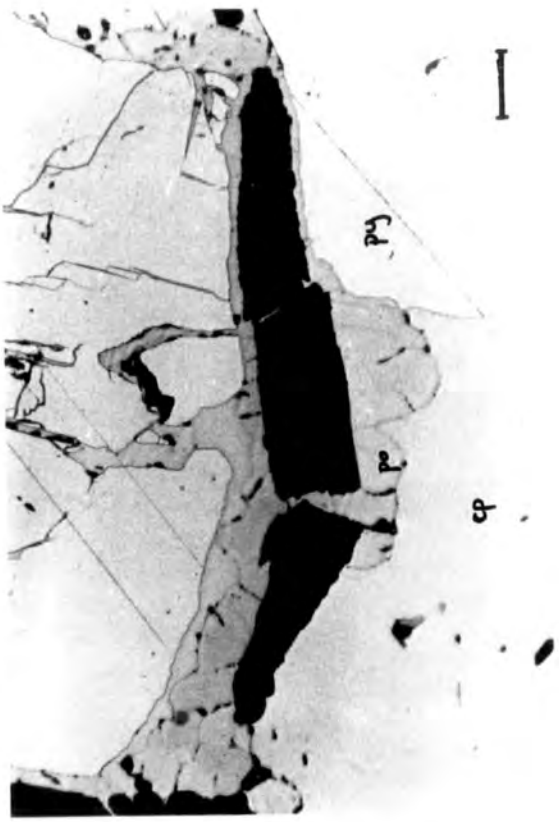

77

74

76

Table 8. MGZ locality. Massive Sulphide Unit.

	pyrrhotite		chalcopyrite		sphalerite	
	mean	range	mean	range	mean	range
S	38.25	37.65-38.83	34.69	34.12-35.45	33.68	33.42-34.19
Mn	0.00	0.00	0.02	0.00-0.05	0.06	0.02-0.14
Fe	61.32	60.99-61.66	30.97	30.54-31.65	6.78	6.09-7.25
Co	0.13	0.07-0.22	0.06	0.00-0.12	na	
Ni	0.01	0.00-0.03	0.04	0.00-0.08	na	
Cu	0.01	0.00-0.03	33.54	33.06-34.37	0.03	0.00-0.13
Zn	0.00	0.00-0.14	0.30	0.06-0.84	59.43	58.54-60.11
Ag	0.01	0.00-0.04	0.05	0.00-0.14	0.00	0.00-0.01
Cd	0.01	0.00-0.02	na		0.00	0.00
Total	99.74		99.67		99.98	

na - not analysed
values in wt%

Transition Zone at L, and following 22 m of aluminous cherts at W, see fig. 40, chapter 7. Sphalerite, chalcopyrite, pyrite and pyrrhotite are present, with sphalerite forming the vast majority of the sulphides, especially in the heavily mineralized parts. The common sulphide occurrences are in thin, 1 mm bands of clear quartz and quartz lenses, and as disseminated grains in sericite-rich horizons.

In sample MA17W2, plate 40, an intrafolial F_1 fold has affected a quartz+sphalerite+chalcopyrite band with subsequent thickening in the fold hinge. The quartz+sulphide bands, and the disseminated horizons are both parallel to lithological layering within the aluminous cherts. Occasional crosscutting veinlets were observed. Within the bands and veins, quartz and sulphides are granular and recrystallized, micaceous minerals form prismatic crystals, and all are of a coarser grain size than the surrounding host rock, plate 78. Margins of the bands are irregular with individual minerals projecting into the matrix.

8.4.2 Pyrite

Pyrite is mainly confined to veins and bands containing quartz, with or without other sulphides. It forms small cubes, though where intergrown with sphalerite these are imperfectly formed, and exhibit coarse round embayments and inclusions typical of recrystallized pyrite (Stanton, 1964; Vokes, 1969).

In the more massive sphalerite+quartz bands, minor amounts of pyrite form small, irregular patches usually

at sphalerite-silicate boundaries. This pyrite is heavily embayed and corroded, and appears to have undergone partial replacement, plate 79.

8.4.3 Sphalerite

Sphalerite is found as small, red-brown, semi-transparent grains disseminated in the aluminous cherts, and with quartz bands and patches, throughout the sequence.

In the disseminated form sphalerite occurs as angular grains, elongate parallel to the schistosity. The angularity is due to the sphalerite being somewhat interstitial to muscovite, plate 80. In places these aligned grains have been deformed by S_2, and are occasionally enclosed by poikiloblastic garnets, plate 81.

Sphalerite forms polygonally granular aggregates in quartz bands. Boundaries with quartz tend to be smooth, although they may appear to be highly irregular and embayed and to have a caries-texture. This is caused by the presence of minute quartz and sphalerite grains along the boundaries forming a micro, mutual boundary texture. Sphalerite is everywhere in equilibrium with associated silicates. In the larger sphalerite bands, contorted and irregular inclusions of muscovite and/or quartz aggregates are common.

Minute blebs of chalcopyrite and, rarely, pyrrhotite form inclusions within the larger sphalerite aggregates.

Electron microprobe analyses of the disseminated and quartz-band variety of sphalerite reveal iron contents of 6.32-6.81 wt% and 5.47-5.94 wt% respectively, table 9. Trace element contents are generally below the limits of

detection, although Mn contents are high. In quartz bands, Mn ranges from 0.10 to 0.13 wt%, while in the sericite horizons analyses from four sphalerites included in a Mn-bearing garnet where 0.14, 0.38, 0.39 and 0.39 wt%. Sphalerite in the same horizon, but outside the garnet, has a Mn content of 0.07 wt%.

8.4.4 Chalcopyrite

This is a relatively minor sulphide, forming <1% of the rock. At the L locality chalcopyrite takes the form of chains of minute blebs outlining individual sphalerite grains, and as intragranular exsolution lamellae. Granular aggregates of chalcopyrite are rare: where present they form mutual boundary textured intergrowths with sphalerite. At the W locality chalcopyrite forms large aggregates within and adjacent to sphalerite. Exsolution and intergranular blebs are rare. Pyrrhotite is present as rare blebs and heavily embayed patches within chalcopyrite.

8.4.5 Pyrrhotite

This is rather a rare mineral and is found in quartz bands as anhedral grains, and in sphalerite aggregates where it forms small, <0.01 mm, grains in mutual boundary texture with sphalerite and chalcopyrite.

8.4.6 Miscellaneous

At W, small rounded grains of a grey-purple mineral were observed within the larger sphalerite aggregates. These grains are isotropic, with a reflectance slightly greater than sphalerite and a much greater hardness. They are thought to be magnetite. In the host rocks, thin

parallel horizons contain minute, corroded or poikiloblastic, homotropic laths of ilmenite. They are euhedral against, and within, sphalerite. This ilmenite is considered to represent an original detrital concentrate.

8.4.7 Summary

Massive sulphides were not located, and are possibly not present at the L and W localities. Sphalerite with minor amounts of chalcopyrite, pyrite and pyrrhotite form disseminations in cherts and aluminous cherts, and within quartz bands and lenses.

The sulphides and gangue minerals, mainly quartz and lesser muscovite and chlorite, have been completely recrystallized. The coarser grain size in the bands, as compared to the host rock, is most likely due to the presence of sulphide (Mallio and Gheith, 1972). Parallelism of the bands and disseminated horizons with sedimentary features in the host rock, and the absence of alteration suggest a similar, sedimentary origin.

At the W locality, Mn-bearing garnets may enclose or occur within sulphide bearing horizons, see also chapter 7. The Mn content of the sphalerites is fairly high suggesting a common source. The variation in Fe content between sphalerite from disseminated horizons and quartz bands is probably caused by a sealing effect in the latter as opposed to a more open environment in the former. Chalcopyrite in sphalerite is the result of exsolution at L and may be of the same origin at W but with increased recrystallization and expulsion from the sphalerite. Alternatively the chalcopyrite may have been originally separate from the sphalerite with only minor amounts of dissolved copper.

Plate 78. Coarse, quartz and sphalerite (opaque) band in micaceous schist, L locality. Sample MA2L1, thin section, crossed polars.

Plate 79. Corroded pyrite in sphalerite and quartz, L locality. Sample MA3L1, reflected light.

Plate 80. Angular sphalerite, interstitial to sericite, and parallel to schistosity, W locality, Sample MA16W2, thin section, plane polarised light.

Plate 81. Garnet enclosing sphalerite, W locality. Sample MA23W2, thin section, plane polarised light.

Scale bar is 100 microns, or 0.1 mm. Q - quartz; G - garnet; py - pyrite; sp - sphalerite.

79

81

78

80

Table 9, Sphalerite analyses from the W locality.

	In quartz bands		Enclosed in garnet		Away from garnet (Two analyses)	
	mean	range	mean	range		
S	33.02	32.87-33.14	33.22	32.69-33.58	32.94	33.46
Mn	0.12	0.10-0.13	0.33	0.14-0.39	0.07	0.07
Fe	5.72	5.47-5.94	6.73	6.63-6.81	6.32	6.41
Cu	0.01	0.00-0.02	0.00	0.00-0.01	0.04	0.00
Zn	60.87	60.24-61.47	59.64	59.32-60.00	60.49	60.82
Se	0.00	0.00-0.02	na		na	na
Cd	0.00	0.00	na		na	na
Sn	0.02	0.00-0.08	na		na	na
Total	99.76		99.92		99.85	100.77

na - not analysed
values in wt%

8.5 Sphalerite Geobarometer

8.5.1 Introduction

The theory behind the sphalerite geobarometer has been discussed by Barton and Toulmin (1966), Scott and Barnes (1971), and Scott (1973, 1976). Briefly the FeS content of sphalerite is a function of temperature (T), pressure (P), and FeS activity.

The FeS activity is not necessarily dependent on P & T, and for geobarometry work must be buffered by one or more iron sulphide phases. When buffered by the divariant system pyrite+hexagonal pyrrhotite, retrograde variation in pyrrhotite composition is not important (Scott, 1976).

Fig. 42, taken from Scott (1976), shows isobars of sphalerite composition along the pyrite+hexagonal pyrrhotite buffer. In applying the sphalerite geobarometer, the following criteria must be fulfilled:

1. Sphalerite must have equilibrated with pyrite and hexagonal pyrrhotite (Scott, 1976). In practice this requires analyses of only those sphalerite grains in mutual contact with, and in equilibrium with, pyrite and hexagonal pyrrhotite. Sphalerite grains in contact with or within a centimeter of only one of the sulphide phases give erroneous results (Bristol, 1979).
2. Temperatures must be greater than 265^{o}C and probably below 600-700^{o}C where the curvature of the isobars is strong (Scott, 1976).

8.5.2 Methods

Samples of massive sulphide from the J deposit were examined for sphalerite+pyrite+pyrrhotite equilibrium assemblages. Treatment with a magnetic colloid solution (Scott, 1974) was used to distinguish between magnetic, monoclinic, and non-magnetic, hexagonal pyrrhotite.

Eighteen analyses were made by electron microprobe, of sphalerite grains in mutual contact with and apparently in equilibrium with pyrite and hexagonal pyrrhotite, table 6. Their mean mol% FeS content is 13.66 with a standard deviation of 1.33 mol%. Previous analyses indicate the Mn content to be <0.03 wt% and Cd content to be <0.01 wt%. The exsolution of copper as chalcopyrite does not appear to significantly alter the utility of the sphalerite geobarometer (Wiggins & Craig, 1980). The results have been plotted on fig.42.

8.5.3 Results

From a study of metamorphic silicate mineral sequences, the temperature of metamorphism did not exceed, but was probably close to 500°C, see chapter 5.

For a temperature of 500°C, the mean FeS composition corresponds to a metamorphic pressure of 5.6 kbar, the range for $\pm$ 1 standard deviation being 4.4 to 7.1 kbar.

This pressure is in reasonable agreement with that estimated for the silicate mineral assemblage which is thought to have formed between 3-5.5 kbar (Winkler, 1974). Minnitt (1975) considered that pressures above 6 kbar could not have developed in the Murchison greenstone belt.

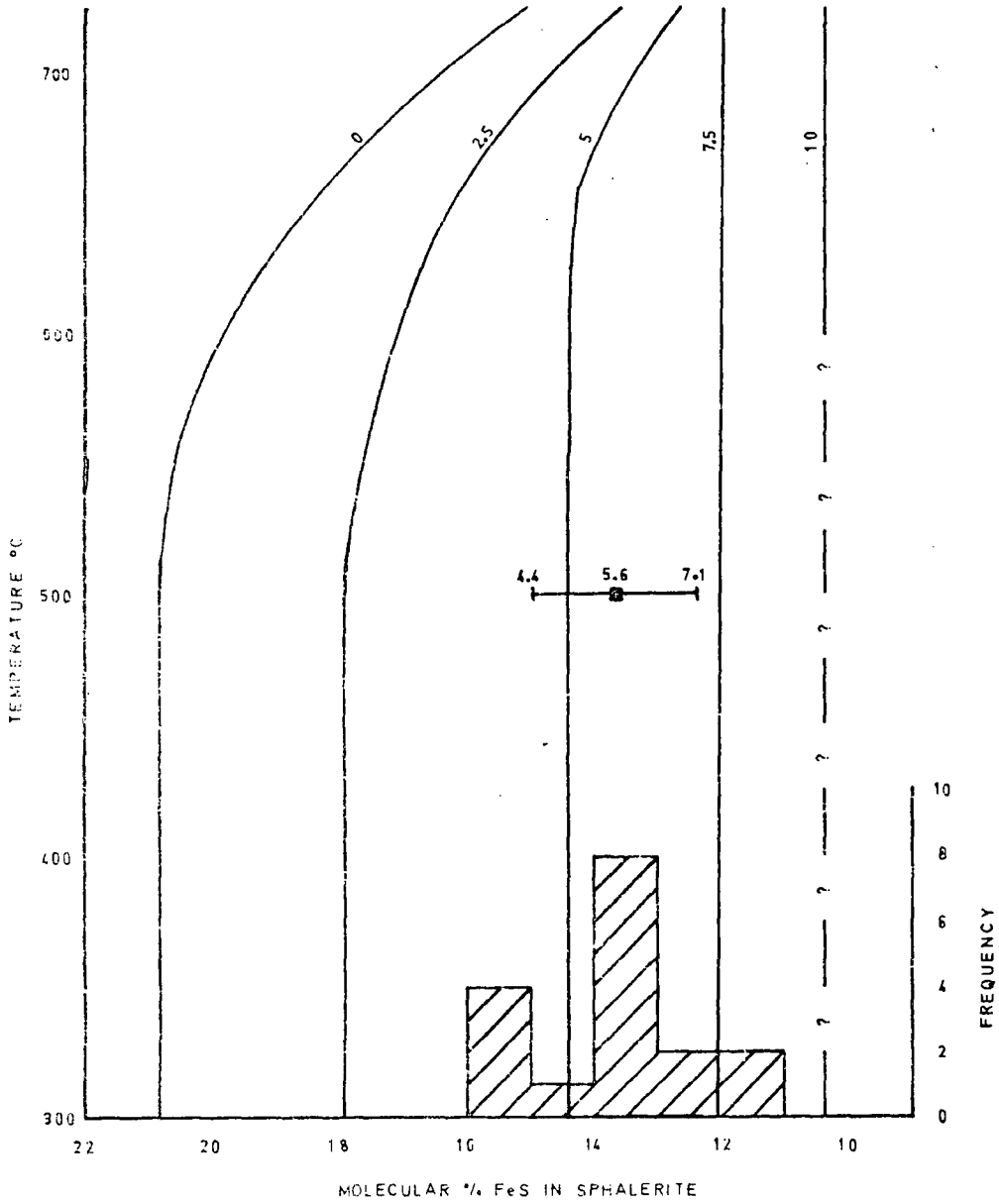

FIG 42

T-X PROJECTION ONTO THE FeS-ZnS JOIN OF SPHALERITE+PYRITE+HEXAGONAL PYRRHOTITE (IN KBAR). FROM SCOTT (1976).

FeS IN SPHALERITE FROM J DEPOSIT SUPERIMPOSED

SPHALERITE+PYRRHOTITE AND SPHALERITE+ PYRITE COEXIST TO THE LEFT AND RIGHT, RESPECTIVELY, OF EACH ISOBAR

PRESSURE RANGE AT 500°C IS 4.4 — 7.1 KBAR
▣ MEAN AT 5.6 KBAR

n = 18

$\bar{x}$ = 13.66

s = 1.33

HORIZONTAL BAR IS ONE STANDARD DEVIATION FeS EITHER SIDE OF MEAN ▣

CHAPTER IX

FOOTWALL ALTERATION

9.1 Introduction

The majority of Archaean, volcanogenic, massive sulphide deposits (Type I) occur in or at the top of piles of acid volcanic rocks which are dominantly pyroclastic (Sangster, 1972; Spence and de Rosen Spence, 1975; Sangster and Scott,1976). The deposits consist of an upper, massive sulphide body which may overlie a stockwork, copper-rich zone. This extends into the footwall and grades into a silicate alteration zone which in turn grades downwards and laterally into "fresh unaltered rocks".

From a close study of the bulk chemical and mineralogical changes of rock that has been progressively and increasingly altered, a picture can be constructed of the chemistry and physical conditions of the fluids which caused the alteration, and which eventually formed the overlying, massive sulphide body.

9.2 Alteration Zone - Geochemistry

Previous investigations into the chemistry of these silicate alteration zones reveal that the sulphide stockwork is surrounded by a chlorite-rich zone which grades outwards to a sericite-rich zone and finally to unaltered volcanic rocks (Franklin et al., 1975; Sangster and Scott, 1976; Riverin and Hodgson, 1980). Chemical analyses show a relative increase in Fe, Mg and S in the alteration zone,

with depletion of Ca and Na (Franklin et al., 1975; Sangster and Scott, 1976; Spitz and Darling, 1978; Riverin and Hodgson, 1980). Alumina tends to be immobile, although at Millenbach, Riverin and Hodgson (1980) report leaching of Al_2O_3, together with K_2O, from the central alteration zone, with additions at the margins. Silica may increase (MacGeehan and MacLean, 1980b) or decrease (Koo and Mossman, 1975; Sangster and Scott, 1976). At the Mattabi deposit the dominant alteration mineral is siderite (Franklin et al., 1975).

The importance of hydrogen metasomatism in the process of alteration has been widely underestimated (Hemley and Jones, 1964). According to Riverin and Hodgson (1980), in the chlorite zone, chlorite is generated from sericite by:

1. $\underset{\text{sericite}}{3KAl_3Si_3O_{10}(OH)_2} + 10(Fe,Mg)^{2+} + 32H_2O =$

$\underset{\text{chlorite}}{2(Mg,Fe)_5Al_2Si_3O_{10}(OH)_8} + 3Si(OH)_4 + \underset{\text{liberated}}{3K^+ + 22H^+ + 5Al(OH)_4^-}$

The liberated ions K^+, H^+ and $Al(OH)_4^-$ are then utilized in the margin to produce sericite from albite by:

2. $\underset{\text{albite}}{NaAlSi_3O_8} + 2Al(OH)_4^- + K^+ + 2H^+ =$

$\underset{\text{sericite}}{KAl_3Si_3O_8(OH)_2} + Na^+ + 4H_2O$

Further chlorite may also be produced from albite and biotite (Meyer and Hemley, 1967):

3. $2NaAlSi_3O_8 + 4(Mg,Fe)^{2+} + 2(Fe,Al)^{3+} + 10H_2O =$
albite

$(Mg,Fe)_4^{2+}(Fe,Al)_2^{3+}Si_2O_{10}(OH)_8 + 4SiO_2 + 2Na^+ + 12H^+$
chlorite liberated

4. $2K(Mg,Fe)_3AlSi_3O_{10}(OH)_2 + 4H^+ =$
biotite

$Al(Mg,Fe)_5AlSi_3O_{10}(OH)_8 + (Mg,Fe)^{2+} + 2K^+ + 3SiO_2$
chlorite liberated

The overall result is fixation of Fe and Mg in the central alteration zone with depletion of Al and K, and production of H^+. These are then fixed in the outer, sericite, zone. These reactions, somewhat simplified, and their possible relationships are summed up in fig. 43. Fluids moving through a volume of rock would thus produce a central zone of chlorite-rich alteration surrounded by sericite-rich alteration. The apparent mobility of silica in these reactions would account for variations in silica content. Silica may be fixed in the sulphide-rich stockwork or carried through in solution.

In the massive sulphide deposits discussed here, alteration is present as a pipe-shaped zone in the footwall, decreasing with depth. The optimum conditions for reaction between host-rock and solution are near the overlying massive sulphide body. Presently-held concepts suggest the massive body to be deposited at the sea-floor (Solomon, 1976; Solomon and Walshe, 1979), and thus the footwall rocks would be water-saturated. Mixing with cold sea-water would set up disequilibrium between rock and fluid causing the various reactions to occur. Some form of

initial barrier or cap rock may well restrict the entry of solutions onto the sea-floor producing an outward diffusion of the rising solutions into the footwall rocks.

9.3 Solutions

Hypotheses for the origin of the hydrothermal solutions responsible for producing both the alteration zone and overlying massive sulphide lens have been reviewed in chapter 3, section 3. Briefly these solutions are considered to have originated as sea-water percolating down through the volcanic pile, becoming heated and modified by reaction with the host rock to produce hot saline brines capable of leaching and transporting base metals. Temperatures of $380\pm30^{o}C$ with pH of 4.7 have been directly measured from hydrothermal solutions venting onto the sea-floor at the East Pacific Rise (Edmond, 1981). Solomon and Walshe (1979), from published fluid inclusion data, estimated salinities to be 1 m NaCl for solutions forming the Kuroko-type deposits, and 0.6 m NaCl for Cyprus-type deposits.

These solutions would thus be buoyant on entering the sea-water and would rise as plumes, entraining and mixing with cold sea-water precipitating sulphides, silica and sulphates (Turner and Gustaffson, 1978; Solomon and Walshe, 1979; RISE Project Group, 1980). From studies by Large (1977), and direct observations by the RISE Project Group (1980), pyrrhotite and chalcopyrite precipitate adjacent to the vent, with pyrite and sphalerite further away.

9.4 Murchison Greenstone Belt

9.4.1 J Locality

A well developed silicate alteration zone underlies the massive sulphide lens at the J locality. This zone forms an oval shaped area grading laterally and downwards, in the original sense, into unaltered tuffs. The most intense alteration, containing appreciable amounts of sulphide, occurs within the coarser, more porous tuffs. Pyrrhotite and chalcopyrite are dominant in the core of the alteration Zone and pyrite and sphalerite at the margins, see fig. 33. Overall, the most intense alteration is chlorite-rich. Local increases in the original clay content, however, have given rise to chlorite schist horizons which are almost impossible to distinguish from this pervasive alteration. Surrounding the chlorite zone is a sericite-rich halo, the full shape and distribution of which is unknown. The petrology of the alteration zone is further complicated by overprinting due to regional and thermal metamorphism.

The most noticeable alteration takes the form of cross-cutting veins and coarse patches of dark green chlorite with lesser biotite, albite and carbonate, plate 28. Quartz$\pm$sulphides occur within these veins and patches, and may form separate veins cutting across these features. A well developed vein comprises a core of quartz$\pm$sulphide$\pm$ chlorite with margins of chlorite$\pm$biotite$\pm$albite$\pm$rare sulphide. All these veins cut the rock into blocks of relatively unaltered tuff which, with increasing size

and frequency of veining, become rounded. The fine grained groundmass to the tuff consists of quartz+chlorite, sericite being absent, and frequently contains clots of coarse chlorite, quartz and sulphide as "diffuse" alteration.

Samples of variously altered tuff were analysed for major and trace elements, and are presented in fig. 44 and Appendix C. With increasing alteration Al_2O_3 and K_2O decrease and total iron and S increase. MgO and SiO_2 remain constant. The decrease in alumina and potash is related to the disappearance of sericite, and the increase in S to the appearance of sulphides. The increase in total iron reflects a general increase in chlorite and sulphide content. Lacharpagne (1979) detected an increase in the Fe/Fe+Mg ratio of the chlorites towards the massive sulphide lens. This is somewhat, though erratically, supported by Electron Microprobe analysis of chlorites from rocks suffering varying degrees of alteration, fig. 45.

9.4.2 MGZ Locality

A footwall alteration zone similar to that at the J locality was not observed. Samples of the footwall tuffs were collected at 5 m intervals along hole MS1, which intersected sulphide mineralization. Equivalent samples were collected from hole MS6, 50 m along strike, which only intersected a thin chloritic horizon. In hand specimen the only difference noted was a slightly greater chlorite content, especially as thin chlorite bands, in hole 6.

From an examination of the sequence in hole 1 the tuffs comprise a fine grained, schistose and braided intergrowth of quartz+chlorite+sericite outlining occasional quartz lenses. Towards the top of the sequence chlorite becomes more abundant and forms finely matted patches. In thin section the interference colour of the chlorite changes from grey-green to an anomalous purple or brown, reflecting a higher Fe^{2+}/Fe^{2+} + Mg ratio. This was the only change noted. Rocks from hole 6 show no such change.

Changes in the bulk chemistry of the rocks from hole 1 can be seen in fig. 46 and also Appendix C. Towards the sulphide horizon, i.e. stratigraphically upwards, there is an increase in total iron and a slight decrease in K_2O. Samples from hole 6 show no discernable trend, although they have a higher iron content, probably reflecting their higher chlorite content.

9.5 Summary and Discussion

A well developed silicate and sulphide alteration zone is present in the tuffs beneath the massive sulphide lens at the J locality. This alteration consists of chlorite with pyrrhotite and chalcopyrite, grading outwards into pyrite and sphalerite accompanied by sericitic alteration. According to Large (1977) the presence of pyrrhotite and chalcopyrite is indicative of a higher temperature environment than for pyrite and sphalerite. This is in agreement with their presence in the centre of the alteration zone.

Bulk chemical analyses show that, with increasing

alteration, the total iron and S contents increase, and K_2O and Al_2O_3 decrease. The increase in iron is paralleled by an increase in the amount of chlorite present, and an increase in the Fe/Fe+Mg ratio of that chlorite.

The solutions responsible for this alteration introduced Fe, S and metals into the tuffs, and leached K and Al. As outlined above in section 2 it is most probable that the chlorite was produced from sericite with the loss of Al and K. Albite was converted to sericite. SiO_2 liberated by these reactions appears to have been reprecipitated with sulphides in veinlets, and as patches, as a separate process from the main chlorite alteration. Lateral enrichment of K and Al was not noted.

A similar alteration zone was not found at the MGZ deposit although chemical analyses of tuffs beneath the sulphide horizon show an increase in total iron and a slight decrease in K_2O towards the sulphides. A control sequence some 50 m away, where sulphides are absent, shows no such variation. These chemical variations suggest that mineralizing solutions did pass through the footwall tuffs beneath the MGZ deposit. No visible alteration minerals or zones were formed in that part of the footwall remaining beneath the MGZ deposit. They were presumably present in the part of the deposit now eroded away.

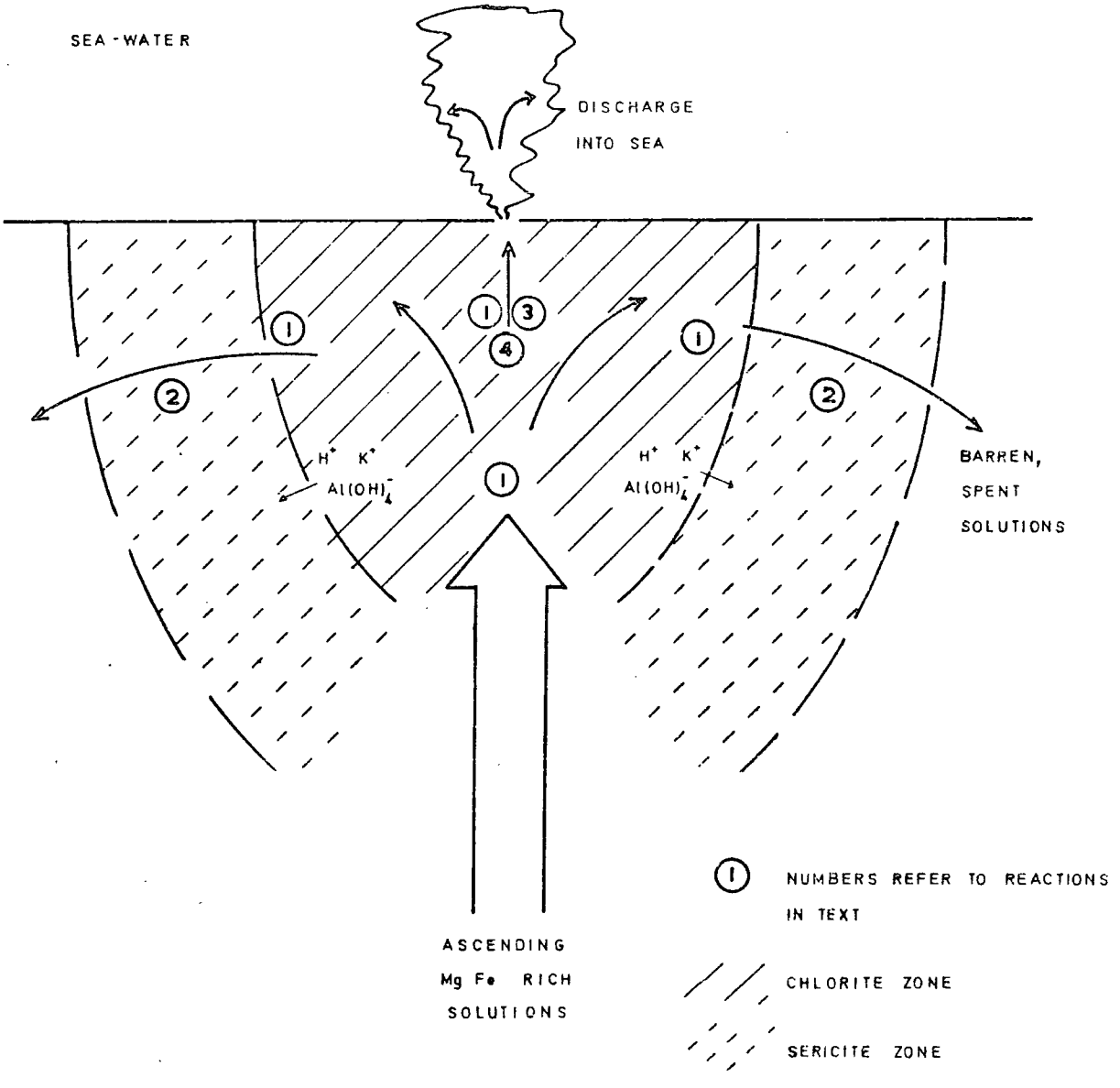

FIG 43 DIAGRAMATIC SECTION THROUGH A HYPOTHETICAL ALTERATION ZONE

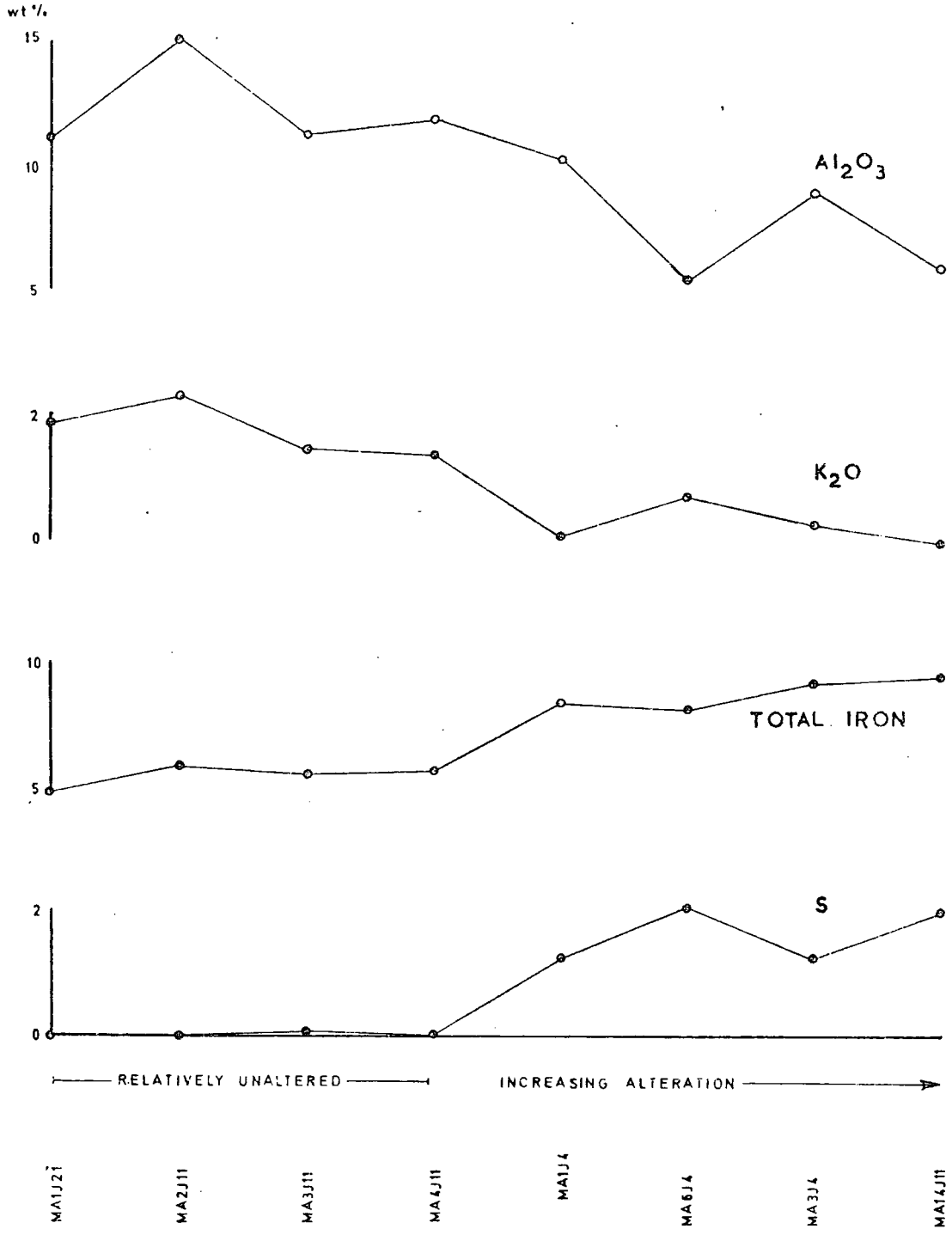

FIG 44 J LOCALITY: FOOTWALL ALTERATION ZONE

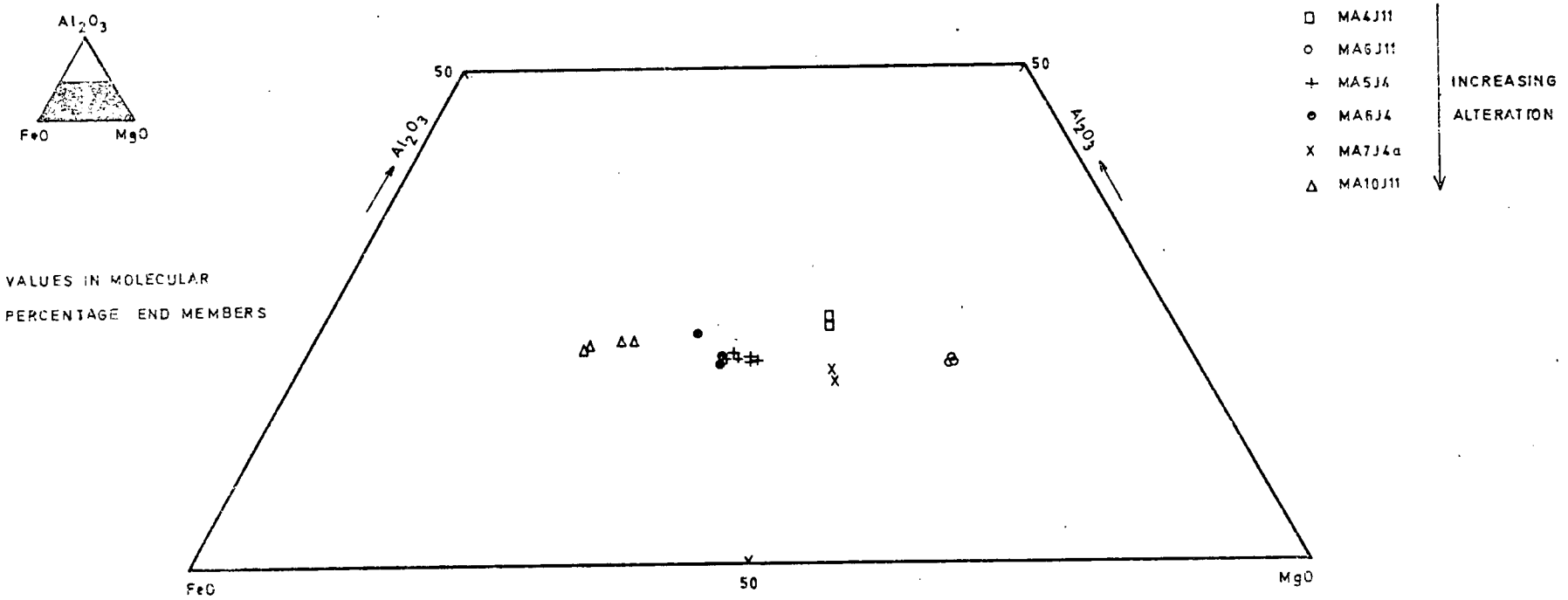

FIG 45 CHLORITE COMPOSITION: FOOTWALL ALTERATION ZONE AT THE J LOCALITY

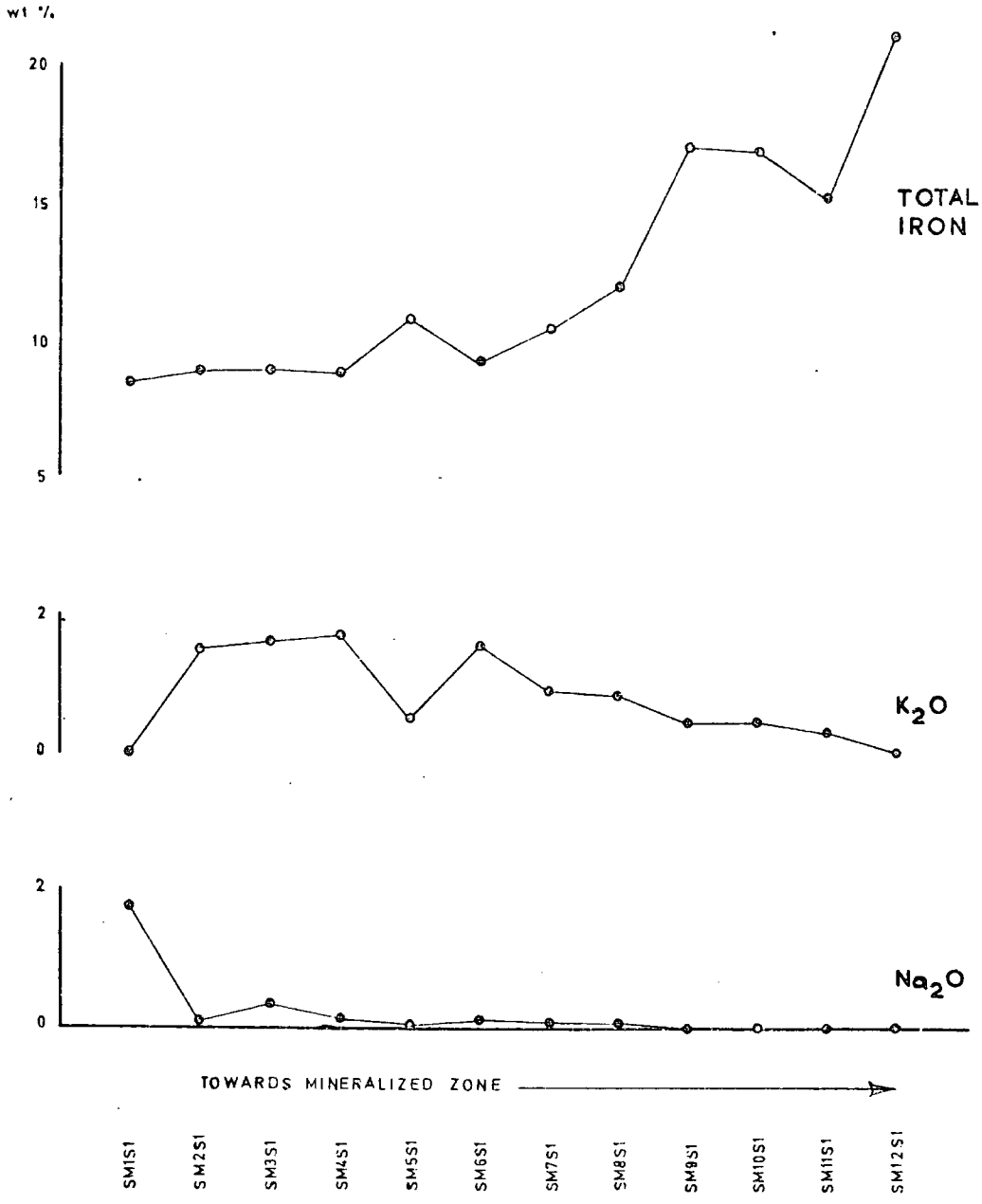

FIG 46 MGZ LOCATION: FOOTWALL TUFFS

CHAPTER X

DISCUSSION

10.1 Geology

The geology of the northern flank of the Murchison greenstone belt was examined north of the town of Gravelotte. From north to south the following lithological units were encountered. All units young consistently to the south.

The northern margin of the belt consists of a large gabbro and quartz-diorite intrusive, the Rooiwater Igneous Complex. In the south this intrudes a thick pile of tuffs and flows of rhyolitic composition. The centre of volcanic activity was at the western extremity of the study area. The top of the volcanic pile is marked by localized, explosive activity at centres approximately 4 to 5 km apart.

Overlying the volcanic pile is a 100 m thick sequence of cherts, reworked felsic volcanic rocks, and acid porphyries or welded tuffs,collectively termed the Transition Zone. The acid porphyries originated from a volcanic centre immediately west of the study area. During the short time interval between the end of volcanism and reworking of the volcanic rocks, ie. the base of the Transition Zone, massive copper-zinc sulphide deposits were formed.

The Transition Zone is conformably overlain by a thick sequence of clastic sediments. These grade upwards from argillaceous to arenaceous sediments with prominent quartzite horizons. The important antimony-sulphide

deposits of the Murchison greenstone belt are hosted by a carbonate-rich horizon at the top of the sedimentary sequence, south of the study area.

The volcanic and sedimentary sequence is intruded by numerous, thick and extensive basic sills. The whole assemblage has been tilted to the vertical, and now strikes east-west.

10.2 Copper-Zinc Sulphide Deposits

Three massive copper-zinc sulphide deposits, the MGZ, D and J, and one area of disseminated sulphides, the L-W, were located in the study area. All overlie the felsic volcanic rocks, and locally form the base of the Transition Zone. Both the J and L-W deposits overlie local, explosive volcanic centres.

The mineralizing fluids which produced the two main deposits, the MGZ and J deposits, were similar. They were initially rich in copper and silica, and later became zinc-rich. At the MGZ deposit this can be observed as a chlorite schist and recrystallized quartz rock (referred to as "chert") containing pyrite, chalcopyrite and pyrrhotite, overlain by massive sulphides consisting of pyrrhotite, sphalerite and chalcopyrite.

At the J deposit, the basal sulphide horizons were originally rich in silica. This silica was replaced by zinc sulphide as the fluids evolved. This gave rise to the uniformly high zinc content throughout the deposit, and lack of metal zonation.

10.3 Model for Sulphide Formation

Present theories concerning the genesis of Archaean, type I, massive sulphide deposits are summarized in chapter 3. A similar origin is proposed for the deposits of the Murchison greenstone belt.

Following accumulation of a pile of felsic tuffs and flows, cessation of volcanism was accompanied by extensive fracturing of the pile, probably as a result of caldera collapse, allowing sea-water to percolate into the rocks (Hodgson and Lydon, 1977; Ohmoto, 1978).

Magma remaining beneath the extrusive pile, possibly a differentiate of that which supplied the volcano, provided a heat source to initiate and drive a circulatory water system within the rock pile (Solomon, 1976). For the Murchison, a suitable heat source would have been the magma of the Rooiwater Igneous Complex, prior to emplacement. According to Elder (1977) such a ground-water system would heat up rapidly, and the temperature would then gradually decay with time. Originally, the felsic volcanic rocks were underlain by tholeiitic and high magnesia basalts, with a total thickness in excess of 5 km. This would be capable of supplying the necessary metals to the circulating, hot, brines. The early fluids, being hotter, would tend to be copper-rich, while later, cooler, fluids would be zinc-rich.

Expulsion of these metalliferous fluids from the system was facilitated by pre-existing channelways and fracture zones associated with local, explosive, volcanic centres. Sulphides were precipitated by the sudden

quenching of the fluids at the rock/seawater interface. The entire system is diagrammatically illustrated in fig. 47.

The horizontal diameter of each circulatory, or convection, cell is given by the distance between the massive sulphide deposits. In the Murchison belt this is mainly 14 km, with one 19 km spacing; a figure similar to the 18 km proposed by Russell et al. (1981). The disseminated sphalerite mineralization at the L-W locality could be produced from a small, shallow, convection cell, possibly later captured by that supplying the J deposit, 5 km to the west (Russell et al., 1981).

The end of the mineralizing episode was possibly caused by minor uplift allowing erosion and reworking of the volcanic rocks to form the Transition Zone sequence. Theoretically this sequence should contain reworked sulphides, but none were found in the area.

10.4 Implications for Exploration in the Murchison Greenstone Belt

In the Murchison greenstone belt, all the known copper-zinc and antimony sulphide deposits are regularly spaced along two parallel stratigraphic horizons, and crop out, or are within one hundred meters of the present surface, fig. 48. This suggests a fortuitous erosion plane.

10.4.1 Copper-Zinc Deposits

The distances separating the known massive copper-zinc sulphide deposits in the Murchison belt are; 14 km

between Mashawa Coppers and Letaba Coppers, 14 km between Letaba Coppers and the MGZ deposit, and 19 km from the MGZ to the J deposit, fig. 48. On Magoboya's Location, 30 km west of the J deposit, a small zinc deposit has been recently discovered (W.G. Hancock - personal communication, 1981), and a copper-zinc deposit is rumoured to exist in between these.

It is of note that the distance separating the MGZ and L-W deposits is also 14 km. This suggests that the convection cell supplying the L-W deposit was controlled by the same system as the others, but was subsequently captured by a stronger cell, or moved 5 km west, to form the J deposit.

Exhaustive exploration between the MGZ (+D), L-W, and J deposits has failed to locate other deposits. Future exploration should thus be concentrated at distances of approximately 14 km east of Mashawa Coppers, and west of the J locality.

10.4.2 Antimony Deposits

Antimony deposits, as prospects, abandoned and working mines, occur at 4-5 km spacings within carbonates of the Antimony Line. This carbonate horizon is only present where sediments overlie felsic volcanic rocks, and antimony deposits are extremely rare elsewhere in the Murchison greenstone belt.

When traced across to the parallel copper-zinc line, each antimony deposit was originally directly underlain by either a massive sulphide deposit, an area of minor sulphide mineralization, or a local centre of explosive

volcanism at the top of the felsic volcanic pile.

As far as the writer is aware, there are no signs of hydrothermal activity between the copper-zinc deposits and the antimony deposits through the 1500 m of intervening sediments. Minnitt (1975) suggests that the antimony deposits were formed from submarine hot-springs, implying the existence of a sub-surface geothermal cell. The present 4-5 km spacing of the deposits would suggest a similar convection cell diameter to that supplying the L-W deposit.

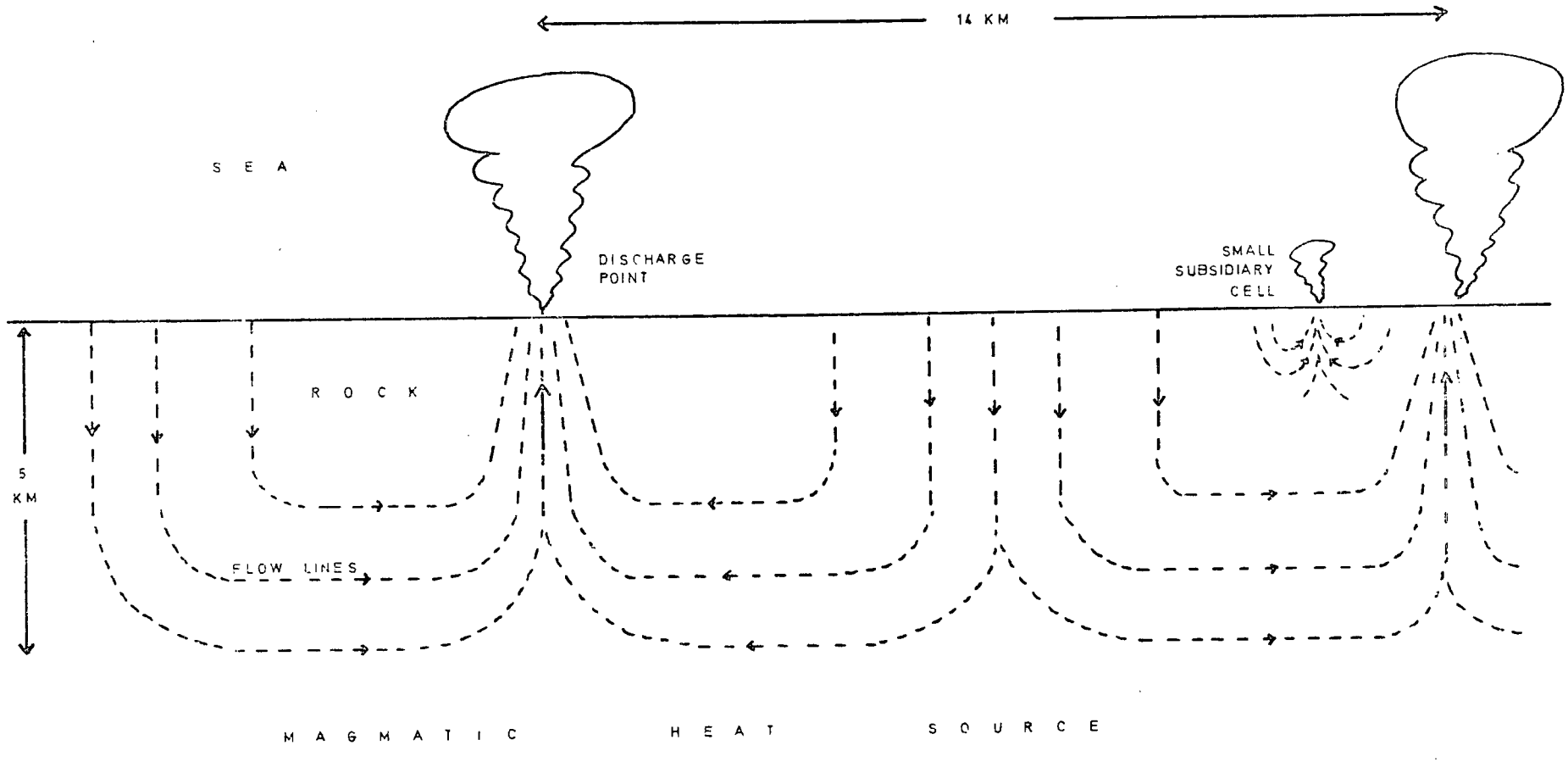

FIG 47 DIAGRAMMATIC SECTION THROUGH A CONVECTION CELL

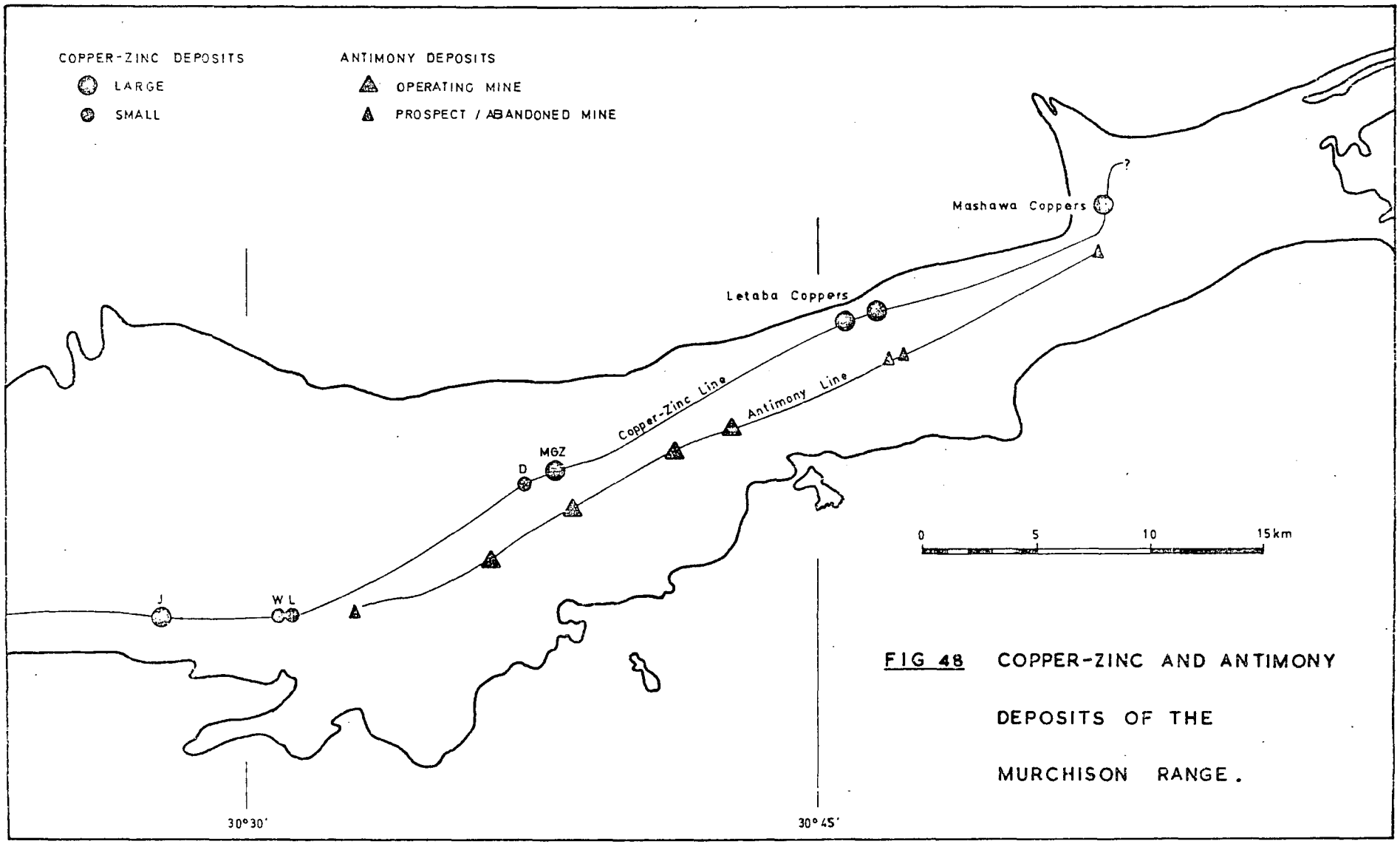

FIG 48 COPPER-ZINC AND ANTIMONY DEPOSITS OF THE MURCHISON RANGE.

REFERENCES

ALABASTER, T. and PEARCE, J.A. (1981).
Geological Setting of Massive Sulphide Deposits in the Oman Ophiolite Complex. Trans. Instn. Min Metall., v.90, abstract, p.B61.

ANDERSON, J.E. Jr. (1969).
Development of Snowflake Texture in a Welded Tuff, Davis Mountains, Texas. Bull. geol. Soc. Am., v.80, pp.2075-2080.

ANDREWS, A.J. and FYFE, W.S. (1976).
Metamorphism and Massive Sulphide Generation in Oceanic Crust. Geosci. Can., v.3, pp.84-94.

ANGER, G. (1971).
Microfabrics in Geosynclinal Sulphide Deposits. Clausthaler Hefte Zur Lagerstättenkunde Und Geochemie Der Mineralischen Rohstoffe. Heft 10.

ANHAEUSSER, C.R. (1973).
Precambrian Tectonic Environments. Inf. Circ. No. 78, Econ. Res. Unit, Univ. Witwatersrand, Johannesburg, 19p.

ANHAEUSSER, C.R. (1972).
The Evolution of the Early Precambrian Crust of Southern Africa. Inf. Circ. No. 70, Econ. Geol. Res. Unit., Univ. Witwatersrand, Johannesburg, 31p.

ANHAEUSSER, C.R., MASON, R., VILJOEN, M.J. and VILJOEN, R.P. (1969). A Reappraisal of Some Aspects of Precambrian Shield Geology. Bull. geol. Soc. Am., v.80, pp.2175-2200.

BAER, A.J., VEIZER, J. and BARAGER, W.R.A. (1978).
Relationships Between Archaean Granites and Greenstones. Geosci. Can., v.5, pp.29-32.

BARTON, P.B. and TOULMIN, P. (1966).
Phase Relations Involving Sphalerite in the Fe-Zn-S System. Econ. Geol., v.61, pp.815-849.

BAYLISS, P. (1977).
Crystal Structure Refinement of a Weakly Anisotropic Pyrite. Am. Miner. v.62, pp.1168-1172.

BISCHOFF, J.L. and DICKSON, F.W. (1975).
Seawater-Basalt Interaction at 200°C and 500 Bars: Implications for Origin of Sea-Floor Heavy-Metal Deposits and Regulation of Seawater Chemistry. Earth Planet. Sci. Lett., v.25, pp.385-397.

BRISTOL, C.C. (1979).
Applications of Sphalerite Geobarometry to Ores From the Ruttan Mine. Econ. Geol., v.74, pp.1496-1503.

CILLIERS, C.J.P. (1975).
Structural Controls of Antimony Mineralization in the Murchison Range with Particular Reference to the Free State and Monarch Orebodies. Abstr. 16th Congr. geol. Soc. S. Afr., pp.22-24.

CLARK, B.R. and KELLY, W.C. (1973).
Sulphide Deformation Studies: I. Experimental Deformation of Pyrrhotite and Sphalerite to 2,000 Bars and 500°C. Econ. Geol., v.68, pp.332-352.

COETZEE, C.B. (1976).
Antimony. in C.B. Coetzee (ed), Mineral Resources of South Africa, Dept. Mines, Geol. Surv., Hbk.7, pp.107-10.

COLLEY, H. and GREENBAUM, D. (1980).
The Mineral Deposits and Metallogenesis of the Fiji Platform. Econ. Geol., v.75, pp.807-829.

CONDIE, K.C., MACKE, J.E. and REIMER, T.O. (1970).
Petrology and Geochemistry of Early Precambrian Greywackes From the Fig Tree Group, South Africa. Bull. geol. Soc. Am., v.81, pp.2759-2776.

CONSTANTINOU, G. and GOVETT, G.J.S. (1973).
Geology, Geochemistry and Genesis of Cyprus Sulphide Deposits. Econ. Geol., v.68, pp.843-858.

CORNELL, D.H. (1977).
Alteration of Volcanic Formations Beneath the Transvaal Volcanosedimentary Pile. Abstr. 17th Congr. geol. Soc. S. Afr.

CRONE, J.D. (1975).
A Ground Pulse Electromagnetic Method and its Application in Mineral Exploration. Paper presented at: Geologoravedka-75, Moscow, Russia, 11p.

DAVIES, J.F., GRANT, R.W.E. and WHITEHEAD, R.E.S. (1979).
Immobile Trace Elements and Archaean Volcanic Stratigraphy in the Timmings Area, Ontario. Can. J. Earth Sci., v.16, pp.305-311.

DEB, M. (1979).
Polymetamorphism of Ores in Precambrian Stratiform Massive Sulphide Deposits at Ambaji-Deri, Western India. Miner. Deposita, v.14, pp.21-31.

DEER, W.A., HOWIE, R.A. and ZUSSMAN, J. (1971).
An Introduction to the Rock-Forming Minerals. Longman, London, 528pp.

DEER, W.A., HOWIE, R.A. and ZUSSMAN, J. (1963).
Rock-Forming Minerals; v.5, Non-Silicates. Longman, London, 371pp.

EDMOND, J.M. (1981).
Hydrothermal Activity at Mid-Ocean Ridge Axes. Nature, v.290, pp.87-88.

EGIN, D. (1978).
Polymetallic, Sulphide Ore Deposits and Associated Volcanic Rocks from the Harsit River Area, N.E. Turkey. Unpublished Ph.D. thesis, University of Durham, 305p.

ELDER, J.W.(1977).
Model of Hydrothermal Ore Genesis. in: Volcanic Processes in Ore Genesis, Inst. Min. Metall., London, pp.4-13.

ENGEL, A.E.J. and ENGEL, C.G. (1962).
Hornblendes formed During Progressive Metamorphism of Amphibolites, Northwest Adirondack Mountains, New York. Bull. geol. Soc. Am., v.73, pp.1499-1514.

ERIKSSON, K.A. (1980).
Transitional Sedimentation Styles in the Moodies and Fig Tree Groups, Barberton Mountain Land, South Africa: Evidence Favouring an Archaean Continental Margin. Precambrian Res., v.12, pp.141-160.

EVANS, J.E.L. (1944).
Porphyry of the Porcupine District, Ontario. Bull. geol. Soc. Am., v.55, pp.1115-1142.

FINLOW-BATES, T. and LARGE, D.E. (1978).
Water Depth As Major Control on the Formation of Submarine Exhalative Ore Deposits. Geol. Jahrb., Ser.D.,v.30, pp.27-39.

FLOYD, P.A., WINCHESTER, J.A. (1978).
Identification and Discrimination of Altered and Metamorphosed Volcanic Rocks Using Immobile Elements. Chem. Geol., v.21, pp.291-306.

FRANKLIN, J.M., KASARDA, J. and POULSEN, K.H. (1975).
Petrology and Chemistry of the Alteration Zone of the Mattabi Massive Sulphide Deposit. Econ. Geol., v.70, pp.63-79.

FRIPP, R.E.P., VANNIEROP, D.A., CALLOW, M.J., LILLY, P.A. and DU PLESSIS, L.U. (1980). Deformation in Part of the Archaean Kaapvaal Craton, South Africa. Precambrian Res., v.13, pp.241-251.

GILL, J.E. (1969).
Experimental Deformation and Annealing of Sulphides and Interpretation of Ore Textures. Econ. Geol., v.64, pp.500-508.

GWOSDZ, W. and KREBS, W. (1977).
Manganese Halo Surrounding Meggen Ore Deposit, Germany. Trans. Instn. Min. Metall., v.86, pp.B73-B77.

HALL, A.L. (1912).
The Geology of the Murchison Range and District. Mem. geol. Surv. Un. S. Afr., 8, 184p.

HAMMERBECK, E.C.I. (1976).
Copper. In: Coetzee (ed.), Mineral Resources of South Africa, Dept. Mines, Geol. Surv., Hbk.7, pp.125-146.

HAMMERBECK, E.C.I. (1976).
Mercury. In: Coetzee (ed.), Mineral Resources of South Africa, Dept. Mines, Geol. Surv., Hbk.7, p.173.

HATCH, F.H., WELLS, A.K. and WELLS, M.K. (1961).
Petrology of the Igneous Rocks, 4th edition. Murby and Co., London.

HAUSMANN, S.G. (1959).
A Mineralogical Investigation of the Letaba Copper-Zinc Ores and the Monarch Cinnibar Deposits Located in the Murchison Range of Eastern Transvaal. Unpublished M.Sc. Thesis, University of the Witwatersrand, 49p.

HEMLEY, J.J. and JONES, W.R. (1964).
Chemical Aspects of Hydrothermal Alteration with Emphasis on Hydrogen Metasomatism. Econ. Geol., v.59, pp.538-569.

HODGSON, C.J. and LYDON, J.W. (1977).
Geological Setting of Volcanogenic Massive Sulphide Deposits and Active Hydrothermal Systems: Some Implications for Exploration. C.I.M. Bull., v.70, pp. 95-106.

HOLLISTER, V.F. (1981).
Relationship of Sulphide Mineralization to Ophiolite Complexes in North America. Min. Engng., v.33, pp. 421-424.

HOPWOOD, T.P. (1978).
Conformable Elongate Ore Bodies and Intrafolial Folds Parallel to a Mineral Streaking Lineation. In: Verwood (ed.), Mineralization in Metamorphic Terrains, Spec. Pub. geol. Soc. S. Afr., 4, pp.41-51.

HOPWOOD, T.P. (1976).
"Quartz-Eye" Bearing Porphyroidal Rocks and Volcanogenic Massive Sulphide Deposits. Econ. Geol., v. 71, pp.589-612.

HUGHES, C.J. (1973).
Spilites, Keratophyres and the Igneous Spectrum. Geol. Mag., v.109, pp.513-527.

HUMPHRIS, S.E. and THOMPSON, G. (1978a).
Hydrothermal Alteration of Oceanic Basalts by Seawater. Geochim. cosmochim. Acta, v.42, pp.107-125.

HUMPHRIS, S.E. and THOMPSON, G. (1978b).
Trace Element Mobility During Hydrothermal Alteration of Oceanic Basalts. Geochim. cosmochim. Acta, v.42, pp.127-136.

HUNTER, D.R. (1974a).
Crustal Development in the Kaapvaal Craton, I: The Archaean. Precambrian Res., v.1, pp.259-294.

HUNTER, D.R. (1974b).
Crustal Development in the Kaapvaal Craton, II: The Proterozoic. Precambrian Res., v.1, pp.295-326.

HUNTER, R.H. (1980).
The Petrology and Geochemistry of the Carrock Fell Gabbro-Granophyre Complex, Cumbria. Unpublished Ph.D. Thesis, University of Durham, 333p.

HUTCHINSON, R.W. (1973).
Volcanogenic Sulphide Deposits and Their Metallogenic Significance. Econ. Geol., v.68, pp.1223-1246.

IRVIN, T.N. and BARAGER, W.R.A. (1971).
A Guide to the Chemical Classification of the Common Volcanic Rocks. Can. J. Earth Sci., v.8, pp. 523-548.

JAMBOR, J.L. (1979).
Mineralogical Evaluation of Proximal-Distal Features in New Brunswick Massive-Sulphide Deposits. Can. Mineralogist, v.17, pp.649-664.

JANTSKY, J.G. (1978).
Proposed Stratigraphy for the Murchison Range. Unpublished Report to the South African Committee for Stratigraphy, 8p.

KAJIWARA, Y. (1973).
Chemical Composition of Ore-Forming Solution Responsible for the Kuroko Type Mineralization in Japan. Geochem. J. (Japan), v.6, pp.141-149.

KANEMIRA, K. and TATSUMI, T. (1970).
Bedded Cupriferous Iron Sulphide Deposits in Japan, A Review. In: Tatsumi (ed.), Volcanism and Ore Genesis: Tokyo, Tokyo Univ. Press, pp.51-76.

KINGSTON, A.J. (1976).
A Cu, Zn Prospect and its Geological Setting, N.E. Transvaal, S. Africa. Unpublished B.Sc. Dissertation, Portsmouth Polytechnical College.

KULLERUD, G. and YODER, H.S. (1959).
Pyrite Stability Relations in the Fe-S System. Econ. Geol., v.54, pp.533-572.

LACHARPAGNE, J.C. (1979).
Massive Sulphide and Wall Rock Alteration - Preliminary Study. S.N.E.A. (P), Unpublished Company Report, 7p.

LAMBERT, I.B. (1976).
The McArthur Zinc-Lead-Silver Deposit: Features, Metallogenesis and Comparisons with some other Stratiform Ores. In: Wolf (ed.), Handbook of Strata-Bound and Stratiform Ore Deposits, v.6, Elsevier, Amsterdam, pp. 535-585.

LAMBERT, I.B. and SATO, T. (1974).
The Kuroko and Associated Ore Deposits of Japan: A Review of Their Features and Metallogenesis. Econ. Geol. v.69, pp.1215-1236.

LARGE, R.R. (1977).
Chemical Evolution and Zonation of Massive Sulphide Deposits in Volcanic Terrains. Econ. Geol. v.72, pp.549-572.

LAWRENCE, L.J. and SAVAGE, E.N. (1976).
Ore Genesis in the Wainivesi Area, Fiji, and some Exploration Implications. Proc. Australas. Inst. Min. Metall., No.260, pp.59-69.

LAZNICKA, P. (1976).
Lead Deposits in the Global Plate Tectonic Model. In: Strong (ed.) - Metallogeny and Plate Tectonics; Geol. Assoc. Can., Spec. Pap. 14, pp.243-271.

LOWE, D.R. and KNAUTH, L.P. (1977).
Sedimentology of the Onverwacht Group (3.4 Billion Years), Transvaal, South Africa, and its bearing on the Characteristics and Evolution of the Early Earth. J. Geol., v.85, pp.699-723.

MACGEEHAN, P.J. and MACLEAN, W.H. (1980a).
Tholeiitic Basalt - Rhyolite Magmatism and Massive Sulphide Deposits at Matagami, Quebec. Nature, v.283, pp.153-157.

MACGEEHAN, P.J. and MACLEAN, W.H. (1980b).
An Archaean Sub-Seafloor Geothermal System, "Calc-Alkali" Trends, and Massive Sulphide Genesis. Nature, v.286, pp.767-771.

MALLIO, W.J. and GHEITH, M.A. (1972).
Textural and Chemical Evidence Bearing on Sulphide-Silicate Reactions in Metasediments. Miner. Deposita, v.7, pp.13-17.

McDONALD, J.A. (1967).
Metamorphism and Its Effects on Sulphide Assemblages. Miner. Deposita, v.2, pp.200-220.

MELLOR, E.T. (1906).
The Geology of the District about Haenartsburg, Leydsdorp and the Murchison Range. Ann. Rept. geol. Surv. S. Afr., pp.23-52.

MENDELSOHN, E. (1938).
Gold Deposits of the Central Murchison Range, Transvaal. Trans. geol. Soc. S. Afr., No.21, pp. 249-272.

MERENSKY, H. (1905).
The Gold Deposits of the Murchison Range in the North Eastern Transvaal. Trans. geol. Soc. S. Afr., No.8, pp.42-46.

MEYER, C. and HEMLEY, J.J. (1967).
Wall Rock Alteration. In: Barnes (ed.), Geochemistry of Hydrothermal Ore Deposits; Holt, Rinehart and Winston, New York, pp.166-235.

MINNITT, R.C.A. (1975).
The Geology of the Eastern Portion of the Murchison Range Between the Quagga Camp Area and the Kruger National Park. Unpublished M.Sc. Thesis, University of the Witwatersrand, 171p.

MITCHELL, A.H. and BELL, J.D. (1973).
Island-Arc Evolution and Related Mineral Deposits. J. Geol., v.81, pp.381-405.

MIYASHIRO, A. (1973).
Metamorphism and Metamorphic Belts.
Allen and Unwin, London, 491p.

MOORE, J. McM. (1975).
Regional Metamorphism as an Ore-Forming Process in the Saudi Arabian Shield. Trans. Instn. Min. Metall., v.84, pp.B59-62.

MORRIS, R.C. and EWERS, W.E. (1978).
A Simple Streak-Print Technique for Mapping Mineral Distribution in Ores and Other Rocks.
Econ. Geol., v.73, pp.562-566.

MOTTL, M.J. and HOLLAND, H.D. (1978).
Chemical Exchange During Hydrothermal Alteration of Basalt by Seawater - I: Experimental Results for Major and Minor Components of Seawater. Geochim. Cosmochim. Acta, v.42, pp.1103-1115.

MUFF, R. (1978).
The Antimony Deposits in the Murchison Range of the Northeastern Transvaal, Republic of South Africa. Monograph Series on Mineral Deposits, 16, Berlin.

OHMOTO, H. (1978).
Submarine Calderas: A Key to the Formation of Volcanogenic Massive Sulphide Deposits? Min. Geol. (Japan), v.28, pp.219-231.

OHMOTO, H. and RYE, R.O. (1979).
Isotopes of Sulfur and Carbon. In: Barnes (ed.), Geochemistry of Hydrothermal Ore Deposits, 2nd Edition, Wiley and Sons, New York, pp.509-567.

PALABORA MINING COMPANY GEOLOGICAL STAFF (1976).
The Geology and the Economic Deposits of Copper, Iron and Vermiculite in the Palabora Igneous Complex: A Brief Review. Econ. Geol., v.71, pp.171-192.

PEARCE, J.A. (1981).
Mineralization in Ophiolites.
Abstr. 28th. Inter-Univ. Geol. Congr., Glasgow.

PEARTON, T.N. (1975).
Geology and Geochemistry of the Monarch Orebody and its Environs. Abstr. 16th Congr. geol. Soc. S. Afr., pp.115-118.

POLLOCK, G.D., SINCLAIR, I.G.L., WARBURTON, A.F. and WIERZBICKI, V. (1972). The Uchi Orebody - A Massive Sulphide Deposit in An Archaean Siliceous Volcanic Environment. 24th. Internat. Geol. Congr., Montreal, Sectn. 4, pp.299-308.

RAMDOHR, P. (1980).
The Ore Minerals and Their Intergrowths, 2nd Edition. Vol.I. Pergamon Press, Oxford.

RAMSAY, J.G. (1967).
Folding and Fracturing of Rocks. McGraw-Hill, New York, 568p.

RAMSAY, J.G. (1963).
Structural Investigations in the Barberton Mountain Land, Eastern Transvaal. Trans. geol. Soc. S. Afr., v.66, pp.354-401.

RAYBOULD, J.G. (1978).
Tectonic Controls on Proterozoic Stratiform Copper Mineralization. Trans. Instn. Min. Metall., v.87, pp.B79-B86.

REYNOLDS, D.G., ALLCHURCH, P.D., BROOK, W.A. and MARSHALL, A.E. (1975). Volcanogenic Copper-Zinc Deposits in the Pilbara and Yilgarn Archaean Blocks. In: Knight (ed.), Economic Geology of Australia and Papua New Guinea. Australas. Inst. Min. Metall., Melbourne.

RICKARD, D.T. and ZWEIFEL, H. (1975).
Genesis of Precambrian Sulphide Ores, Skellefte District, Sweden. Econ. Geol., v.70, pp.255-274.

RISE PROJECT GROUP (1980).
East Pacific Rise: Hot Springs and Geophysical Experiments. Science, v.207, pp.1421-1433.

RIVERIN, G. and HODGSON, C.J. (1980).
Wall-Rock Alteration at the Millenbach Cu-Zn Mine, Noranda, Quebec. Econ. Geol., v.75, pp. 424-444.

ROBB, L.J. (1978).
A General Geological Description of the Archaean Granitic Terrane between Nelspruit and Bushbuckridge, Eastern Transvaal. Trans. geol. Soc. S. Afr., v.81, pp.331-338.

ROBERTS, R.G. (1975).
The Geological Setting of the Mattagami Lake Mine, Quebec: A Volcanogenic Massive Sulphide Deposit. Econ. Geol., v.70, pp.115-129.

RUSSELL, M.J. (1981).
Genesis of the Major Exhalative Zinc + Lead ± Copper Deposits. Abstr. 28th. Inter-Univ. Geol. Congr., Glasgow.

RUSSELL, M.J. (1975).
Lithogeochemical Environment of the Tynagh Base-Metal Deposit, Ireland, and its bearing on Ore Deposition. Trans. Instn. Min. Metall., v.84, pp.B128-B133.

RUSSELL, M.J., SOLOMON, M. and WALSHE, J.L. (1981).
The Genesis of Sediment-Hosted, Exhalative Zinc+Lead Deposits. Miner. Deposita, v.16, pp.113-127.

RYE, D.M. and WILLIAMS, N. (1981).
Studies of Base Metal Sulphide Deposits at McArthur River, Northern Territory, Australia: III. The Stable Isotope Geochemistry of the H.Y.C., Ridge and Cooley Deposits. Econ. Geol., v.76, pp.1-26.

SANGSTER, D.F. (1972).
Precambrian Volcanogenic Massive Sulphide Deposits in Canada - A Review. Geol. Soc. Can., Pap.72-22, 44p.

SANGSTER, D.F. and SCOTT, S.D. (1976).
Precambrian, Strata-Bound, Massive Cu-Zn-Pb Sulfide Ores of North America. In: Wolf (ed.), Handbook of Strata-Bound and Stratiform Ore Deposits, v.6, Elsevier, Amsterdam, pp.129-222.

SARKAR, S.C., BHATTACHARYYA, P.K. and MUKHERJEE, A.D. (1980). Evolution of the Sulphide Ores of Saladipura, Rajasthan, India. Econ. Geol., v.75, pp.1152-1167.

SAWKINS, F.J., CHASE, C.G., DARBY, D.G. and RAPP, G. (1974). The Evolving Earth, MacMillan, New York, 476p.

SAWYER, A.R. (1892). Mining: A Geological and General Guide to the Murchison Range. John Heywood, London, 96p.

SCHWELLNUS, C.M. (1937). Short Notes on the Phalaborwa Smelting Ovens. S. Afr. J. Sci., v.33, pp.904-912.

SCOTT, S.D. (1976). Application of the Sphalerite Geobarometer To Regionally Metamorphosed Terrains. Am. Miner., v.61, pp.661-670.

SCOTT, S.D. (1974). Experimental Methods in Sulfide Synthesis. In: Ribbe (ed.), Sulphide Mineralogy, Short Course Notes, v.1, Min. Soc. Am., pp.51-538.

SCOTT, S.D. (1973). Experimental Callibration of the Sphalerite Geobarometer. Econ. Geol., v.68, pp.466-474.

SCOTT, S.D. and BARNES, H.L. (1971). Sphalerite Geothermometry and Geobarometry. Econ. Geol., v.66, pp.653-669.

SCOTT, S.D., BOTH, R.A. and KISSIN, S.A. (1977). Sulfide Petrology of the Broken Hill Region, New South Wales. Econ. Geol., v.72, pp.1410-1425.

SEYFRIED, W.E. Jr. and BISCHOFF, J.L. (1981). Experimental Seawater-Basalt Interaction At 300^{o}C, 500 Bars, Chemical Exchange Secondary Mineral Formation and Implications For the Transport of Heavy Metals. Geochim. cosmochim. Acta, v.45, pp.135-147.

SHADLUN, T.N. (1971). Metamorphic Textures and Structures of Sulphide Ores. Soc. Min. Geologists Japan, Spec. Issue 3, pp.241-250.

SIEVER, R. (1962). Silica Solubility 0-200^{o}C, and the Diagenesis of Siliceous Sediments. J. Geol., v.70, pp.127-150.

SILLITOE, R.H. (1973). Environments of Formation of Volcanogenic Massive Sulphide Deposits. Econ. Geol., v.68, pp.1321-1325.

SOLOMON, M. (1976).
"Volcanic" Massive Sulphide Deposits and Their Host Rocks - A Review and An Explanation. In: Wolf (ed.) - Handbook of Stratabound and Stratiform Ore Deposits, v.6, Elsevier, pp.21-54.

SOLOMON, M. and WALSHE, J.L. (1979).
The Formation of Massive Sulfide deposits on the sea floor. Econ. Geol., v.74, pp.797-813.

SOUTH AFRICAN COMMITTEE FOR STRATIGRAPHY
Stratigraphy of South Africa. Part I. (Comp. L.E. Kent). Lithostratigraphy of the Republic of South Africa, South West Africa/Namibia, and the Republics of Bophuthatswana, Transkei and Venda. Handbook Geol. Surv. S. Afr., 8.,

SPENCE, C.D. and DEROSEN-SPENCE, A.F. (1975).
The Place of Sulphide Mineralization in the Volcanic Sequence at Noranda, Quebec. Econ. Geol., v.70, pp.90-101.

SPITZ, G. and DARLING, R. (1978).
Major and Minor Element Lithogeochemical Anomalies Surrounding the Louvem Copper Deposit, Val d'Or, Quebec. Can J. Earth Sci., v.15, pp.1161-1169.

SPITZ, G. and DARLING, R. (1975).
The Petrochemistry of Altered Volcanic Rocks: Surrounding the Louvem Copper Deposit, Val d'Or, Quebec. Can J. Earth Sci., v.12, pp.1820-1849.

SPOONER, E.T.C. and BRAY, C.J. (1977).
Hydrothermal Fluids of Seawater Salinity in Ophiolitic Sulphide Ore Deposits in Cyprus. Nature, v.266, pp.808-812.

STANTON, R.L. (1972).
Ore Petrology. McGraw-Hill, New York, 713p.

STANTON, R.L. (1964).
Mineral Interfaces in Stratiform Ores. Trans. Instn. Min. Metall., v.74 pt.2, pp.45-79.

STANTON, R.L. and GORMAN, H. (1968).
A Phenomenological Study of Grain Boundary Migration In Some Common Sulphides. Econ. Geol., v.63, pp.907-923.

STRAUSS, G.K. and MADEL, J. (1974).
Geology of Massive Sulphide Deposits in the Spanish-Portuguese Pyrite Belt. Geol. Rdsch., v.63, pp.191-211.

STURT, B.A. (1962).
The Composition of Garnets From Pelitic Schists in Relation to the Grade of Regional Metamorphism. J. Petrology, v.3, pp.181-191.

SUTTON, J. (1967).
The Extension of the Geological Record into the PreCambrian. Proc. geol. Ass., v.78, pp.493-534.

SWEATMAN, T.R. and LONG, V.P. (1969).
Quantitative Electron-Probe Microanalysis of Rock-Forming Minerals. J. Petrology, v.10, pp.332-379.

TATSUMI, T. and CLARK, L.A. (1972).
Chemical Composition of Acid Volcanic Rocks Genetically Related to Formation of the Kuroko Deposits. J. geol. Soc. Japan, v.78, pp.191-201.

TATSUMI, T. and WATANABE, T. (1971).
Geological Environment of formation of the Kuroko type Deposits. Soc. Min. Geologists Japan, Spec. Issue 3, pp.216-220.

TAYLOR, H.P. (1979).
Oxygen and Hydrogen Isotope. Relations in Hydrothermal Mineral Deposits. In: Barnes (ed.) Geochemistry of Hydrothermal Ore Deposits, 2nd ed., Wiley and Sons, New York, pp.236-277.

TREVOR, T.G. (1912).
Some Observations on Ancient Mine Workings in the Transvaal. J. chem. metall. Min.Soc. S. Afr., pp.267-275.

TURNER, F.J. (1968).
Metamorphic Petrology. McGraw-Hill, New York, 403p.

TURNER, F.J. and VERHOOGEN, J. (1960).
Igneous and Metamorphic Petrology, 2nd Edition. McGraw-Hill, New York, 694p.

TURNER, J.S. and GUSTAFSON, L.B. (1978).
The Flow of Hot Saline Solutions from Vents in the Sea Floor - Some Implications for Exhalative Massive Sulphide and Other Ore Deposits. Econ. Geol., v.73 pp.1082-1100.

VAN EEDEN, O.R., PARTRIDGE, F.C., KENT, L.D. and BRANDT, J.W. (1939). The Mineral Deposits of the Murchison Range East of Leydsdorp. Mem. geol. Surv. Un. S. Afr., 36.

VAN VUUREN, C.J. (1975).
Aspects of the Geology and Geochemistry of the Gravelotte/Alpha Orebody, Murchison Range. Abstr. 16th Congr. geol. Soc. S. Afr., pp.156-159.

VILJOEN, M.J. and VILJOEN, R.P. (1969a).
An Introduction to the Geology of the Barberton Granite-Greenstone Terrain. Spec. Pub. geol. Soc. S. Afr., 2, pp.9-28.

VILJOEN, M.J. and VILJOEN, R.P. (1969b).
The Geology and Geochemistry of the Lower Ultramafic Unit of the Onverwacht Group and a Proposed New Class of Igneous Rocks. Spec. Pub. geol. Soc. S. Afr., 2, pp.55-85.

VILJOEN, R.P. and VILJOEN, M.J. (1969c).
The Geological and Geochemical Significance of the Upper Formations of the Onverwacht Group. Spec. Pub. geol. Soc. S. Afr., 2, pp.113-152.

VILJOEN, M.J., PEARTON, T.N., MINNITT, R.C.A. and ANHAEUSSER, C.R. (1979). Proposed Lithostratigraphic Subdivision of the Swaziland Supergroup in the Murchison Range. Unpublished Report to the South African Committee for Stratigraphy, 12p.

VILJOEN, M.J., VAN VUUREN, C.J.J., PEARTON, T.N., MINNITT, R.C.A., MUFF, R. and CILLIERS, P. (1978).
The Regional Geological Setting of Mineralization in the Murchison Range with Particular Reference to Antimony. In: Verwood (ed.), Mineralization in Metamorphic Terrains, Spec. Pub. geol. Soc. S. Afr., 4, pp.55-76.

VINE, F.J. and MATTHEWS, D.H. (1963).
Magnetic Anomalies Over Oceanic Ridges. Nature, v.199, pp.947-949.

VOKES, F.M. (1969).
A Review of the Metamorphism of Sulphide Deposits. Earth Sci. Rev., v.5, pp.99-143.

WALKER, R.N., LOGAN, R.G. and BINNEKAMP, J.G. (1977).
Recent Geological Advances Concerning the HYC and Associated Deposits, McArthur River, N.T. J. geol. Soc. Aust., v.24, pp.365-380.

WIGGINS, L.B. and CRAIG, J.R. (1980).
Reconnaissance of the Cu-Fe-Zn-S System: Sphalerite Phase Relationships. Econ. Geol., v.75, pp.742-751.

WILSON, H.D.B., ANDREWS, P., MOXHAM, R.L. and RAMAL, K. (1965). Archaean Volcanism in the Canadian Shield. Can. J. Earth Sci., v.2, pp.161-175.

WILSON-MOORE, C. (1896).
The Economic Importance of the Murchison Range. Trans. geol. Surv. S. Afr., v.1, pp.51-60.

WINCHESTER, J.A. and FLOYD, P.A. (1977).
Geochemical Discrimination of Different Magma Series and Their Differentiation Products Using Immobile Elements. Chem. Geol., v.20, pp.325-343.

WINKLER, H.G.F. (1974).
Petrogenesis of Metamorphic Rocks, 3rd Edition. Springer-Verlag, Berlin, 334p.

WINKLER, H.G.F. (1967).
Petrogenesis of Metamorphic Rocks, Revised Second Edition. Springer-Verlag, Berlin, 237p.

WINTER, P.E. (1975).
Report of Visit to Consolidated Murchison Antimony Mines. A.S.T.E., Unpublished Company Report, 4p.

APPENDIX A

SAMPLE COLLECTION

A1. Whole Rock Analyses

Samples for whole-rock chemical analyses were taken from fresh drill core, or from the freshest available surface material. Weathered, altered, or veined material was avoided. Approximately 1 kg of material was collected. This was crushed in the field using an iron pestle and mortar, and later, finely powdered in a tungsten carbide Temar Mill. The powder was then stored in air-tight plastic bottles.

Contamination between samples was reduced by crushing, and rejecting, pieces of white, barren quartz between each rock sample. Iron contamination from the mortar and pestle was negligible. A piece of each sample was retained for thin section preparation.

A2. Rock Textures and Sulphide Samples

Samples of various textures and mineral assemblages in silicate and sulphide rocks were taken from drill core by cutting either ½ core or 5 mm thick slices. Where this was not possible streak prints were taken of the relevant texture (Morris and Ewers, 1978).

A3. Nomenclature

Each sample was numbered. Samples taken from surface exposures were designated by two letters followed by a number, eg. SM10. The letters refer to the farm

name, where SM - Solomons Mine; MD - Mon Desir; GE - Gravelotte; RV - Rubbervale; CD - Cottondale; MA - Maranda; RW - Rooiwater; and QA - Quagga (north of Rubbervale). The number is the sample number. For samples from drill core the following system was used eg. MA14W2, where MA - farm name; 14 - sample number; W - locality; and 2 - drill hole number. The MGZ locality is designated S.

Samples referred to in the text and Appendices are listed below, and are located on map 4.

a - albite
act - actinolite
b - biotite
c - chlorite
cz - clinozoisite
cc - calcite
e - epidote
f - fuchsite
g - garnet
p - plagioclase
q - quartz
s - sericite
z - zoisite

Surface Samples, and from Isolated Drillholes

MINERALOGY

SAMPLE NUMBER	GROUNDMASS	PHENOCRYSTS/ PORPHYROBLASTS	ORIGINAL ROCK
SM1	q-c-cc	q,a	coarse tuff
SM4	q-c-b		flow
SM6	q-c-s		tuff
SM10	q-c		tuff
SM11	q-c-s	q	tuff
SM12	q-a-b-s		quartz-diorite
SM16	q-z-f		quartzite
SM17	q-c	a	flow
SM154	q-c-s-b		tuff
SM204	q-a-c	q,a	tuff
MS7/4	q-c-b	q,a,g	interflow sediment
SM4S7	q-s-c-b	g,q	ditto
SM5S7	q-s-c	g	ditto
SM1S9	q-c	a,q	tuff
SM3S9	q-s-c	b,a,q	tuff
SM5S9	q-c-s	q,a	tuff
SM6S9	q-c	b,a,q	tuff
SM7S9	a-e-act-cz-c-q-cc		basic intrusive
MD1	act-e-p-a-cz-q		gabbro
MD3	q-s-f		quartzite
GE3	q-c	q,a	flow
GE5	q-c	q,a	flow
GE8	q-c-cc	q,a	flow
GE114	q-c-a-cc	a,q	coarse tuff
RV1	q-b		flow
RV2	q-s		tuff
RV3	q-s-c	q	tuff
RV4	q-s-c		coarse tuff
RV5	q-c-s	q	tuff
RV6	q-s	q	tuff
RV7	q-s-c	q	flow
CD4	q-s-c-cc	a	flow
CD18	q-c-e-s		flow
CD21	q-a-s-c		quartz-diorite
CD23	q-s	q	flow
MA1	q-c	q	tuff
MA2	q-c-s		coarse tuff
MA3	q-c-s		coarse tuff
MA25	a-act-e-cc-q-c		basic intrusive
MA29	q-s-c		tuff
RW2	q-s-c		tuff
QA1A	amphibole-q-c-opaques		amphibolite

Samples from Individual Localities

SAMPLE NUMBER	MINERALOGY GROUNDMASS	PHENOCRYSTS/ PORPHYROBLASTS	ORIGINAL ROCK
MGZ LOCALITY			
SM1S1 to SM12S1	q-c-s	(q)	tuff
SM1S2	c-a-cc-a-b		chlorite schist
SM3S2	q-sulphides		mineralized chert
SM4S2	q-sulphides		ditto
SM8S2	c-z-b-cc-opaques	c,b	chlorite schist
SM2S3	c-q-cc	act	ditto
SM4AS3	c-sulphides	act	ditto
SM5S3	q-sulphides		mineralized chert
SM11S3	q-c	a,b	cherty tuff
SM16S3	q-c	a,q	ditto
SM17S3	q-c-cc-magnetite		basic intrusive
SM9S6	q-c-a-e-sulphide		mineralized tuff
SM3P4	massive sulphides		sulphides
SM5P4	massive sulphides		ditto
Θ LOCALITY, 300 m SOUTH OF MGZ, IN SEDIMENTS			
SM2Θ1	q-c		greywacke
SM4Θ1	a-act-q-cz-c		basic intrusive
SM5Θ1	q-s		greywacke
D LOCALITY			
MD1D2	q-c	q	tuff
MD3D2	act-c-a-q-magnetite		basic intrusive
MD4D2	act-c-a-q-cz		ditto
MD4D6	act-c-a-q-cz		ditto
L LOCALITY			
MA2L1	q-sphalerite		chert
MA3L1	q-sphalerite		chert
MA1L2	q-s		flow
W LOCALITY			
MA2W2 to MA18W2	q-s-c±sphalerite	g,a,b	aluminous chert
MA20W2	q-s-c		ditto
MA23W2	q-s-c-sphalerite	g	ditto
MA28W2	q-s	b,a	ditto
MA29W2	q-s-c	g,a	ditto
MA3W1	q-b		flow
MA1W3	q-c-s		tuff

Samples from Individual Localities

MINERALOGY

SAMPLE NUMBER	GROUNDMASS	PHENOCRYSTS/ PORPHYROBLASTS	ORIGINAL ROCK
K LOCALITY, ON MARANDA-COTTONDALE BOUNDARY			
MA1K1	amphibole-a-q-cc		basic intrusive
MA4K1	amphibole-a-cz-q		ditto
J LOCALITY			
MA1J4	q-c	b	tuff
MA3J4	q-c	b,a	tuff
MA4J4	c-q-e	act	chlorite schist
MA5J4	q-c	b	tuff
MA6J4	q-c	b,a	tuff
MA7J4	c-act-b		chlorite schist
MA9J4	pyrite in chlorite schist		ditto
MA2J11	q-c-s	q	tuff
MA3J11	q-c-s		tuff
MA4J11	q-c-s		tuff
MA6J11	q-c		tuff
MA7J11	c-a-cc-magnetite		basic intrusive
MA9J11	c	c	chlorite schist
MA10J11	q-c-a		tuff
MA14J11	q-c-sulphides		chert?
MA15J11	massive sulphides		sulphides
MA16J11	massive sulphides		ditto
MA17J11	massive sulphides		ditto
MA18J11	massive sulphides		ditto
MA20J11	massive sulphides		ditto
MA21J11	q-c-cc-a		basic intrusive
MA22J11	q-c-s		aluminous chert
MA1J15	massive pyrite		sulphides
MA2J15	massive pyrite		sulphides
MA6J15	massive, pyrite and sphalerite		ditto
MA9J15	massive sulphides		ditto
MA11J15	massive, pyrite and sphalerite		ditto
MA2J18	banded sulphide-silicate		ditto
MA1J21	q-s		flow
MA2J25	q-c-s		aluminous chert
MA1J38	q-c-s		ditto
MA2J38	q-c-s		ditto
MA3J38	q-c-s		ditto

Samples of acid porphyry from the J locality:

MA1J1, MA1J2, MA1J3, MA1AJ4, MA1J5A, MA1J7, MA1J8, MA1J10, MA1J11, MA1J15, MA1J16, MA1J18, MA1J22, MA1J23, MA1J24, MA1J25, MA1J26, MA1J27, MA2J29, MA1J30, MA1J31, MA1J36, MA1J37.

Mineralogy: q-a-s-c with q,a phenocrysts.

APPENDIX B

ELECTRON MICROPROBE ANALYSES

B 1. Operating Conditions

Mineral analyses were performed on a Cambridge Instrument Company "Geoscan - Mark II" electron microprobe analyser, at the University of Durham, using methods similar to those of Sweatman and Long (1969). Data was handled by an on-line Varian 620/100 computer. The programme TIM4 was written by Dr. A. Peckett of the Department, and performs the necessary corrections for atomic number, mass absorption, and fluorescence, on peak and background data for standards and samples. The programme was also used to calculate FeO and Fe_2O_3 for chlorites and amphiboles, and to assign a water component. The results for amphiboles are estimates only.

The wave dispersive system of analysis was used, with two spectrometers and three analysing crystals, LiF, PET, and KAP. Three, ten second count accumulations were used for each peak and background position, although up to five accumulations were used for Co and Ni analyses in sulphides. The Geoscan was operated under a high vacuum with an accelerating voltage of 15 kV for silicate minerals, 20 kV for sulphides, and a probe current of 40 nanoamps for silicates, 20 nanoamps for sulphides. The electron beam was focussed and held in one position to produce a spot diameter of 2-5 microns. A defocussed beam was used for feldspar analysis to overcome mineral decomposition.

The standard error for each element varies with concentration, but is approximated by:

wt.% oxide/element	relative error
10 - 50	2%
1 - 10	5%
1	10%

The standards used, and operating conditions, are shown in the accompanying table.

Operating conditions for Geoscan Electron Microprobe

ATOMIC NUMBER	ELEMENT	LINE	CRYSTAL	COUNTER 2	PEAK	STANDARD USED
11	Na	$K\alpha_1$	KAP	FLOW	53°18'	jadeite
12	Mg	$K\alpha_1$	KAP	"	43°45'	MgO
13	Al	$K\alpha_1$	KAP	"	36°37'	jadeite
14	Si	$K\alpha_1$	PET	"	109°9'	wollastonite
16	S	$K\alpha_1$	PET	"	75°46'	FeS_2
19	K	$K\alpha_1$	PET	"	50°25'	AF15
20	Ca	$K\alpha_1$	LiF	"	113°21'	wollastonite
22	Ti	$K\alpha_1$	LiF	"	86°5'	TiO_2
23	V	$K\alpha_1$	LiF	"	76°50'	V_2O_5
24	Cr	$K\alpha_1$	LiF	"	69°17'	Cr
25	Mn	$K\alpha_1$	LiF	"	62°50'	rhodonite
26	Fe	$K\alpha_1$	LiF	"	57°23'	FeS_2 Fe
27	Co	$K\alpha_1$	LiF	"	52°51'	Co
28	Ni	$K\alpha_1$	LiF	"	48°32'	Ni
29	Cu	$K\alpha_1$	LiF	"	44°50'	Cu
30	Zn	$K\alpha_1$	LiF	"	41°34'	Zn
33	As	$L\alpha_1$	KAP	"	41°21'	As
34	Se	$L\alpha_1$	LiF	"	32°18'	Cd Se
47	Ag	$L\alpha_1$	PET	"	56°37'	Ag
48	Cd	$L\alpha_1$	PET	"	53°35'	CdSe
50	Sn	$L\alpha_1$	LiF	"	126°47'	Sn
51	Sb	$L\alpha_1$	LiF	"	117°22'	Sb
52	Te	$L\alpha_1$	LiF	"	109°34'	Te
82	Pb	$M\alpha_1$	PET	"	74°15'	PbS
83	Bi	$M\beta_1$	PET	"	68°10'	Bi

B2. Results

Results of silicate and sulphide analyses are set out in the following tables.

Abbreviations used:

na - not analysed

c - core analysis

m - margin analysis

Regional Dynamothermal Metamorphism - Chlorite

ANAL	10	11	17	18	37	38	39	45	168	169	191	192
SAMPLE	SM11S3	SM11S3	SM11S3	SM11S3	SM2S1	SM2S1	SM2S1	SM2S1	MA4J11	MA4J11	SM9S6	SM9S6
SiO_2	25.29	22.70	24.40	23.99	25.32	24.25	24.71	25.13	25.22	25.34	25.07	26.89
TiO_2	0.08	0.08	0.06	0.13	0.11	0.06	0.10	0.07	0.02	0.02	0.01	0.04
Al_2O_3	21.17	20.88	21.00	21.00	22.35	21.57	22.22	22.22	23.80	23.30	21.23	21.02
Cr_2O_3	0.00	0.00	0.00	0.01	0.00	0.37	0.00	0.03	na	na	na	na
Fe_2O_3	0.00	3.12	1.07	1.25	0.15	1.41	0.91	0.00	0.00	0.00	3.36	
FeO	24.91	21.58	24.36	23.74	21.19	19.12	19.85	20.37	21.03	20.81	19.88	22.62
MnO	0.33	0.34	0.35	0.36	0.08	0.10	0.27	0.11	0.07	0.04	0.26	0.28
MgO	15.01	15.04	14.92	14.78	17.80	17.90	17.95	17.64	18.00	17.38	17.94	16.44
CaO	0.01	0.02	0.01	0.03	0.08	0.09	0.04	0.06	0.02	0.00	0.06	0.01
Na_2O	0.05	0.00	0.00	0.00	0.04	0.02	0.03	0.02	0.00	0.00	0.20	0.00
K_2O	0.05	0.04	0.05	0.12	0.05	0.07	0.05	0.00	0.00	0.00	0.00	0.00
H_2O	11.29	10.86	11.16	11.06	11.57	11.28	11.45	11.42	11.74	11.59	11.60	11.54
TOTAL	98.19	94.65	97.38	96.46	98.74	96.24	97.58	97.12	99.90	98.49	99.60	98.84
Cations per 36 oxygens												
Si	5.376	5.014	5.247	5.206	5.252	5.156	5.179	5.281	5.153	5.245	5.186	5.589
Ti	0.013	0.013	0.010	0.021	0.017	0.010	0.016	0.011	0.003	0.003	0.001	0.006
Al	5.307	5.439	5.326	5.374	5.467	5.409	5.493	5.507	5.734	5.688	5.181	5.153
Cr				0.002		0.062		0.005				
Fe^{3+}		0.518	0.174	0.204	0.024	0.225	0.143				0.523	
Fe^{2+}	4.428	3.985	4.382	4.308	3.676	3.401	3.480	3.580	3.593	3.602	3.439	3.933
Mn	0.059	0.064	0.064	0.066	0.014	0.018	0.048	0.020	0.012	0.007	0.045	0.050
Mg	4.755	4.951	4.782	4.780	5.502	5.672	5.607	5.525	5.480	5.362	5.532	5.095

Regional Dynamothermal Metamorphism - Chlorite (continued)

ANAL	10	11	17	18	37	38	39	45	168	169	191	192
SAMPLE	SM11S3	SM11S3	SM11S3	SM11S3	SM2S1	SM2S1	SM2S1	SM2S1	MA4J11	MA4J11	SM9S6	SM9S6
Cations per 36 oxygens (continued)												
Ca	0.002	0.005	0.002	0.007	0.018	0.021	0.009	0.014	0.004		0.013	0.002
Na	0.021				0.016	0.008	0.012	0.008			0.079	
K	0.014	0.011	0.014	0.033	0.013	0.019	0.013	0.013				
H	16.00	16.00	16.00	16.00	16.00	16.00	16.00	16.00	16.00	16.00	16.00	16.00
RATIOS												
Fe^{2+}	0.4822	0.4460	0.4782	0.4740	0.4005	0.3748	0.3830	0.3932	0.3960	0.4018	0.3833	0.4356
Mg	0.5178	0.5540	0.5218	0.5260	0.5995	0.6252	0.6170	0.6068	0.6040	0.5982	0.6167	0.5644

ANAL	260	261	262	263	76	146	147
SAMPLE	MA4K1	MA4K1	MA4K1	MA4K1	SM16*	MA6J4	MA6J4
SiO_2	37.90	38.58	38.49	38.25	38.07	34.49	32.49
TiO_2	0.03	0.00	0.19	0.19	0.10	0.10	0.17
Al_2O_3	21.46	21.60	22.21	22.94	31.73	22.13	18.37
Fe_2O_3	14.15	13.23	13.51	12.43	0.62	10.30	7.50
FeO	0.40	0.28	0.00	0.00	0.00	2.60	5.85
MnO	0.16	0.23	0.18	0.31	0.04	0.25	0.33
MgO	0.10	0.25	0.13	0.20	0.11	0.51	0.25
CaO	22.47	22.93	22.49	22.50	23.64	17.72	14.68
Na_2O	0.20	0.17	0.54	0.32	0.06	0.23	0.25
K_2O	0.03	0.03	0.02	0.02	0.01	0.06	0.06
H_2O	1.86	1.87	1.88	1.88	1.91	1.71	1.53
TOTAL	98.77	99.19	99.64	99.03	96.43	90.10	81.48
Cations per 13 oxygens							
Si	3.063	3.094	3.068	3.058	2.995	3.0298	3.1789
Ti	0.002		0.011	0.012	0.0059	0.0066	0.0125
Al	2.045	2.043	2.088	2.162	2.9440	2.2927	2.1198
Fe^{3+}	0.860	0.798	0.810	0.747	0.0368	0.6808	0.5523
Fe^{2+}	0.027	0.019				0.1912	0.4787
Mn	0.011	0.016	0.012	0.021	0.0027	0.0186	0.0273
Mg	0.012	0.030	0.016	0.024	0.0129	0.0668	0.0365
Ca	1.946	1.970	1.922	1.927	1.9927	1.6679	1.5390
Na	0.031	0.027	0.083	0.049	0.0092	0.0392	0.0474
K	0.003	0.003	0.003	0.002	0.0010	0.0067	0.0075
H	1.000	1.000	1.000	1.000	1.0011	1.0000	1.0000
RATIOS							
Fe^{2+}	0.6914	0.3885	0	0	0	0.7412	0.9292
Mg	0.3086	0.6115	1.0	1.0	1.0	0.2588	0.0708

*Contains 0.14 wt% Cr_2O_3

ANAL	1	2	3	4	5	6	20	21	22	23
SAMPLE	SM11S3	SM11S3	SM11S3	SM11S3	SM11S3	SM11S3	SM204	SM204	SM204	SM204
SiO_2	66.20	65.58	68.22	66.68	65.78	65.01	69.96	66.83	71.17	69.30
TiO_2	0.00	0.00	0.00	0.00	0.02	0.01	0.02	0.04	0.00	0.06
Al_2O_3	19.41	19.38	19.61	19.16	19.60	19.68	19.68	19.63	19.65	19.68
Cr_2O_3	0.00	0.01	0.02	0.02	0.00	0.02	0.02	0.03	0.04	0.00
FeO	0.00	0.00	0.08	0.18	0.03	0.04	0.00	0.07	0.06	0.49
MnO	0.00	0.02	0.01	0.02	0.02	0.00	0.01	0.01	0.03	0.01
MgO	0.03	0.05	0.07	0.06	0.06	0.03	0.03	0.05	0.02	0.06
CaO	0.59	0.80	0.50	0.47	0.25	0.34	0.33	0.25	0.16	0.19
Na_2O	10.96	11.38	10.61	12.08	11.53	11.91	11.18	11.94	11.78	11.76
K_2O	0.09	0.07	0.10	0.11	0.24	0.10	0.08	0.10	0.09	0.09
TOTAL	97.30	97.27	99.26	98.73	97.52	97.14	101.31	98.94	103.00	101.64
Cations per 8 oxygens										
Si	2.973	2.9561	2.994	2.966	2.957	2.939	3.008	2.962	3.014	2.986
Ti			0.001		0.001		0.001	0.001		0.002
Al	1.028	1.0301	1.015	1.006	1.039	1.049	0.998	1.026	0.981	1.000
Cr		0.0004	0.001			0.001	0.001	0.001	0.001	
Fe			0.003	0.007	0.001	0.001		0.002	0.002	0.018
Mn		0.0008		0.001	0.001				0.001	
Mg	0.002	0.0034	0.005	0.004	0.004	0.002	0.002	0.003	0.001	0.004
Ca	0.029	0.0386	0.023	0.022	0.012	0.017	0.015	0.012	0.007	0.009
Na	0.954	0.9945	0.902	1.043	1.005	1.044	0.932	1.026	0.967	0.983
K		0.0040	0.006	0.006	0.014	0.006	0.005	0.006	0.005	0.005
Ca	5.069	3.72	2.521	2.090	1.170	1.562	1.611	1.146	0.734	0.874
Na	94.158	95.89	96.852	97.350	97.489	97.902	97.910	98.297	98.760	98.625
K	0.773	0.39	0.627	0.560	1.340	0.536	0.479	0.557	0.506	0.501

ANAL	24	35	36	264	265
SAMPLE	GE3	SM4Θ1	SM4Θ1	MA4K1	MA4K1
SiO_2	70.04	70.31	69.87	67.91	67.92
TiO_2	0.01	0.00	0.05	0.01	0.03
Al_2O_3	20.41	20.25	19.66	19.90	19.19
Cr_2O_3	0.02	0.00	0.00	na	na
FeO	0.01	0.10	0.14	0.43	0.39
MnO	0.01	0.03	0.03	0.01	0.00
MgO	0.03	0.03	0.03	0.08	0.09
CaO	0.04	0.25	0.29	0.56	0.28
Na_2O	11.97	12.08	12.11	11.12	10.53
K_2O	0.07	0.06	0.07	0.07	0.07
TOTAL	102.60	103.12	102.24	100.10	98.50
Cations per 8 oxygens					
Si	2.981	2.982	2.991	2.969	3.004
Ti			0.002		0.001
Al	1.025	1.013	0.993	1.026	1.001
Cr	0.001				
Fe		0.004	0.005	0.016	0.015
Mn		0.001	0.001		
Mg	0.002	0.002	0.002	0.006	0.006
Ca	0.002	0.011	0.013	0.026	0.014
Na	0.987	0.993	1.005	0.943	0.903
K	0.004	0.003	0.004	0.004	0.004
Ca	0.173	1.136	1.294	2.710	1.470
Na	99.447	98.520	98.319	96.900	98.130
K	0.381	0.344	0.387	0.390	0.400

Regional dynamothermal metamorphism - Mica

	Biotite			Sericite				Chrome-rich sericite (fuchsite)	
ANAL	70	71	81	74	86	174	175	72	73
SAMPLE	RV1	RV1	SM4	RV1	SM12	MA4J11	MA4J11	SM16	SM16
SiO_2	34.63	35.07	38.02	47.29	44.77	46.14	47.43	46.66	46.09
TiO_2	2.60	2.36	1.66	0.33	0.35	0.16	0.18	0.15	0.29
Al_2O_3	15.65	15.46	15.74	28.42	31.04	35.78	35.74	34.87	33.79
Cr_2O_3	0.09	0.06	0.07	0.01	0.03	na	na	0.58	1.24
FeO	29.94	28.67	20.75	6.51	6.45	1.81	1.32	0.66	0.70
MnO	0.38	0.28	0.16	0.05	0.06	0.00	0.00	0.01	0.02
MgO	4.30	4.22	11.02	1.44	0.25	1.45	1.01	0.97	0.96
CaO	0.10	0.04	0.00	0.01	0.04	0.02	0.05	0.06	0.00
Na_2O	0.03	0.12	0.11	0.12	0.29	1.08	0.84	0.85	0.66
K_2O	9.24	9.02	9.60	10.84	9.82	8.59	9.16	8.58	9.91
TOTAL	96.97	95.30	97.13	95.03	93.10	95.02	95.72	93.39	93.66
Cations per 22 oxygen									
Si	5.490	5.610	5.705	6.500	6.251	6.113	6.223	6.248	6.226
Ti	0.310	0.284	0.187	0.034	0.037	0.016	0.017	0.016	0.029
Al	2.926	2.916	2.786	4.607	5.116	5.592	5.530	5.506	5.383
Cr	0.012	0.007	0.008	0.001	0.003			0.061	0.133
Fe	3.970	3.835	2.605	0.748	0.753	0.200	0.145	0.074	0.078
Mn	0.052	0.038	0.020	0.006	0.007			0.001	0.002
Mg	1.016	1.006	2.464	0.296	0.053	0.286	0.197	0.194	0.194
Ca	0.016	0.006		0.002	0.005	0.003	0.008	0.009	
Na	0.009	0.039	0.033	0.032	0.079	0.278	0.214	0.220	0.172
K	1.869	1.840	1.837	1.901	1.751	1.451	1.533	1.466	1.708

ANAL	57	58	59	60	65	66	67	68	176	177	178	179
SAMPLE	SM4AS3	SM4AS3	SM4AS3	SM4AS3	SM4AS3	SM1S2	SM1S2	SM1S2	SM2S3	SM2S3	SM2S3	SM2S3
SiO_2	53.06	52.56	53.49	53.97	53.83	47.69	50.51	50.99	56.98	56.61	56.92	55.58
TiO_2	0.04	0.08	0.08	0.13	0.06	0.26	0.12	0.19	0.01	0.06	0.06	0.12
Al_2O_3	1.91	2.51	2.94	2.43	2.37	8.57	5.28	4.90	1.29	2.27	2.01	2.50
Cr_2O_3	0.00	0.04	0.02	0.03	0.01	0.03	0.03	0.01	na	na	na	na
Fe_2O_3	5.44	7.61	8.04	6.70	6.46	9.26	10.54	9.32	0.00	0.00	1.13	1.44
FeO	7.23	4.06	5.59	6.49	5.98	6.83	5.99	5.39	7.06	6.91	5.25	5.52
MnO	0.32	0.30	0.42	0.32	0.32	0.31	0.35	0.27	0.24	0.28	0.32	0.31
MgO	17.25	17.73	17.15	17.19	17.53	13.71	15.04	15.69	19.59	19.07	20.34	19.53
CaO	11.38	11.68	11.67	12.00	11.54	11.42	11.36	11.38	12.01	11.64	11.70	11.46
Na_2O	0.49	0.70	0.77	0.63	0.70	1.57	1.24	1.01	0.30	0.63	0.55	0.56
K_2O	0.00	0.11	0.11	0.11	0.11	0.26	0.17	0.16	0.02	0.03	0.03	0.04
H_2O	2.09	2.11	2.16	2.15	2.14	2.11	2.13	2.12	2.15	2.15	2.17	2.14
TOTAL	99.21	99.48	102.44	102.15	101.04	101.96	102.77	101.43	99.66	99.65	100.48	99.19
Cations per 24 oxygens												
Si	7.609	7.478	7.442	7.528	7.561	6.784	7.097	7.210	7.956	7.898	7.848	7.785
Ti	0.004	0.009	0.008	0.014	0.006	0.028	0.013	0.020	0.001	0.007	0.006	0.012
Al	0.323	0.421	0.482	0.400	0.393	1.438	0.875	0.816	0.212	0.373	0.327	0.412
Cr		0.005	0.002	0.003	0.001	0.003	0.003	0.001				
Fe^{3+}	0.587	0.815	0.842	0.704	0.683	0.991	1.115	0.990			0.117	0.152
Fe^{2+}	0.867	0.483	0.651	0.757	0.702	0.813	0.705	0.636	0.825	0.807	0.605	0.647
Mn	0.039	0.036	0.050	0.038	0.038	0.037	0.042	0.032	0.029	0.034	0.037	0.036
Mg	3.687	3.760	3.556	3.573	3.669	2.906	3.150	3.303	4.077	3.964	4.179	4.077
Ca	1.759	1.781	1.740	1.794	1.737	1.741	1.710	1.722	1.797	1.740	1.728	1.719
Na	0.136	0.193	0.208	0.170	0.191	0.417	0.338	0.277	0.082	0.170	0.146	0.152
K		0.020	0.020	0.020	0.020	0.047	0.031	0.029	0.004	0.006	0.006	0.007
H	2.000	2.000	2.000	2.000	2.000	2.000	2.000	2.000	1.998	2.000	2.000	2.000
RATIOS												
Fe	0.1903	0.1138	0.1547	0.1748	0.1606	0.2185	0.1828	0.1615	0.1683	0.1691	0.1265	0.1369
Mg	0.8097	0.8862	0.8453	0.8252	0.8394	0.7815	0.8172	0.8385	0.8317	0.8309	0.8735	0.8631

Thermal Metamorphism - Amphibole (continued)

ANAL	153	154	155	156	157	158	159	160	161	162	163
SAMPLE	MA7J4a	MA7J4a	MA7J4a	MA7J4a	MA7J4a	MA7J4a	MA7J4a	MA7J4a	MA7J4a	MA7J4a	MA7J4a
SiO_2	55.03	53.95	54.14	54.75	54.02	53.20	54.90	54.47	54.73	54.40	54.40
TiO_2	0.01	0.08	0.03	0.07	0.07	0.09	0.06	0.06	0.09	0.04	0.05
Al_2O_3	1.04	2.65	2.21	2.20	2.28	3.01	2.10	2.74	2.19	2.80	1.95
Cr_2O_3	na	na	na	na	na	na	na	na	na	na	na
Fe_2O_3	1.88	4.02	3.76	3.90	3.75	5.35	2.19	3.16	2.80	3.66	3.71
FeO	11.09	8.47	8.40	8.19	8.57	8.17	9.36	9.36	9.48	8.65	8.45
MnO	0.22	0.19	0.23	0.19	0.21	0.25	0.19	0.21	0.31	0.20	0.23
MgO	16.42	16.14	17.12	16.93	16.58	16.14	17.05	16.31	16.73	16.62	17.20
CaO	11.63	11.55	11.08	11.54	11.40	10.78	10.98	11.04	11.17	10.94	11.06
Na_2O	0.26	0.82	0.61	0.76	0.69	0.89	0.67	0.82	0.65	0.86	0.65
K_2O	0.26	0.05	0.05	0.05	0.05	0.07	0.06	0.05	0.05	0.05	0.04
H_2O	2.10	2.11	2.11	2.13	2.10	2.10	2.11	2.12	2.12	2.12	2.11
TOTAL	99.93	100.02	99.75	100.72	99.73	100.04	99.66	100.33	100.30	100.34	99.86
Cations per 24 oxygens											
Si	7.870	7.672	7.699	7.712	7.699	7.579	7.798	7.714	7.753	7.690	7.727
Ti	0.001	0.008	0.003	0.008	0.008	0.010	0.006	0.006	0.009	0.005	0.005
Al	0.175	0.444	0.373	0.365	0.383	0.506	0.352	0.458	3.366	0.466	0.327
Fe^{3+}	0.202	0.431	0.402	0.413	0.403	0.574	0.234	0.337	0.298	0.390	0.397
Fe^{2+}	1.326	1.008	0.999	0.965	1.021	0.973	1.112	1.108	1.123	1.022	1.004
Mn	0.027	0.023	0.028	0.023	0.025	0.030	0.023	0.025	0.037	0.024	0.028
Mg	3.499	3.420	3.628	3.554	3.521	3.427	3,610	3.443	3.531	3.501	3.641
Ca	1.782	1.760	1.689	1.742	1.741	1.646	1.671	1.675	1.696	1.657	1.684
Na	0.071	0.225	0.169	0.208	0.190	0.245	0.184	0.224	0.179	0.237	0.180
K	0.048	0.010	0.008	0.010	0.010	0.012	0.010	0.010	0.009	0.008	0.008
H	2.000	2.000	2.000	2.000	2.000	2.000	2.000	2.000	2.000	2.000	2.000
RATIOS											
Fe2+	0.2748	0.2276	0.2159	0.2136	0.2248	0.2212	0.2355	0.2435	0.2412	0.2260	0.2161
Mg	0.7252	0.7724	0.7841	0.7864	0.7752	0.7788	0.7645	0.7565	0.7588	0.7740	0.7839

Thermal Metamorphism - Biotite

ANAL	9	19	56	c 131	cm 132	m 133	152	164	165
SAMPLE	SM11S3	SM11S3	SM8S2	MA5J4	MA5J4	MA6J4	MA6J4	MA7J4a	MA7J4a
SiO_2	36.58	36.75	38.44	40.56	36.84	34.52	36.86	40.74	39.96
TiO_2	1.47	1.62	1.52	1.44	1.51	1.05	1.50	0.48	0.47
Al_2O_3	16.12	16.49	15.53	14.45	15.06	14.87	16.37	12.14	12.53
Cr_2O_3	0.02	0.03	0.00	na	na	na	na	na	na
FeO	18.74	18.46	16.84	18.93	20.94	28.00	21.30	15.85	15.75
MnO	0.17	0.19	0.06	0.08	0.07	0.09	0.05	0.05	0.05
MgO	12.57	11.44	14.63	14.04	13.32	12.36	11.00	17.21	17.28
CaO	0.01	0.00	0.00	0.04	0.01	0.04	0.03	0.03	0.01
Na_2O	0.13	0.03	0.11	0.05	0.03	0.01	0.07	0.00	0.07
K_2O	9.52	10.01	8.74	9.59	8.74	5.42	9.38	8.25	8.46
TOTAL	95.32	95.11	95.86	99.18	96.51	96.36	95.55	94.75	94.59
Cations per 22 oxygens									
Si	5.563	5.603	5.705	5.875	5.566	5.335	5.506	6.059	5.970
Ti	0.168	0.185	0.169	0.157	0.171	0.122	0.134	0.054	0.053
Al	2.891	2.966	2.717	2.469	2.683	2.710	2.965	2.129	2.209
Cr	0.003	0.003							
Fe	2.383	2.354	2.091	2.294	2.645	3.619	2.735	1.971	1.967
Mn	0.021	0.025	0.007	0.010	0.009	0.012	0.007	0.006	0.006
Mg	2.848	2.599	3.235	3.032	2.999	2.847	2.517	3.816	3.848
Ca	0.001	0.015		0.006	0.001	0.007	0.004	0.004	0.002
Na	0.039	0.008	0.031	0.015	0.008	0.004	0.021		0.021
K	1.847	1.947	1.654	1.772	1.685	1.069	1.837	1.566	1.613

c - orange core of zoned biotite
cm - mid-point
m - green margin

Thermal Metamorphism - Chlorite

ANAL SAMPLE	48 SM8S2	49 SM8S2	50 SM8S2
SiO_2	26.35	26.19	27.75
TiO_2	0.06	0.06	0.09
Al_2O_3	20.62	21.18	18.64
Cr_2O_3	0.00	0.00	0.00
Fe_2O_3	0.57	0.00	0.00
FeO	20.70	20.93	19.64
MnO	0.22	0.20	0.17
MgO	18.88	18.37	19.68
CaO	0.03	0.01	0.05
Na_2O	0.00	0.00	0.02
K_2O	0.04	0.04	0.05
H_2O	11.62	11.57	11.53
TOTAL	99.09	98.55	97.62
Cations per 36 oxygens			
Si	5.441	5.431	5.772
Ti	0.009	0.009	0.014
Al	5.022	5.180	4.573
Cr			
Fe^{3+}	0.089		
Fe^{2+}	3.574	3.630	3.417
Mn	0.039	0.035	0.030
Mg	5.810	5.677	6.101
Ca	0.007	0.002	0.011
Na			0.008
K	0.011	0.011	0.013
H	16.00	16.00	16.00

ANAL SAMPLE	48 SM8S2	49 SM8S2	50 SM8S2
RATIOS			
Fe^{2+}	0.3809	0.3900	0.3590
Mg	0.6191	0.6100	0.6410

ANAL	142	143	144	151	186	187	189	188	190
SAMPLE	MA6J4	MA6J4	MA6J4	MA6J4	MA10J11	MA10J11	SM9S6	SM9S6	SM9S6
SiO_2	65.03	67.26	65.16	65.62	68.26	70.18	69.90	67.63	68.57
TiO_2	0.0	0.01	0.01	0.08	0.03	0.03	0.02	0.06	0.01
Al_2O_3	22.05	21.88	22.81	22.39	20.19	18.84	18.43	19.84	18.52
FeO	0.10	0.38	0.12	0.40	0.23	0.12	0.04	0.15	0.10
MnO	0.06	0.01	0.00	0.03	0.05	0.03	0.02	0.02	0.02
MgO	0.03	0.07	0.04	0.04	0.04	0.04	0.01	0.05	0.03
CaO	2.45	2.76	3.08	3.01	0.30	0.24	0.19	0.09	0.07
Na_2O	10.31	7.85	7.53	9.32	11.89	12.04	12.01	11.64	11.99
K_2O	0.07	0.08	0.07	0.09	0.08	0.08	0.08	0.08	0.08
TOTAL	100.10	100.32	98.83	100.96	101.06	101.60	100.69	99.56	99.40
Cations per 8 oxygens									
Si	2.860	2.919	2.872	2.858	2.960	3.020	3.033	2.971	3.017
Ti		0.001	0.001	0.003	0.001	0.001	0.001	0.002	0.004
Al	1.144	1.120	1.186	1.150	1.033	0.956	0.943	1.028	0.961
Fe	0.004	0.014	0.004	0.014	0.008	0.004	0.002	0.006	0.004
Mn	0.002	0.001	0.000	0.001	0.002	0.001	0.001	0.001	0.001
Mg	0.002	0.005	0.003	0.003	0.002	0.003	0.001	0.003	0.002
Ca	0.115	0.128	0.146	0.140	0.014	0.011	0.009	0.004	0.003
Na	0.879	0.661	0.644	0.787	1.000	1.005	1.010	0.991	1.023
K	0.004	0.005	0.004	0.005	0.004	0.004	0.005	0.005	0.005
Ca	11.56	16.16	18.34	15.05	1.37	1.08	0.84	0.43	0.32
Na	88.05	83.27	81.15	84.41	98.20	98.50	98.70	99.12	99.24
K	0.39	0.57	0.51	0.54	0.44	0.43	0.46	0.46	0.44

Thermal Metamorphism - Feldspar (continued)

ANAL	232	233	234	235	236	348	349	350
SAMPLE	MA14W2	MA14W2	MA14W2	MA14W2	MA14W2	MA29W2	MA29W2	MA29W2
SiO_2	67.90	67.21	67.66	67.30	67.42	68.34	68.38	67.91
TiO_2	0.04	0.02	0.03	0.03	0.03	0.02	0.01	0.02
Al_2O_3	20.64	20.47	20.70	20.06	20.16	20.41	19.74	20.01
FeO	0.05	0.09	0.06	0.21	0.15	0.08	0.02	0.04
MnO	0.03	0.00	0.02	0.03	0.03	0.00	0.04	0.02
MgO	0.03	0.03	0.03	0.04	0.04	0.05	0.04	0.03
CaO	0.83	1.06	0.85	0.60	0.72	0.68	0.46	0.84
Na_2O	10.23	10.08	11.15	10.36	10.88	11.03	11.31	11.55
K_2O	0.07	0.07	0.07	0.07	0.08	0.09	0.10	0.10
TOTAL	99.84	99.03	100.55	98.71	99.52	100.70	100.12	100.52
Cations per 8 oxygens								
Si	2.9626	2.9585	2.9442	2.9725	2.9612	2.9644	2.9836	2.9605
Ti	0.0015	0.0007	0.0009	0.0009	0.0011	0.0006	0.0004	0.0007
Al	1.0620	1.0629	1.0622	1.0449	1.0444	1.0440	1.0158	1.0289
Fe	0.0019	0.0033	0.0022	0.0078	o.0057	0.0028	0.0011	0.0015
Mn	0.0010		0.0006	0.0011	0.0011	0.0002	0.0013	0.0006
Mg	0.0022	0.0018	0.0019	0.0029	0.0027	0.0031	0.0028	0.0018
Ca	0.0388	0.0500	0.0394	0.0283	0.0340	0.0315	0.01	0.0394
Na	0.8655	0.8604	0.9406	0.8875	0.9264	0.9281	0.9572	0.9761
K	0.0041	0.0042	0.0038	0.0041	0.0047	0.0051	0.0053	0.0054
Ca	4.28	5.47	4.01	3.08	3.52	3.26	2.20	3.86
Na	95.28	94.07	95.60	96.47	95.99	96.21	97.25	95.61
K	0.45	0.46	0.39	0.45	0.49	0.53	0.54	0.53

	c	m	c	m	c	m	c	cm	m	c	m
ANAL	342	343	344	345	346	347	281	282	283	284	285
SAMPLE	MA29W2	MA29W2	MA29W2	MA29W2	MA29W2	MA29W2	MA23W2	MA23W2	MA23W2	MA23W2	MA23W2
SiO_2	36.38	36.19	36.73	37.24	36.89	36.54	36.34	36.57	37.76	37.00	37.93
TiO_2	0.07	0.05	0.04	0.07	0.07	0.05	0.06	0.05	0.00	0.03	0.00
Al_2O_3	20.61	20.51	21.12	20.39	20.67	21.11	21.02	20.18	20.72	20.94	19.85
FeO	17.00	20.96	17.14	21.20	17.98	20.80	20.98	20.16	20.00	20.10	19.88
MnO	22.81	17.93	22.77	18.81	22.28	19.00	17.35	17.92	16.35	17.52	15.89
MgO	0.56	0.69	0.54	0.64	0.45	0.60	0.54	0.56	0.44	0.57	0.50
CaO	1.11	2.23	1.18	1.58	1.27	1.99	3.00	3.11	4.22	2.94	4.28
Na_2O	0.12	0.12	0.13	0.00	0.02	0.05	0.01	0.00	0.09	0.05	0.14
K_2O	0.00	0.00	0.01	0.00	0.00	0.00	0.00	0.00	0.01	0.00	0.00
TOTAL	98.66	98.63	99.65	99.95	99.63	100.14	99.31	98.55	99.59	99.15	98.46
Cations per 24 oxygen											
Si	6.0218	5.9908	6.0088	6.0809	6.0470	5.927	5.9636	6.0486	6.1223	6.0493	6.2129
Ti	0.0084	0.0059	0.0053	0.0083	0.0090	0.0061	0.0079	0.0058		0.0037	
Al	4.0226	4.0030	4.0742	3.9272	3.999	4.0629	4.0695	3.9366	3.9615	4.0377	3.8346
Fe	2.3530	2.9010	2.3449	2.8949	2.4649	2.8395	2.8796	2.7880	2.7126	2.7491	2.7229
Mn	3.1974	2.5139	3.1548	2.6021	3.094	2.6262	2.4116	2.5105	2.2461	2.4267	2.2044
Mg	0.1386	0.1713	0.1325	0.1561	0.1090	0.1468	0.1314	0.1371	0.1062	0.1384	0.1210
Ca	0.1968	0.3962	0.2070	0.2772	0.2232	0.3480	0.5282	0.5508	0.7332	0.5155	0.7513
Na	0.0397	0.0388	0.0412		0.0061	0.0151	0.0042		0.0285	0.0155	0.0452
K			0.0015						0.0017		
PYROPE	2.35	2.86	2.27	2.65	1.85	2.46	2.21	2.32	1.83	2.37	2.10
SPESS	54.32	42.02	54.03	44.17	52.52	44.06	40.53	42.51	38.74	41.63	38.32
GROSS	3.34	6.62	3.55	4.70	3.79	5.84	8.88	9.33	12.65	8.84	13.06
ALM	39.98	48.49	40.16	48.47	41.84	47.64	48.39	45.84	46.78	47.16	46.51
%	98.23	99.57	97.50	98.50	98.50	99.30	99.20	98.56	97.17	97.55	96.52

c - core of garnet
m - margin of garnet

	c	cm	m	c	cm	m	c	m
ANAL	329	330	331	332	333	334	335	336
SAMPLE	SM4S7	SM4S7	SM4S7	SM4S7	SM4S7	SM4S7	SM4S7	SM4S7
SiO_2	37.05	37.02	36.94	37.01	35.85	35.84	36.60	36.63
TiO_2	0.18	0.06	0.02	0.09	0.08	0.07	0.06	0.04
Al_2O_3	20.12	19.84	20.41	20.19	21.46	22.37	20.08	21.35
FeO	32.99	32.98	33.02	32.44	32.65	35.46	32.80	31.63
MnO	8.01	7.55	8.62	8.14	7.66	4.82	8.57	8.62
MgO	0.84	0.70	0.75	0.75	0.79	0.83	0.76	0.66
CaO	1.23	1.93	1.01	1.30	0.88	0.75	0.84	1.61
Na_2O	0.00	0.00	0.00	0.02	0.02	0.09	0.01	0.00
K_2O	0.00	0.00	0.00	0.00	0.00	0.00	0.00	0.00
TOTAL	100.41	100.07	100.78	99.93	99.39	100.23	99.70	100.55
Cations per 24 oxygens								
Si	6.0532	6.0724	6.0245	6.0663	5.9041	5.8428	6.0368	5.9579
Ti	0.0216	0.0071	0.0026	0.0109	0.0099	0.0084	0.0072	0.0052
Al	3.8771	3.8384	3.9264	3.9027	4.1690	4.3013	3.9048	4.0951
Fe	4.5069	4.5242	4.5048	4.4478	4.4977	4.8339	4.5234	4.3023
Mn	1.1081	1.0496	1.1909	1.1304	1.0684	0.6650	1.1965	1.1882
Mg	0.2044	0.1702	0.1833	0.1823	0.1943	0.2027	0.1857	0.1595
Ca	0.2150	0.3393	0.1772	0.2276	0.1545	0.1305	0.1482	0.2811
Na				0.0068	0.0078	0.0269	0.0020	
K								
PYROPE	3.51	2.96	3.11	3.11	3.29	3.47	3.17	2.69
SPESS	19.05	18.23	20.22	19.31	18.10	11.60	20.43	20.03
GROSS	3.70	5.89	3.01	3.89	2.62	2.24	2.53	4.74
ALM	73.73	72.92	73.66	73.69	76.00	82.89	73.87	72.54
%	97.01	95.95	98.10	97.72	98.37	97.13	97.59	98.92

c - core of garnet
m - margin of garnet

	c	m	c		m
ANAL	337	338	339	340	341
SAMPLE	SM5S7	SM5S7	SM5S7	SM5S7	SM5S7
SiO_2	36.60	37.29	36.95	36.91	36.27
TiO_2	0.15	0.04	0.07	0.09	0.16
Al_2O_3	20.83	19.87	20.32	20.36	20.42
FeO	30.91	29.09	30.98	31.19	30.49
MnO	7.37	5.57	5.94	6.50	6.28
MgO	1.06	1.45	1.10	1.04	0.92
CaO	3.38	7.37	3.94	3.73	4.60
Na_2O	0.02	0.00	0.01	0.00	0.02
K_2O	0.00	0.02	0.00	0.00	0.00
TOTAL	100.32	100.70	99.31	99.82	99.15
Cations per 24 oxygen					
Si	5.9509	6.0098	6.0420	6.0209	5.9605
Ti	0.0187	0.0044	0.0089	0.0111	0.0197
Al	3.9947	3.7778	3.9195	3.9177	3.9574
Fe	4.2041	3.9213	4.2371	4.2553	4.1913
Mn	1.0147	0.7599	0.8224	0.8983	0.8737
Mg	0.2569	0.3476	0.2688	0.2534	0.2258
Ca	0.5897	1.2736	0.6895	0.6520	0.8094
Na	0.0066		0.0019		0.0067
K		0.0048			
PYROPE	4.32	6.13	4.57	4.31	3.80
SPESS	17.05	13.41	13.99	15.29	14.72
GROSS	9.91	22.48	11.73	11.09	13.64
ALM	68.72	57.98	69.71	69.31	67.84
%	98.96	93.86	98.05	97.89	98.66

c - core of garnet
m - margin of garnet

	c	m					c	m	c	m	c	m
ANAL	28	27	29	30	31	32	33	34	77	78	79	80
SAMPLE	MA4K1	MA4K1	MA4K1	MA4K1	MA4K1	MA4K1	SM401	SM401	SM401	SM401	SM401	SM401
SiO_2	43.90	45.13	48.45	52.39	43.98	42.65	51.03	43.01	52.10	42.84	53.52	41.70
TiO_2	0.51	0.32	0.22	0.15	0.31	0.35	0.16	0.22	0.07	0.35	0.03	0.29
Al_2O_3	10.68	11.79	8.09	4.71	13.03	12.55	4.73	11.82	2.29	12.32	2.25	14.59
Fe_2O_3	6.23	2.48	4.66	0.00	7.31	4.96	0.01	4.15	6.05	5.18	2.13	6.03
FeO	16.40	19.66	16.26	18.07	15.82	16.70	17.15	17.57	11.52	16.78	14.46	16.11
MnO	0.25	0.22	0.18	0.18	0.26	0.24	0.22	0.21	0.27	0.28	0.29	0.17
MgO	7.19	6.98	9.55	10.78	7.26	6.88	10.87	6.69	14.00	7.18	13.36	6.32
CaO	11.34	11.97	11.80	12.09	11.34	11.01	11.70	11.15	11.87	11.30	11.98	11.08
Na_2O	1.16	1.59	1.15	0.79	1.93	2.10	0.77	1.59	0.37	1.81	0.30	1.84
K_2O	0.19	0.32	0.11	0.08	0.11	0.08	0.10	0.39	0.14	0.57	0.15	0.39
H_2O	1.99	2.03	2.07	2.06	2.06	1.98	2.02	1.96	2.07	2.00	2.07	2.00
TOTAL	99.84	102.49	102.53	101.30	103.41	99.50	98.76	98.76	100.75	100.62	100.55	100.53
Cations per 24 oxygens												
Si	6.6183	6.6528	7.0251	7.6035	6.3969	6.4555	7.584	6.572	7.533	6.437	7.744	6.252
Ti	0.0578	0.0355	0.0240	0.0164	0.0339	0.0398	0.018	0.025	0.008	0.040	0.003	0.034
Al	1.8990	2.0498	1.3835	0.8062	2.2352	2.2403	0.829	2.130	0.391	2.183	0.384	2.580
Fe^{3+}	0.7070	0.2754	0.5080		0.8004	0.5648	0.001	0.477	0.658	0.586	0.233	0.681
Fe^{2+}	2.0682	2.4234	1.9718	2.1933	1.9244	2.1138	2.132	2.245	1.593	2.108	1.750	2.020
Mn	0.0319	0.0275	0.0221	0.0221	0.0320	0.0308	0.028	0.027	0.033	0.036	0.036	0.022
Mg	1.6155	1.5335	2.0637	2.3317	1.5737	1.5520	2.408	1.524	3.017	1.608	2.881	1.412
Ca	1.8319	1.8907	1.8333	1.8801	1.7673	1.7856	1.863	1.826	1.839	1.819	1.858	1.780
Na	0.3391	0.4545	0.3233	0.2223	0.5443	0.6163	0.222	0.471	0.104	0.527	0.084	0.535
K	0.0365	0.0602	0.0203	0.0148	0.0204	0.0154	0.019	0.076	0.026	0.109	0.028	0.075
H	2.0000	2.0000	1.9999	1.9966	2.0000	1.9999	2.000	2.000	2.000	2.000	2.000	2.000
RATIOS												
Fe^{2+}	0.5614	0.6125	0.4886	0.4847	0.5501	0.5766	0.4697	0.5957	0.3158	0.5674	0.3779	0.5886
Mg	0.4386	0.3875	0.5114	0.5153	0.4499	0.4234	0.5303	0.4043	0.6842	0.4326	0.6221	0.4114

c - core of zoned amphibole; m - margin of zoned amphibole.

	c	m	c	m	c	m
ANAL	255	254	256	257	259	258
SAMPLE	MA4K1	MA4K1	MA4K1	MA4K1	MD4D6	MD4D6
SiO_2	48.11	42.99	53.28	44.48	52.76	44.02
TiO_2	0.20	0.29	0.15	0.25	1.35	0.41
Al_2O_3	6.89	11.27	2.55	10.87	2.63	12.67
Fe_2O_3	5.97	6.31	0.00	6.88	0.00	2.79
FeO	13.67	15.61	16.66	15.00	14.19	17.88
MnO	0.23	0.28	0.24	0.28	0.21	0.29
MgO	10.37	7.44	11.97	8.07	13.76	7.11
CaO	11.33	11.00	12.16	11.31	12.80	11.68
Na_2O	0.88	1.83	0.51	1.43	0.42	1.47
K_2O	0.16	0.12	0.08	0.19	0.10	0.42
H_2O	2.03	1.98	2.04	2.02	2.06	2.01
TOTAL	99.83	99.13	99.64	100.77	100.30	100.76
Cations per 24 oxygens						
Si	7.110	6.526	7.814	6.610	7.635	6.565
Ti	0.022	0.034	0.016	0.028	0.147	0.046
Al	1.201	2.018	0.441	1.906	0.449	2.228
Fe^{3+}	0.664	0.721		0.770		0.313
Fe^{2+}	1.689	1.982	2.043	1.865	1.718	2.230
Mn	0.029	0.036	0.030	0.035	0.026	0.037
Mg	2.285	1.683	2.617	1.787	2.969	1.580
Ca	1.794	1.790	1.911	1.801	1.986	1.866
Na	0.251	0.540	0.146	0.411	0.119	0.425
K	0.030	0.023	0.015	0.036	0.019	0.079
H	2.000	2.000	1.994	2.000	1.991	2.000
RATIOS						
Fe^{2+}	0.4251	0.5408	0.4385	0.5106	0.3665	0.5853
Mg	0.5749	0.4592	0.5615	0.4894	0.6335	0.4147

c - core of zoned amphibole; m - margin of zoned amphibole.

Rooiwater Igneous Complex: Quartz-Diorite$_c$ Phase. Feldspar$_m$ Feldspar$_o$

ANAL	82	83	84	85	368	369	370	371
SAMPLE	SM12	SM12	SM12	SM12	SM12	SM12	SM12	SM12
SiO_2	69.68	68.59	67.97	67.69	67.28	68.57	68.70	68.91
TiO_2	0.05	0.05	0.03	0.03	0.02	0.01	0.04	0.00
Al_2O_3	19.00	19.56	19.34	19.93	21.05	20.19	19.31	19.80
Cr_2O_3	0.06	0.03	0.06	0.04	na	na	na	na
FeO	0.06	0.08	0.11	0.05	0.39	0.00	0.07	0.04
MnO	0.06	0.04	0.04	0.03	0.01	0.08	0.02	0.00
MgO	0.03	0.01	0.03	0.03	0.05	0.03	0.03	0.03
CaO	0.26	0.25	0.30	0.21	0.68	0.31	0.23	0.23
Na_2O	9.69	11.02	12.63	11.24	11.19	11.24	11.30	11.12
K_2O	0.09	0.10	0.15	0.08	0.73	0.10	0.10	0.10
TOTAL	98.98	99.71	100.66	99.33	101.38	100.53	99.79	100.23
Cations per 8 oxygen								
Si	3.046	2.998	2.970	2.975	2.9209	2.9767	3.0032	2.9958
Ti	0.001	0.002	0.001	0.001	0.0007	0.0002	0.0012	-
Al	0.979	1.008	0.996	1.0331	1.0777	1.0339	0.9958	1.0153
Cr	0.002	0.001	0.002	0.001				
Fe	0.002	0.002	0.004	0.002	0.0141		0.0024	0.0013
Mn	0.002	0.001	0.001	0.001	0.0003	0.0031	0.0006	
Mg	0.002	0.001	0.002	0.002	0.0033	0.0021	0.0020	0.0022
Ca	0.012	0.012	0.014	0.010	0.0315	0.0143	0.0108	0.0105
Na	0.821	1.434	1.070	0.958	0.9417	0.9459	0.9577	0.9370
K	0.005	0.005	0.008	0.005	0.0403	0.0058	0.0056	0.0057
Ca	1.47	1.21	1.27	1.02	0.0311	0.0148	0.0111	0.0110
Na	97.91	98.23	97.96	98.51	0.9292	0.9792	0.9831	0.9829
K	0.62	0.56	0.77	0.47	0.0397	0.0062	0.0058	0.0060

c - core of large feldspar
m - margin
o - overgrowth

Koolwater Igneous Complex: Gabbro Phase: Amphibolite

	c	m	c	m	c	m	c	m	c	m		
ANAL.	351	352	353	354	355	356	357	358	359	360	361	362
SAMPLE	QA1A	QA1A	QA1A	QA1A	QA1A	QA1A	QA1A	QA1A	MD1	MD1	MD1	MD1
SiO_2	41.18	43.53	42.82	42.86	40.13	44.87	40.97	42.34	46.32	46.32	46.22	46.56
TiO_2	0.10	0.31	0.37	0.20	0.37	0.30	0.23	0.30	0.68	0.14	0.10	0.11
Al_2O_3	15.60	11.13	13.79	12.89	17.02	10.65	15.60	12.76	10.65	10.40	11.38	11.51
Fe_2O_3	3.66	2.92	5.37	0.00	0.00	4.63	2.72	2.74	5.14	11.96	2.12	8.68
FeO	14.48	17.34	12.70	19.39	17.96	15.03	15.53	16.93	8.20	2.32	10.84	4.97
MnO	0.23	0.20	0.20	0.20	0.16	0.18	0.21	0.20	0.19	0.21	0.32	0.02
MgO	7.71	7.66	9.02	8.12	6.61	8.77	7.44	7.38	13.20	14.33	12.42	13.20
CaO	11.82	11.43	11.47	13.72	13.70	11.15	11.84	11.34	11.85	11.07	12.06	10.28
Na_2O	1.77	1.66	1.88	1.95	1.92	1.65	1.93	1.93	1.43	1.16	1.90	1.93
K_2O	0.19	0.37	0.07	0.12	0.22	0.33	0.17	0.38	0.14	0.13	0.02	0.15
H_2O	1.99	1.96	2.02	2.00	1.97	2.01	1.98	1.96	2.07	2.10	2.06	2.09
TOTAL	98.72	98.51	99.71	101.46	100.06	99.58	98.62	98.26	99.78	100.14	99.44	99.51
Cations per 24 oxygen												
Si	6.2096	6.6438	6.3523	6.4027	6.0505	6.7092	6.2042	6.4759	6.6883	6.6053	6.7394	6.6823
Ti	0.0114	0.0357	0.0410	0.0229	0.0417	0.0336	0.0266	0.0343	0.0736	0.0155	0.0113	0.0121
Al	2.7740	2.0041	2.4128	2.2714	3.0251	1.8778	2.7871	2.3015	1.8167	1.7490	1.9572	1.9481
Fe^{3+}	0.4158	0.3356	0.5992	-	-	0.5213	0.3100	0.3156	0.5597	1.2839	0.2326	0.9375
Fe^{2+}	1.8258	2.2129	1.5151	2.4229	2.2640	1.8800	1.9668	2.1651	0.9919	0.2770	1.3222	0.5960
Mn	0.0289	0.0257	0.0250	0.0252	0.0206	0.0231	0.0265	0.0257	0.0237	0.0249	0.0390	0.0024
Mg	1.7333	1.7421	1.9939	1.8082	1.4812	1.9549	1.6787	1.6819	2.8464	3.0444	2.6983	2.8216
Ca	1.9091	1.8685	1.8240	2.1959	2.2133	1.7865	1.9207	1.8577	1.8363	1.6912	1.8844	1.5807
Na	0.5170	0.4921	0.5421	0.5641	0.5609	0.4798	0.5666	0.5729	0.4018	0.3194	0.5362	0.5373
K	0.0356	0.0721	0.0126	0.0222	0.0424	0.0623	0.0331	0.0742	0.0257	0.0238	0.0039	0.0269
H	1.9998	2.0000	1.9999	1.9928	1.9824	1.9829	2.0000	2.0000	2.0000	2.0000	2.0000	2.0000
RATIOS												
Fe^{2+}	0.5130	0.5595	0.4413	0.5726	0.6037	0.4902	0.5395	0.5628	0.2584	0.0834	0.3289	0.1744
Mg	0.4870	0.4405	0.5587	0.4274	0.3963	0.5098	0.4605	0.4372	0.7416	0.9166	0.6711	0.8256

ANAL.	372	373
SAMPLE	MD1	MD1
SiO_2	25.78	25.57
TiO_2	0.10	0.04
Al_2O_3	21.62	21.10
Fe_2O_3	0.00	0.01
FeO	17.20	17.09
MnO	0.22	0.32
MgO	20.30	20.13
CaO	0.04	0.05
Na_2O	0.00	0.00
K_2O	0.00	0.00
H_2O	11.55	11.41
TOTAL	96.82	95.73
Cations per 36 oxygen		
Si	5.3536	5.3755
Ti	0.0160	0.0069
Al	5.2947	5.2335
Fe^{3+}		0.0018
Fe^{2+}	2.9880	3.0054
Mn	0.0391	0.0571
Mg	6.2820	6.3092
Ca	0.0097	0.0109
Na		
K		
H	16.00	15.9995
RATIOS		
Fe^{2+}	0.3223	0.3227
Mg	0.6777	0.6773

Rockwater Lyttelton Complex: Stable Phase Continued: Feldspar.

ANAL. SAMPLE	363 MD1	367 MD1	364 MD1	365 MD1	366 MD1	374 MD1	375 MD1
SiO	57.20	56.05	59.27	64.48	62.26	38.91	38.96
TiO_2	0.03	0.01	0.05	0.03	0.03	0.00	0.04
Al_2O_3	27.51	28.09	25.42	23.25	24.03	29.42	30.67
Fe_2O_3						3.47	3.88
FeO	0.14	0.10	0.42	0.14	0.05	0.00	0.78
MnO	0.01	0.00	0.03	0.01	0.02	0.09	0.09
MgO	0.05	0.09	0.06	0.06	0.06	0.06	0.08
CaO	9.13	8.40	6.67	3.65	4.07	27.16	23.42
Na_2O	6.67	7.03	8.16	9.22	9.60	0.10	0.00
K_2O	0.10	0.10	0.10	0.11	0.11	0.02	0.01
H_2O						1.98	1.95
TOTAL	100.84	99.86	100.18	100.95	100.23	101.23	99.90
Cations per 8 oxygen						Cations per 13 oxygen	
Si	2.5474	2.5209	2.6464	2.8145	2.7523	2.9794	2.9953
Ti	0.0011	0.0002	0.0018	0.0010	0.0010		0.0024
Al	1.4450	1.4897	1.3386	1.1971	1.2530	2.6565	2.7811
Fe^{3+}						0.2000	0.2247
Fe^{2+}	0.0052	0.0038	0.0156	0.0050	0.0017	-	0.0502
Mn	0.0005		0.0012	0.0002	0.0009	0.0060	0.0060
Mg	0.0036	0.0057	0.0039	0.0038	0.0039	0.0073	0.0097
Ca	0.4357	0.4046	0.3193	0.1709	0.1930	2.2283	1.9292
Na	0.5757	0.6126	0.7061	0.7805	0.8227	0.0154	-
K	0.0054	0.0059	0.0055	0.0062	0.0064	0.0017	0.0013
Ca	42.85	39.54	30.97	17.85	18.80		
Na	56.62	59.88	68.50	81.51	80.50		
K	0.53	0.58	0.53	0.65	0.62		

N.B. analyses 363, 364, 365 and 367 are from the same feldspar.

ANAL	168	169	170	171	172	173	134	135	136	137	138	141
SAMPLE	MA4J11	MA4J11	MA6J11	MA6J11	MA6J11	MA6J11	MA5J4	MA5J4	MA5J4	MA5J4	MA5J4	MA5J4
SiO_2	25.22	25.34	26.68	26.57	28.38	27.97	27.65	25.04	27.68	26.13	25.94	25.34
TiO_2	0.02	0.02	0.00	0.03	0.01	0.05	0.03	0.04	0.03	0.03	0.02	0.08
Al_2O_3	23.80	23.30	20.87	20.77	21.00	20.63	20.19	20.30	20.10	19.57	20.68	20.21
Fe_2O_3	0.00	0.00	1.64	2.15		0.01		0.67				1.39
FeO	21.03	20.81	13.83	13.64	15.63	15.52	27.86	25.71	26.96	26.04	27.26	27.12
MnO	0.07	0.04	0.04	0.00	0.02	0.02	0.19	0.16	0.19	0.18	0.19	0.22
MgO	18.00	17.38	23.41	23.49	23.45	23.50	15.74	14.81	14.20	15.33	14.54	14.32
CaO	0.02	0.00	0.00	0.00	0.00	0.01	0.00	0.00	0.00	0.00	0.00	0.00
Na_2O	0.00	0.00	0.00	0.00	0.00	0.02	0.00	0.00	0.00	0.01	0.00	0.00
K_2O	0.00	0.00	0.00	0.00	0.00	0.00	0.00	0.00	0.00	0.00	0.00	0.04
H_2O	11.74	11.59	11.88	11.89	12.16	12.04	11.82	11.18	11.55	11.28	11.41	11.34
TOTAL	99.90	98.49	98.36	98.55	100.67	99.78	103.48	97.92	100.72	98.56	100.04	100.04
Cations per 36 oxygens												
Si	5.153	5.245	5.389	5.362	5.597	5.571	5.611	5.371	5.748	5.555	5.456	5.361
Ti	0.003	0.003		0.004	0.002	0.008	0.004	0.006	0.005	0.005	0.003	0.012
Al	5.734	5.688	4.972	4.942	4.885	4.846	4.833	5.137	4.923	4.907	5.131	5.043
Fe^{3+}			0.250	0.327		0.002		0.109				0.221
Fe^{2+}	3.593	3.602	2.336	2.302	2.579	2.585	4.729	4.612	4.682	4.631	4.795	4.800
Mn	0.012	0.007	0.007		0.004	0.004	0.033	0.028	0.033	0.032	0.033	0.039
Mg	5.480	5.362	7.046	7.062	6.892	6.975	4.761	4.736	4.394	4.857	4.553	4.515
Ca	0.004					0.003						
Na						0.006				0.003		
K												0.010
H	16.000	16.000	16.000	16.000	16.000	16.00	15.999	16.00	16.00	15.999	16.00	16.00
RATIOS												
Fe^{2+}	0.3960	0.4018	0.2490	0.2458	0.2723	0.2704	0.4983	0.4934	0.5159	0.4881	0.5127	0.5153
Mg	0.6040	0.5982	0.7510	0.7542	0.7277	0.7296	0.5017	0.5066	0.4841	0.5119	0.4873	0.4847

N.B. Increasing alteration of samples from left to right.

ANAL	148	149	150	166	167	182	183	184	185
SAMPLE	MA6J4	MA6J4	MA6J4	MA7J4a	MA7J4a	MA10J11	MA10J11	MA10J11	MA10J11
SiO_2	24.97	25.10	23.79	26.53	26.66	24.16	24.18	24.52	23.79
TiO_2	0.05	0.02	0.04	0.00	0.01	0.04	0.04	0.09	0.07
Al_2O_3	20.29	19.51	22.32	18.83	18.14	20.39	20.90	21.94	21.02
Fe_2O_3	0.87	1.31	0.97	1.30	1.18	1.18	0.63	1.62	0.00
FeO	26.76	27.21	27.99	21.48	21.47	34.00	34.42	32.15	31.99
MnO	0.11	0.12	0.10	0.13	0.12	0.23	0.26	0.34	0.21
MgO	14.13	13.96	12.76	18.46	18.44	9.01	9.12	11.04	9.94
CaO	0.00	0.01	0.00	0.02	0.03	0.09	0.01	0.01	0.00
Na_2O	0.03	0.00	0.00	0.00	0.00	0.08	0.00	0.00	0.00
K_2O	0.00	0.00	0.00	0.00	0.00	0.00	0.00	0.00	0.00
H_2O	11.18	11.13	11.20	11.43	11.34	10.97	11.03	11.44	10.85
TOTAL	98.38	98.38	99.17	98.19	97.38	100.14	100.58	103.17	97.87
Cations per 36 oxygens									
Si	5.359	5.411	5.095	5.567	5.641	5.285	5.261	5.143	5.261
Ti	0.008	0.003	0.007		0.002	0.006	0.007	0.015	0.012
Al	5.136	4.960	5.639	4.660	4.526	5.261	5.362	5.429	5.482
Fe^{3+}	0.141	0.213	0.157	0.206	0.188	0.194	0.103	0.257	
Fe^{2+}	4.804	4.905	5.013	3.769	3.800	6.219	6.263	5.641	5.917
Mn	0.020	0.022	0.018	0.023	0.021	0.042	0.047	0.061	0.040
Mg	4.520	4.484	4.072	5.771	5.816	2.937	2.956	3.452	3.275
Ca		0.002		0.004	0.006	0.021	0.002	0.002	
Na	0.012					0.036			
K									
H	16.00	16.00	16.00	16.00	16.00	16.00	16.00	16.00	16.00
RATIOS									
Fe^{2+}	0.5153	0.5224	0.5518	0.3951	0.3952	0.6793	0.6794	0.6204	0.6437
Mg	0.4847	0.4776	0.4482	0.6049	0.6048	0.3207	0.3206	0.3796	0.3563

N.B. Increasing alteration of samples from left to right.

J Locality - Massive Sulphides

COARSE SUBHEDRAL PYRITE

SAMPLE MA15J11a

	c	m	c	m	c	m	c	m	c	m	MA15J11d c	m
ANAL	239	240	241	242	243	244	245	246	247	248	252	253
S	53.75	53.14	53.35	53.06	53.02	52.49	53.15	52.72	53.41	53.31	52.64	53.66
Mn	0.00	0.00	0.02	0.00	0.00	0.01	0.00	0.00	0.00	0.01	0.00	0.00
Fe	46.99	47.04	45.93	47.38	47.15	46.64	46.58	46.16	47.04	46.87	46.92	46.56
Co	0.06	0.15	0.15	0.13	0.09	0.22	0.01	0.36	0.05	0.11	0.36	0.14
Ni	0.05	0.02	0.00	0.00	0.06	0.00	0.05	0.00	0.01	0.02	0.03	0.04
Cu	0.06	0.05	0.03	0.01	0.05	0.05	0.04	0.20	0.05	0.10	0.00	0.05
Zn	0.02	0.02	0.00	0.02	0.00	0.50	0.00	0.00	0.09	0.00	0.01	0.02
Se	0.00	0.01	0.00	0.01	0.00	0.00	0.00	0.03	0.00	0.02	0.00	0.00
Ag	0.00	0.02	0.00	0.00	0.00	0.00	0.00	0.00	0.00	0.00	0.00	0.00
TOTAL	100.93	100.45	99.48	100.62	100.38	99.46	99.82	99.29	100.65	100.44	99.97	100.47
Number of atoms												
S	2.0000	1.9999	2.0000	1.9998	2.0000	2.0000	2.0000	1.9996	2.0000	1.9997	2.0000	2.0000
Mn			0.0005			0.0002				0.0003	0.0001	
Fe	1.0037	1.0162	0.9883	1.0249	1.0208	1.0200	1.0061	1.0049	1.0110	1.0094	1.0233	0.9961
Co	0.0013	0.0032	0.0030	0.0028	0.0018	0.0045	0.0002	0.0075	0.0010	0.0022	0.0075	0.0028
Ni	0.0009	0.0005			0.0012		0.0009	0.0004	0.0002	0.0005	0.0006	0.0009
Cu	0.0011	0.0010	0.0006	0.0002	0.0010	0.0009	0.0008		0.0009	0.0019	0.0001	0.0010
Zn	0.0004	0.0004		0.0003		0.0009			0.0017		0.0001	0.0003
Se		0.0001		0.0002				0.0004		0.0003		
Ag		0.0002										

c - core of grain

m - margin

J Locality - Massive Sulphides : Banded Sphalerite + Pyrite

FINE EUHEDRAL PYRITE

SAMPLE	MA6J15c							
ANAL	395	396	401	402	403	406	407	408
S	53.08	52.82	53.00	53.16	52.89	53.02	52.91	52.35
Mn	0.00	0.01	0.01	0.00	0.02	0.01	0.00	0.00
Fe	46.57	46.59	46.48	46.71	46.41	46.71	47.17	47.33
Co	0.19	0.22	0.23	0.19	0.14	0.22	0.40	0.41
Ni	0.00	0.02	0.00	0.00	0.01	0.00	0.04	0.01
Cu	0.01	0.10	0.00	0.26	0.01	0.00	0.03	0.01
Zn	0.17	0.38	0.39	0.98	0.23	0.15	0.46	0.03
Se	0.04	0.03	0.04	0.06	0.00	0.06	0.08	0.07
Ag	0.00	0.01	0.00	0.02	0.00	0.00	0.00	0.01
TOTAL	100.07	100.17	100.15	101.38	99.72	100.16	101.08	100.21
Number of atoms								
S	1.9994	1.9996	1.9994	1.9990	2.0000	1.9991	1.9988	1.9989
Mn		0.0002	0.0002		0.0004	0.0001		
Fe	1.0069	1.0124	1.0064	1.0082	1.0075	1.0110	1.0230	1.0373
Co	0.0039	0.0045	0.0048	0.0039	0.0029	0.0045	0.0082	0.0084
Ni		0.0004			0.0001		0.0008	0.0003
Cu	0.0002	0.0019		0.0048	0.0002		0.0006	0.0001
Zn	0.0032	0.0070	0.0072	0.0180	0.0043	0.0028	0.0085	0.0005
Se	0.0007	0.0004	0.0006	0.0010		0.0009	0.0012	0.0011
Ag		0.0002		0.0003				0.0002

c - core of grain

m - margin

J Locality - Massive Sulphides: Banded Sphalerite + Pyrite

Associated Sieve-Textured Pyrite

SAMPLE	MA6J15c					
	c	m	c	m	c	m
ANAL	397	398	399	400	409	410
S	53.08	52.93	52.78	52.92	52.13	52.71
Mn	0.00	0.00	0.01	0.02	0.00	0.01
Fe	46.70	46.76	46.60	47.02	47.01	46.50
Co	0.06	0.12	0.18	0.14	0.27	0.13
Ni	0.00	0.00	0.03	0.00	0.00	0.00
Cu	0.00	0.00	0.02	0.02	0.02	0.00
Zn	0.16	0.11	0.03	0.19	0.00	0.02
Se	0.02	0.04	0.00	0.07	0.03	0.04
Ag	0.03	0.00	0.03	0.00	0.01	0.01
TOTAL	100.05	99.96	99.68	100.39	99.46	99.42
Number of atoms						
S	1.9997	1.9995	2.0000	1.9989	1.9995	1.9993
Mn			0.0001	0.0003		0.0002
Fe	1.0099	1.0140	1.0135	1.0194	1.0350	1.0124
Co	0.0013	0.0024	0.0036	0.0029	0.0056	0.0026
Ni			0.0006			
Cu			0.0005	0.0004	0.0004	
Zn	0.0030	0.0021	0.0005	0.0036		0.0004
Se	0.0003	0.0005		0.0011	0.0005	0.0007
Ag	0.0003		0.0004		0.0001	0.0001

c - core of grain

m - margin

J Locality - Massive Sulphides

CHALCOPYRITE

SAMPLE	MA16J11b			
ANAL	319	318	325	326
S	34.40	34.68	34.09	34.52
Mn	0.00	0.00	0.02	0.00
Fe	31.67	31.11	31.20	31.06
Co	0.00	0.03	0.14	0.08
Ni	0.00	0.00	0.00	0.00
Cu	34.25	34.07	33.67	33.85
Zn	0.10	0.09	0.13	0.11
Ag	0.06	0.04	0.07	0.04
TOTAL	100.48	100.01	99.34	99.66
Number of atoms				
S	2.0000	2.0000	2.0000	2.0000
Mn			0.0005	
Fe	1.0572	1.0299	1.0508	1.0331
Co	0.0001	0.0008	0.0044	0.0026
Cu	1.0050	0.9913	0.9972	0.9896
Zn	0.0028	0.0026	0.0039	0.0032
Ag	0.0011	0.0007	0.0011	0.0007

SAMPLE	MA9J15d
ANAL	130
S	34.35
Mn	na
Fe	30.54
Cu	33.72
Zn	0.48
Ag	0.03
Sb	0.00
Te	0.03
Bi	0.00
Pb	0.11
Cd	0.00
As	0.00
Se	0.04
TOTAL	99.30

S	2.0000
Fe	1.0207
Cu	0.9907
Zn	0.0138
Ag	0.0005
Sb	
Te	0.0004
Bi	
Pb	0.0009
Cd	
As	
Se	0.0010

J Locality - Massive Sulphides

PYRRHOTITE

SAMPLE	MA16J116				SAMPLE	MA17J11
ANAL	316	317	327	328	ANAL	91
S	38.84	38.70	38.82	38.65	S	38.16
Mn	0.00	0.02	0.01	0.04	Mn	0.02
Fe	60.90	60.47	59.75	59.81	Fe	60.22
Co	0.13	0.13	0.19	0.10	Co	0.14
Ni	0.00	0.00	0.00	0.01	Ni	0.01
Cu	0.60	1.26	0.43	0.46	Cu	0.06
Zn	0.03	0.01	0.04	0.00	Zn	0.55
Ag	0.03	0.03	0.01	0.03	Se	0.15
					Ag	0.04
TOTAL	100.52	100.62	99.24	99.11	Cd	0.01
					Pb	0.00
					TOTAL	99.35
Number of atoms						
S	1.0000	1.0000	1.0000	1.0000		
Mn		0.0003	0.0001	0.0007		
Fe	0.8999	0.8969	0.8834	0.8883		
Co	0.0018	0.0019	0.0026	0.0014		
Ni				0.0001		
Cu	0.0078	0.1650	0.0056	0.0060		
Zn	0.0004	0.0001	0.0005			
Ag	0.0002	0.0002	0.0001	0.0003		

J Locality - Massive Sulphides

SPHALERITE

SAMPLE	MA16J11a										
ANAL	97	98	99	100	101	102	103	105	106	107	108
S	33.01	33.19	33.01	33.63	32.81	33.10	33.28	32.14	32.35	33.20	33.18
Mn											
Fe	8.46	8.04	9.24	6.97	7.18	8.82	8.91	8.07	7.58	8.08	9.15
Co											
Ni											
Cu											
Zn	57.58	58.39	57.96	60.95	60.13	57.88	58.64	58.80	59.27	58.19	57.73
Se				0.00	0.00	0.00	0.00	0.24	0.00		
Ag											
Cd				0.00	0.00	0.00	0.00	0.00	0.00		
Pb											
TOTAL	99.05	99.62	100.22	100.55	100.12	99.80	100.83	99.25	99.21	99.47	100.06

N.B. Sphalerite in equilibrium with hexagonal pyrrhotite.

J Locality - Massive Sulphide (continued)

SPAHLERITE

SAMPLE	MA16J11a					
ANAL	109	110	112	113	115	116
S	32.63	32.84	32.59	32.54	32.43	33.01
Mn						
Fe	8.08	7.46	6.44	7.67	7.99	7.71
Co						
Ni						
Cu						
Zn	58.81	59.63	60.63	58.87	59.62	59.70
Se						
Ag						
Cd						
Pb						
TOTAL	99.52	99.93	99.65	99.08	100.03	100.42

N.B. Sphalerite in equilibrium with hexagonal pyrrhotite.

J Locality - Massive Sulphides

MAGNETITE

SAMPLE MA15J11d

	c	m	c	m	
ANAL	378	379	380	381	382
SiO_2	0.01	0.02	0.03	0.03	0.02
TiO_2	0.13	0.06	0.10	0.08	0.06
Al_2O_3	0.09	0.07	0.02	0.00	0.00
V_2O_3	0.00	0.03	0.04	0.05	0.00
Cr_2O_3	0.02	0.03	0.08	0.00	0.00
Fe_2O_3	69.42	69.19	68.83	67.89	68.13
FeO	31.52	31.36	31.26	30.77	30.79
MnO	0.01	0.00	0.01	0.00	0.00
MgO	0.02	0.00	0.01	0.00	0.01
TOTAL	101.22	100.75	100.37	98.81	99.02
Cations per 4 oxygen					
Si	0.0004	0.0009	0.0010	0.0010	0.0009
Ti	0.0036	0.0016	0.0028	0.0023	0.0018
Al	0.0042	0.0031	0.0011		
V		0.0008	0.0011	0.0015	
Cr	0.0005	0.0009	0.0025		
Fe^{3+}	1.9873	1.9902	1.9877	1.9918	1.9946
Fe^{2+}	1.0028	1.0025	1.0031	1.0033	1.0020
Mn	0.0003		0.0004		
Mg	0.0009		0.0004		0.0006

MGZ LOCALITY - Massive Sulphide Unit

PYRRHOTITE

SAMPLE	SM3P4a		c	m	SM5P4		
ANAL	293	294	295	296	313	314	315
S	38.57	38.29	38.67	38.83	37.95	37.82	37.65
Mn	0.00	0.00	0.00	0.00	0.00	0.00	0.00
Fe	61.36	61.47	61.35	60.99	61.11	61.27	61.66
Co	0.07	0.07	0.14	0.13	0.22	0.21	0.07
Ni	0.00	0.01	0.02	0.00	0.03	0.03	0.01
Cu	0.00	0.00	0.01	0.03	0.03	0.00	0.00
Zn	0.00	0.00	0.14	0.00	0.00	0.00	0.00
Ag	0.00	0.02	0.00	0.00	0.00	0.04	0.01
Cd	0.00	0.02	0.00	0.02	na	na	na
TOTAL	100.01	99.88	100.33	100.01	99.34	99.38	99.39
Number of atoms							
S	1.0000	1.0000	1.0000	1.0000	1.0000	1.0000	1.0000
Mn							
Fe	0.9132	0.9215	0.9106	0.9016	0.9243	0.9299	0.9400
Co	0.0010	0.0010	0.0019	0.0018	0.0031	0.0030	0.0011
Ni		0.0001	0.0002		0.0005	0.0005	0.0001
Cu			0.0001	0.0004	0.0004		
Zn			0.0018				
Ag		0.0002				0.0003	
Cd		0.0002		0.0002			

c - core of grain

m - margin

MGZ LOCALITY - Massive Sulphide Unit (continued)

CHALCOPYRITE

SAMPLE	SM3P4a				SM5P4			
ANAL	297	298	299	300	309	310	311	312
S	34.35	34.55	34.42	35.20	35.19	35.45	34.26	34.12
Mn	0.04	0.048	0.03	0.00	0.00	0.01	0.01	0.00
Fe	30.72	30.69	30.54	31.10	31.27	31.65	31.04	30.75
Co	0.07	0.11	0.07	0.12	0.09	0.05	0.00	0.00
Ni	0.00	0.08	0.07	0.10	0.04	0.04	0.00	0.01
Cu	33.06	32.82	33.31	33.53	33.65	33.22	34.37	34.32
Zn	0.18	0.76	0.84	0.19	0.10	0.06	0.12	0.14
Ag	0.00	0.05	0.07	0.01	0.06	0.09	0.07	0.04
Cd	0.00	0.00	0.00	0.00	na	na	na	na
TOTAL	98.41	99.12	99.35	100.25	100.39	100.56	99.84	99.38
Number of atoms								
S	2.0000	2.0000	2.0000	2.0000	2.0000	2.0000	2.0000	2.0000
Mn	0.0014	0.0016	0.0010			0.005	0.0004	0.0001
Fe	1.0268	1.0197	1.0189	1.0143	1.0201	1.0248	1.0400	1.0349
Co	0.0022	0.0035	0.0023	0.0036	0.0028	0.0015		
Ni	0.0038	0.0025	0.0022	0.0031	0.0013	0.0011		0.0004
Cu	0.9712	0.9590	0.9766	0.9614	0.9650	0.9457	1.0123	1.0152
Zn	0.0052	0.0215	0.0240	0.0054	0.0028	0.0017	0.0034	0.0040
Ag		0.0009	0.0012	0.0002	0.0009	0.0014	0.0008	0.0006
Cd								

c - core of grain

m - margin

MGZ LOCALITY - Massive Sulphide Unit (continued)

SPHALERITE

SAMPLE	SM3P4a				SM5P4			
ANAL	301	302	303	304	305	306	307	308
S	33.78	34.19	33.53	33.90	33.50	33.67	33.42	33.48
Mn	0.02	0.06	0.04	0.14	0.05	0.09	0.05	0.06
Fe	6.82	7.13	6.86	7.01	6.09	6.57	6.49	7.25
Co		na	na	na	na	na	na	na
Ni		na	na	na	na	na	na	na
Cu	0.00	0.00	0.00	0.00	0.13	0.00	0.07	0.02
Zn	59.27	59.50	58.54	58.62	60.11	59.71	60.05	59.63
Ag	0.01	0.01	0.00	0.00	0.01	0.00	0.00	0.00
Cd	0.00	0.00	0.00	0.00	0.00	0.00	0.00	0.00
TOTAL	99.90	100.89	98.98	99.67	99.89	100.05	100.09	100.43
S	1.0000	1.0000	1.0000	1.0000	1.0000	1.0000	1.0000	1.0000
Mn	0.0003	0.0011	0.0008	0.0024	0.0008	0.0015	0.0009	0.0010
Fe	0.1159	0.1197	0.1175	0.1186	0.1044	0.1121	0.1114	0.1243
Co								
Ni								
Cu					0.0020		0.0011	0.0003
Zn	0.8604	0.8537	0.8564	0.8481	0.8802	0.8698	0.8812	0.8737
Ag	0.0001	0.0001			0.0001			
Cd								

c - core of grain

m - margin

L-W Locality - Sphalerite

	IN QUARTZ BANDS				ENCLOSED IN GARNET				DISSEMINATED AWAY FROM GARNET	
SAMPLE	MA17W2				MA23W2				MA23W2	
ANAL	266	267	268	269	271	272	270	273	274	275
S	32.96	33.11	33.14	32.87	32.69	33.33	33.58	33.26	32.94	33.46
Mn	0.13	0.11	0.10	0.12	0.39	0.39	0.14	0.38	0.07	0.07
Fe	5.94	5.80	5.68	5.47	6.65	6.81	6.63	6.81	6.32	6.41
Cu	0.02	0.01	0.00	0.00	0.00	0.01	0.00	0.00	0.04	0.00
Zn	61.12	61.47	60.24	60.65	59.79	59.44	59.32	60.00	60.49	60.82
Se	0.00	0.00	0.02	0.00	0.00	na	0.00	na	na	na
Cd	0.00	0.00	0.00	0.00	0.00	na	0.00	na	na	na
Sn	0.08	0.00	0.00	0.01	0.00	na	0.00	na	na	na
TOTAL	100.24	100.51	99.17	99.12	99.52	99.98	99.66	100.44	99.85	100.77
Number of Atoms										
S	1.0000	1.0000	0.9998	1.0000	1.0000	1.0000	1.0000	1.0000	1.0000	1.0000
Mn	0.0024	0.0019	0.0017	0.0021	0.0070	0.0068	0.0024	0.0067	0.0012	0.0013
Fe	0.1034	0.1006	0.0983	0.0956	0.1168	0.1173	0.1133	0.1175	0.1101	0.1100
Cu	0.0003	0.0002				0.001			0.005	
Zn	0.9095	0.9105	0.8914	0.9050	0.8971	0.8747	0.8663	0.8848	0.9099	0.8915
Se			0.0002							
Cd										
Sn	0.0006			0.0001						

APPENDIX C

WHOLE ROCK ANALYSES

C1 Sample Preparation

Between 100 and 200 gm of the finely powdered sample were pressed into briquettes using a hydraulic ram operating at 7 tons/sq. inch. A few drops of "Mowiol" were used as a binder.

C2 Operating Conditions

The briquettes were analysed by X-ray fluorescence using a Philips PW1400 Spectrometer with a Rhodium tube. This enabled both major and trace elements to be analysed simultaneously. The operating conditions for the various elements are presented in the accompanying table.

C3 Results

Analytical results were compiled on a water-free basis, normalised to 100%, and are presented in the following tables. The total iron content is calculated as Fe_2O_3.

Element	Line	Collimator (1)	Detector (2)	Crystal (3)	Upper Level	Lower Level	KV	mA	Angle	Background +	Background - (Offset)
Na	KA	C	F	4	75	30	35	80	55.165	3.50	0.00
Mg	KA	C	F	4	70	35	35	80	45.220	2.40	0.00
Al	KA	C	F	3	75	30	35	80	145.225	0.00	0.00
Si	KA	C	F	3	80	25	35	80	109.230	0.00	0.00
P	KA	C	F	5	70	30	70	40	141.100	2.40	0.00
S	KA	C	F	3	75	30	60	50	75.890	1.20	0.00
K	KA	C	F	2	70	30	35	80	136.820	0.00	0.00
Ca	KA	C	F	2	70	30	35	80	113.280	0.00	0.00
Ti	KA	C	F	2	75	30	35	80	86.275	0.00	0.00
Mn	KA	C	F	1	70	40	50	60	95.320	2.00	0.00
Fe	KA	F	F	2	70	35	35	80	57.635	0.00	0.00
Ni	KA	C	S	1	75	25	80	35	71.280	2.00	1.50
Cu	KA	C	S	1	70	30	80	35	65.575	1.00	0.80
Zn	KA	C	S	1	60	40	80	35	60.615	1.10	1.30
Rb	KA	C	S	1	60	40	90	30	37.990	1.70	1.00
Sr	KA	C	S	1	60	40	90	30	35.845	1.00	1.00
Y	KA	C	S	1	60	40	90	30	33.905	1.00	0.90
Zr	KA	C	S	1	60	40	90	30	32.095	0.90	1.20
Nb	KA	C	S	1	60	40	90	30	30.450	0.50	0.00
Ba	KA	F	S	1	60	40	90	30	15.575	1.50	0.90
La	LA	C	F	1	70	30	35	80	139.095	2.00	2.00
Ce	LA	C	F	1	70	30	35	80	111.840	2.00	2.00

(1) C - coarse; F - fine.

(2) F - flow; S - scintillometer

(3) 1 - LiF_{220}
2 - LiF_{200}
3 - PET
4 - ThAP
5 - Ge

Table of Operating Conditions for PW1400 X-ray Spectrometer

Rubbervale Subgroup: Flows, low Na, high K/K+Na

Sample (wt%)	RV7	CD18	MA1	MA1L2	MA1J21
SiO_2	67.29	68.74	72.55	76.37	76.48
Al_2O_3	15.71	15.61	14.52	14.43	12.41
Fe_2O	8.19	8.31	8.71	4.09	4.98
MgO	5.93	4.88	0.78	1.65	3.82
CaO	0.00	0.00	0.00	0.00	0.00
Na_2O	0.09	0.17	0.15	0.24	0.14
K_2O	2.38	1.77	2.85	2.99	1.90
TiO_2	0.30	0.41	0.26	0.18	0.22
MnO	0.05	0.02	0.16	0.04	0.02
S	0.01	0.01	0.01	0.00	0.00
P_2O_5	0.06	0.09	0.02	0.01	0.02
TOTAL	100.01	100.01	100.01	100.00	99.99
ppm					
Ba	510	625	523	661	359
Nb	24	31	53	48	47
Zr	569	638	789	657	710
Y	134	123	158	145	142
Sr	9	11	4	4	9
Rb	27	20	23	29	25
Zn	128	22	443	197	56
Cu	5	10	41	43	46
Ni	12	8	8	15	12
Cr	40	61	47	28	37
La	6	51	3	59	88
Ce	64	117	41	86	180

Rubbervale Subgroup: Flows, high Na, low K/K+Na

Sample (wt%)	SM17	SM4	GE3	GE5	GE8	RV1	MA3W1
SiO_2	77.14	73.29	71.87	72.34	73.43	74.57	74.48
Al_2O_3	11.39	12.95	12.32	12.31	12.59	12.10	12.67
Fe_2O_3	4.54	4.32	6.19	4.71	4.33	4.36	4.20
MgO	1.46	1.92	2.34	0.97	1.00	0.55	1.26
CaO	0.00	0.61	1.04	2.20	1.05	0.32	0.21
Na_2O	5.09	3.81	4.63	6.42	6.51	5.97	4.93
K_2O	0.03	2.72	0.42	0.06	0.14	1.53	1.89
TiO_2	0.24	0.28	0.81	0.73	0.71	0.43	0.28
MnO	0.09	0.06	0.05	0.08	0.06	0.10	0.03
S	0.00	0.02	0.16	0.01	0.01	0.02	0.03
P_2O_5	0.02	0.02	0.18	0.18	0.18	0.06	0.02
TOTAL	100.00	100.00	100.01	100.01	100.01	100.01	100.00
ppm							
Ba	33	493	197	69	82	264	455
Nb	30	74	66	64	71	52	68
Zr	545	815	765	781	701	814	900
Y	122	437	313	292	295	215	262
Sr	31	24	56	49	35	26	22
Rb	1	36	7	1	3	21	22
Zn	150	177	77	46	89	84	190
Cu	5	24	8	3	11	6	20
Ni	13	24	19	19	15	13	19
Cr	35	36	46	31	36	25	13
La	39	129	83	83	83	56	68
Ce	121	221	198	203	211	147	191

Rubbervale Subgroup: Tuffs

Sample (wt%)	SM1S9	SM3S9	SM6	SM10	SM11	MD1D2	GE114	RV5	RV6	CD23	MA2
SiO_2	72.82	68.46	68.55	61.39	66.27	70.98	69.58	67.53	66.18	75.04	73.62
Al_2O_3	12.08	14.29	17.45	17.68	14.07	12.12	11.77	17.28	17.36	14.77	12.84
Fe_2O_3	3.31	6.84	7.21	8.95	8.40	7.73	6.68	5.13	4.59	2.37	6.72
MgO	1.62	2.57	3.63	8.47	10.80	4.21	1.14	7.12	9.00	4.88	4.96
CaO	2.50	1.46	0.00	0.21	0.00	0.66	4.18	0.00	0.00	0.00	0.00
Na_2O	6.22	1.79	0.23	0.15	0.07	3.14	5.58	0.28	0.21	0.65	0.22
K_2O	0.16	2.80	2.45	1.85	0.03	0.07	0.00	2.34	2.22	1.97	1.27
TiO_2	0.87	0.93	0.40	0.98	0.25	0.80	0.74	0.22	0.37	0.26	0.22
MnO	0.04	0.07	0.03	0.04	0.02	0.06	0.11	0.02	0.02	0.01	0.04
S	0.11	0.59	0.01	0.06	0.03	0.01	0.01	0.01	0.00	0.01	0.08
P_2O_5	0.26	0.22	0.04	0.22	0.07	0.22	0.20	0.07	0.04	0.04	0.03
TOTAL	99.99	100.02	100.00	100.00	100.01	100.00	99.99	100.00	99.99	100.00	100.00
ppm											
Ba	48	1153	663	398	41	26	30	735	401	583	350
Nb	39	36	60	34	26	33	45	25	35	30	45
Zr	601	521	985	621	520	558	828	617	609	575	718
Y	164	143	197	176	97	155	211	136	79	109	146
Sr	55	59	8	15	7	44	59	10	15	16	4
Rb	3	39	23	17	2	2	2	24	26	22	16
Zn	21	112	30	56	14	227	137	47	43	0	129
Cu	14	21	4	9	1	8	0	8	2	4	9
Ni	19	53	16	19	0	16	27	11	8	5	10
Cr	53	198	56	48	14	43	19	73	44	12	28
La	19	29	21	66	14	43	9	1	23	41	3
Ce	86	92	93	168	39	125	24	139	152	78	14

Rubbervale Subgroup: Tuffs

Sample (wt%)	MA3	MA29	RW2
SiO_2	67.85	66.24	77.79
Al_2O_3	17.47	18.31	13.54
Fe_2O_3	6.58	5.86	2.71
MgO	4.87	6.38	3.21
CaO	0.00	0.00	0.00
Na_2O	0.31	0.28	0.64
K_2O	2.48	2.45	1.65
TiO_2	0.32	0.39	0.31
MnO	0.02	0.04	0.01
S	0.01	0.00	0.05
P_2O_5	0.10	0.05	0.09
TOTAL	100.01	100.00	100.00
ppm			
Ba	1009	168	
Nb	51	68	
Zr	916	944	
Y	182	295	
Sr	13	9	
Rb	23	28	
Zn	11	159	
Cu	5	5	
Ni	15	14	
Cr	10	36	
La	67	75	
Ce	150	204	

Rubbervale Subgroup: Transition Zone above the sulphide horizon at the MGZ locality.

Sample (wt%)	SM5S9	SM6S9	SM16S3
SiO_2	67.22	71.36	73.21
Al_2O_3	11.40	12.57	12.74
Fe_2O_3	7.44	6.23	5.56
MgO	2.54	3.06	2.69
CaO	3.75	1.53	0.00
Na_2O	4.85	3.23	5.26
K_2O	0.35	1.14	0.16
TiO_2	0.81	0.63	0.28
MnO	0.08	0.06	0.08
S	1.37	0.03	0.00
P_2O_5	0.19	0.15	0.04
TOTAL	100.00	99.99	100.02
ppm			
Ba	101	326	55
Nb	51	63	31
Zr	654	728	571
Y	249	248	122
Sr	65	50	31
Rb	7	15	3
Zn	137	103	242
Cu	67	3	13
Ni	21	14	16
Cr	48	43	49
La	63	58	55
Ce	171	163	123

Rubbervale Subgroup: Transition Zone, "aluminous cherts" from hole MW2.

Sample (wt%)	MA10W2	MA9W2	MA8W2	MA7W2	MA2W2	MA3W2	MA4W2	MA5W2	MA6W2	MA11W2	MA12W2
SiO_2	74.19	70.94	72.02	68.41	70.19	69.31	70.09	68.40	71.85	71.33	48.09
Al_2O_3	14.40	14.33	15.57	16.68	14.96	14.84	16.32	16.20	15.55	15.20	12.18
Fe_2O_3	3.69	7.19	5.12	8.26	8.21	8.46	6.25	7.40	6.06	6.81	17.30
MgO	0.79	1.29	1.30	1.96	1.90	3.19	3.08	2.35	2.06	2.07	6.09
CaO	0.11	0.00	0.02	0.00	0.00	0.00	0.00	0.80	0.00	0.00	10.88
Na_2O	3.54	0.28	2.18	0.20	0.29	0.22	0.24	0.28	0.39	0.41	2.10
K_2O	2.86	3.70	2.81	3.39	2.84	2.46	3.15	3.13	2.97	2.82	0.01
TiO_2	0.32	0.29	0.33	0.33	0.28	0.27	0.29	0.31	0.28	0.26	2.13
MnO	0.04	0.09	0.10	0.20	0.20	0.26	0.14	0.21	0.16	0.21	0.57
S	0.03	1.84	0.51	0.54	1.10	0.96	0.41	0.89	0.65	0.86	0.13
P_2O_5	0.04	0.05	0.04	0.04	0.03	0.03	0.03	0.03	0.03	0.03	0.52
TOTAL	100.01	100.00	100.00	100.01	100.00	100.00	100.00	100.00	100.00	100.00	100.00
ppm											
Ba	873	760	467	473	556	528	485	422	442	496	5
Nb	63	47	63	58	51	50	52	56	53	50	13
Zr	900	725	932	857	761	771	826	836	774	767	260
Y	214	157	253	210	200	193	216	246	227	176	58
Sr	24	14	20	10	9	8	11	17	11	11	41
Rb	57	53	42	46	35	31	41	37	37	34	1
Zn	160	2741	2014	2323	5754	4024	1614	2331	3632	7607	424
Cu	16	37	73	24	95	93	42	171	103	256	44
Ni	17	7	18	12	15	13	19	14	17	13	45
Cr	15	26	20	20	21	28	30	20	24	20	45
La	60	60	57	86	87	86	97	105	78	53	12
Ce	170	173	159	210	206	212	223	238	205	155	70

Rubbervale Subgroup: Transition Zone, "aluminous cherts" from hole MW2 (continued).

Sample (wt%)	MA13W2	MA14W2	MA15W2	MA16W2
SiO_2	68.22	73.28	68.82	71.98
Al_2O_5	18.20	15.38	15.82	17.30
Fe_2O_3	6.95	5.10	6.92	1.68
MgO	1.99	1.28	0.97	0.46
CaO	0.00	0.00	0.00	0.00
Na_2O	0.29	0.43	1.05	1.16
K_2O	3.60	3.43	3.26	4.29
TiO_2	0.29	0.25	0.25	0.30
MnO	0.19	0.10	0.10	0.03
S	0.26	0.74	2.80	2.79
P_2O_5	0.02	0.02	0.01	0.02
TOTAL	100.01	100.01	100.00	100.01
ppm				
Ba	514	443	393	406
Nb	65	51	52	59
Zr	1022	823	798	908
Y	192	187	198	194
Sr	13	12	17	15
Rb	49	46	42	53
Zn	395	2245	10200	38000
Cu	78	117	152	60
Ni	18	15	15	12
Cr	18	24	30	30
La	44	73	73	36
Ce	146	190	194	128

N.B. Sampled at 2 m intervals from base of Transition Zone to sphalerite-bearing chert, below the acid porphyries.

Rubbervale Subgroup: Transition Zone, "aluminous cherts" above the massive sulphides at the J Locality.

Sample (wt%)	MA22J11	MA2J25	MA3J38
SiO_2	67.98	72.68	65.92
Al_2O_3	17.10	14.40	14.12
Fe_2O_3	6.28	3.87	7.15
MgO	4.65	1.89	1.90
CaO	0.00	1.87	5.83
Na_2O	0.33	2.27	0.32
K_2O	3.21	2.50	3.69
TiO_2	0.31	0.30	0.43
MnO	0.04	0.09	0.14
S	0.05	0.09	0.45
P_2O_5	0.04	0.05	0.06
TOTAL	99.99	100.01	100.01
ppm			
Ba	548	494	565
Nb	55	29	24
Zr	503	484	368
Y	225	121	96
Sr	15	40	82
Rb	49	43	71
Zn	139	432	3172
Cu	8	10	315
Ni	39	17	91
Cr	39	14	91
La	72	44	30
Ce	150	85	65

Rubbervale Subgroup: Acid Porphyries from the J locality

Sample (wt%)	MA1J1	MA1J2	MA1J3	MA1AJ4	MA1J5A	MA1J7	MA1J8	MA1J10	MA1J11	MA1J15	MA1J16
SiO_2	71.60	70.40	73.07	71.81	71.80	71.16	70.86	73.72	71.30	69.89	71.59
Al_2O_3	13.05	13.28	12.47	11.77	12.67	12.90	13.57	10.33	11.58	13.44	13.22
Fe_2O_3	5.16	6.68	6.05	5.45	4.77	5.42	5.82	5.95	4.85	6.65	6.51
MgO	2.92	4.32	2.53	1.88	3.42	3.99	4.08	2.86	3.51	5.14	4.47
CaO	1.38	0.00	0.00	1.97	1.23	2.18	0.08	0.79	2.77	0.06	0.00
Na_2O	2.63	3.34	4.50	4.92	4.34	1.53	2.64	4.04	4.41	2.05	1.10
K_2O	1.98	0.85	0.27	0.35	0.62	1.90	1.23	0.37	0.38	1.09	1.66
TiO_2	0.64	0.65	0.67	0.64	0.64	0.51	0.67	0.85	0.63	0.68	0.64
MnO	0.06	0.09	0.07	0.05	0.06	0.03	0.06	0.08	0.09	0.06	0.07
S	0.45	0.29	0.25	1.03	0.34	0.27	0.87	0.62	0.38	0.81	0.65
P_2O_5	0.12	0.10	0.12	0.12	0.11	0.12	0.11	0.40	0.11	0.12	0.10
TOTAL	99.99	100.00	100.00	99.99	100.00	100.01	99.99	100.01	100.01	99.99	100.01
Ba	534	193	336		193	365	185	63	100	122	257
Nb	52	52	48		53	49	56	31	53	52	52
Zr	646	646	667		667	638	692	444	640	649	643
Y	186	199	178		217	192	221	167	208	176	217
Sr	36	22	26		34	34	23	35	53	24	16
Rb	28	14	7		12	31	22	18	7	21	26
Zn	239	0	3354		218	339	2196	412	169	1153	3114
Cu	8	3	14		10	59	98	19	15	53	83
Ni	16	20	9		13	12	13	13	14	14	13
Cr	10	62	13		7	12	13	83	14	19	10
La	54	63	79		67	51	68	44	77	60	57
Ce	128	139	168		150	117	168	97	166	137	127

Rubbervale Subgroup: Acid Porphyries from the J locality

Sample (wt%)	MA1J18	MA1J22	MA1J23	MA1J24	MA1J25	MA1J26	MA1J27	MA2J29	MA1J30	MA1J31	MA1J36	MA1J37
SiO_2	69.56	71.51	72.45	70.68	73.87	71.67	70.87	71.09	71.33	71.55	69.32	69.71
Al_2O_3	13.81	12.79	11.22	12.85	14.06	12.95	12.02	12.55	13.51	11.61	13.64	12.86
Fe_2O_3	6.57	4.75	5.03	6.92	3.94	5.89	6.00	6.00	5.40	5.77	6.67	6.74
MgO	3.50	3.15	1.74	2.69	2.03	3.17	3.32	2.63	3.46	2.00	1.65	2.00
CaO	0.31	1.97	2.86	0.87	0.08	0.53	0.53	1.84	0.37	2.04	2.73	1.72
Na_2O	1.93	4.42	5.37	4.34	2.58	1.75	4.92	3.28	3.10	4.21	3.11	4.36
K_2O	1.87	0.54	0.34	0.36	2.18	1.89	0.10	1.31	1.63	0.72	1.90	1.55
TiO_2	0.63	0.64	0.65	0.69	0.57	0.63	0.62	0.67	0.68	0.65	0.78	0.77
MnO	0.09	0.04	0.08	0.08	0.07	0.06	0.05	0.08	0.05	0.09	0.05	0.06
S	1.61	0.07	0.14	0.40	0.52	1.35	1.46	0.43	0.38	1.24	0.04	0.12
P_2O_5	0.11	0.12	0.11	0.12	0.09	0.10	0.12	0.12	0.10	0.12	0.12	0.13
TOTAL	99.99	100.00	99.99	100.00	99.99	99.99	100.00	100.00	100.01	100.00	100.01	100.02
ppm												
Ba		99	120	481	395	289	31	572	447	84	415	492
Nb		55	52	51	40	52	54	52	56	49	60	65
Zr		680	658	659	850	658	656	646	705	609	687	682
Y		224	218	190	261	204	209	201	230	201	260	248
Sr		33	55	38	26	23	30	57	25	32	51	80
Rb		12	9	7	40	30	6	15	31	13	27	19
Zn		122	357	1316	3048	792	655	269	3896	937	45	103
Cu		7	10	97	24	74	57	41	14	47	91	13
Ni		14	13	13	23	16	13	17	20	14	15	13
Cr		21	21	15	15	9	45	19	14	8	15	10
La		69	76	69	51	70	66	59	85	51	71	65
Ce		157	158	154	114	147	150	142	179	125	191	187

BASIC SILLS

Sample (wt%)	SM7S9	SM17S3	SM4Θ1	MD3D2	MD4D2	CD4	MA25	MA1K1	MA4K1	MA7J11	MA21J11
SiO_2	46.47	47.16	49.52	47.76	47.76	49.68	49.52	44.52	48.33	45.66	47.21
Al_2O_3	14.34	12.03	12.43	11.82	11.34	13.74	13.77	13.76	12.07	12.70	13.27
Fe_2O_3	17.71	17.82	16.72	18.65	19.17	14.86	16.31	17.76	18.11	16.94	18.00
MgO	8.26	6.40	6.82	7.50	7.32	7.75	8.41	11.09	6.03	8.87	6.69
CaO	8.36	10.91	9.78	9.91	8.89	8.71	7.79	9.14	8.77	11.72	9.21
Na_2O	2.11	2.51	2.76	1.59	1.91	3.53	1.64	1.80	3.07	2.01	3.34
K_2O	0.02	0.00	0.11	0.12	0.15	0.15	0.06	0.00	0.06	0.00	0.00
TiO_2	1.10	2.28	1.15	1.73	2.63	1.04	1.68	1.20	2.49	1.70	1.44
MnO	0.17	0.21	0.18	0.20	0.20	0.24	0.21	0.21	0.18	0.19	0.22
S	1.02	0.07	0.05	0.23	0.02	0.01	0.01	0.09	0.27	0.01	0.25
P_2O_5	0.42	0.62	0.48	0.50	0.61	0.27	0.61	0.43	0.62	0.19	0.37
TOTAL	99.98	100.01	100.01	100.01	100.00	99.98	100.01	100.00	100.00	99.99	100.00
ppm											
Ba	29	15	23	33	47	239	77	15	30	4	12
Nb	5	12	8	6	9	4	6	5	9	6	5
Zr	179	269	209	171	192	155	247	134	192	102	160
Y	37	65	45	37	51	28	38	27	52	27	34
Sr	134	89	118	146	117	156	150	67	116	139	103
Rb	1	0	1	1	2	4	2	1	2	1	0
Zn	283	107	137	124	148	113	133	103	114	211	147
Cu	168	49	84	147	44	96	88	97	96	53	84
Ni	84	56	73	87	90	118	133	174	76	74	63
Cr	101	44	81	42	59	78	154	296	89	147	79
La	6	16	9	8	7	10	6	0	8	5	8
Ce	39	69	56	44	46	41	47	33	55	36	51

MGZ Locality - Footwall Tuffs, Hole MS1

Sample (wt%)	SM1S1	SM2S1	SM2S1	SM4S1	SM5S1	SM6S1	SM7S1	SM8S1	SM9S1	SM10S1	SM11S1	SM12S1
SiO_2	66.95	63.90	62.29	62.37	60.92	62.38	63.69	60.04	52.77	55.85	61.42	31.47
Al_2O_3	12.85	15.70	16.70	16.98	15.11	16.48	14.63	16.07	17.98	16.66	14.16	22.24
Fe_2O_3	8.49	8.83	8.96	8.87	10.89	9.39	10.45	12.07	17.17	17.07	15.47	22.04
MgO	8.81	8.63	8.64	8.56	11.19	8.64	9.03	9.62	10.09	8.80	7.64	20.68
CaO	0.18	0.14	0.18	0.15	0.15	0.18	0.11	0.13	0.41	0.19	0.12	1.34
Na_2O	1.74	0.07	0.34	0.11	0.02	0.10	0.03	0.05	0.01	0.00	0.00	0.00
K_2O	0.00	1.53	1.62	1.73	0.48	1.56	0.93	0.87	0.44	0.48	0.36	0.04
TiO_2	0.69	0.94	0.99	0.99	0.99	1.00	0.88	0.89	0.74	0.66	0.58	0.71
MnO	0.07	0.05	0.04	0.04	0.05	0.05	0.07	0.06	0.06	0.05	0.06	0.18
S	0.01	0.01	0.01	0.00	0.01	0.01	0.00	0.01	0.01	0.01	0.01	1.11
P_2O_5	0.20	0.20	0.22	0.21	0.20	0.22	0.18	0.19	0.33	0.25	0.17	0.18
TOTAL	99.99	100.00	99.99	100.01	100.01	100.01	100.00	100.00	100.01	100.02	99.99	99.99
ppm												
Ba	11	551	446	401	106	382	239	194	87	128	163	0
Nb	28	35	36	34	32	34	30	30	26	28	26	38
Zr	459	536	606	587	562	584	523	553	685	673	508	846
Y	124	178	172	167	144	145	79	119	117	153	148	166
Sr	12	7	8	7	4	6	4	5	5	4	4	4
Rb	1	15	15	16	5	15	10	9	5	6	4	3
Zn	166	92	53	48	51	47	63	66	78	123	241	919
Cu	2	3	4	4	0	3	2	7	3	8	7	3940
Ni	24	19	16	19	13	17	12	8	13	11	13	8
Cr	40	32	54	31	28	36	29	32	38	40	45	9
La	40	37	46	43	65	32	25	55	96	17	48	29
Ce	120	121	134	109	164	92	85	139	211	62	111	97

N.B. Samples taken every 5 m along drillhole towards sulphide horizon.

J Locality - Footwall alteration

Sample (wt%)	1 MA1J21	2 MA2J11	3 MA3J11	4 MA4J11	5 MA1J4	6 MA6J4	7 MA3J4	8 MA14J11
SiO_2	76.48	71.58	74.77	73.71	70.68	77.98	75.16	75.74
Al_2O_3	12.41	15.29	12.84	13.04	10.98	6.03	8.15	7.04
Fe_2O_3	4.98	5.95	5.63	5.75	8.47	8.29	9.33	9.53
MgO	3.82	4.23	4.66	5.48	6.30	3.57	4.59	5.27
CaO	0.00	0.00	0.00	0.00	0.00	0.27	0.00	0.00
Na_2O	0.14	0.28	0.30	0.28	1.88	0.45	0.89	0.06
K_2O	1.90	2.35	1.48	1.44	0.12	0.76	0.32	0.00
TiO_2	0.22	0.27	0.23	0.22	0.25	0.37	0.17	0.24
MnO	0.02	0.03	0.03	0.02	0.03	0.03	0.03	0.05
S	0.00	0.00	0.04	0.02	1.32	2.10	1.32	2.02
P_2O_5	0.02	0.02	0.03	0.02	0.03	0.15	0.05	0.06
TOTAL	99.99	100.00	100.01	99.98	100.06	100.00	100.01	100.01
ppm								
Ba	359	486		194	37		28	11
Nb	47	51		42	39		24	15
Zr	710	788		696	628		366	57
Y	142	172		110	102		86	566
Sr	9	12		9	27		17	1
Rb	25	27		16	6		13	1
Zn	56	51		120	1043		1179	621
Cu	46	113		63	368		282	602
Ni	12	12		4	0		0	142
Cr	37	17		15	27		12	195
La	88	70		3	37		126	43
Ce	180	261		5	101		331	82

Columns 1-4 Relatively unaltered tuffs.

Columns 5-8 Increasingly altered tuffs.

APPENDIX D

ETCH TECHNIQUES FOR SULPHIDES

Structure etching was carried out where necessary on polished specimens of sulphide assemblages using the reagents and methods set out in the accompanying table. Each sample was first lightly polished with alumina powder to remove any surface tarnish, washed and dried. It was then immersed in the reagent for the required time, or until an etch developed. The sample was then cleaned thoroughly with water.

Over-etching, surface tarnish, or non-uniform etches can be reduced by light polishing with alumina powder. Surface scratches due to the initial polishing tend to be emphasized during etching and cannot be eliminated.

Examples of etched sulphides can be seen in plates 53, 54, 55, 56, 57, 58, 62, and 65.

Structure etching of Sulphides

Mineral	Method	Observations	Reference
Sphalerite	47% HI for 15-20 seconds. Clean in water.	Good clear etch. Deeply etches pyrrhotite, and tarnishes chalcopyrite.	Stanton and Gorman (1968), Clark and Kelly (1973).
Pyrite	Conc. HNO_3 for up to 1½ minutes. Clean in water.	Good etch. Time required depends on grain size, degree of weathering. May be tarnished but this can be removed by light polishing with alumina powder. Deeply etches other sulphides.	Richard and Zweifel (1975).
Pyrrhotite	47% HI for 5-10 seconds. Clean in water.	Non-uniform etch. Some grains deeply tarnished Deeply etches chalcopyrite	Clark and Kelly (1973). Scott, Both and Kissin (1977).
Chalco-pyrite	H_2O_2 (100 volumes) + NH_4OH (conc.) 30 seconds etch time.	Excellent, uniform etch. Slight etching of pyrrhotite to blue-grey-brown.	Stanton and Gorman (1968).
Galena	HI/HBr, time unspecified.	Not used in this study, but included for completeness	Stanton and Gorman (1968), see also Ramdohr (1980), page 649.

SOLOMONS MINE
762 LT
MON DESIR
782 LT
RUBBERVALE
784 LT
GRAVELOTTE
783 LT
BEESPLAAS
676 LT
COTTONDALE
674 LT
ROOIWATER
673 LT
MARANDA
675 LT
CLAIMLAND 780
GRAVELOTTE
GRANITE
ROOIWATER GABBRO
M.N.
T.N.
LEGEND
RECENT
Soil and alluvium
POST-SWAZILAND INTRUSIVES
Dolerite dyke
SWAZILAND SUPERGROUP (ARCHAEAN)
YOUNGER INTRUSIVES
Granite
MURCHISON GROUP INTRUSIVES
Gabbro
Quartz-diorite
Rooiwater Igneous Complex
Basic sills
GRAVELOTTE SUBGROUP
Metasediments: phyllites, greywacks, quartzites
TRANSITION ZONE
Chert, cherty tuff, reworked volcanic rocks
Acid porphyries
RUBBERVALE SUBGROUP
Felsic volcanic rocks
Flows
Tuffs
Fragmentals
Acid intrusives
Hexagonal cooling joints
MINERALIZATION
Massive gossan
Disseminated gossan
Antimony prospect
Antimony mine
SYMBOLS
Geological contact - known
Geological contact - inferred
Geological contact - estimated
Fault/photolineament
Pulse E.M. anomaly
Target area/locality
S1 dip and strike
S1 vertical
S2 vertical
L1 plunge and direction
L1 vertical
MAP I
MURCHISON AREA
CENTRAL SECTOR
DETAIL GEOLOGY
SKETCH GEOLOGY IN NORTH AND SOUTH FROM VAN EEDEN et al. (1939)
SCALE 1:20000
GEOLOGY R. S. Taylor


SOLOMONS MINE
762 LT
MON DESIR
782 LT
RUBBERVALE
784 LT
GRAVELOTTE
783 LT
BEESPLAAS
676 LT
COTTONDALE
674 LT
ROOIWATER
673 LT
MARANDA
675 LT
CLAIM LAND 780
from Tzaneen
GRAVELOTTE
TRANSITION ZONE
M.N.
T.N.
MD1
MD3
SM12
SM11
SM17
SM14
SM16
SM154
GE3
GE114
GE5
GE8
RV6
RV7
RV5
RV4
RV3
RV2
RV1
RW2
CD21
CD18
CD23
CD4
MA1
MA2
MA3
MA29
MA23
D
J
W
L
LEGEND
RECENT
Soil and alluvium
POST-SWAZILAND INTRUSIVES
Dolerite dyke
SWAZILAND SUPERGROUP
(ARCHAEAN)
YOUNGER INTRUSIVES
Granite
MURCHISON GROUP
INTRUSIVES
Gb Gabbro
G Quartz-diorite
Bi Basic sills
Rooiwater Igneous Complex
GRAVELOTTE SUBGROUP
S Metasediments: phyllites, greywacks, quartzites
TRANSITION ZONE
Chert, reworked volcanic rocks, acid porphyries
RUBBERVALE SUBGROUP
Felsic volcanic rocks
Ai Acid intrusives
MINERALIZATION
Massive gossan
Disseminated gossan
SYMBOLS
Geological contact
Fault/photolineament
D Target area/locality
SM1 Sample locality
MAP 4
MURCHISON AREA
CENTRAL SECTOR
SIMPLIFIED GEOLOGICAL MAP
SHOWING SAMPLE LOCALITIES
SCALE 1:20000
GEOLOGY R.S. Taylor
TZ 432

LEGEND

VOLCANIC ROCKS

- A — Acid schist (metalavas)
- A-IΔ — Felsic tuffs
- AT — Cherty tuffs, aluminous cherts
- ATT — Acid porphyry

METASEDIMENTS

- S — Sedimentary schist
- Quartz vein

INTRUSIVES

- Ai — Acid intrusive
- Bi — Basic intrusive
- ^ ^ — Dolerite

MINERALISATION

- Gossan
- Stringer sulphides

SYMBOLS

- Diamond drill hole collar
- Percussion drill hole
- Pulse E M anomaly (8 channel)
- Fault / shear zone
- 60 — Dip and strike of foliation

NOTE

ALL PERCUSSION HOLES ARE DRILLED AT 60° INCLINATION.
ALL DIAMOND DRILL HOLES ARE DRILLED AT 75° INCLINATION EXCEPT WHERE SHOWN OTHERWISE.

MAP 2

MURCHISON AREA

MARANDA

TARGET J

GEOLOGY

SCALE 1 2000

TZ 380

360 E
380 E
420 E
460 E
500 E
Regional Grid 1400 W
BASE LINE
10 040 N
10 000 N
9 960 N
9 920 N
MW4 80°
MW1 75°
MW2 75°
MW3 70°
MP 210
MP 211
MP 212
65°W
FENCE
ROAD
Base of hill
M N
A
AT
ATT
Bi
65° 70°
50° 64°
84°
76° 41°
55° 63°
66° 82°
50°
64°
f
1600 W Regional grid
10 0 50m
SCALE

LEGEND

- A — ACID VOLCANICS (RHYOLITES)
- AT — ALUMINOUS CHERT
- ATT — ACID PORPHYRY
- Bi — BASIC INTRUSIVE
- # # — STRINGER MINERALIZATION PROJECTED TO SURFACE
- 76° — FOLIATION, DIP AND STRIKE S_1
- 41° — LINEATION PLUNGE L_1
- ANCIENT SMELTER SITE
- MW3 70° — DIAMOND DRILL HOLE COLLAR
- PERCUSSION DRILL HOLE COLLAR

MAP 3

MURCHISON AREA

MARANDA

TARGET W

GEOLOGY